Appendix A

EQUATIONS OF MOTION IN THE STATE AND CONFIGURATION SPACES

A.1 EQUATIONS OF MOTION OF DISCRETE LINEAR SYSTEMS

A.1.1 Configuration space

Consider a system with a single degree of freedom and assume that the equation expressing its dynamic equilibrium is a second order ordinary differential equation (ODE) in the generalized coordinate x. Assume as well that the forces entering the dynamic equilibrium equation are

- a force depending on acceleration (inertial force),
- a force depending on velocity (damping force),
- a force depending on displacement (restoring force),
- a force, usually applied from outside the system, that depends neither on coordinate x nor on its derivatives, but is a generic function of time (external forcing function).

If the dependence of the first three forces on acceleration, velocity and displacement respectively is linear, the system is linear. Moreover, if the constants of such a linear combination, usually referred to as mass m, damping coefficient c and stuffiness k do not depend on time, the system is time-invariant. The dynamic equilibrium equation is then

$$m\ddot{x} + c\dot{x} + kx = f(t) \; . \tag{A.1}$$

If the system has a number n of degrees of freedom, the most general form for a linear, time invariant set of second order ordinary differential equations is

$$\mathbf{A}_1\ddot{\mathbf{x}} + \mathbf{A}_2\dot{\mathbf{x}} + \mathbf{A}_3\mathbf{x} = \mathbf{f}(t) \ , \tag{A.2}$$

where:

- $\mathbf{x}$ is a vector of order n (n is the number of degrees of freedom of the system) where the generalized coordinates are listed;
- $\mathbf{A}_1$, $\mathbf{A}_2$ and $\mathbf{A}_3$ are matrices, whose order is $n \times n$; they contain the characteristics (independent of time) of the system;
- $\mathbf{f}$ is a vector function of time containing the forcing functions acting on the system.

Matrix $\mathbf{A}_1$ is usually symmetrical. The other two matrices in general are not. They can be written as the sum of a symmetrical and a skew-symmetrical matrices

$$\mathbf{M}\ddot{\mathbf{x}} + (\mathbf{C} + \mathbf{G})\,\dot{\mathbf{x}} + (\mathbf{K} + \mathbf{H})\,\mathbf{x} = \mathbf{f}(t) \ , \tag{A.3}$$

where:

- $\mathbf{M}$, the *mass matrix* of the system, is a symmetrical matrix of order $n \times n$ (coincides with $\mathbf{A}_1$). Usually it is not singular.
- $\mathbf{C}$ is the real symmetric *viscous damping matrix* (the symmetric part of $\mathbf{A}_2$).
- $\mathbf{K}$ is the real symmetric *stiffness matrix* (the symmetric part of $\mathbf{A}_3$).
- $\mathbf{G}$ is the real skew-symmetric *gyroscopic matrix* (the skew-symmetric part of $\mathbf{A}_2$).
- $\mathbf{H}$ is the real skew-symmetric *circulatory matrix* (the skew-symmetric part of $\mathbf{A}_3$).

Remark A.1 *Actually it is possible to write the set of linear differential Equations (A.2) in such a way that no matrix is either symmetric or skew symmetric (it is enough to multiply one of the equations by a constant other than 1). A better way to say this is that* $\mathbf{M}$, $\mathbf{C}$, *and* $\mathbf{K}$ *can be reduced to symmetric matrices by the same linear transformation that reduces* $\mathbf{G}$ *and* $\mathbf{H}$ *into skew-symmetric matrices.*

Remark A.2 *The same form of Equation (A.2) may result from mathematical modeling of physical systems whose equations of motion are obtained by means of space discretization techniques, such as the well-known finite elements method.*

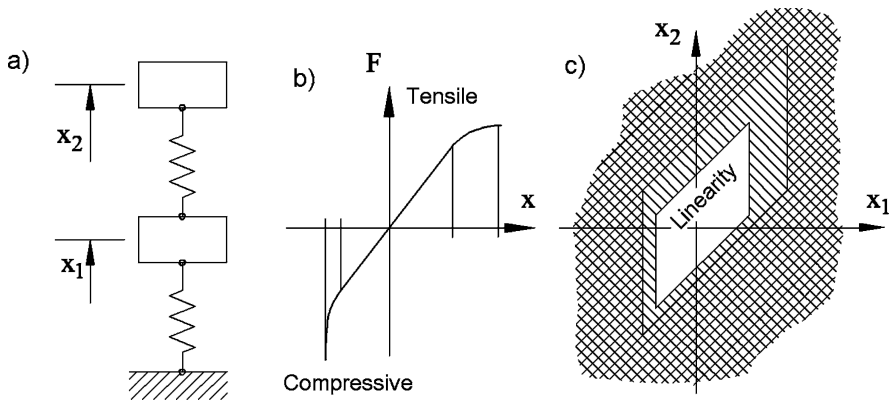

FIGURE A.1. Sketch of a system with two degrees of freedom (a) made by two masses and two springs, whose characteristics (b) are linear only in a zone about the equilibrium position. Three zones can be identified in the configuration space (c): in one the system behaves linearily, in another the system is nonlinear. The latter zone is surrounded by a 'forbidden' zone.

$\mathbf{x}$ is a vector in the sense it is a column matrix. Indeed, any set of n numbers may be interpreted as a vector in an n-dimensional space. This space containing vector $\mathbf{x}$ is usually referred to as *configuration space*, because any point in this space may be associated with a configuration of the system. Actually, not all points of the configuration space, intended to be an infinite n-dimensional space, correspond to configurations that are physically possible for the system: It is then possible to define a subset of possible configurations. Moreover, even systems that are dealt with using linear equations of motion are linear only for configurations little displaced from a reference configuration (usually the equilibrium configuration) and thus the linear equation (A.2) applies in an even smaller subset of the configuration space.

A simple system with two degrees of freedom is shown in Fig. A.1a; it consists of two masses and two springs whose behavior is linear in a zone around the equilibrium configuration with $x_1 = x_2 = 0$, but behave in a nonlinear way to fail at a certain elongation. In the configuration space, which in the case of a system with two degrees of freedom has two dimensions and thus is a plane, there is a linearity zone, surrounded by a zone where the system behaves in nonlinear way. Around the latter is another zone where the system loses its structural integrity.

A.1.2 State space

A set of n second order differential equations is a set of order $2n$ that can be expressed in the form of a set of $2n$ first order equations.

In a way similar to above, a generic linear differential equation with constant coefficients can be written in the form of a set of first order differential equations

$$\mathbf{A}_1\dot{\mathbf{x}} + \mathbf{A}_2\mathbf{x} = \mathbf{f}(t) \; . \tag{A.4}$$

In system dynamics this set of equations is usually solved in the first derivatives (monic form) and the forcing function is written as the linear combination of the minimum number of functions expressing the *inputs* of the system. The independent variables are said to be *state variables* and the equation is written as

$$\dot{\mathbf{z}} = \mathbf{A}\mathbf{z} + \mathbf{B}\mathbf{u} \; , \tag{A.5}$$

where

- $\mathbf{z}$ is a vector of order m, in which the state variables are listed (m is the number of the state variables);
- $\mathbf{A}$ is a matrix of order $m \times m$, independent of time, called the *dynamic matrix*;
- $\mathbf{u}$ is a vector function of time, where the inputs acting on the system are listed (if r is the number of inputs, its size is $r \times 1$);
- $\mathbf{B}$ is a matrix independent of time that states how the various inputs act in the various equations. It is called the input gain matrix and its size is $m \times r$.

As was seen for vector $\mathbf{x}$, $\mathbf{z}$ is also a column matrix that may be considered as a vector in an m-dimensional space. This space is usually referred to as the *state space*, because each point of this space corresponds to a given state of the system.

Remark A.3 *The configuration space is a subspace of the space state.*

If Eq. (A.5) derives from Eq. (A.2), a set of n auxiliary variables must be introduced to transform the system from the configuration to the state space. Although other choices are possible, the simplest choice is to use the derivatives of the generalized coordinates (generalized velocities) as auxiliary variables. Half of the state variables are then the generalized coordinates $\mathbf{x}$, while and the other half are the generalized velocities $\dot{\mathbf{x}}$.

If the state variables are ordered with velocities first and then coordinates, it follows that

$$\mathbf{z} = \left\{ \begin{array}{c} \dot{\mathbf{x}} \\ \mathbf{x} \end{array} \right\} \; .$$

A number n of equations expressing the link between coordinates and velocities must be added to the n equations (A.2). By using symbol $\mathbf{v}$ for the

generalized velocities $\dot{\mathbf{x}}$, and solving the equations in the derivatives of the state variables, the set of $2n$ equations corresponding to Eq. (A.3) is then

$$\begin{cases} \dot{\mathbf{v}} = -\mathbf{M}^{-1}(\mathbf{C}+\mathbf{G})\,\mathbf{v} - \mathbf{M}^{-1}(\mathbf{K}+\mathbf{H})\,\mathbf{x} + \mathbf{M}^{-1}\mathbf{f}(t) \\ \dot{\mathbf{x}} = \mathbf{v}\ . \end{cases} \tag{A.6}$$

Assuming that inputs $\mathbf{u}$ coincide with the forcing functions $\mathbf{f}$, matrices $\mathbf{A}$ and $\mathbf{B}$ are then linked to $\mathbf{M}$,$\mathbf{C}$, $\mathbf{K}$, $\mathbf{G}$ and $\mathbf{H}$ by the following relationships

$$\mathbf{A} = \begin{bmatrix} -\mathbf{M}^{-1}(\mathbf{C}+\mathbf{G}) & -\mathbf{M}^{-1}(\mathbf{K}+\mathbf{H}) \\ \mathbf{I} & \mathbf{0} \end{bmatrix}, \tag{A.7}$$

$$\mathbf{B} = \begin{bmatrix} \mathbf{M}^{-1} \\ \mathbf{0} \end{bmatrix}. \tag{A.8}$$

The first n out of the $m = 2n$ equations constituting the state equation (A.5) are the dynamic equilibrium equations. These are usually referred to as dynamic equations. The other n express the relationship between the position and the velocity variables. These are usually referred to as kinematic equations.

Often what is more interesting than the state vector $\mathbf{z}$ is a given linear combination of states $\mathbf{z}$ and inputs $\mathbf{u}$, usually referred to as the *output vector*. The state equation (A.5) is then associated with an *output equation*

$$\mathbf{y} = \mathbf{C}\mathbf{z} + \mathbf{D}\mathbf{u}\ , \tag{A.9}$$

where

- $\mathbf{y}$ is a vector where the output variables of the system are listed (if the number of outputs is s, its size is $s \times 1$);
- $\mathbf{C}$ is a matrix of order $s \times m$, independent of time, called the *output gain matrix*;
- $\mathbf{D}$ is a matrix independent of time that states how the inputs enter the linear combination yielding the output of the system. It is called the *direct link matrix* and its size is $s \times r$. In many cases the inputs do not enter the linear combination yielding the outputs, and $\mathbf{D}$ is nil.

The four matrices $\mathbf{A}$, $\mathbf{B}$, $\mathbf{C}$ and $\mathbf{D}$ are usually referred to as the quadruple of the dynamic system.

Summarizing, the equations that define the dynamic behavior of the system, from input to output, are

$$\begin{cases} \dot{\mathbf{z}} = \mathbf{A}\mathbf{z} + \mathbf{B}\mathbf{u} \\ \mathbf{y} = \mathbf{C}\mathbf{z} + \mathbf{D}\mathbf{u}. \end{cases} \tag{A.10}$$

Remark A.4 *While the state equations are differential equations, the output equations are algebraic. The dynamics of the system is then concentrated in the former.*

The input-output relationship described by Eq. (A.10) may be described by the block diagram shown in Fig. A.2.

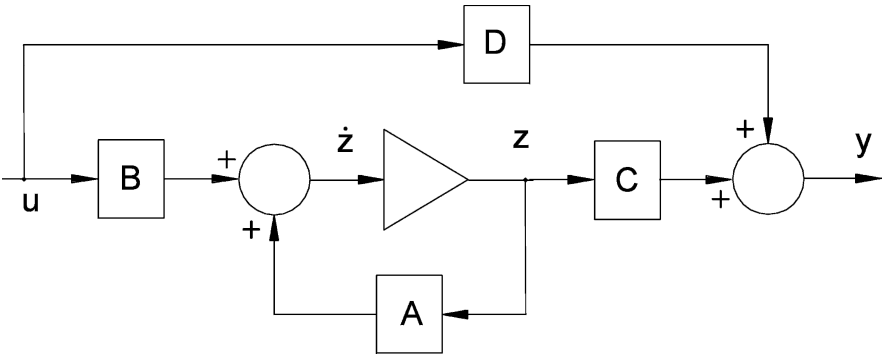

FIGURE A.2. Block diagram corresponding to Eq. (A.10).

A.2 STABILITY OF LINEAR DYNAMIC SYSTEMS

The linearity of a set of equations allows one to state that a solution exists and is unique. The general solution of the equation of motion is the sum of the general solution of the homogeneous equation associated with it and a particular solution of the complete equation. This is true for any differential linear set of equations, even if it is not time-invariant.

The former is the free response of the system, the latter the response to the forcing function.

Consider the equation of motion written in the configuration space (A.2). As already stated, matrix $\mathbf{A}_1$ is symmetrical, while the other two may not be.

The homogeneous equation

$$\mathbf{A}_1\ddot{\mathbf{x}}(t) + \mathbf{A}_2\dot{\mathbf{x}}(t) + \mathbf{A}_3\mathbf{x}(t) = 0 \tag{A.11}$$

describes the free motion of the system and allows its stability to be studied.

The solution of Eq. (A.11) may be written as

$$\mathbf{x}(t) = \mathbf{x}_0\, e^{st}\ , \tag{A.12}$$

where $\mathbf{x}_0$ and s are a vector and a scalar, respectively, both complex and constant. To state the time history of the solution allows the differential equation to be transformed into an algebraic equation

$$\left(\mathbf{A}_1 s^2 + \mathbf{A}_2 s + \mathbf{A}_3\right)\mathbf{x}_0 = \mathbf{0}\ . \tag{A.13}$$

This is a set of linear algebraic homogeneous equations, whose coefficients matrix is a second order *lambda matrix*[1]; it is square and, because the mass matrix $\mathbf{A}_1 = \mathbf{M}$ is not singular, the lambda matrix is said to be *regular*.

[1]The term *lambda matrix* comes from the habit of using the symbol λ for the coefficient appearing in the solution $\mathbf{q}(t) = \mathbf{q}_0\, e^{\lambda t}$. Here symbol s has been used instead of λ, following a more modern habit.

The equation of motion (A.11) has solutions different from the trivial

$$\mathbf{x}_0 = \mathbf{0} \tag{A.14}$$

if and only if the determinant of the matrix of the coefficients vanishes:

$$\det\left(\mathbf{A}_1 s^2 + \mathbf{A}_2 s + \mathbf{A}_3\right) = 0 \ . \tag{A.15}$$

Equation (A.15) is the characteristic equation of a generalized eigenproblem. Its solutions s_i are the eigenvalues of the system and the corresponding vectors $\mathbf{x}_{0_i}$ are its eigenvectors. The rank of the matrix of the coefficients obtained in correspondence of each eigenvalue s_i defines its multiplicity: If the rank is $n-\alpha_i$, the multiplicity is α_i. The eigenvalues are $2n$ and, correspondingly, there are $2n$ eigenvectors.

A.2.1 Conservative natural systems

If the gyroscopic matrix $\mathbf{G}$ is not present the system is said to be *natural*. If the damping and circulatory matrices $\mathbf{C}$ and $\mathbf{H}$ also vanish the system is *conservative*. A system with $\mathbf{G} = \mathbf{C} = \mathbf{H} = \mathbf{0}$ (or, as is usually referred to, an MK system) is then both natural and conservative. The characteristic equation reduces to the algebraic equation

$$\det\left(\mathbf{M}s_i^2 + \mathbf{K}\right) = 0 \ . \tag{A.16}$$

The eigenproblem can be reduced in canonical form

$$\mathbf{D}\mathbf{x}_i = \mu_i \mathbf{x}_i, \tag{A.17}$$

where the dynamic matrix in the configuration space $\mathbf{D}$ (not to be confused with the dynamic matrix in the state space $\mathbf{A}$) is

$$\mathbf{D} = \mathbf{M}^{-1}\mathbf{K} \ , \tag{A.18}$$

and the parameter in which the eigenproblem is written is

$$\mu_i = -s_i^2 \ . \tag{A.19}$$

Because matrices $\mathbf{M}$ and $\mathbf{K}$ are positive defined (or, at least, semi-defined), the n eigenvalues μ_i are all real and positive (or zero) and then the eigenvalues in terms of s_i are $2n$ imaginary numbers in pairs with opposite sign

$$(s_i, \overline{s}_i) = \pm i\sqrt{\mu_i} \ . \tag{A.20}$$

The n eigenvectors $\mathbf{x}_i$ of size n are real vectors.

When the eigenvalue s_i is imaginary, the solution (A.12) reduces to an undamped harmonic oscillation

$$\mathbf{x}(t) = \mathbf{x}_0\, e^{i\omega t} \ , \tag{A.21}$$

where

$$\omega = is = \sqrt{\mu} \tag{A.22}$$

is the (circular) frequency.

The n values of ω_i, computed from the eigenvalues μ_i, are the natural frequencies or eigenfrequencies of the system, usually referred to as ω_{n_i}.

If $\mathbf{M}$ or $\mathbf{K}$ are not positive defined or semidefined, at least one of the eigenvalues μ_i is negative, making one of the pair of solutions in s real, being made of a positive and a negative value. As will be seen below, the real negative solution corresponds to a time history that decays in time in a non-oscillatory way, the positive solution to a time history that increases in time in an unbounded way. The system is then unstable.

A.2.2 Natural nonconservative systems

If matrix $\mathbf{C}$ does not vanish while $\mathbf{G} = \mathbf{H} = \mathbf{0}$, the system is still natural and non-circulatory, but is no longer conservative.

The characteristic equation (A.15) cannot be reduced to an eigenproblem in canonical form in the configuration space and the state space formulation must be used.

The general solution of the homogeneous equation associated with Eq. (A.5) is of the type

$$\mathbf{z} = \mathbf{z}_0 e^{st} \ , \tag{A.23}$$

where s is generally a complex number. Its real and imaginary parts are usually indicated with symbols ω and σ

$$\begin{array}{l} \omega = \Im\left(s\right) \\ \sigma = \Re\left(s\right) \end{array} \tag{A.24}$$

and represent the frequency of the free oscillations and the decay rate. Solution (A.23) can in fact be written in the form

$$\mathbf{z} = \mathbf{z}_0 e^{\sigma t} e^{i\omega t} \ , \tag{A.25}$$

or, because both σ and ω are real numbers,

$$\mathbf{z} = \mathbf{z}_0 e^{\sigma t} \left[\cos\left(\omega t\right) + i \sin\left(\omega t\right)\right] \ . \tag{A.26}$$

By introducing solution (A.23) into the homogeneous equation associated with Eq. (A.5), the latter transforms from a set of differential equations to a (homogeneous) set of algebraic equations

$$s\mathbf{z}_0 = \mathbf{A}\mathbf{z}_0 \ , \tag{A.27}$$

i.e.

$$\left(\mathbf{A} - s\mathbf{I}\right)\mathbf{z}_0 = 0 \ . \tag{A.28}$$

As seen for the equation of motion in the configuration space, the homogeneous equations will have solutions other than the trivial solution $\mathbf{z}_0 = 0$ only if the determinant of the coefficients matrix vanishes

$$\det(\mathbf{A} - s\mathbf{I}) = 0 \,. \tag{A.29}$$

Equation (A.29) can be interpreted as an algebraic equation in s, i.e. the characteristic equation of the dynamic systems. It is an equation of power $2n$, yielding the $2n$ values of s. The $2n$ values of s are the eigenvalues of the system and the corresponding $2n$ values of $\mathbf{z}_0$ are the eigenvectors. In general, both eigenvalues and eigenvectors are complex.

If matrix $\mathbf{A}$ is real, as is usually the case, the solutions are either real or complex conjugate. The corresponding time histories are (Fig. A.3):

- Real solutions ($\omega = 0$, $\sigma \neq 0$): Either exponential time histories, with monotonic decay of the amplitude if the solution is negative (stable, non-oscillatory behavior), or exponential time histories, with monotonic increase of the amplitude if the solution is positive (unstable, non-oscillatory behavior).

- Complex conjugate solutions ($\omega \neq 0$, $\sigma \neq 0$): Oscillating time histories, expressed by Eq. (A.26) with amplitude decay if the real part of the solution

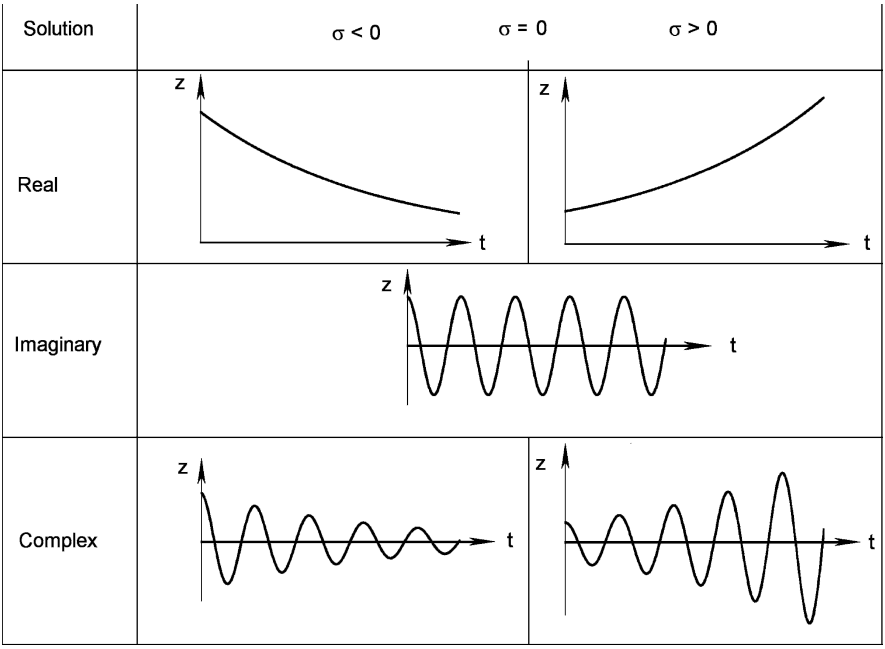

FIGURE A.3. Time history of the free motion for the various types of the eigenvalues of the system

is negative (stable, oscillatory behavior) or amplitude increase in time if the real part of the solution is positive (unstable, oscillatory behavior). If the system is stable, stability is asymptotic.

To these two cases, that previously seen for conservative systems may be added:

- Imaginary solutions ($\omega \neq 0$, $\sigma = 0$): Harmonic time histories (sine or cosine waves, undamped oscillatory behavior). In this case stability is non-asymptotic.

The necessary and sufficient condition for stable behavior is thus that the real part of all eigenvalues is negative.

If any one of the real parts of the eigenvalues is zero, the behavior is still stable (because the amplitude does not grow uncontrolled in time) but not asymptotically stable.

If at least one of the real parts of the eigenvalues is positive, the system is unstable.

If the system is little damped, i.e. the eigenvalues are conjugate and the decay rates σ are small, the values of the natural frequencies ω are close to those of the corresponding undamped system, i.e. to those of the MK system obtained by simply neglecting the damping matrix $\mathbf{C}$. In this case the natural frequencies ω_{n_i} are still those of the corresponding undamped systems.

The general solution of the homogeneous equation is a linear combination of the $2n$ solutions

$$\mathbf{z} = \sum_{i=1}^{2n} C_i \mathbf{z}_{0i} e^{s_i t} \ , \tag{A.30}$$

where the $2n$ constants C_i must be obtained from the initial conditions, i.e. from vector $\mathbf{z}(0)$.

The equation allowing constants C_i to be computed can be written as

$$\mathbf{z}(0) = \left[\begin{array}{cccc} \mathbf{z}_{01} & \mathbf{z}_{02} & ... & \mathbf{z}_{02n} \end{array} \right] \left\{ \begin{array}{c} C_1 \\ C_2 \\ .... \\ C_{2n} \end{array} \right\} = \mathbf{\Phi C} \ , \tag{A.31}$$

where $\mathbf{\Phi}$ is the matrix of the complex eigenvectors.

A real and negative eigenvalue corresponds to an *overdamped* behavior, which is non-oscillatory, of the relevant mode. If the eigenvalue is complex (with negative real part) the mode has an *underdamped* behavior, i.e. has a damped oscillatory time history. A system with all underdamped modes is said to be underdamped, while if only one of the modes is overdamped, the system is said to be overdamped. If all modes are overdamped, the system cannot have free oscillations, but can oscillate if forced to do so.

It must be noted that if all matrices $\mathbf{M}$, $\mathbf{K}$ and $\mathbf{C}$ are positive defined (or at least semidefined), as in the case of a structure with viscous damping with

positive stiffness and damping, there is no eigenvalue with positive real part and hence the system is stable. If all matrices are strictly positive defined, there is no eigenvalue with vanishing real part and the system is asymptotically stable.

A.2.3 Systems with singular mass matrix

If matrix $\mathbf{M}$ is singular, it is impossible to write the dynamic matrix in the usual way. This usually occurs because a vanishingly small inertia is associated with some degrees of freedom, as for instance in the case of the driveline models shown in Fig. 30.9, where the tire is modelled as a spring and a damper in series, with no mass between them. Clearly the problem may be circumvented by associating a very small mass with the relevant degrees of freedom: A new very high natural frequency that has no physical meaning is thus introduced and, if this is done carefully, no numerical instability problem results. However, it makes little sense to resort to tricks of this kind when it is possible to overcome the problem in a more correct and essentially simple way.

The degrees of freedom can be subdivided into two sets: A vector $\mathbf{x}_1$ containing those with which a non-vanishing inertia is associated, and a vector $\mathbf{x}_2$, containing all others. All matrices and forcing functions may be similarly split . The mass matrix $\mathbf{M}_{22}$ vanishes, and if the mass matrix is diagonal, $\mathbf{M}_{12}$ and $\mathbf{M}_{21}$ also vanish.

Assuming that $\mathbf{M}_{12}$ and $\mathbf{M}_{21}$ are zero, the equations of motion become

$$\left\{ \begin{array}{l} \mathbf{M}_{11}\ddot{\mathbf{x}}_1 + \mathbf{C}_{11}\dot{\mathbf{x}}_1 + \mathbf{C}_{12}\dot{\mathbf{x}}_2 + \mathbf{K}_{11}\mathbf{x}_1 + \mathbf{K}_{12}\mathbf{x}_2 = \mathbf{f}_1(t) \\ \mathbf{C}_{21}\dot{\mathbf{x}}_1 + \mathbf{C}_{22}\dot{\mathbf{x}}_2 + \mathbf{K}_{21}\mathbf{x}_1 + \mathbf{K}_{22}\mathbf{x}_2 = \mathbf{f}_2(t) \ . \end{array} \right. \tag{A.32}$$

To simplify the equations of motion neither the gyroscopic nor the circulator matrices are explicitly written, but in what follows no assumption on the symmetry of the stiffness and damping matrices will be made. The equations also hold for gyroscopic and circulatory systems.

By introducing the velocities $\mathbf{v}_1$ together with generalized coordinates $\mathbf{x}_1$ and $\mathbf{x}_2$ as state variables, the state equation is

$$\mathbf{M}^* \left\{ \begin{array}{c} \mathbf{v}_1 \\ \mathbf{x}_1 \\ \mathbf{x}_2 \end{array} \right\} = \mathbf{A}^* \left\{ \begin{array}{c} \mathbf{v}_1 \\ \mathbf{x}_1 \\ \mathbf{x}_2 \end{array} \right\} + \left[\begin{array}{cc} \mathbf{I} & \mathbf{0} \\ \mathbf{0} & \mathbf{I} \\ \mathbf{0} & \mathbf{0} \end{array} \right] \left\{ \begin{array}{c} \mathbf{f}_1(t) \\ \mathbf{f}_2(t) \end{array} \right\} , \tag{A.33}$$

where

$$\mathbf{M}^* = \left[\begin{array}{ccc} \mathbf{M}_{11} & \mathbf{0} & \mathbf{C}_{12} \\ \mathbf{0} & \mathbf{0} & \mathbf{C}_{22} \\ \mathbf{0} & \mathbf{I} & \mathbf{0} \end{array} \right] , \ \mathbf{A}^* = - \left[\begin{array}{ccc} \mathbf{C}_{11} & \mathbf{K}_{11} & \mathbf{K}_{12} \\ \mathbf{C}_{21} & \mathbf{K}_{21} & \mathbf{K}_{22} \\ -\mathbf{I} & \mathbf{0} & \mathbf{0} \end{array} \right] . \tag{A.34}$$

The dynamic matrix and the input gain matrix are

$$\mathbf{A} = \mathbf{M}^{*-1}\mathbf{A}^* \ , \ \mathbf{B} = \mathbf{M}^{*-1} \left[\begin{array}{cc} \mathbf{I} & \mathbf{0} \\ \mathbf{0} & \mathbf{I} \\ \mathbf{0} & \mathbf{0} \end{array} \right] . \tag{A.35}$$

Alternatively, the expressions of $\mathbf{M}^*$ and $\mathbf{A}^*$ can be

$$\mathbf{M}^* = \begin{bmatrix} \mathbf{M}_{11} & \mathbf{C}_{11} & \mathbf{C}_{12} \\ \mathbf{0} & \mathbf{C}_{21} & \mathbf{C}_{22} \\ \mathbf{0} & \mathbf{I} & \mathbf{0} \end{bmatrix} , \quad \mathbf{A}^* = - \begin{bmatrix} \mathbf{0} & \mathbf{K}_{11} & \mathbf{K}_{12} \\ \mathbf{0} & \mathbf{K}_{21} & \mathbf{K}_{22} \\ -\mathbf{I} & \mathbf{0} & \mathbf{0} \end{bmatrix} . \tag{A.36}$$

If vector $\mathbf{x}_1$ contains n_1 elements and $\mathbf{x}_2$ contains n_2 elements, the size of the dynamic matrix $\mathbf{A}$ is $2n_1 + n_2$.

A.2.4 Conservative gyroscopic systems

If matrix $\mathbf{G}$ is not zero, while both $\mathbf{C}$ and $\mathbf{H}$ vanish, the dynamic matrix reduces to

$$\mathbf{A} = \begin{bmatrix} -\mathbf{M}^{-1}\mathbf{G} & -\mathbf{M}^{-1}\mathbf{K} \\ \mathbf{I} & \mathbf{0} \end{bmatrix} . \tag{A.37}$$

By premultiplying the first n equations by $\mathbf{M}$ and the other n by $\mathbf{K}$, it follows that

$$\mathbf{M}^*\dot{\mathbf{z}} + \mathbf{G}^*\mathbf{z} = \mathbf{0} , \tag{A.38}$$

where

$$\mathbf{M}^* = \begin{bmatrix} \mathbf{M} & \mathbf{0} \\ \mathbf{0} & \mathbf{K} \end{bmatrix} , \quad \mathbf{G}^* = \begin{bmatrix} \mathbf{G} & \mathbf{K} \\ -\mathbf{K} & \mathbf{0} \end{bmatrix} . \tag{A.39}$$

The first matrix is symmetrical, while the second is skew symmetrical.

By introducing solutions (A.23) into the equation of motion, the following homogeneous equation

$$s\mathbf{M}^*\mathbf{z}_0 + \mathbf{G}^*\mathbf{z}_0 = \mathbf{0} \tag{A.40}$$

is obtained.

The corresponding eigenproblem has imaginary solutions like those of an MK system, even if the structure of the eigenvectors is different. In any case the time history of the free oscillations is harmonic and undamped, because the decay rate $\sigma = \Re(s)$ is zero.

A.2.5 General dynamic systems

The situation is similar to that seen for natural non-conservative systems, in the sense that the time histories of the free oscillations are those seen in Fig. A.3 and stability is dominated by the sign of the real part of s.

Remark A.5 *In general, the presence of a gyroscopic matrix does not reduce the stability of the system, while the presence of a circulatory matrix has a destabilizing effect.*

Consider, for instance, a two degrees of freedom system made by two independent MK system; each with a single degree of freedom, and assume that the two masses are equal. The equations for free motion are

$$\begin{cases} m\ddot{x}_1 + k_1 x_1 = 0 \\ m\ddot{x}_2 + k_2 x_2 = 0 \ . \end{cases} \tag{A.41}$$

Introduce now a coupling term in both equations, introducing for instance a spring with stiffness k_{12} between the two masses. The equations of motion become

$$\begin{cases} m\ddot{x}_1 + (k_1 + k_{12})\, x_1 - k_{12} x_2 = 0 \ , \\ m\ddot{x}_2 - k_{12} x_1 + (k_1 + k_{12})\, x_2 = 0 \ . \end{cases} \tag{A.42}$$

By introducing parameters

$$\omega_0^2 = \frac{k_1 + k_2 + 2k_{12}}{2m} \ , \quad \alpha = \frac{k_2 - k_1}{2m\Omega_0^2} \ , \quad \epsilon = \frac{k_{12}}{m\Omega_0^2} \ , \tag{A.43}$$

the equation of motion can be written as

$$\begin{Bmatrix} \ddot{x} \\ \ddot{y} \end{Bmatrix} + \omega_0^2 \begin{bmatrix} 1-\alpha & \epsilon \\ \epsilon & 1+\alpha \end{bmatrix} \begin{Bmatrix} x \\ y \end{Bmatrix} = \mathbf{0} \ . \tag{A.44}$$

Note that

$$-1 \le \alpha \le 1 \ . \tag{A.45}$$

The matrix that multiplies the generalized coordinates is symmetrical and is thus a true stiffness matrix. The coupling is said in this case to be *non-circolatory* or *conservative.* Because there is no damping matrix and the stiffness matrix is positive defined ($-1 \le \alpha \le 1$), the eigenvalues are imaginary and the system is stable, even if it is not asymptotically stable as it would be if a positive defined damping matrix were present.

The natural frequencies of the system, made nondimensional by dividing them by ω_0, depend upon two parameters, α and ϵ. They are shown in Fig. A.4(a) as functions of α for some values of ϵ. The distance between the two curves (one for $\omega > \omega_0$ and the other for $\omega < \omega_0$) increases if the coupling term ϵ increases. For this reason this type of coupling is said to be *repulsive.*

Consider now the case with coupling term ϵ in the form

$$\begin{Bmatrix} \ddot{x} \\ \ddot{y} \end{Bmatrix} + \Omega_0^2 \begin{bmatrix} 1-\alpha & \epsilon \\ -\epsilon & 1+\alpha \end{bmatrix} \begin{Bmatrix} x \\ y \end{Bmatrix} = \mathbf{0} \ . \tag{A.46}$$

The terms outside the main diagonal of the stiffness matrix now have the same modulus but opposite sign. The matrix multiplying the displacements is made up of a symmetrical part (the stiffness matrix) and a skew-symmetrical part (the circulatory matrix). A coupling of this type is said to be *circulatory* or *non-conservative*.

While in the previous case the effect could be caused by the presence of a spring between the two masses, it cannot be due to springs or similar elements here. There are situations of practical interest where circulatory coupling occurs.

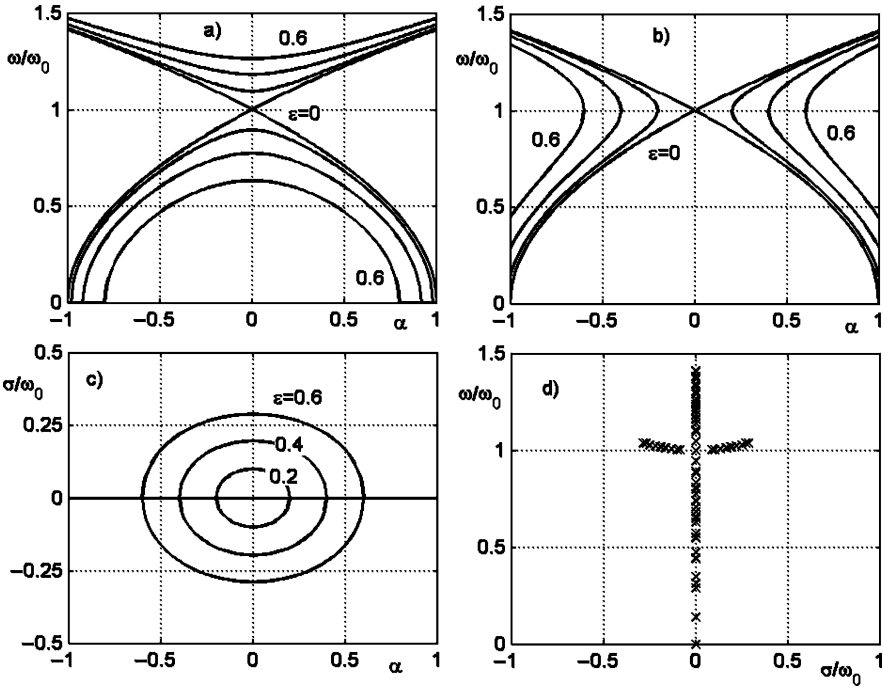

FIGURE A.4. Nondimensional natural frequencies as functions of parameters α and ϵ for a system with two degrees of freedom with non-circulatory (a) and circulatory (b) coupling. Decay rate (c) and roots locus (d) for the system with circulatory coupling.

The natural frequencies of the system in this case also depend on the two parameters α and ϵ. These are plotted in nondimensional form, by dividing them by ω_0, in Fig. A.4(b) as functions of α for some values of ϵ. The two curves now close on each other. Starting from the condition with $\alpha = -1$, the two curves meet for a certain value of α in the interval $(-1,\ 0)$. There is a range, centered in the point with $\alpha = 0$, where the solutions of the eigenproblem are complex. Beyond this range the two curves separate again.

Because the two curves approach each other and finally meet, this type of coupling is said to be *attractive*.

In the range where the values of s are complex, one of the two solutions has a positive real part: It follows that an unstable solution exists, as can be seen from the decay rate plot in Fig. A.4(c) and from the roots locus in Fig. A.4(d).

Remark A.6 *Instability is linked with the skew-symmetric matrix due to coupling, i.e. because of the fact that a circulatory matrix exists.*

A.3 CLOSED FORM SOLUTION OF THE FORCED RESPONSE

The particular solution of the complete equation depends on the time history of the forcing function (input) $\mathbf{u}(t)$. In case of harmonic input

$$\mathbf{u} = \mathbf{u}_0 e^{i\omega t} \ , \tag{A.47}$$

the response is harmonic as well

$$\mathbf{z} = \mathbf{z}_0 e^{i\omega t} \ , \tag{A.48}$$

and has the same frequency as the forcing function ω. As usual, by introducing the time history of the forcing function and the response into the equation of motion, it transforms into an algebraic equation

$$(\mathbf{A} - i\omega \mathbf{I})\, \mathbf{z}_0 + \mathbf{B}\mathbf{u}_0 = 0, \tag{A.49}$$

that allows the amplitude of the response to be computed

$$\mathbf{z}_0 = -\left(\mathbf{A} - i\omega \mathbf{I}\right)^{-1} \mathbf{B}\mathbf{u}_0 \ . \tag{A.50}$$

If the input is periodic, it may be decomposed in Fourier series and the response to each of its harmonic components computed. The results are then added. This is possible only because the system is linear.

If the input is not harmonic or at least periodic, it is possible to resort to Laplace transforms or the Duhamel integral. These techniques apply only to linear systems.

Remark A.7 *Linear models allow closed form solutions to be obtained and stability, in particular, to be studied. In linear systems, moreover, stability is a property of the system and not of its peculiar working conditions.*

A.4 NONLINEAR DYNAMIC SYSTEMS

The state equations of dynamic systems are often nonlinear. The reasons for the presence of nonlinearities may differ, owing to the presence of elements behaving in an intrinsically nonlinear way (e.g. springs producing a force dependent in a nonlinear way on the displacement), or the presence of trigonometric functions of some of the generalized coordinates in the dynamic or kinematic equations. If inertial forces are linear in the accelerations, the equations of motion can be written in the form

$$\mathbf{M}\ddot{\mathbf{x}} + \mathbf{f}_1(\mathbf{x}, \dot{\mathbf{x}}) = \mathbf{f}(t) \ . \tag{A.51}$$

Function $\mathbf{f}_1$ may often be considered as the sum of a linear and nonlinear part. The equation of motion can then be written as

$$\mathbf{M}\ddot{\mathbf{x}} + (\mathbf{C}+\mathbf{G})\,\dot{\mathbf{x}} + (\mathbf{K}+\mathbf{H})\,\mathbf{x} + \mathbf{f}_2(\mathbf{x},\,\dot{\mathbf{x}}) = \mathbf{f}(t)\ , \tag{A.52}$$

where function $\mathbf{f}_2$ contains only the nonlinear part of the dynamic system.

The state equations corresponding to Eq. (A.51) and Eq. (A.52) are

$$\dot{\mathbf{z}} = \mathbf{f}_1(\mathbf{z}) + \mathbf{B}\mathbf{u}\ , \tag{A.53}$$

or, by separating the linear from the nonlinear part,

$$\dot{\mathbf{z}} = \mathbf{A}\mathbf{z} + \mathbf{f}_2(\mathbf{z}) + \mathbf{B}\mathbf{u}\ . \tag{A.54}$$

Another way to express the equation of motion or the state equation of a nonlinear system is by writing equations (A.3) or (A.10), where the various matrices are functions of the generalized coordinates and their derivatives, or of the state variables. In the state space it follows that

$$\begin{cases} \dot{\mathbf{z}} = \mathbf{A}(\mathbf{z})\mathbf{z} + \mathbf{B}(\mathbf{z})\mathbf{u} \\ \mathbf{y} = \mathbf{C}(\mathbf{z})\mathbf{z} + \mathbf{D}(\mathbf{z})\mathbf{u}\ . \end{cases} \tag{A.55}$$

If the system is not time-invariant, the various matrices may also be explicit functions of time

$$\begin{cases} \dot{\mathbf{z}} = \mathbf{A}(\mathbf{z},\,t)\mathbf{z} + \mathbf{B}(\mathbf{z},\,t)\mathbf{u} \\ \mathbf{y} = \mathbf{C}(\mathbf{z},\,t)\mathbf{z} + \mathbf{D}(\mathbf{z},\ t)\mathbf{u}\ . \end{cases} \tag{A.56}$$

Remark A.8 *It is not possible to obtain a closed form solution of nonlinear systems, and concepts like natural frequency or decay rate lose their meaning. It is not even possible to distinguish between free and forced behavior, in the sense that the free oscillations depend upon the zone of the state space where the system operates.*

In some zones of the state space the behavior of the system may be stable, while in others it may be unstable.

In any case it is often possible to linearize the equations of motion about any given working conditions, i.e. any given point of the state space, and to use the linearized model so obtained in that area of the space state to study the motion of the system and above all its stability. In this case the motion and stability are studied *in the small*. It is, however, clear that no general result may be obtained in this way.

If the state equation is written in the form (A.53), its linearization about a point of coordinates $\mathbf{z}_0$ in the state space is

$$\dot{\mathbf{z}} = \left(\frac{\partial \mathbf{f}_1}{\partial \mathbf{z}}\right)_{\mathbf{z}=\mathbf{z}_0} \mathbf{z} + \mathbf{B}\mathbf{u}\ , \tag{A.57}$$

where $\left(\frac{\partial \mathbf{f}_1}{\partial \mathbf{z}}\right)_{\mathbf{z}=\mathbf{z}_0}$ is the Jacobian matrix of function $\mathbf{f}_1$ computed in $\mathbf{z}_0$.

If the formulation (A.55) is used, the linearized dynamics of the system about point $\mathbf{z}_0$ may be studied through the linear equation

$$\begin{cases} \dot{\mathbf{z}} = \mathbf{A}(\mathbf{z}_0)\mathbf{z} + \mathbf{B}(\mathbf{z}_0)\mathbf{u} \\ \mathbf{y} = \mathbf{C}(\mathbf{z}_0)\mathbf{z} + \mathbf{D}(\mathbf{z}_0)\mathbf{u} \, . \end{cases} \tag{A.58}$$

Remark A.9 *While the motion and stability in the small can be studied in closed form, studying the motion* in the large *requires resorting to the numerical integration of the equations of motion, that is, resorting to numerical simulation.*

A.5 LAGRANGE EQUATIONS IN THE CONFIGURATION AND STATE SPACE

In relatively simple systems it is possible to write the equations of motion directly in the form of Eq. (A.3), by writing all forces, internal and external to the system, acting on its various parts. However, if the system is complex, and in particular if the number of degrees of freedom is large, it is expedient to resort to the methods of analytical mechanics.

One of the simplest approaches to writing the equations of motion of multi-degrees of freedom systems is by resorting to Lagrange equations. Consider a generic mechanical system with n degrees of freedom, i.e. one whose configuration may be expressed using n generalized coordinates x_i. Its equations of motion can in general be written in the form

$$\frac{d}{dt}\left(\frac{\partial \mathcal{T}}{\partial \dot{x}_i}\right) - \frac{\partial \mathcal{T}}{\partial x_i} + \frac{\partial \mathcal{U}}{\partial x_i} + \frac{\partial \mathcal{F}}{\partial \dot{x}_i} = Q_i \qquad (i = 1,...., n), \tag{A.59}$$

where:

- $\mathcal{T}$ is the kinetic energy of the system. This allows inertial forces to be written in a synthetic way. In general,

  $$\mathcal{T} = \mathcal{T}(\dot{x}_i, x_i, t) \, .$$

  The kinetic energy is basically a quadratic function of the generalized velocities

  $$\mathcal{T} = \mathcal{T}_0 + \mathcal{T}_1 + \mathcal{T}_2 \, , \tag{A.60}$$

  where $\mathcal{T}_0$ does not depend on the velocities, $\mathcal{T}_1$ is linear and $\mathcal{T}_2$ is quadratic.

  In linear systems, the kinetic energy must contain terms of the velocities and coordinates having no powers higher than 2 or products of more than two of them. As a consequence, $\mathcal{T}_2$ cannot contain displacements

  $$\mathcal{T}_2 = \frac{1}{2}\sum_{i=1}^{n}\sum_{j=1}^{n} m_{ij} x_i x_j = \frac{1}{2}\dot{\mathbf{x}}^T \mathbf{M}\dot{\mathbf{x}} \, , \tag{A.61}$$

  where the terms m_{ij} don't depend on either $\mathbf{x}$ or $\dot{\mathbf{x}}$. If the system is time-invariant, $\mathbf{M}$ is constant.

$\mathcal{T}_1$ is linear in the velocities, and thus, if the system is linear, cannot contain terms other than constant or linear in the displacements

$$\mathcal{T}_1 = \frac{1}{2}\dot{\mathbf{x}}^T \left(\mathbf{M}_1\mathbf{x} + \mathbf{f}_1\right) , \tag{A.62}$$

where matrix $\mathbf{M}_1$ and vector $\mathbf{f}_1$ do not contain the generalized coordinates, even if $\mathbf{f}_1$ may be a function of time even in time-invariant systems.

$\mathcal{T}_0$ does not contain generalized velocities but, in the case of linear systems, only contains terms with power not greater than 2 in the generalized coordinates:

$$\mathcal{T}_o = \frac{1}{2}\mathbf{x}^T\mathbf{M}_g\mathbf{x} + \mathbf{x}^T\mathbf{f}_2 + e , \tag{A.63}$$

where matrix $\mathbf{M}_g$, vector $\mathbf{f}_2$ and scalar e are constant. Constant e does not enter the equations of motion. As will be seen later, the structure of $\mathcal{T}_o$ is similar to that of the potential energy. The term

$$\mathcal{U} - \mathcal{T}_0$$

is often referred to as *dynamic potential*.

- $\mathcal{U}$ is the potential energy. It allows conservative forces to be expressed in a synthetic form. In general,

$$\mathcal{U} = \mathcal{U}(x_i) .$$

In linear systems, the potential energy is a quadratic form in the generalized coordinates and, apart from a constant term that does not enter the equations of motion and thus has no importance, can be written as

$$\mathcal{U} = \frac{1}{2}\mathbf{x}^T\mathbf{K}\mathbf{x} + \mathbf{x}^T\mathbf{f}_0 , \tag{A.64}$$

By definition the potential energy does not depend on the generalized velocities and its derivatives with respect to the generalized velocities $\dot{x}_i$ vanish. Equation (A.59) is often written with reference to the *Lagrangian function*

$$\mathcal{L} = \mathcal{T} - \mathcal{U}$$

and becomes

$$\frac{d}{dt}\left[\frac{\partial \mathcal{L}}{\partial \dot{x}_i}\right] - \frac{\partial \mathcal{L}}{\partial x_i} + \frac{\partial \mathcal{F}}{\partial \dot{x}_i} = Q_i . \tag{A.65}$$

- $\mathcal{F}$ is the Raleigh dissipation function. It allows some types of damping forces to be expressed in a synthetic form. In many cases $\mathcal{F} = \mathcal{F}(\dot{x}_i)$, but it may also depend upon the generalized coordinates. In linear systems, the dissipation function is a quadratic form in the generalized velocities and, apart from terms not depending upon $\dot{x}_i$ that do not enter the equation of motion and thus have no importance, may be written as

$$\mathcal{F} = \frac{1}{2}\dot{\mathbf{x}}^T\mathbf{C}\dot{\mathbf{x}} + \frac{\mathbf{1}}{\mathbf{2}}\dot{\mathbf{x}}^{\mathbf{T}}\left(\mathbf{C_1}\mathbf{x} + \mathbf{f_3}\right) . \tag{A.66}$$

- Q_i are generalized forces that cannot be expressed using the above mentioned functions. In general, $Q_i = Q_i(\dot{q}_i, q_i, t)$. In the case of linear systems, these forces do not depend on the generalized coordinates and velocities, and then

$$Q_i = Q_i(t) \ . \tag{A.67}$$

In linear systems, by performing the relevant derivatives

$$\frac{\partial(\mathcal{T}-\mathcal{U})}{\partial \dot{x}_i} = \mathbf{M}\dot{\mathbf{x}} + \frac{1}{2}\left(\mathbf{M}_1\mathbf{x} + \mathbf{f}_1\right) \ , \tag{A.68}$$

$$\frac{d}{dt}\left[\frac{\partial(\mathcal{T}-\mathcal{U})}{\partial \dot{x}_i}\right] = \mathbf{M}\ddot{\mathbf{x}} + \frac{1}{2}\mathbf{M}_1\dot{\mathbf{x}} + \dot{\mathbf{f}}_1 \ , \tag{A.69}$$

$$\frac{\partial(\mathcal{T}-\mathcal{U})}{\partial x_i} = \frac{1}{2}\mathbf{M}_1^T\dot{\mathbf{x}} + \mathbf{M}_g\mathbf{x} - \mathbf{K}\mathbf{x} + \mathbf{f}_2 - \mathbf{f}_0 \ , \tag{A.70}$$

$$\frac{\partial \mathcal{F}}{\partial \dot{x}_i} = \mathbf{C}\dot{\mathbf{x}} + \mathbf{C}_1\mathbf{x} + \mathbf{f}_3 \ , \tag{A.71}$$

the equation of motion becomes

$$\mathbf{M}\ddot{\mathbf{x}} + \frac{1}{2}\left(\mathbf{M}_1 - \mathbf{M}_1^T\right)\dot{\mathbf{x}} + \mathbf{C}\dot{\mathbf{x}} + (\mathbf{K} - \mathbf{M}_g + \mathbf{C}_1)\,\mathbf{x} = -\dot{\mathbf{f}}_\mathbf{1} + \mathbf{f}_2 - \mathbf{f}_3 - \mathbf{f}_0 + \mathbf{Q} \ . \tag{A.72}$$

Matrix $\mathbf{M}_1$ is normally skew-symmetric. However, even if it is not, it may be written as the sum of a symmetrical and a skew-symmetrical part

$$\mathbf{M}_1 = \mathbf{M}_{1symm} + \mathbf{M}_{1skew} \ . \tag{A.73}$$

By introducing this form into Eq. (A.72), the term

$$\mathbf{M}_1 - \mathbf{M}_1^T$$

becomes

$$\mathbf{M}_{1symm} + \mathbf{M}_{1skew} - \mathbf{M}_{1symm} + \mathbf{M}_{1skew} = 2\mathbf{M}_{1skew} \ .$$

Only the skew-symmetric part of $\mathbf{M}_1$ is included in the equation of motion. $\mathbf{C}_1$ is usually skew-symmetrical.

Writing $\mathbf{M}_{1skew}$ as $\mathbf{G}$ and $\mathbf{C}_1$ (or at least its skew-symmetric part; if a symmetric part existed, it could be included into matrix $\mathbf{K}$) as $\mathbf{H}$, and including vectors $\mathbf{f}_0$, $\dot{\mathbf{f}}_1$, $\mathbf{f}_2$ and $\mathbf{f}_3$ into forcing functions $\mathbf{Q}$, the equation of motion becomes

$$\mathbf{M}\ddot{\mathbf{x}} + (\mathbf{C} + \mathbf{G})\,\dot{\mathbf{x}} + (\mathbf{K} - \mathbf{M}_g + \mathbf{H})\,\mathbf{x} = \mathbf{Q} \ . \tag{A.74}$$

The mass, stiffness, gyroscopic and circulatory matrices $\mathbf{M}$, $\mathbf{K}$, $\mathbf{G}$ and $\mathbf{H}$ have already been defined. The symmetric matrix $\mathbf{M}_g$ is often defined as a *geometric matrix*[2].

[2]Here the symbol $\mathbf{M}_g$ is used instead of the more common $\mathbf{K}_g$ to emphasize that it comes from the kinetic energy.

As already stated, a system in which $\mathcal{T}_1$ is not present is said to be *natural*. Its equation of motion does not contain a gyroscopic matrix. In many cases $\mathcal{T}_0$ also is absent and the kinetic energy is expressed by Eq. (A.61).

The linearized equation of motion of a nonlinear system can be written in two possible ways. The first is by writing the complete expression of the energies, performing the derivatives obtaining the complete equations of motion and then cancelling nonlinear terms.

The second is by reducing the expression of the energies to quadratic forms, developing their expressions in power series and then truncating them after the quadratic terms. The linearized equations of motion are then directly obtained.

Remark A.10 *These two approaches yield the same result, but the first is usually more computationally intensive. At any rate, a set of n second order equations are obtained: These are either linear or nonlinear depending on the system under study.*

To write the state equations, a number n of kinematic equations must be written

$$\dot{x}_i = v_i \qquad (i = 1,...., n). \tag{A.75}$$

If the state vector is defined in the usual way

$$\mathbf{z} = \left\{ \begin{array}{c} \mathbf{v} \\ \mathbf{x} \end{array} \right\} ,$$

this procedure is straightforward.

A.6 HAMILTON EQUATIONS AND PHASE SPACE

If the generalized momenta are used as auxiliary variables instead of the generalized velocities, the equations are written with reference to the *phase space* and *phase vector* instead of the state space and vector.

The generalized momenta are defined, starting from the Lagrangian $\mathcal{L}$, as

$$\mathbf{p} = \frac{\partial \mathcal{L}}{\partial \dot{x}_i} . \tag{A.76}$$

If the system is a natural linear system, this definition reduces to the usual one

$$\mathbf{p} = \mathbf{M}\dot{\mathbf{x}} . \tag{A.77}$$

By including the forces coming from the dissipation function in the generalized forces Q_i, the Lagrange equation simplifies as

$$\dot{p}_i = \frac{\partial \mathcal{L}}{\partial x_i} + Q_i . \tag{A.78}$$

A function $\mathcal{H}(\dot{x}_i, x_i, t)$, called the *Hamiltonian function*, is defined as

$$\mathcal{H} = \mathbf{p}^T \dot{\mathbf{x}} - \mathcal{L} \ . \tag{A.79}$$

Because $\mathcal{H}$ is a function of p_i, x_i and t ($\mathcal{H}(p_i, x_i, t)$), the differential $\delta\mathcal{H}$ is

$$\delta\mathcal{H} = \sum_{i=1}^{n} \left(\frac{\partial \mathcal{H}}{\partial p_i} \delta p_i + \frac{\partial \mathcal{H}}{\partial x_i} \delta x_i \right) \ . \tag{A.80}$$

On the other hand, Eq. (A.79) yields

$$\begin{aligned} \delta\mathcal{H} &= \sum_{i=1}^{n} \left(p_i \delta\dot{x}_i + \dot{x}_i \delta p_i - \frac{\partial \mathcal{L}}{\partial x_i} \delta x_i - \frac{\partial \mathcal{L}}{\partial \dot{x}_i} \delta\dot{x}_i \right) = \\ &= \sum_{i=1}^{n} \left(\dot{x}_i \delta p_i - \frac{\partial \mathcal{L}}{\partial x_i} \delta x_i \right) \ , \end{aligned} \tag{A.81}$$

and then

$$\frac{\partial \mathcal{H}}{\partial p_i} = \dot{x}_i \ \ , \qquad \frac{\partial \mathcal{H}}{\partial x_i} = -\frac{\partial \mathcal{L}}{\partial x_i} \ . \tag{A.82}$$

The $2n$ phase space equations are then

$$\begin{cases} \dot{x}_i = \dfrac{\partial \mathcal{H}}{\partial p_i} \\ \\ \dot{p}_i = -\dfrac{\partial \mathcal{H}}{\partial x_i} + Q_i \ . \end{cases} \tag{A.83}$$

A.7 LAGRANGE EQUATIONS IN TERMS OF PSEUDO COORDINATES

While in vehicle dynamics Hamilton equations are seldom used, the state equations are often written with reference to generalized velocities that are not simply the derivatives of the generalized coordinates. In particular, it is often expedient to use suitable combinations of the derivatives of the coordinates $v_i = \dot{x}_i$ as generalized velocities

$$\{w_i\} = \mathbf{A}^T \{\dot{x}_i\} \ , \tag{A.84}$$

where the coefficients of the linear combinations included into matrix $\mathbf{A}^T$ may be constant, but in general are functions of the generalized coordinates.

Equation (A.84) may be inverted, obtaining

$$\{\dot{x}_i\} = \mathbf{B} \{w_i\} \ , \tag{A.85}$$

where

$$\mathbf{B} = \mathbf{A}^{-T} \tag{A.86}$$

and symbol $\mathbf{A}^{-T}$ indicates the inverse of the transpose of matrix $\mathbf{A}$.

In some cases matrix $\mathbf{A}^T$ is a rotation matrix whose inverse coincides with its transpose. In such cases

$$\mathbf{B} = \mathbf{A}^{-T} = \mathbf{A} \ .$$

However, this generally does not occur and

$$\mathbf{B} \neq \mathbf{A} \ .$$

While v_i are the derivatives of the coordinates x_i, it is usually not possible to express w_i as the derivatives of suitable coordinates. Eq. (A.84) can be written in the infinitesimal displacements dx_i

$$\{d\theta_i\} = \mathbf{A}^T \{dx_i\} \ , \tag{A.87}$$

obtaining a set of infinitesimal displacements $d\theta_i$, corresponding to velocities w_i. Equations (A.87) can be integrated, yielding displacements θ_i corresponding to the velocities w_i, only if

$$\frac{\partial a_{js}}{\partial x_k} = \frac{\partial a_{ks}}{\partial x_j} \ .$$

Otherwise equations (A.87) cannot be integrated and velocities w_i cannot be considered as the derivatives of true coordinates. In such cases they are said to be the derivatives of pseudo-coordinates.

As a first consequence of the non-existence of coordinates corresponding to velocities w_i, Lagrange equation (A.59) cannot be written directly using velocities w_i (which cannot be considered as derivatives of the new coordinates), but must be modified to allow the use of velocities and coordinates that are not direct derivatives of each other.

The use of pseudo-coordinates is fairly common, particularly in vehicle dynamics. If, for instance, the generalized velocities in a reference frame following the body in its motion are used in the dynamics of a rigid body, while the coordinates x_i are the displacements in an inertial frame, matrix $\mathbf{A}^T$ is simply the rotation matrix allowing passage from one reference frame to the other. Matrix $\mathbf{B}$ then coincides with $\mathbf{A}$, but neither is symmetrical. The velocities in the body-fixed frame cannot therefore be considered as the derivatives of the displacements in that frame.

Remark A.11 *The body-fixed frame rotates continuously so that it is not possible to integrate the velocities along the body-fixed axes to obtain the displacements along the same axes. This fact notwithstanding, it is possible to use the components of the velocity along the body-fixed axes to write the equations of motion.*

The kinetic energy can be written in general in the form

$$\mathcal{T} = \mathcal{T}(w_i, x_i, t) \ .$$

The derivatives $\frac{\partial \mathcal{T}}{\partial \dot{x}_i}$ included into the equations of motion are

$$\frac{\partial \mathcal{T}}{\partial \dot{x}_k} = \sum_{i=1}^{n} \frac{\partial \mathcal{T}}{\partial w_i} \frac{\partial w_i}{\partial \dot{x}_k} \ , \tag{A.88}$$

i.e., in matrix form,

$$\left\{ \frac{\partial \mathcal{T}}{\partial \dot{x}} \right\} = \mathbf{A} \left\{ \frac{\partial \mathcal{T}}{\partial w} \right\} \ , \tag{A.89}$$

where

$$\left\{ \frac{\partial \mathcal{T}}{\partial \dot{x}} \right\} = \left[\begin{array}{ccc} \frac{\partial \mathcal{T}}{\partial \dot{x}_1} & \frac{\partial \mathcal{T}}{\partial \dot{x}_2} & \ldots \end{array} \right]^T \ ,$$

$$\left\{ \frac{\partial \mathcal{T}}{\partial w} \right\} = \left[\begin{array}{ccc} \frac{\partial \mathcal{T}}{\partial w_1} & \frac{\partial \mathcal{T}}{\partial w_2} & \ldots \end{array} \right]^T \ .$$

By differentiating with respect to time, it follows that

$$\frac{\partial}{\partial t} \left(\left\{ \frac{\partial \mathcal{T}}{\partial \dot{x}} \right\} \right) = \mathbf{A} \frac{\partial}{\partial t} \left(\left\{ \frac{\partial \mathcal{T}}{\partial w} \right\} \right) + \dot{\mathbf{A}} \left\{ \frac{\partial \mathcal{T}}{\partial w} \right\} \ , \tag{A.90}$$

The generic element $\dot{a}_{jk}$ of matrix $\dot{\mathbf{A}}$ is

$$\dot{a}_{jk} = \sum_{i=1}^{n} \frac{\partial a_{jk}}{\partial x_i} \dot{x}_i = \dot{\mathbf{x}}^T \left\{ \frac{\partial a_{jk}}{\partial x} \right\} \ , \tag{A.91}$$

and then

$$\dot{a}_{jk} = \mathbf{w}^T \mathbf{B}^T \left\{ \frac{\partial a_{jk}}{\partial x} \right\} \ . \tag{A.92}$$

The various $\dot{a}_{jk}$ so computed can be written in matrix form

$$\dot{\mathbf{A}} = \left[\mathbf{w}^T \mathbf{B}^T \left\{ \frac{\partial a_{jk}}{\partial x} \right\} \right] \ . \tag{A.93}$$

The computation of the derivatives of the generalized coordinates $\left\{ \frac{\partial \mathcal{T}}{\partial x} \right\}$ is usually less straightforward. The generic derivative $\frac{\partial \mathcal{T}}{\partial x_k}$ is

$$\frac{\partial \mathcal{T}^*}{\partial x_k} = \frac{\partial \mathcal{T}}{\partial x_k} + \sum_{i=1}^{n} \frac{\partial \mathcal{T}}{\partial w_i} \frac{\partial w_i}{\partial x_k} = \frac{\partial \mathcal{T}}{\partial x_k} + \sum_{i=1}^{n} \frac{\partial \mathcal{T}}{\partial w_i} \sum_{j=1}^{n} \frac{\partial a_{ij}}{\partial x_k} \dot{x}_j \ , \tag{A.94}$$

where $\mathcal{T}^*$ is the kinetic energy expressed as a function of the generalized coordinates and their derivatives (the expression to be introduced into the Lagrange equation in its usual form), while $\mathcal{T}$ is expressed as a function of the generalized

coordinates and of the velocities in the body-fixed frame. Equation (A.94) can be written as

$$\frac{\partial \mathcal{T}^*}{\partial x_k} = \frac{\partial \mathcal{T}}{\partial x_k} + \mathbf{w}^T \mathbf{B}^T \frac{\partial \mathbf{A}}{\partial x_k} \left\{ \frac{\partial \mathcal{T}}{\partial w} \right\} , \tag{A.95}$$

where product $\mathbf{w}^T \mathbf{B}^T \frac{\partial \mathbf{A}}{\partial x_k}$ yields a row matrix with n elements, which multiplied by the column matrix $\left\{ \frac{\partial \mathcal{T}}{\partial w} \right\}$ yields the required number.

By combining these row matrices, a square matrix is obtained

$$\left[\mathbf{w}^T \mathbf{B}^T \frac{\partial \mathbf{A}}{\partial x_k} \right] , \tag{A.96}$$

and then the column containing the derivatives with respect to the generalized coordinates is

$$\left\{ \frac{\partial \mathcal{T}^*}{\partial x} \right\} = \left\{ \frac{\partial \mathcal{T}}{\partial x} \right\} + \left[\mathbf{w}^T \mathbf{B}^T \frac{\partial \mathbf{A}}{\partial x} \right] \left\{ \frac{\partial \mathcal{T}}{\partial w} \right\} . \tag{A.97}$$

By definition, the potential energy does not depend on the generalized velocities. Thus the term $\frac{\partial \mathcal{U}}{\partial x_i}$ is not influenced by the way the generalized velocities are written. Finally, the derivatives of the dissipation function are

$$\left\{ \frac{\partial \mathcal{F}}{\partial \dot{x}} \right\} = \mathbf{A} \left\{ \frac{\partial \mathcal{F}}{\partial w} \right\} \tag{A.98}$$

The equation of motion (A.59) is then

$$\mathbf{A} \frac{\partial}{\partial t} \left(\left\{ \frac{\partial \mathcal{T}}{\partial w} \right\} \right) + \mathbf{\Gamma} \left\{ \frac{\partial \mathcal{T}}{\partial w} \right\} - \left\{ \frac{\partial \mathcal{T}}{\partial x} \right\} + \left\{ \frac{\partial \mathcal{U}}{\partial x} \right\} + \mathbf{A} \left\{ \frac{\partial \mathcal{F}}{\partial w} \right\} = \mathbf{Q} , \tag{A.99}$$

where

$$\mathbf{\Gamma} = \left[\mathbf{w}^T \mathbf{B}^T \left\{ \frac{\partial a_{jk}}{\partial x} \right\} \right] - \left[\mathbf{w}^T \mathbf{B}^T \frac{\partial \mathbf{A}}{\partial x_k} \right] \tag{A.100}$$

and $\mathbf{Q}$ is a vector containing the n generalized forces Q_i.

By premultiplying all terms by matrix $\mathbf{B}^T = \mathbf{A}^{-1}$ and attaching the kinematic equations to the dynamic equations, the final form of the state space equations is obtained

$$\begin{cases} \dfrac{\partial}{\partial t} \left(\left\{ \dfrac{\partial \mathcal{T}}{\partial w} \right\} \right) + \mathbf{B^T \Gamma} \left\{ \dfrac{\partial \mathcal{T}}{\partial w} \right\} - \mathbf{B}^T \left\{ \dfrac{\partial \mathcal{T}}{\partial x} \right\} + \mathbf{B}^T \left\{ \dfrac{\partial \mathcal{U}}{\partial x} \right\} + \left\{ \dfrac{\partial \mathcal{F}}{\partial w} \right\} = \mathbf{B}^T \mathbf{Q} \\ \{ \dot{q}_i \} = \mathbf{B} \{ w_i \} \ . \end{cases} \tag{A.101}$$

A.8 MOTION OF A RIGID BODY

A.8.1 Generalized coordinates

Consider a rigid body free in tri-dimensional space. Define an inertial reference frame OXYZ and a frame Gxyz fixed to the body and centred in its center of mass. The position of the rigid body is defined once the position of frame Gxyz is defined with respect to OXYZ, that is, once the transformation leading OXYZ to coincide with Gxyz is defined. It is well known that the motion of the second frame can be considered as the sum of a displacement plus a rotation. The parameters to be defined are therefore 6: 3 components of the displacement, two of the components of the unit vector defining the rotation axis (the third component need not be defined and may be computed from the condition that the unit vector has unit length) and the rotation angle. A rigid body thus has six degrees of freedom in tri-dimensional space.

There is no problem in defining the generalized coordinates for the translational degrees of freedom, because the coordinates of the center of mass G in any inertial reference frame (in particular, in frame OXYZ) are usually the simplest, and the most obvious, choice. For the other generalized coordinates the choice is much more complicated. It is possible to resort, for instance, to two coordinates of a second point and to one of the coordinates of a third point (not on a straight line through the other two), but this choice is far from being the most expedient.

An obvious way to define the rotation of frame Gxyz with respect to OXYZ is to directly express the rotation matrix linking the two reference frames. It is a square matrix of size 3×3 (in tri-dimensional space) and thus has 9 elements. Three of these are independent, while the other 6 may be obtained from the first 3 using suitable equations.

Alternatively, the position of the body-fixed frame can be defined with a sequence of three rotations about the axes. Because rotations are not vectors, the order in which they are performed must be specified.

Start rotating, for instance, the inertial frame about the X-axis. The second rotation may be performed about axes Y or Z (obviously in the position they take after the first rotation), but not about X-axis, because in the latter case the two rotations would simply add to each other and would amount to a single rotation. Assume, for instance, that the frame is rotated about the Y-axis. The third rotation may occur about either the X-axis or the Z-axis (in the new position, taken after the second rotation), but not about the Y-axis.

The possible rotation sequences are 12, but may be subdivided into two types: Those like $X \to Y \to X$ or $X \to Z \to X$, where the third rotation occurs about the same axis as the first, and those like $X \to Y \to Z$ or $X \to Z \to Y$, where the third rotation is performed about a different axis.

In the first cases the angles are said to be *Euler angles*, because they are of the same type as the angles Euler proposed to study the motion of gyroscopes

(precession ϕ about the Z-axis, nutation θ about the X-axis and rotation ψ, again about the Z-axis). In the second case they are said to be *Tait-Bryan angles*[3].

The possible rotation sequences are reported in the following table

First	X				Y				Z			
Second	Y		Z		X		Z		X		Y	
Third	X	Z	X	Y	Y	Z	Y	X	Z	Y	Z	X
Type	E	TB	E	TB	E	TB	E	TB	E	TB	E	TB

In the case of vehicle dynamics Euler angles have the drawback of being indeterminate when plane xy of the rigid body is parallel to THE XY-plane of the inertial frame. They also yield indications that are less intuitively clear.

In the dynamics of vehicles the most common approach is to use Tait-Bryan angles of the type $Z \to Y \to X$ so defined (Fig. A.5):

- Rotate frame XYZ (whose XY plane is parallel to the ground) about the Z-axis until axis X coincides with the projection of the x-axis on plane XY (Fig. A.5a). Such a position of the X-axis can be indicated as x^*; the rotation angle between axes X and x^* is the yaw angle ψ. The rotation matrix allowing passage from the x^*y^*Z frame, which will be defined as the *intermediate frame*, to the inertial frame XYZ is

$$\mathbf{R}_1 = \begin{bmatrix} \cos(\psi) & -\sin(\psi) & 0 \\ \sin(\psi) & \cos(\psi) & 0 \\ 0 & 0 & 1 \end{bmatrix} . \tag{A.102}$$

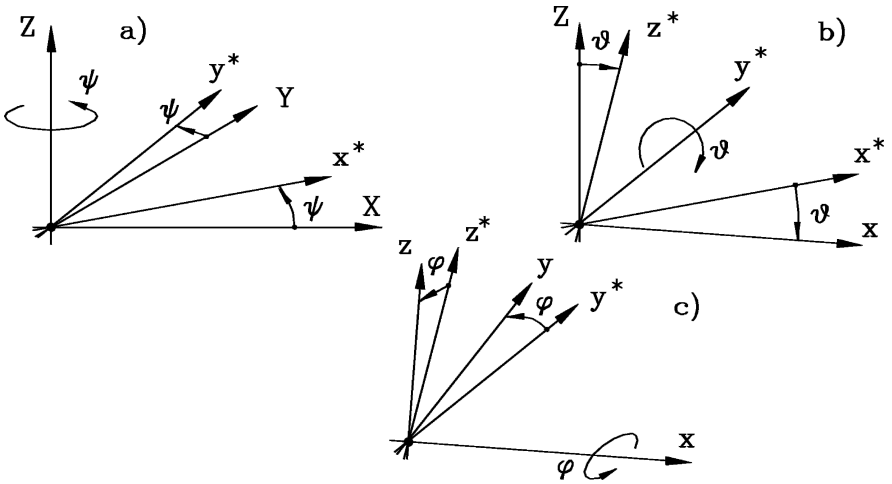

FIGURE A.5. Definition of angles: yaw ψ (a), pitch θ (b) and roll ϕ (c).

[3]Sometimes all sets of three ordered angles are said to be Euler angles. With this wider definition Tait-Brian angles are also considered as Euler angles.

- The second rotation is the pitch rotation θ about the y^*-axis, so that axis x^* reaches the position of the x-axis (Fig. A.5b). The rotation matrix is

$$\mathbf{R}_2 = \begin{bmatrix} \cos(\theta) & 0 & \sin(\theta) \\ 0 & 1 & 0 \\ -\sin(\theta) & 0 & \cos(\theta) \end{bmatrix} . \tag{A.103}$$

- The third rotation is the roll rotation ϕ about the x-axis, so that axes y^* and z^* coincide with axes y and z (Fig. A.5c). The rotation matrix is

$$\mathbf{R}_3 = \begin{bmatrix} 1 & 0 & 0 \\ 0 & \cos(\phi) & -\sin(\phi) \\ 0 & \sin(\phi) & \cos(\phi) \end{bmatrix} . \tag{A.104}$$

The rotation matrix allowing any vector in the body-fixed frame xyz to be rotated to the inertial frame XYZ is clearly the product of the three matrices

$$\mathbf{R} = \mathbf{R}_1\mathbf{R}_2\mathbf{R}_3 . \tag{A.105}$$

Deriving the product of the rotation matrices, it follows that

$$\mathbf{R}= \begin{bmatrix} c(\psi)c(\theta) & c(\psi)s(\theta)s(\phi) - s(\psi)c(\phi) & c(\psi)s(\theta)c(\phi) + s(\psi)s(\phi) \\ s(\psi)c(\theta) & s(\psi)s(\theta)s(\phi) + c(\psi)c(\phi) & s(\psi)s(\theta)c(\phi) - c(\psi)s(\phi) \\ -s(\theta) & c(\theta)s(\phi) & c(\theta)c(\phi) \end{bmatrix} , \tag{A.106}$$

where symbols cos and sin have been replaced by c and s.

Roll and pitch angles are sometimes small. In this case it is expedient to keep the last two rotations separate from the first ones, which cannot usually be linearized.

The product of the rotation matrices related to the last two rotations is

$$\mathbf{R}_2\mathbf{R}_3. = \begin{bmatrix} \cos(\theta) & \sin(\theta)\sin(\phi) & \sin(\theta)\cos(\phi) \\ 0 & \cos(\phi) & -\sin(\phi) \\ -\sin(\theta) & \cos(\theta)\sin(\phi) & \cos(\theta)\cos(\phi) \end{bmatrix} , \tag{A.107}$$

which becomes, in the case of small angles

$$\mathbf{R}_2\mathbf{R}_3 \approx \begin{bmatrix} 1 & 0 & \theta \\ 0 & 1 & -\phi \\ -\theta & \phi & 1 \end{bmatrix} . \tag{A.108}$$

The angular velocities $\dot{\psi}$, $\dot{\theta}$ and $\dot{\phi}$ are not applied along the x, y and z axes, and thus are not the components Ω_x, Ω_y and Ω_z of the angular velocity in the body-fixed reference frame[4]. Their directions are those of axes Z, y^* and x, and then the angular velocity in the body-fixed frame is

[4]Symbols p, q and r are often used for the components of the angular velocity in the body-fixed frame.

$$\left\{ \begin{array}{c} \Omega_x \\ \Omega_y \\ \Omega_z \end{array} \right\} = \dot{\phi}\mathbf{e}_x + \dot{\theta}\mathbf{R}_3^T\mathbf{e}_y + \dot{\psi}\big[\mathbf{R}_2\mathbf{R}_3\big]^T\mathbf{e}_z \ , \tag{A.109}$$

where the unit vectors are obviously

$$\mathbf{e}_x = \left\{ \begin{array}{c} 1 \\ 0 \\ 0 \end{array} \right\} \ , \ \mathbf{e}_y = \left\{ \begin{array}{c} 0 \\ 1 \\ 0 \end{array} \right\} \ , \ \mathbf{e}_z = \left\{ \begin{array}{c} 0 \\ 0 \\ 1 \end{array} \right\} \ . \tag{A.110}$$

By deriving the products, it follows that

$$\left\{ \begin{array}{l} \Omega_x = \dot{\phi} - \dot{\psi}\sin(\theta) \\ \Omega_y = \dot{\theta}\cos(\phi) + \dot{\psi}\sin(\phi)\cos(\theta) \\ \Omega_z = \dot{\psi}\cos(\theta)\cos(\phi) - \dot{\theta}\sin(\phi) \ , \end{array} \right. \tag{A.111}$$

or, in matrix form

$$\left\{ \begin{array}{c} \Omega_x \\ \Omega_y \\ \Omega_z \end{array} \right\} = \left[\begin{array}{ccc} 1 & 0 & -\sin(\theta) \\ 0 & \cos(\phi) & \sin(\phi)\cos(\theta) \\ 0 & -\sin(\phi) & \cos(\phi)\cos(\theta) \end{array} \right] \left\{ \begin{array}{c} \dot{\phi} \\ \dot{\theta} \\ \dot{\psi} \end{array} \right\} \ . \tag{A.112}$$

If the pitch and roll angles are small enough to linearize the relevant trigonometric functions, the components of the angular velocity may be approximated as

$$\left\{ \begin{array}{l} \Omega_x = \dot{\phi} - \theta\dot{\psi} \\ \Omega_y = \dot{\theta} + \phi\dot{\psi} \\ \Omega_z = \dot{\psi} - \phi\dot{\theta} \ . \end{array} \right. \tag{A.113}$$

Other alternatives sometimes used in vehicle modelling, such as quaternions, will not be dealt with here.

A.8.2 Equations of motion - Lagrangian approach

Consider a rigid body in tri-dimensional space and chose as generalized coordinates the displacements X, Y and Z of its center of mass and angles ψ, θ and ϕ. Assuming that the body axes xyz are principal axes of inertia, the kinetic energy of the rigid body is

$$\begin{array}{r} \mathcal{T} = \frac{1}{2}m\left(\dot{X}^2 + \dot{Y}^2 + \dot{Z}^2\right) + \frac{1}{2}J_x\left[\dot{\phi} - \dot{\psi}\sin(\theta)\right]^2 + \\ +\frac{1}{2}J_y\left[\dot{\theta}\cos(\phi) + \dot{\psi}\sin(\phi)\cos(\theta)\right]^2 + \\ +\frac{1}{2}J_z\left[\dot{\psi}\cos(\theta)\cos(\phi) - \dot{\theta}\sin(\phi)\right]^2 \ . \end{array} \tag{A.114}$$

Introducing the kinetic energy into the Lagrange equations

$$\frac{d}{dt}\left(\frac{\partial\mathcal{T}}{\partial\dot{q}_i}\right) - \frac{\partial\mathcal{T}}{\partial q_i} = Q_i \ ,$$

and performing the relevant derivatives, the six equations of motion are directly obtained. The three equations for translational motion are

$$\begin{cases} m\ddot{X} = Q_X \\ m\ddot{Y} = Q_Y \\ m\ddot{Z} = Q_Z \ . \end{cases} \tag{A.115}$$

The equations for rotational motion are much more complicated

$$\begin{aligned} &\ddot{\psi}\left[J_x \sin^2(\theta) + J_y \sin^2(\phi)\cos^2(\theta) + J_z \cos^2(\phi)\cos^2(\theta)\right] + \\ &-\ddot{\phi} J_x \sin(\theta) + \ddot{\theta}\left(J_y - J_z\right)\sin(\phi)\cos(\phi)\cos(\theta) + \\ &+\dot{\phi}\dot{\theta}\cos(\theta)\left\{\left[1 - 2\sin^2(\phi)\right]\left(J_y - J_z\right) - J_x\right\} + \\ &+2\dot{\phi}\dot{\psi}\left(J_y - J_z\right)\cos(\phi)\cos^2(\theta)\sin(\phi) + \\ &+2\dot{\theta}\dot{\psi}\sin(\theta)\cos(\theta)\left[J_x - \sin^2(\phi)J_y - \cos^2(\phi)J_z\right] + \\ &+\dot{\theta}^2\left(-J_y + J_z\right)\sin(\phi)\cos(\phi)\sin(\theta) = Q_\psi, \end{aligned}$$

$$\begin{aligned} &\ddot{\psi}\left(J_y - J_z\right)\sin(\phi)\cos(\theta)\cos(\phi) + \ddot{\theta}\left[J_y \cos^2(\phi) + J_z \sin^2(\phi)\right] + \\ &+2\dot{\phi}\dot{\theta}\left(J_z - J_y\right)\sin(\phi)\cos(\phi) + \dot{\phi}\dot{\psi}\left(J_y - J_z\right)\cos(\theta)\left[1 - 2\sin^2(\phi)\right] + \\ &+\dot{\psi}\dot{\phi}J_x\cos(\theta) - \dot{\psi}^2\sin(\theta)\cos(\theta)\left[J_x - J_y\sin^2(\phi) - J_z\cos^2(\phi)\right] = Q_\theta, \end{aligned} \tag{A.116}$$

$$\begin{aligned} &J_x\ddot{\phi} - \sin(\theta)J_x\ddot{\psi} - \dot{\theta}\dot{\psi}J_z\sin^2(\phi)\cos(\theta) + \\ &-\dot{\psi}\dot{\theta}\cos(\theta)\left\{J_x + J_y\left[1 - 2\sin^2(\phi)\right] - J_z\cos^2(\phi)\right\} + \\ &+\dot{\theta}^2\left(J_y - J_z\right)\sin(\phi)\cos(\phi) - \dot{\psi}^2\left(J_y - J_z\right)\cos(\phi)\cos^2(\theta)\sin(\phi) = Q_\phi \ . \end{aligned}$$

Angle ψ does not appear explicitly in the equations of motion. If the roll and pitch angles are small all trigonometric functions can be linearized. If the angular velocities are also small, the equations of motion for rotations reduce to

$$\begin{cases} J_z\ddot{\psi} = Q_\psi \\ J_y\ddot{\theta} = Q_\theta \\ J_x\ddot{\phi} = Q_\phi \ . \end{cases} \tag{A.117}$$

In this case, the kinetic energy may be directly simplified, by developing the trigonometric functions in Taylor series and neglecting all terms containing products of three or more small quantities. For instance, the term

$$\left[\dot{\phi} - \dot{\psi}\sin(\theta)\right]^2$$

reduces to

$$\left[\dot{\phi} - \dot{\psi}\theta + \dot{\psi}\theta^3/6 + ...\right]^2$$

and then to $\dot{\phi}^2$, because all other terms contain products of at least three small quantities. The kinetic energy then reduces to

$$\mathcal{T} \approx \frac{1}{2}m\left(\dot{X}^2 + \dot{Y}^2 + \dot{Z}^2\right) + \frac{1}{2}\left(J_x\dot{\phi}^2 + J_y\dot{\theta}^2 + J_z\dot{\psi}^2\right) \ . \tag{A.118}$$

Remark A.12 *This approach is simple only if the roll and pitch angles are small. If they are not, the equations of motion obtained in this way in terms of angular velocities $\dot{\phi}$, $\dot{\theta}$ and $\dot{\psi}$ are quite complicated and another approach is more expedient.*

A.8.3 Equations of motion using pseudo-coodinates

Because the forces and moments applied to the rigid body are often written with reference to the body-fixed frame, the equations of motion are best written with reference to the same frame. The kinetic energy can then be written in terms of the components v_x, v_y and v_z (often referred to as u, v and w) of the velocity and Ω_x, Ω_x e Ω_x (often referred to as p, q and r) of the angular velocity.

If the body fixed frame is a principal frame of inertia, the expression of the kinetic energy is

$$\mathcal{T} = \frac{1}{2} m \left(v_x^2 + v_y^2 + {v_z}^2 \right) + \frac{1}{2} \left(J_x \Omega_x^2 + J_y \Omega_y^2 + J_z \Omega_z^2 \right) \ .$$

The components of the velocity and the angular velocity in the body fixed frame are not the derivatives of coordinates, but are linked to the coordinates by the six kinematic equations

$$\left\{ \begin{array}{c} v_x \\ v_y \\ v_z \end{array} \right\} = \mathbf{R}^T \left\{ \begin{array}{c} \dot{X} \\ \dot{Y} \\ \dot{Z} \end{array} \right\} \ , \tag{A.119}$$

$$\left\{ \begin{array}{c} \Omega_x \\ \Omega_y \\ \Omega_z \end{array} \right\} = \left[\begin{array}{ccc} 1 & 0 & -\sin(\theta) \\ 0 & \cos(\phi) & \sin(\phi)\cos(\theta) \\ 0 & -\sin(\phi) & \cos(\theta)\cos(\phi) \end{array} \right] \left\{ \begin{array}{c} \dot{\phi} \\ \dot{\theta} \\ \dot{\psi} \end{array} \right\} \ , \tag{A.120}$$

that is, in more compact form,

$$\mathbf{w} = \mathbf{A}^T \dot{\mathbf{q}} \ , \tag{A.121}$$

where the vectors of the generalized velocities and of the derivatives of the generalized coordinates are

$$\mathbf{w} = \left[\begin{array}{cccccc} v_x & v_y & v_z & \Omega_x & \Omega_y & \Omega_z \end{array} \right]^T \ , \tag{A.122}$$

$$\dot{\mathbf{q}} = \left[\begin{array}{cccccc} \dot{X} & \dot{Y} & \dot{Z} & \dot{\phi} & \dot{\theta} & \dot{\psi} \end{array} \right]^T \tag{A.123}$$

and matrix $\mathbf{A}$ is

$$\mathbf{A} = \left[\begin{array}{cc} \mathbf{R} & \mathbf{0} \\ \mathbf{0} & \left[\begin{array}{ccc} 1 & 0 & -\sin(\theta) \\ 0 & \cos(\phi) & \sin(\phi)\cos(\theta) \\ 0 & -\sin(\phi) & \cos(\theta)\cos(\phi) \end{array} \right]^T \end{array} \right] \ . \tag{A.124}$$

Note that the second submatrix is not a rotation matrix (the first submatrix is) and then

$$\mathbf{A}^{-1} \neq \mathbf{A}^T \; ; \qquad \mathbf{B} \neq \mathbf{A} \; . \tag{A.125}$$

The inverse transformation is Eq. (A.85)

$$\dot{\mathbf{q}} = \mathbf{B}\mathbf{w} \; ,$$

where $\mathbf{B} = \mathbf{A}^{-\mathbf{T}}$.

None of the velocities included in vector $\mathbf{w}$ can be integrated to obtain a set of generalized coordinates, and must all be considered as derivatives of pseudo-coordinates.

The state space equation, made up of the six dynamic and the six kinematic equations, is then equation (A.101), simplified because in the present case neither the potential energy nor the dissipation function are present

$$\begin{cases} \dfrac{\partial}{\partial t}\left(\left\{\dfrac{\partial \mathcal{T}}{\partial w}\right\}\right) + \mathbf{B}^{\mathbf{T}}\boldsymbol{\Gamma}\left\{\dfrac{\partial \mathcal{T}}{\partial w}\right\} - \mathbf{B}^T\left\{\dfrac{\partial \mathcal{T}}{\partial q}\right\} = \mathbf{B}^T\mathbf{Q} \\ \\ \{\dot{q}_i\} = \mathbf{B}\,\{w_i\} \; . \end{cases} \tag{A.126}$$

Here $\mathbf{B}^T\mathbf{Q}$ is simply a column matrix containing the three components of the force and the three components of the moment applied to the body along the body-fixed axes x, y, z.

The most difficult part of the computation is writing matrix $\mathbf{B}^{\mathbf{T}}\boldsymbol{\Gamma}$. Performing rather difficult computations it follows that

$$\mathbf{B}^{\mathbf{T}}\boldsymbol{\Gamma} = \begin{bmatrix} \widetilde{\boldsymbol{\Omega}} & \mathbf{0} \\ \widetilde{\mathbf{V}} & \widetilde{\boldsymbol{\Omega}} \end{bmatrix} \; . \tag{A.127}$$

where $\widetilde{\boldsymbol{\Omega}}$ and $\widetilde{\mathbf{V}}$ are skew-symmetric matrices containing the components of the angular and linear velocities

$$\widetilde{\boldsymbol{\Omega}} = \begin{bmatrix} 0 & -\Omega_z & \Omega_y \\ \Omega_z & 0 & -\Omega_x \\ -\Omega_y & \Omega_x & 0 \end{bmatrix} \; , \; \widetilde{\mathbf{V}} = \begin{bmatrix} 0 & -v_z & v_y \\ v_z & 0 & -v_x \\ -v_y & v_x & 0 \end{bmatrix} \; . \tag{A.128}$$

If the body-fixed axes are principal axes of inertia, the dynamic equations are simply

$$\begin{cases} m\dot{v}_x = m\Omega_z v_y - m\Omega_y v_z + F_x \\ m\dot{v}_y = m\Omega_x v_z - m\Omega_z v_x + F_y \\ m\dot{v}_z = m\Omega_y v_x - m\Omega_x v_y + F_z \\ J_x\dot{\Omega}_x = \Omega_y\Omega_z\,(J_y - J_z) + M_x \\ J_y\dot{\Omega}_y = \Omega_x\Omega_z\,(J_z - J_x) + M_y \\ J_z\dot{\Omega}_z = \Omega_x\Omega_y\,(J_x - J_y) + M_x \end{cases} \tag{A.129}$$

Remark A.13 *The equations so obtained are much simpler than equations (A.116). The last three equations are nothing other than Euler equations.*

Appendix B
DYNAMICS OF MOTOR CYCLES

When studying the handling behavior of a two-wheeled vehicle, rolling motions and, to a lesser extent, gyroscopic moments must not be neglected. A linearized model similar in many respects to that seen in Part IV for single-track vehicles may be built.

Linearization obviously requires that the roll angle be small, severely limiting the applicability of such a model to the study of stability on straight roads and operating conditions where the lateral acceleration is small compared to gravitational acceleration.

The mass of the driver, who controls the vehicle not only by acting on the steering but also displacing his body, can be a substantial fraction of the total mass. Moreover, a two-wheeled vehicle is intrinsically unstable. The driver thus has to perform as a stabilizer for the capsize mode.

Finally, the body of the driver, acting as an aerodynamic brake or control surface, contributes in a substantial way to aerodynamic forces. To model a two-wheeled vehicle without modelling the driver is merely a first approximation approach, useful for conditions in which only low performance is required.

In such cases the vehicle can be modelled as a rigid body that also includes the driver. A sketch of the vehicle model is shown in Fig. B.1. The reference frame Hxyz is fixed to such a rigid body, with origin at point H defined in the same way as for the model of the vehicle on elastic suspensions. Its position is defined by the yaw and roll angles ψ and ϕ; the first is defined as for a vehicle with four wheels. The roll angle is defined as the angle between the z axis and the perpendicular to the ground. The roll axis is assumed to pass through the centers of the contact areas of the tires, a rough approximation only because motor cycle

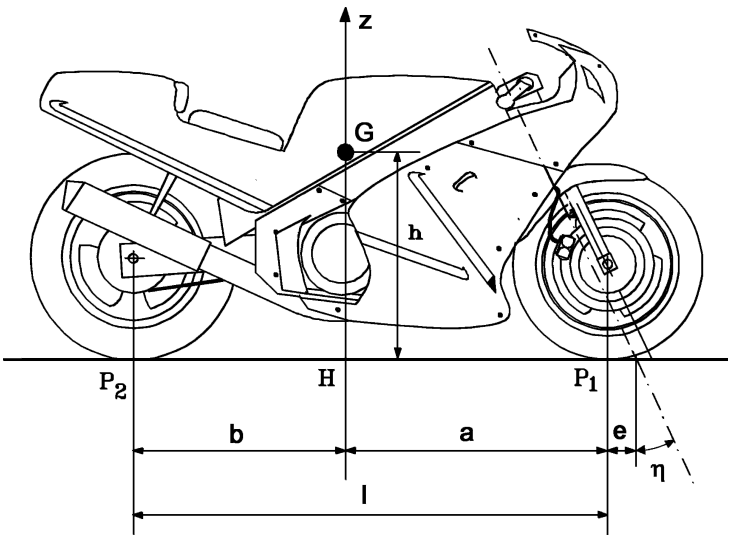

FIGURE B.1. Model for a two wheeled vehicle; reference frames and main geometrical definitions

tires usually have a considerably rounded transversal profile. In locked control dynamics the steering angle δ is an input, while in free control dynamics it is one of the variables of motion.

The main difficulty is linked to the high values, even larger than 45°, that the roll angle may take: In these conditions, assumption of small angles does not hold. The kinematic of the steering system is further complicated by the large values that the caster angle (η in Fig. B.1) may take. The caster offset, shown in the figure with symbol e, may be relatively large and is an important parameter in the study of the behavior of motor cycles.

Since angle η may be not small, the steering angle δ_s measured on the ground does not coincide with the steering angle δ at the handlebar. If the roll angle is small, it follows that

$$\delta_s \approx \delta \cos(\eta) \ . \tag{B.1}$$

The trajectory curvature gain in kinematic conditions is then

$$\left(\frac{1}{R\delta}\right)_c \approx \frac{1}{l}\delta \cos(\eta) \ . \tag{B.2}$$

It follows that the more the steering axis is inclined with respect to the vertical, the lower the trajectory curvature gain and the less manoeuvrable the vehicle.

B.1 BASIC DEFINITIONS

The generalized coordinates are the coordinates X and Y of point H in the inertial frame XYZ and the yaw ψ and roll ϕ angles. The steering angle δ may be considered as a variable of the motion (free controls) or an input (locked controls).

The components of the velocity in the body-fixed frame u and v are linked to the derivatives of the generalized coordinates $\dot{X}$, $\dot{Y}$ in the inertial frame by the usual relationship

$$\left\{ \begin{array}{c} u \\ v \\ 0 \end{array} \right\} = \mathbf{R}_1^T \left\{ \begin{array}{c} \dot{X} \\ \dot{Y} \\ 0 \end{array} \right\} = \left[\begin{array}{ccc} \cos(\psi) & \sin(\psi) & 0 \\ -\sin(\psi) & \cos(\psi) & 0 \\ 0 & 0 & 1 \end{array} \right] \left\{ \begin{array}{c} \dot{X} \\ \dot{Y} \\ 0 \end{array} \right\} , \tag{B.3}$$

where $\mathbf{R}_1$ is the yaw rotation matrix.

The angular velocities Ω_x, Ω_y and Ω_z about the body axes are linked to the roll velocity $p = \dot{\phi}$ and yaw velocity $r = \dot{\psi}$ by the relationship

$$\mathbf{\Omega} = \left\{ \begin{array}{c} \Omega_x \\ \Omega_y \\ \Omega_z \end{array} \right\} = \left\{ \begin{array}{c} \dot{\phi} \\ 0 \\ 0 \end{array} \right\} + \mathbf{R}_2^T \left\{ \begin{array}{c} 0 \\ 0 \\ \dot{\psi} \end{array} \right\} , \tag{B.4}$$

where $\mathbf{R}_2$ is the roll rotation matrix

$$\mathbf{R}_2 = \left[\begin{array}{ccc} 1 & 0 & 0 \\ 0 & \cos(\phi) & -\sin(\phi) \\ 0 & \sin(\phi) & \cos(\phi) \end{array} \right] .$$

Performing the relevant computations, the relationship linking the angular velocities about the axes of the body-fixed frame and the derivatives of the generalized coordinates is

$$\mathbf{\Omega} = \left\{ \begin{array}{c} \Omega_x \\ \Omega_y \\ \Omega_z \end{array} \right\} = \mathbf{A}^T \left\{ \begin{array}{c} \dot{\phi} \\ \dot{\psi} \end{array} \right\} = \left\{ \begin{array}{c} \dot{\phi} \\ \dot{\psi}\sin(\phi) \\ \dot{\psi}\cos(\phi) \end{array} \right\} , \tag{B.5}$$

where

$$\mathbf{A}^T = \left[\begin{array}{cc} 1 & 0 \\ 0 & \sin(\phi) \\ 0 & \cos(\phi) \end{array} \right] . \tag{B.6}$$

The angular velocity of the steering system $\mathbf{\Omega}_1$ must be explicitly computed when studying motion in free controls conditions

$$\mathbf{\Omega}_1 = \left\{ \begin{array}{c} 0 \\ 0 \\ \dot{\delta} \end{array} \right\} + \mathbf{R}_3^T \mathbf{R}_\eta^T \left\{ \begin{array}{c} \dot{\phi} \\ 0 \\ 0 \end{array} \right\} + \mathbf{R}_3^T \mathbf{R}_\eta^T \mathbf{R}_2^T \left\{ \begin{array}{c} 0 \\ 0 \\ \dot{\psi} \end{array} \right\} , \tag{B.7}$$

i.e.

$$\mathbf{\Omega}_1 = \left\{ \begin{array}{c} 0 \\ 0 \\ \dot{\delta} \end{array} \right\} + \mathbf{R}_3^T \mathbf{R}_\eta^T \mathbf{\Omega} \, , \tag{B.8}$$

where matrices $\mathbf{R}_3$ (steering rotation) and $\mathbf{R}_\eta^T$ (matrix defining the direction of the steering axis) are

$$\mathbf{R}_3 = \left[\begin{array}{ccc} \cos(\delta) & -\sin(\delta) & 0 \\ \sin(\delta) & \cos(\delta) & 0 \\ 0 & 0 & 1 \end{array} \right] \, , \quad \mathbf{R}_\eta = \left[\begin{array}{ccc} \cos(\eta) & 0 & -\sin(\eta) \\ 0 & 1 & 0 \\ \sin(\eta) & 0 & \cos(\eta) \end{array} \right] \, .$$

The final expression of the angular velocity of the steering system is

$$\mathbf{\Omega}_1 = \left\{ \begin{array}{c} \dot{\phi}\cos(\eta)\cos(\delta) + \dot{\psi}\left[\cos(\phi)\sin(\eta)\cos(\delta) + \sin(\phi)\sin(\delta)\right] \\ -\dot{\phi}\cos(\eta)\sin(\delta) + \dot{\psi}\left[-\cos(\phi)\sin(\eta)\sin(\delta) + \sin(\phi)\cos(\delta)\right] \\ \dot{\delta} - \dot{\phi}\sin(\eta) + \dot{\psi}\cos(\phi)\cos(\eta) \end{array} \right\} \, . \tag{B.9}$$

The position of the mass center G is

$$(\overline{\mathrm{G-O}}) = \left\{ \begin{array}{c} X \\ Y \\ 0 \end{array} \right\} + \mathbf{R}_1 \mathbf{R}_2 \left\{ \begin{array}{c} 0 \\ 0 \\ h \end{array} \right\} \, . \tag{B.10}$$

The velocity of the same point is then

$$V_{\mathrm{G}} = \left\{ \begin{array}{c} \dot{X} \\ \dot{Y} \\ 0 \end{array} \right\} + \left(\dot{\mathbf{R}}_1 \mathbf{R}_2 + \mathbf{R}_1 \dot{\mathbf{R}}_2 \right) \left\{ \begin{array}{c} 0 \\ 0 \\ h \end{array} \right\} \, , \tag{B.11}$$

that is

$$V_{\mathrm{G}} = \left\{ \begin{array}{c} \dot{X} + h\dot{\psi}\cos(\psi)\sin(\phi) + h\dot{\phi}\sin(\psi)\cos(\phi) \\ \dot{Y} + h\dot{\psi}\sin(\psi)\sin(\phi) - h\dot{\phi}\cos(\psi)\cos(\phi) \\ -h\dot{\phi}\sin(\phi) \end{array} \right\} \, . \tag{B.12}$$

In the study of free controls dynamics, the position and velocity of the center of mass will be assumed to be unaffected by the steering angle δ.

The translational and rotational kinetic energies are respectively:

$$\mathcal{T}_t = \frac{1}{2} m V_{\mathrm{G}}^2 \, , \tag{B.13}$$

$$\mathcal{T}_r = \frac{1}{2} \left\{ \begin{array}{c} \Omega_x \\ \Omega_y \\ \Omega_z \end{array} \right\}^T \left[\begin{array}{ccc} J_x & 0 & J_{xz} \\ 0 & J_y & 0 \\ J_{xz} & 0 & J_z \end{array} \right] \left\{ \begin{array}{c} \Omega_x \\ \Omega_y \\ \Omega_z \end{array} \right\} \, ,$$

i.e.

$$\mathcal{T}_r = \frac{1}{2} \left\{ \begin{array}{c} \dot{\phi} \\ \dot{\psi} \end{array} \right\}^T \mathbf{A} \left[\begin{array}{ccc} J_x & 0 & J_{xz} \\ 0 & J_y & 0 \\ J_{xz} & 0 & J_z \end{array} \right] \mathbf{A}^T \left\{ \begin{array}{c} \dot{\phi} \\ \dot{\psi} \end{array} \right\} \, .$$

The expression of the kinetic energy of the system is

$$\begin{aligned}\mathcal{T} = \frac{1}{2}m\left(\dot{X}^2 + \dot{Y}^2\right) + \frac{1}{2}\dot{\phi}^2 J_x^* + \frac{1}{2}\dot{\psi}^2\left[J_z\cos^2(\phi) + J_y^*\sin^2(\phi)\right] + \\ + \dot{\psi}\dot{\phi}J_{xz}\cos(\phi) + mh\left[\dot{X}\dot{\psi}\sin(\phi) - \dot{Y}\dot{\phi}\cos(\phi)\right]\cos(\psi) + \\ + mh\left[\dot{X}\dot{\phi}\cos(\phi) + \dot{Y}\dot{\psi}\sin(\phi)\right]\sin(\psi)\ ,\end{aligned} \tag{B.14}$$

where

$$J_x^* = J_x + mh^2, \quad J_y^* = J_y + mh^2$$

are the roll and pitch moments of inertia with respect to a reference frame set on the ground.

The kinetic energy of the steering system due to steering motion, needed to study the free controls behavior, is

$$\mathcal{T}_{r_1} = \frac{1}{2}\boldsymbol{\Omega}_1{}^T\mathbf{J}_1\boldsymbol{\Omega}_1\ , \tag{B.15}$$

where $\mathbf{J}_1$ is the inertia tensor of the steering system. The kinetic energy of the steering system and the front wheel were already partly taken into account in the expression of the kinetic energy of the vehicle.

Since the steering angle is small in normal vehicle use, the trigonometric functions of δ will be linearized when computing the kinetic energy $\mathcal{T}_{r_1}$. It then follows that

$$\begin{aligned}\mathcal{T}_{r_1} = \mathcal{T}_{0_1} + \frac{1}{2}J_{z1}\dot{\delta}^2 + \dot{\delta}\dot{\psi}\left[J_{z1}\cos(\eta) + J_{xz1}\sin(\eta)\cos(\phi)\right] + \\ + \dot{\delta}\dot{\psi}\left[-J_{z1}\sin(\eta) + J_{xz1}\cos(\eta)\right] + A_1\delta\dot{\psi}^2 + A_2\delta\dot{\phi}^2 + A_3\delta\dot{\psi}\dot{\phi}\ ,\end{aligned} \tag{B.16}$$

where the terms that do not depend on δ, and thus have already been accounted for in the expression used for locked controls motion, are included in $\mathcal{T}_{0_1}$. Terms A_i are:

$$\begin{aligned}A_1 &= \left(J_{x1} - J_{y1}\right)\sin(\phi)\cos(\phi)\sin(\eta) + J_{xz1}\left[\sin(\phi)\cos(\phi)\cos(\eta)\right], \\ A_2 &= J_{xz1}\sin(\phi), \\ A_3 &= \left(J_{x1} - J_{y1}\right)\cos(\eta)\sin(\phi) - J_{xz1}\sin^2(\eta)\ .\end{aligned} \tag{B.17}$$

These will be neglected in the following equations.

The kinetic energy of the wheels due to rotation about their axis must be computed to take into account their gyroscopic moments as well.

If χ_i is the rotation angle of the ith wheel, the angular velocity of the rear wheel is

$$\boldsymbol{\Omega}_{w2} = \begin{Bmatrix}\dot{\phi}\\ \dot{\chi}_2\\ 0\end{Bmatrix} + \mathbf{R}_2^T\begin{Bmatrix}0\\ 0\\ \dot{\psi}\end{Bmatrix} = \boldsymbol{\Omega} + \begin{Bmatrix}0\\ \dot{\chi}_2\\ 0\end{Bmatrix}\ , \tag{B.18}$$

i.e.,

$$\mathbf{\Omega}_{w2} = \left\{ \begin{array}{c} \dot{\phi} \\ \dot{\psi}\sin(\phi) + \dot{\chi}_2 \\ \dot{\psi}\cos(\phi) \end{array} \right\} . \tag{B.19}$$

Things are more complicated for the front wheel, because it can steer:

$$\mathbf{\Omega}_{w1} = \mathbf{\Omega}_1 + \left\{ \begin{array}{c} 0 \\ \dot{\chi}_1 \\ 0 \end{array} \right\} . \tag{B.20}$$

In locked controls motion the kinetic energy of the ith wheel is

$$\mathcal{T}_{r_i} = \frac{1}{2}\mathbf{\Omega}_{wi}^T \mathbf{J}_{wi} \mathbf{\Omega}_{wi} , \tag{B.21}$$

where, because the wheels are gyroscopic solids (two of their moments of inertia are equal to each other) the inertia matrix $\mathbf{J}_{r_i}$ reduces to

$$\mathbf{J}_{w_i} = \left[\begin{array}{ccc} J_{t_i} & 0 & 0 \\ 0 & J_{p_i} & 0 \\ 0 & 0 & J_{t_i} \end{array} \right] .$$

Stating $\mathbf{\Omega}_1 = \mathbf{\Omega}$, and remembering that, at least as a first approximation, the angular velocity of the wheel is

$$\dot{\chi}_i = \frac{V}{R_{e_i}} , \tag{B.22}$$

the kinetic energy is

$$\mathcal{T}_{r_i} = \frac{1}{2}J_{t_i}\dot{\phi}^2 + \frac{1}{2}J_{t_i}\dot{\psi}^2\cos^2(\phi) + \frac{1}{2}J_{p_i}\dot{\psi}^2\sin^2(\phi) + \frac{1}{2}V^2\frac{J_{pi}^2}{R_{ei}^2} + V\dot{\psi}\sin(\phi)\frac{J_{p_i}}{R_{e_i}} . \tag{B.23}$$

The first three terms were already included in the rotational kinetic energy of the vehicle. It then becomes possible to account for the energy due to wheel rotation simply by adding the term

$$\Delta\mathcal{T} = \frac{1}{2}V^2\left(\frac{J_{p_1}^2}{R_{e_1}^2} + \frac{J_{p_2}^2}{R_{e_2}^2}\right) + V\dot{\psi}\sin(\phi)\left(\frac{J_{p_1}}{R_{e_1}} + \frac{J_{p_2}}{R_{e_2}}\right) , \tag{B.24}$$

to the already computed value of the kinetic energy.

If the steering control is free, the expression of the kinetic energy is much more complicated. With somewhat complex computations, assuming that angle δ is small, a further increase of the kinetic energy is obtained

$$\Delta\mathcal{T}_1 = -V\frac{J_{p_1}}{R_{e_1}}\delta\left[\dot{\psi}\cos(\phi)\sin(\eta) + \dot{\phi}\cos(\eta)\right] . \tag{B.25}$$

The gravitational potential energy is:

$$\mathcal{U} = mgh\cos(\phi) . \tag{B.26}$$

B.2 LOCKED CONTROLS MODEL

B.2.1 Equations of motion

The locked controls Lagrangian function is

$$\begin{aligned}\mathcal{L} = &\frac{1}{2}m\left(\dot{X}^2+\dot{Y}^2\right)+\frac{1}{2}\dot{\phi}^2 J_x^*+\frac{1}{2}\dot{\psi}^2\left[J_z\cos^2(\phi)+J_y^*\sin^2(\phi)\right]+\\ &+\dot{\psi}\dot{\phi}J_{xz}\cos(\phi)\;+\;mh\left[\dot{X}\dot{\psi}\sin(\phi)-\dot{Y}\dot{\phi}\cos(\phi)\right]\cos(\psi)+\\ &+mh\left[\dot{X}\dot{\phi}\cos(\phi)+\dot{Y}\dot{\psi}\sin(\phi)\right]\sin(\psi)+\frac{1}{2}V^2\left(\frac{J_{p_1}^2}{R_{e_1}^2}+\frac{J_{p_2}^2}{R_{e_2}^2}\right)+\\ &+V\dot{\psi}\sin(\phi)\left(\frac{J_{p_1}}{R_{e_1}}+\frac{J_{p_2}}{R_{e_2}}\right)-mgh\cos(\phi)\;.\end{aligned} \tag{B.27}$$

First two equations of motion

The derivatives entering the first two equations are

$$\begin{aligned}\frac{\partial\mathcal{L}}{\partial\dot{X}} &= m\left[\dot{X}+h\dot{\psi}\sin(\phi)\cos(\psi)+h\dot{\phi}\cos(\phi)\sin(\psi)\right]\;,\\ \frac{\partial\mathcal{L}}{\partial\dot{Y}} &= m\left[\dot{Y}+h\dot{\psi}\sin(\phi)\sin(\psi)-h\dot{\phi}\cos(\phi)\cos(\psi)\right]\;,\\ \frac{\partial\mathcal{L}}{\partial X} &= \frac{\partial\mathcal{L}}{\partial Y}=0\;.\end{aligned} \tag{B.28}$$

Remembering that

$$\left\{\begin{array}{c}\dot{X}\\ \dot{Y}\end{array}\right\}=\left[\begin{array}{cc}\cos(\psi) & -\sin(\psi)\\ \sin(\psi) & \cos(\psi)\end{array}\right]\left\{\begin{array}{c}u\\ v\end{array}\right\}=\mathbf{R}_1\left\{\begin{array}{c}u\\ v\end{array}\right\}\;, \tag{B.29}$$

it follows that

$$\begin{aligned}\frac{\partial\mathcal{T}}{\partial\dot{X}} &= m\left[u+h\dot{\psi}\sin(\phi)\right]\cos(\psi)-m\left[v-h\dot{\phi}\cos(\phi)\right]\sin(\psi)\;,\\ \frac{\partial\mathcal{T}}{\partial\dot{Y}} &= m\left[u+h\dot{\psi}\sin(\phi)\right]\sin(\psi)+m\left[v-h\dot{\phi}\cos(\phi)\right]\cos(\psi)\;.\end{aligned} \tag{B.30}$$

By performing the derivatives with respect to time, and collecting the terms in $\cos(\psi)$ and $\sin(\psi)$, the following equations of motion can be obtained

$$m\left[\begin{array}{cc}\cos(\psi) & -\sin(\psi)\\ \sin(\psi) & \cos(\psi)\end{array}\right]\times \tag{B.31}$$

$$\times \left\{ \begin{array}{c} \dot{u} - h\dot{\psi}v + h\ddot{\psi}\sin(\phi) + 2h\dot{\psi}\dot{\phi}\cos(\phi) \\ \dot{v}+u\dot{\psi} - h\ddot{\phi}\cos(\phi) + h\dot{\phi}^2\sin(\phi) + h\dot{\psi}^2\sin(\phi)\ . \end{array} \right\} = \left\{ \begin{array}{c} Q_X \\ Q_Y \end{array} \right\}\ .$$

Remembering that

$$\left\{ \begin{array}{c} Q_X \\ Q_Y \end{array} \right\} = \left[\begin{array}{cc} \cos(\psi) & -\sin(\psi) \\ \sin(\psi) & \cos(\psi) \end{array} \right] \left\{ \begin{array}{c} Q_x \\ Q_y \end{array} \right\} = \mathbf{R}_1 \left\{ \begin{array}{c} Q_x \\ Q_y \end{array} \right\}\ , \tag{B.32}$$

the first two equations reduce to

$$\left\{ \begin{array}{l} m\left[\dot{u} - h\dot{\psi}v + h\ddot{\psi}\sin(\phi) + 2h\dot{\psi}\dot{\phi}\cos(\phi)\right] = Q_x\ , \\ m\left[\dot{v}+u\dot{\psi} - h\ddot{\phi}\cos(\phi) + h\dot{\phi}^2\sin(\phi) + h\dot{\psi}^2\sin(\phi)\right] = Q_y\ . \end{array} \right. \tag{B.33}$$

Third equation of motion

The third equation, describing the yaw angle ψ, can be obtained in the same way. The derivatives are

$$\begin{array}{l} \dfrac{\partial \mathcal{L}}{\partial \dot{\psi}} = \dot{\psi}\left[J_z\cos^2(\phi) + J_y^*\sin^2(\phi)\right] + \dot{\phi}J_{xz}\cos(\phi) + \\ \qquad + mh\sin(\phi)\left[\dot{X}\cos(\psi) + \dot{Y}\sin(\psi)\right] + V\sin(\phi)\left(\frac{J_{p1}}{R_{e1}} + \frac{J_{p2}}{R_{e2}}\right), \\ \dfrac{\partial \mathcal{L}}{\partial \psi} = -mh\left[\dot{X}\dot{\psi}\sin(\phi) - \dot{Y}\dot{\phi}\cos(\phi)\right]\sin(\psi) + \\ \qquad + mh\left[\dot{X}\dot{\phi}\cos(\phi) + \dot{Y}\dot{\psi}\sin(\phi)\right]\cos(\psi)\ , \end{array} \tag{B.34}$$

and then

$$\begin{array}{l} \dfrac{d}{dt}\left(\dfrac{\partial \mathcal{L}}{\partial \dot{\psi}}\right) = \ddot{\psi}\left[J_z\cos^2(\phi) + J_y^*\sin^2(\phi)\right] + 2\dot{\psi}\dot{\phi}\left(-J_z + J_y^*\right)\sin(\phi)\cos(\phi) \\ \qquad + \ddot{\phi}J_{xz}\cos(\phi) - \dot{\phi}^2 J_{xz}\sin(\phi) + mh\dot{\phi}\cos(\phi)\left[\dot{X}\cos(\psi) + \dot{Y}\sin(\psi)\right] + \\ \qquad + mh\sin(\phi)\left[\ddot{X}\cos(\psi) + \ddot{Y}\sin(\psi)\right] + + V\dot{\phi}\cos(\phi)\left(\frac{J_{p1}}{R_{e1}} + \frac{J_{p2}}{R_{e2}}\right) + \\ \qquad + mh\dot{\psi}\sin(\phi)\left[-\dot{X}\sin(\psi) + \dot{Y}\cos(\psi)\right] + \dot{V}\sin(\phi)\left(\frac{J_{p1}}{R_{e1}} + \frac{J_{p2}}{R_{e2}}\right)\ . \end{array} \tag{B.35}$$

The third equation is then

$$\begin{array}{c} \ddot{\psi}\left[J_z\cos^2(\phi) + J_y^*\sin^2(\phi)\right] + 2\dot{\psi}\dot{\phi}\left(-J_z + J_y^*\right)\sin(\phi)\cos(\phi) + \\ + \ddot{\phi}J_{xz}\cos(\phi) - \dot{\phi}^2 J_{xz}\sin(\phi) + + mh\sin(\phi)\left[\ddot{X}\cos(\psi) + \ddot{Y}\sin(\psi)\right] + \\ + \dot{V}\sin(\phi)\left(\frac{J_{p1}}{R_{e1}} + \frac{J_{p2}}{R_{e2}}\right) + V\dot{\phi}\cos(\phi)\left(\frac{J_{p1}}{R_{e1}} + \frac{J_{p2}}{R_{e2}}\right) = Q_\psi\ . \end{array} \tag{B.36}$$

Because

$$\ddot{X}\cos(\psi) + \ddot{Y}\sin(\psi) = \dot{u} - v\dot{\psi}, \tag{B.37}$$

its final form is

$$\begin{aligned}\ddot{\psi}\left[J_z\cos^2(\phi)+J_y^*\sin^2(\phi)\right]+2\dot{\psi}\dot{\phi}\left(-J_z+J_y^*\right)\sin(\phi)\cos(\phi)+\\ +\ddot{\phi}J_{xz}\cos(\phi)-\dot{\phi}^2J_{xz}\sin(\phi)+mh\sin(\phi)\left(\dot{u}-v\dot{\psi}\right)+\\ +\dot{V}\sin(\phi)\left(\tfrac{J_{p1}}{R_{e_1}}+\tfrac{J_{p2}}{R_{e_2}}\right)+V\dot{\phi}\cos(\phi)\left(\tfrac{J_{p1}}{R_{e_1}}+\tfrac{J_{p2}}{R_{e_2}}\right)=Q_\psi\ .\end{aligned} \tag{B.38}$$

Fourth equation of motion

The fourth equation, describing the roll angle ϕ, may be obtained in the same way. The derivatives are

$$\begin{aligned}\frac{\partial\mathcal{L}}{\partial\dot{\phi}}&=\dot{\phi}J_x^*+\dot{\psi}J_{xz}\cos(\phi)+mh\cos(\phi)\left[-\dot{Y}\cos(\psi)+\dot{X}\sin(\psi)\right],\\ \frac{\partial\mathcal{L}}{\partial\phi}&=\dot{\psi}^2\left[-J_z+J_y^*\right]\cos(\phi)\sin(\phi)-\dot{\psi}\dot{\phi}J_{xz}\sin(\phi)+\\ &\quad+mh\left[\dot{X}\dot{\psi}\cos(\phi)+\dot{Y}\dot{\phi}\sin(\phi)\right]\cos(\psi)+mgh\sin(\phi)+\\ &\quad+mh\left[-\dot{X}\dot{\phi}\sin(\phi)+\dot{Y}\dot{\psi}\cos(\phi)\right]\sin(\psi)+V\dot{\psi}\cos(\phi)\left(\tfrac{J_{p1}}{R_{e_1}}+\tfrac{J_{p2}}{R_{e_2}}\right),\end{aligned} \tag{B.39}$$

and then

$$\begin{aligned}\frac{d}{dt}\left(\frac{\partial\mathcal{L}}{\partial\dot{\phi}}\right)&=\ddot{\phi}J_x^*+\ddot{\psi}J_{xz}\cos(\phi)-\dot{\psi}\dot{\phi}J_{xz}\sin(\phi)+\\ &\quad-mh\dot{\phi}\sin(\phi)\left[-\dot{Y}\cos(\psi)+\dot{X}\sin(\psi)\right]+mh\cos(\phi)\left[-\ddot{Y}\cos(\psi)+\right.\\ &\quad\left.+\ddot{X}\sin(\psi)\right]++mh\dot{\psi}\cos(\phi)\left[\dot{Y}\sin(\psi)+\dot{X}\cos(\psi)\right].\end{aligned} \tag{B.40}$$

The fourth equation is

$$\begin{aligned}\ddot{\phi}J_x^*+\ddot{\psi}J_{xz}\cos(\phi)-\dot{\psi}^2\left[-J_z+J_y^*\right]\cos(\phi)\sin(\phi)+\\ +mh\cos(\phi)\left[-\ddot{Y}\cos(\psi)+\ddot{X}\sin(\psi)\right]+\\ -V\dot{\psi}\cos(\phi)\left(\tfrac{J_{p1}}{R_{e_1}}+\tfrac{J_{p2}}{R_{e_2}}\right)-mgh\sin(\phi)=Q_\phi\ .\end{aligned} \tag{B.41}$$

Because

$$\ddot{Y}\cos(\psi)+\ddot{X}\sin(\psi)=\dot{v}+u\dot{\psi}, \tag{B.42}$$

it may be written in the form

$$\begin{aligned}\ddot{\phi}J_x^*+\ddot{\psi}J_{xz}\cos(\phi)-\dot{\psi}^2\left[-J_z+J_y^*\right]\cos(\phi)\sin(\phi)+\\ -mh\cos(\phi)\left(\dot{v}+u\dot{\psi}\right)-V\dot{\psi}\cos(\phi)\left(\tfrac{J_{p1}}{R_{e_1}}+\tfrac{J_{p2}}{R_{e_2}}\right)-mgh\sin(\phi)=Q_\phi\ .\end{aligned} \tag{B.43}$$

B.2.2 Linearization of the equations of motion

If the values of ϕ and v are small, it is possible to linearize the equations of motion. As usual in linearized models, V and u are interchangeable and the terms containing the products of small quantities may be neglected. It then follows that

$$\left\{\begin{array}{l} m\dot{V} = Q_x \ , \\ m\dot{v} + mV\dot{\psi} - mh\ddot{\phi} = Q_y \ , \\ J_z\ddot{\psi} + J_{xz}\ddot{\phi} + m\phi h\dot{V} + V\dot{\phi}\left(\frac{J_{p1}}{R_{e_1}} + \frac{J_{p2}}{R_{e_2}}\right) + \dot{V}\phi\left(\frac{J_{p1}}{R_{e_1}} + \frac{J_{p2}}{R_{e_2}}\right) = Q_\psi \ , \\ J_x\ddot{\phi} + J_{xz}\ddot{\psi} - mh\dot{v} - mhV\dot{\psi} - V\dot{\psi}\left(\frac{J_{p1}}{R_{e_1}} + \frac{J_{p2}}{R_{e_2}}\right) - mgh\phi = Q_\phi \ . \end{array}\right. \tag{B.44}$$

B.2.3 Generalized forces

The forces at the wheel-ground contact may be computed in a way similar to that for the vehicle with two axles, with the monotrack model being no longer a simplification but a realistic model.

The sideslip angle of the ith wheel is

$$\alpha_i = \arctan\left(\frac{v + \dot{\psi}x_i}{u}\right) - \delta_i \ . \tag{B.45}$$

The rear wheel usually does not steer, while the front wheel steers about an axis that is inclined with respect to the vertical. If the inclination angle is γ, it follows that

$$\delta_1 = \delta\cos(\gamma) \ , \qquad \delta_2 = 0 \ . \tag{B.46}$$

The linearized expression of the sideslip angle is then identical to that of two-axles vehicles

$$\left\{\begin{array}{l} \alpha_1 = \beta + \dfrac{a}{V}r - \delta\cos(\eta) \ , \\ \alpha_2 = \beta - \dfrac{b}{V}r \ . \end{array}\right. \tag{B.47}$$

The virtual displacement of the center of the contact zone of the ith wheel in the reference frame of the vehicle is

$$\delta u_i = \left\{\begin{array}{c} \delta x \\ \delta y + \delta\psi x_i \end{array}\right\} \ . \tag{B.48}$$

The virtual work of forces F_{x_i} and F_{y_i} and of the moment M_{z_i} exchanged between wheel and ground is

$$\delta\mathcal{L} = F_{x_i}\delta x + F_{y_i}(\delta y + \delta\psi x_i) + M_{z_i}\delta\psi \ . \tag{B.49}$$

The aerodynamic forces are applied at the center of mass of the vehicle. Assuming that the force components F_{xa}, F_{ya} and F_{za} and the components of

the moment M_{za} and M_{xa} are referred to the x and y axes laying on the ground and to a vertical z axis, the virtual displacement of the center of mass of the vehicle is

$$\delta u_{\mathrm{G}} = \left\{ \begin{array}{c} \delta x + h\delta\psi \sin(\phi) \\ \delta y - h\delta\phi \cos(\phi) \\ -h\delta\phi \sin(\phi) \end{array} \right\} . \tag{B.50}$$

The virtual work of the aerodynamic forces and moments is then

$$\begin{aligned} \delta\mathcal{L} = \; & F_{xa}\left[\delta x + h\delta\psi \sin(\phi)\right] + F_{ya}\left[\delta y - h\delta\phi \cos(\phi)\right] + \\ & + F_{za}\left[-h\delta\phi \sin(\phi)\right] + M_{za}\delta\psi + M_{xa}\delta\phi \; . \end{aligned} \tag{B.51}$$

The generalized forces that must be introduced into the equations are then

$$\left\{ \begin{array}{l} Q_x = F_{x_1} + F_{x_2} + F_{xa} \; , \\ Q_y = F_{y_1} + F_{y_2} + F_{ya} \; , \\ Q_\psi = F_{y_1} a - F_{y_2} b + M_{z_1} + M_{z_2} - F_{xa} h \sin(\phi) + M_{za} \; , \\ Q_\phi = -hF_{ya} \cos(\phi) - F_{za} h \sin(\phi) + M_{xa} \; . \end{array} \right. \tag{B.52}$$

Side forces depend in this case not only on the slip angle but also on the camber angle, which is here equal to the roll angle.

B.2.4 Linearized expression of the generalized forces

As in the case of four-wheeled vehicles, the generalized forces may be linearized. Remembering that for small angles

$$\beta = \frac{v}{V} \; , \tag{B.53}$$

and proceeding as seen in the previous models, it follows that

$$Q_y = Y_v v + Y_r \dot{\psi} + Y_\phi \phi + Y_\delta \delta + F_{y_e} \; , \tag{B.54}$$

where

$$\left\{ \begin{array}{l} Y_v = \frac{1}{V}\left[-C_1 - C_2 + \frac{1}{2}\rho V_r^2 S (C_y)_{,\beta}\right] \; , \\ Y_r = -\frac{1}{V}\left(aC_1 - bC_2\right) \; , \\ Y_\phi = (F_{y_1})_{,\gamma} + (F_{y_2})_{,\gamma} \; , \\ Y_\delta = C_1 \cos(\eta) \; , \end{array} \right. \tag{B.55}$$

and where $(F_{y_i})_{,\gamma}$ is the camber stiffness. Moreover,

$$Q_\psi = N_v v + N_r r + N_\phi \phi + N_\delta \delta + M_{z_e} \; , \tag{B.56}$$

where

$$\left\{\begin{array}{l} N_v = -aC_1 + bC_2 + (M_{z_1})_{,\alpha} + (M_{z_1})_{,\alpha} + \frac{1}{2}\rho V_r^2 S (C_{M_z})_{,\beta} \ , \\ N_r = \frac{1}{V}\left[-a^2 C_1 - b^2 C_2 + (M_{z_1})_{,\alpha} a - (M_{z_2})_{,\alpha} b\right] \ , \\ N_\phi = a(F_{y_1})_{,\gamma} - b(F_{y_2})_{,\gamma} - \frac{1}{2}\rho V_r^2 S h C_x \ , \\ N_\delta = \left[C_1 a - (M_{z_1})_{,\alpha}\right]\cos(\gamma) \ . \end{array}\right. \tag{B.57}$$

At last

$$Q_\phi = L_v v + L_\phi \phi \ , \tag{B.58}$$

where

$$\left\{\begin{array}{l} L_v = \frac{1}{2}\rho V_r S\left[l(C_{M_x})_{,\beta} - h(C_y)_{,\beta}\right] \ , \\ L_\phi = -\frac{1}{2}\rho V_r^2 S h C_z \ . \end{array}\right. \tag{B.59}$$

B.2.5 Final expression of the linearized equations of motion

The linearized equations may be uncoupled, as in the case of four wheeled vehicles, by assuming that the forward velocity V is a known function of time instead of being a variable of motion. The first equation is the usual one

$$m\dot{V} = F_{x_1} + F_{x_2} + F_{xa} \ . \tag{B.60}$$

It allows the driving (or braking) force needed to follow a given law $V(t)$ to be computed.

The other three equations may be written as

$$\begin{bmatrix} m & 0 & -mh \\ 0 & J_z & J_{xz} \\ -mh & J_{xz} & J_x \end{bmatrix} \begin{Bmatrix} \dot{v} \\ \ddot{\psi} \\ \ddot{\phi} \end{Bmatrix} + \begin{bmatrix} -Y_v & mV - Y_r & 0 \\ -N_v & -N_r & N_g \\ -L_v & -mhV - VN_g & 0 \end{bmatrix} \begin{Bmatrix} v \\ \dot{\psi} \\ \dot{\phi} \end{Bmatrix} + \tag{B.61}$$

$$+ \begin{bmatrix} 0 & 0 & -Y_\phi \\ 0 & 0 & mh\dot{V} + \dot{V}\left(\frac{J_{p_1}}{R_{e_1}} + \frac{J_{p_2}}{R_{e_2}}\right) - N_\phi \\ 0 & 0 & -mgh - L_\phi \end{bmatrix} \begin{Bmatrix} y \\ \psi \\ \phi \end{Bmatrix} = \begin{Bmatrix} Y_\delta \delta + F_{y_e} \\ N_\delta \delta + M_{z_e} \\ 0 \end{Bmatrix} \ ,$$

where

$$N_g = V\left(\frac{J_{p_1}}{R_{e_1}} + \frac{J_{p_2}}{R_{e_2}}\right) \ . \tag{B.62}$$

The three matrices included in the equation of motion in the configuration space are normally defined as mass, stiffness and damping matrices (**M**, **C** and **K**). The first is symmetrical, while the other two are not. As usual in vehicle dynamics, the first two columns of the stiffness matrix vanish, because coordinates

y[1] and ψ do not appear directly in the equations. The order of the linearized set of equations is then 4 and not 6, and the state space model is made by four first-order differential equations.

The state space open loop model is the usual one

$$\dot{\mathbf{z}} = \mathbf{A}\mathbf{z} + \mathbf{B}_c\mathbf{u}_c + \mathbf{B}_e\mathbf{u}_e \ , \tag{B.63}$$

where

$$\mathbf{z} = \left[\begin{array}{cccc} v & r & p & v_\delta \end{array} \right]^T \ ,$$

r and p are the derivatives of ψ and ϕ with respect to time;

$$\mathbf{A} = \left[\begin{array}{cc} -\mathbf{M}^{-1}\mathbf{C} & -\mathbf{M}^{-1}\mathbf{K}^* \\ 0 \quad 0 \quad 1 & 0 \end{array} \right] ,$$

where $\mathbf{K}^*$ has been obtained by cancelling the first two columns of $\mathbf{K}$, and

$$\mathbf{B}_c = \left[\begin{array}{c} \mathbf{M}^{-1} \left[\begin{array}{ccc} Y_\delta & N_\delta & 0 \\ & 0 & \end{array} \right]^T \end{array} \right] \ , \quad \mathbf{B}_e = \left[\begin{array}{c} \mathbf{M}^{-1} \\ 0 \end{array} \right] \ ,$$

$$\mathbf{u}_c = \delta \ , \qquad \mathbf{u}_e = \left\{ \begin{array}{c} F_{y_e} \\ M_{z_e} \\ 0 \end{array} \right\} \ .$$

B.3 LOCKED CONTROLS STABILITY

Stability with locked controls may be studied simply by searching the eigenvalues of the dynamic matrix $\mathbf{A}$. The eigenproblem usually yields two real eigenvalues and one complex conjugated pair. Of the real solutions, one is negative and has little importance in the behavior of the system, while the other is positive and hence unstable. The latter corresponds to the capsize mode and must be stabilized by the driver or by some control device. This eigenvalue decreases with increasing speed, as gyroscopic moments of the wheels reduce the velocity at which the motorcycle leans to the side.

The two complex conjugate pairs are related to the so-called weave mode; this mode is primarily a yaw oscillation of the whole vehicle but it also involves the roll and steering degrees of freedom. Weave oscillation is usually damped, at least in locked control motion. At low speed it may not involve a true oscillation (the imaginary part of the eigenvalue may be equal to zero, but in any case the real part is negative).

Remark B.1 *Weave motion usually becomes less stable with increasing speed, i.e. the modulus of its real part decreases while the frequency increases. At high speed it may be difficult for the driver to control the motion, because its frequency is high enough to produce instability.*

[1] v is the derivative of a pseudo-coordinate here and thus y has no physical meaning.

B.3.1 Capsize motion

An extremely simplified model for capsize motion is an inverted pendulum (Fig. B.2a). The linearized equation of a pendulum with length h and baricentric moment of inertia J_x is the usual one

$$\left(J_x + mh^2\right)\ddot{\phi} - mgh\phi = 0 \,, \tag{B.64}$$

where a (-) sign has been introduced in the gravitational term to take into account the fact that the pendulum is inverted (the suspension point is below the center of mass).

The characteristic equation may be obtained by introducing expression

$$\phi = \phi_0 e^{st} \,,$$

into the equation of motion. It is

$$s^2\left(J_x + mh^2\right) - mgh = 0 \,, \tag{B.65}$$

which yields

$$s = \pm\sqrt{\frac{mgh}{J_x + mh^2}} \,. \tag{B.66}$$

The positive solution shows that the capsize motion is unstable. Its time constant is

$$\tau = \frac{1}{s} = \pm\sqrt{\frac{J_x + mh^2}{mgh}} \,. \tag{B.67}$$

Actually the motorcycle does not behave as an inverted pendulum and the time constant increases (that is, s decreases) with increasing speed. This is due both to gyroscopic effect and the camber thrust of the tires caused by roll.

A way to factor in the latter effect is to build a simple model made by an inverted pendulum whose supporting point is free to move horizontally (Fig. B.2b). The position of point P is

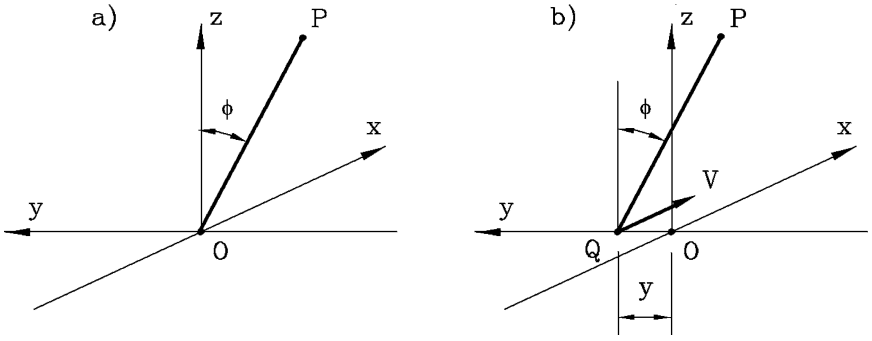

FIGURE B.2. Simplified models for capsize motion. a) Inverted pendulum; b) inverted pendulum with moving supporting point

$$\left(\overline{\mathrm{P}-\mathrm{O}}\right) = \left\{ \begin{array}{l} 0 \\ h\cos(\phi) \\ y - h\sin(\phi) \end{array} \right\} \tag{B.68}$$

and its velocity is

$$V_{\mathrm{P}} = \left\{ \begin{array}{l} 0 \\ -h\dot{\phi}\sin(\phi) \\ \dot{y} - h\dot{\phi}\cos(\phi) \end{array} \right\} . \tag{B.69}$$

The kinetic energy of the system is then

$$\mathcal{T} = \frac{1}{2}m\left[\dot{y}^2 - 2h\dot{y}\dot{\phi}\cos(\phi) + h^2\dot{\phi}^2\right] + \frac{1}{2}J_x\dot{\phi}^2 . \tag{B.70}$$

The gravitational potential energy is

$$\mathcal{U} = mgh\cos(\phi) . \tag{B.71}$$

The equations of motion obtained through Lagrange equations by performing the relevant derivatives of the Lagrangian function $\mathcal{T} - \mathcal{U}$ and linearizing are

$$\left\{ \begin{array}{l} m\ddot{y} - mh\ddot{\phi} = Q_y , \\ -mh\ddot{y} + \left(mh^2 + J_x\right)\ddot{\phi} - mgh\phi = Q_\phi . \end{array} \right. \tag{B.72}$$

The side force acting on point Q is due to the tires, which work with both a sideslip and camber angle. If the virtual displacement of point Q is δy and the usual linearized expression is used for the side force F_y

$$F_y = -C\alpha + (F_y)_{,\gamma}\,\phi , \tag{B.73}$$

where the cornering stiffness C and the camber stiffness $(F_y)_{,\gamma}$ are those of the whole vehicle (the sum of the stiffness referred to the two tires), the virtual work is

$$\delta\mathcal{L} = \delta y\left[-C\alpha + (F_y)_{,\gamma}\,\phi\right] . \tag{B.74}$$

Assuming that the system moves along the x axis at a speed V, the velocity of point Q is

$$V_{\mathrm{Q}} = \left[\begin{array}{ccc} V & \dot{y} & 0 \end{array}\right]^T . \tag{B.75}$$

The sideslip angle of the wheels is then

$$\alpha = \mathrm{artg}\left(\frac{\dot{y}}{V}\right) \approx \frac{\dot{y}}{V} . \tag{B.76}$$

By differentiating the virtual work with respect to the virtual displacement the generalized forces are immediately obtained,

$$Q_y = -C\frac{\dot{y}}{V} + (F_y)_{,\gamma}\,\phi \quad , \quad Q_\phi = 0 . \tag{B.77}$$

The equation of motion is then

$$\begin{bmatrix} m & -mh \\ -mh & mh^2 + J_x \end{bmatrix} \begin{Bmatrix} \ddot{y} \\ \ddot{\phi} \end{Bmatrix} + \frac{1}{V} \begin{bmatrix} C & 0 \\ 0 & 0 \end{bmatrix} \begin{Bmatrix} \dot{y} \\ \dot{\phi} \end{Bmatrix} + \\ + \begin{bmatrix} 0 & -(F_y)_{,\gamma} \\ 0 & -mgh \end{bmatrix} \begin{Bmatrix} y \\ \phi \end{Bmatrix} = \mathbf{0} \ . \tag{B.78}$$

This equation coincides with Eq. (B.61), where the second row and column have been cancelled in all matrices and aerodynamic terms have been neglected.

The characteristic equation allowing the natural frequencies to be computed is

$$\det \begin{bmatrix} ms^2 + \frac{C}{V}s & -mhs^2 - (F_y)_{,\gamma} \\ -mhs^2 & \left(mh^2 + J_x\right) s^2 - mgh \end{bmatrix} = 0 \ , \tag{B.79}$$

and then

$$s \left\{ mJ_x V s^3 + C \left(mh^2 + J_x\right) s^2 + mhV \left[-(F_y)_{,\gamma} - mg \right] s - Cmgh \right\} = 0 \ . \tag{B.80}$$

One solution is obviously $s = 0$; out of the other three, one is real and positive (capsize motion) while the other two are complex with a negative real part. The latter represent a kind of weave motion, but because the model does not take yaw rotation into account, an important factor in weave motion, these solutions have no physical meaning. In this way the time constant of capsize motion becomes a function of speed.

B.3.2 Weave motion

It is possible to build a much simplified model for weave motion as well. Because weave motion primarily involves the vehicle body and not the steering system, a model based on an almost horizontal pendulum hinged on the steering axis (axis H_1H_2 in Fig. B.3) can be built. The length of such a pendulum is GH_1,

$$\overline{GH_1} = l_1 = [a + e - h \tan(\eta)] \cos(\eta) \ . \tag{B.81}$$

The distance of the point where the side force of the rear tire is applied from the hinge axis is P_2H_2:

$$\overline{P_2H_2} = l_2 = (l + e) \cos(\eta) \ . \tag{B.82}$$

If the rotation angle of the pendulum about the steering axis is θ, the steering angle with respect to the xz plane of the rear wheel is

$$\theta \cos(\eta)$$

and its lateral velocity is $\dot{\theta} l_2$. The sideslip angle of the rear wheel is then

$$\alpha_2 = \theta \cos(\eta) + \dot{\theta} \frac{l_2}{V} \ . \tag{B.83}$$

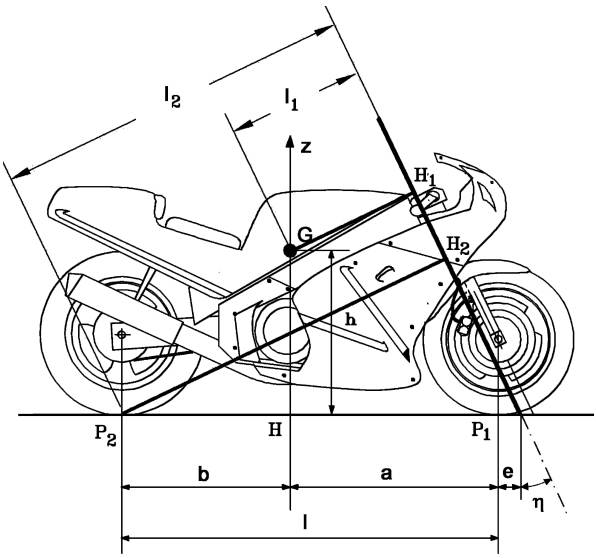

FIGURE B.3. Simplified model for weave motion

Because the roll angle has been assumed to be zero, the side force on the tire is

$$F_{y_2} = -C_2\alpha_2 = -C_2\left[\theta\cos(\eta) + \dot{\theta}\frac{l_2}{V}\right] \ . \tag{B.84}$$

The equation of motion of the vehicle body about the steering axis is

$$J\ddot{\theta} + \frac{C_2 l_2^2}{V}\dot{\theta} + l_2 C_2\theta\cos(\eta) = 0 \ , \tag{B.85}$$

where J is its moment of inertia about the same axis.

A rough approximation is

$$J = J_z + ml_1^2$$

where J_z is the moment of inertia of the whole vehicle about the z axis and m refers to the whole vehicle.

The pole for weave motion is

$$s = \frac{-C_2 l_2^2 \pm \sqrt{C_2^2 l_2^4 - 4V^2 J l_2 C_2\cos(\eta)}}{2VJ} \ . \tag{B.86}$$

At low speed the two solutions are both real and negative, so that weave is stable and not oscillatory (weave is a misnomer in this case). Starting from a speed

$$V = \frac{l_2}{2}\sqrt{\frac{C_2 l_2}{J\cos(\eta)}} \tag{B.87}$$

the roots become complex conjugate and the motion is oscillatory. At low speed the motion is damped, but at high speed the real part may become positive and weave motion may become unstable.

Example B.1 *Study the locked controls stability of the motorcycle of Appendix E.10. Plot the eigenvalues as functions of the speed and the roots locus.*

To correctly compute the roots locus the cornering stiffness of the tires must be computed correctly. The forces on the ground F_{z_i} were then computed, factoring in aerodynamic forces and rolling resistance. The effect of driving forces can also be accounted for, at least using the elliptical approximation.

The values of the cornering and camber stiffness at standstill, at 100 and at 200 km/h are

V	F_{z1}	F_{z2}	C_1	C_2	$(F_{y1})_\gamma$	$(F_{y2})_\gamma$
km/h	*N*	*N*	*N/rad*	*N/rad*	*N/rad*	*N/rad*
0	*1,451*	*1,394*	*39,600*	*41,400*	$-1,708$	$-1,905$
100	*1,384*	*1,414*	*37,700*	*38,600*	$-1,630$	$-1,933$
200	*1,183*	*1,473*	*32,300*	*32,300*	$-1,392$	$-2,013$

The roots locus and the plot of the eigenvalues versus the speed are reported in Fig. B.4.

Weave is oscillatory from about 100 km/h and becomes unstable slightly above 240 km/h, while capsize is, as is normal for motorcycles, unstable.

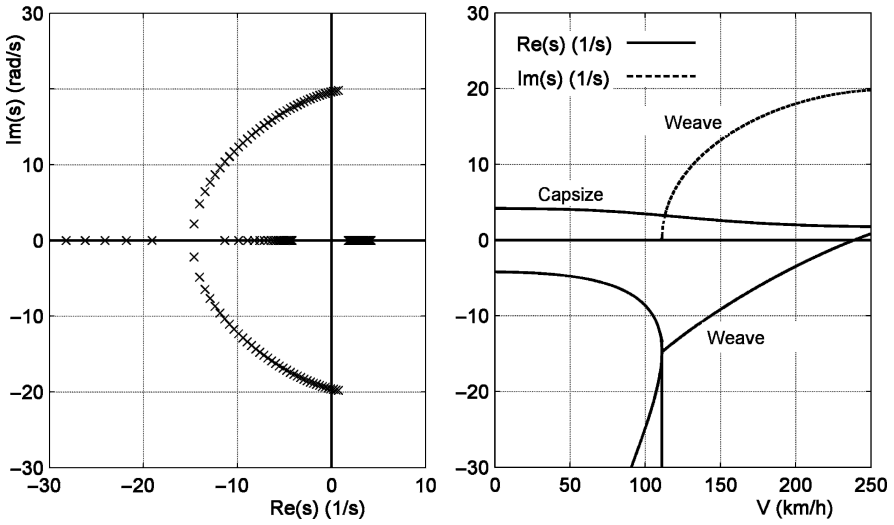

FIGURE B.4. Locked controls stability of a motor cycle. Roots locus and plot of the eigenvalues versus the forward speed

The values of the natural frequencies and of the time constant of capsize motion at three values of speed are

V	s_{cap}	τ_{cap}	s_{weave}	τ^*_{cap}	τ^{**}_{cap}	s^*_{weave}
km/h	*1/s*	*s*	*1/s*	*s*	*s*	*1/s*
0	*4.20*	*0.24*	*–*	*0.33*	*0.33*	*–*
100	*3.44*	*0.29*	*–8.76*	*0.33*	*0.37*	*–10.8±17.6i*
200	*2.00*	*0.50*	*–3.45±18.0 i*	*0.33*	*0.41*	*–4.26±17.8i*

*The values of the capsize time constants and of the eigenvalue for weave computed using the simplified models (values with * and **), are also reported. The latter model largely underestimates the speed at which weave becomes oscillatory (52 km/h against about 100 in the model with three degrees of freedom), but once motion is oscillatory, allows its frequency to be computed in a way that is surprisingly consistent with the value obtained from the more complex model.*

B.4 STEADY-STATE MOTION

Equation (B.61) may be used to compute the steady-state response by simply assuming that v, r, ϕ, δ, and the speed V are constant. A simple way to compute the steady-state response is to fix a certain value of either r or δ and then solve the equations for v, ϕ, δ or r. Perhaps the most immediate approach is the first, because in steady-state conditions, to state r means to state a value of the radius of the path R. The problem is then stated in this form: Given a certain circular path, a value of the speed and perhaps also of external forces, compute sideslip, roll and steering angles ($\beta = v/V$, ϕ and δ). The relevant equation is

$$\begin{bmatrix} C_{11} & K_{13} & -Y_\delta \\ C_{21} & K_{23} & -N_\delta \\ C_{31} & K_{33} & 0 \end{bmatrix} \begin{Bmatrix} V\beta \\ \phi \\ \delta \end{Bmatrix} = r \begin{Bmatrix} -C_{12} \\ -C_{22} \\ -C_{32} \end{Bmatrix} + \begin{Bmatrix} F_{y_e} \\ M_{z_e} \\ 0 \end{Bmatrix} . \tag{B.88}$$

By solving Eq. (B.88) it is possible to compute

- the path curvature gain:
$$\frac{1}{R\delta} = \frac{r}{V\delta} ;$$
- the sideslip angle gain
$$\frac{\beta}{\delta} = \frac{v}{V\delta} ;$$
- the roll angle gain
$$\frac{\phi}{\delta} .$$

Owing to the linearity of the model, if the external forces are assumed to be equal to zero, the mentioned gains are a function of the velocity only; i.e., they do not depend on the radius of the trajectory. Equation (B.88) can thus be assumed to hold for very high speeds as well, if a large enough radius R is considered.

Once the trajectory curvature gain has been obtained, the usual definitions of understeer, neutral steer and oversteer can be applied.

The present model is linearized and hence holds only if the relevant angles are small enough to allow the linearization of their trigonometric functions. The limit in this case is primarily due to the roll angle ϕ which can easily exceed the value of about 20° that can be considered a limit for linearization.

The computation of the steady-state response assumes that the motion is possible, implying that the driver stabilizes the capsize mode, which is unstable in open-loop operation.

Example B.2 *Compute the steady-state steering response of the motorcycle of Appendix E.10, assuming that no external force is present. Compute the values of β, δ, and ϕ on a curve with a radius of 200 m at a speed of 80 km/h.*

The various gains are plotted versus the speed in Fig. B.5. The nondimensional curves hold for any value of the radius R: They are plotted for speeds up to 240 km/h, although on a curve with a radius of 200 m the limit for linearization occurs at speeds slightly in excess of 80 km/h.

At 80 km/h their values are $1/R\delta = 0.56$ 1/m; $\beta/\delta = 0.77$, and $\phi/\delta = -28.5$. On a curve of 200 m radius the steering angle is $\delta = 0.0090$ rad $= 0.52\,^\circ$. Because the

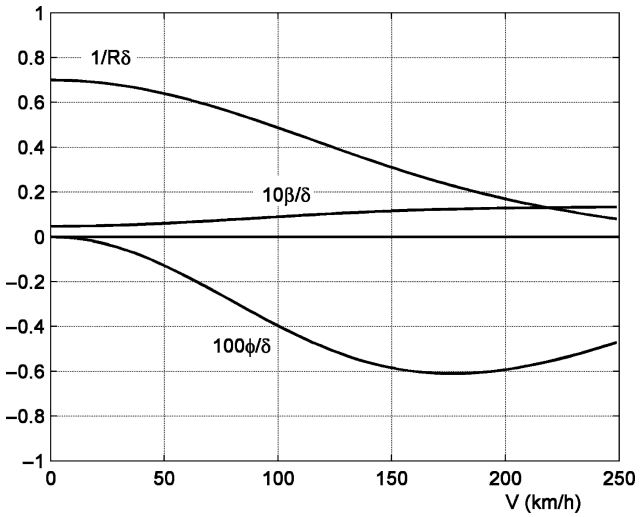

FIGURE B.5. Values of the path curvature gain $1/R\delta = r/V\delta$, the sideslip angle gain $\beta/\delta = v/V\delta$ and the roll angle gain ϕ/δ for the motorcycle of Appendix E.10 versus the speed V

wheelbase is 1.316 m, the kinematic value of the trajectory curvature gain is 0.70 and the steering angle is then $\delta_c = 0.0071$ rad $= 0.41°$. The vehicle is then understeer.

The other values are $\beta = 0.0069$ rad $= 0.40°$, and $\phi = -0.257$ rad $= -14.7°$. The value of the roll angle is quite close to the limit for linearization.

B.5 FREE CONTROLS MODEL

The Lagrangian function for a system with free controls is that already seen for the locked controls model, with some additional terms

$$\begin{aligned}\Delta\mathcal{L} &= \frac{1}{2}J_{z1}\dot{\delta}^2 + \dot{\delta}\dot{\psi}\left[J_{z1}\cos(\eta) + J_{xz1}\sin(\eta)\cos(\phi)\right] + \\ &+ \dot{\delta}\dot{\phi}\left[-J_{z1}\sin(\eta) + J_{xz1}\cos(\eta)\right] + A_1\delta\dot{\psi}^2 + A_2\delta\dot{\phi}^2 + \\ &+ A_3\delta\dot{\psi}\dot{\phi} - V\frac{J_{p_1}}{R_{e_1}}\delta\left[\dot{\psi}\cos(\phi)\sin(\eta) + \dot{\phi}\cos(\eta)\right] .\end{aligned}$$

First two equations of motion

$\Delta\mathcal{L}$ Does not contain either X or Y or their derivatives. The first two equations are not changed by the free controls assumptions.

Third equation of motion

When linearizing the equation, terms in A_i disappear. The derivatives included in the third equation are

$$\begin{aligned}\frac{\partial\Delta\mathcal{L}}{\partial\dot{\psi}} &= \dot{\delta}\left[J_{z1}\cos(\eta) + J_{xz1}\sin(\eta)\right] - V\frac{J_{p_1}}{R_{e_1}}\delta\sin(\eta) , \\ \frac{\partial\Delta\mathcal{L}}{\partial\psi} &= 0\end{aligned} \tag{B.89}$$

and then

$$\frac{d}{dt}\left(\frac{\partial\Delta\mathcal{L}}{\partial\dot{\psi}}\right) = \ddot{\delta}\left[J_{z1}\cos(\eta) + J_{xz1}\sin(\eta)\right] - \dot{V}\frac{J_{p_1}}{R_{e_1}}\delta\sin(\eta) - V\frac{J_{p_1}}{R_{e_1}}\dot{\delta}\sin(\eta) . \tag{B.90}$$

The third equation is then

$$\begin{aligned}&J_z\ddot{\psi} + J_{xz}\ddot{\phi} + \ddot{\delta}\left[J_{z1}\cos(\eta) + J_{xz1}\sin(\eta)\right] + m\phi h\dot{V} + V\dot{\phi}\left(\tfrac{J_{p_1}}{R_{e_1}} + \tfrac{J_{p_2}}{R_{e_2}}\right) + \\ &-V\tfrac{J_{p_1}}{R_{e_1}}\dot{\delta}\sin(\eta) + \dot{V}\phi\left(\tfrac{J_{p_1}}{R_{e_1}} + \tfrac{J_{p_2}}{R_{e_2}}\right) - \dot{V}\tfrac{J_{p_1}}{R_{e_1}}\delta\sin(\eta) = Q_\psi .\end{aligned} \tag{B.91}$$

Fourth equation of motion

The fourth equation, dealing with the roll angle ϕ, may be obtained in the same way. The derivatives are

$$\begin{aligned}\frac{\partial \Delta\mathcal{L}}{\partial \dot{\phi}} &= \dot{\delta}\left[-J_{z1}\sin(\eta) + J_{xz1}\cos(\eta)\right] - V\frac{J_{p_1}}{R_{e_1}}\delta\cos(\eta)\,,\\ \frac{\partial \Delta\mathcal{L}}{\partial \phi} &= 0\end{aligned} \tag{B.92}$$

and then

$$\frac{d}{dt}\left(\frac{\partial \Delta\mathcal{L}}{\partial \dot{\phi}}\right) = \ddot{\delta}\left[-J_{z1}\sin(\eta) + J_{xz1}\cos(\eta)\right] - V\frac{J_{p_1}}{R_{e_1}}\dot{\delta}\cos(\eta) - \dot{V}\frac{J_{p_1}}{R_{e_1}}\delta\cos(\eta)\ . \tag{B.93}$$

The fourth equation is then

$$\begin{aligned}&J_x\ddot{\phi} + J_{xz}\ddot{\psi} + \ddot{\delta}\left[-J_{z1}\sin(\eta) + J_{xz1}\cos(\eta)\right] - mh\dot{v} - mhV\dot{\psi} + \\ &-V\dot{\psi}\left(\frac{J_{p_1}}{R_{e_1}} + \frac{J_{p_2}}{R_{e_2}}\right) - V\frac{J_{p_1}}{R_{e_1}}\dot{\delta}\cos(\eta) - \dot{V}\frac{J_{p_1}}{R_{e_1}}\delta\cos(\eta) - mgh\phi = Q_\phi\ .\end{aligned} \tag{B.94}$$

Fifth equation of motion

A further equation describing the motion of the steering system must be added to the first four equations. The relevant derivatives are

$$\begin{aligned}\frac{\partial \Delta\mathcal{L}}{\partial \dot{\delta}} &= J_{z1}\dot{\delta} + \dot{\psi}\left[J_{z1}\cos(\eta) + J_{xz1}\sin(\eta)\right] + \dot{\phi}\left[-J_{z1}\sin(\eta) + J_{xz1}\cos(\eta)\right]\ ,\\ \frac{\partial \Delta\mathcal{L}}{\partial \delta} &= -V\frac{J_{p_1}}{R_{e_1}}\left[\dot{\psi}\sin(\eta) + \dot{\phi}\cos(\eta)\right]\ ,\end{aligned} \tag{B.95}$$

and then

$$\begin{aligned}\frac{d}{dt}\left(\frac{\partial \Delta\mathcal{L}}{\partial \dot{\delta}}\right) = J_{z1}\ddot{\delta} + \ &\ddot{\psi}\left[J_{z1}\cos(\eta) + J_{xz1}\sin(\eta)\right] + \\ &+\ddot{\phi}\left[-J_{z1}\sin(\eta) + J_{xz1}\cos(\eta)\right]\ .\end{aligned} \tag{B.96}$$

The fifth equation is

$$\begin{aligned}&J_{z1}\ddot{\delta} + \ddot{\psi}\left[J_{z1}\cos(\eta) + J_{xz1}\sin(\eta)\right] + \ddot{\phi}\left[-J_{z1}\sin(\eta) + J_{xz1}\cos(\eta)\right] + \\ &+ V\frac{J_{p_1}}{R_{e_1}}\left[\dot{\psi}\sin(\eta) + \dot{\phi}\cos(\eta)\right] = Q_\delta\ .\end{aligned} \tag{B.97}$$

B.5.1 Generalized forces

The virtual displacement of the center of the contact zone of the rear wheel is the same as seen for the case of locked controls motion. The sideslip angle of the

front wheel, assuming that the steering angle is small, is

$$\alpha_1 = \arctan\left(\frac{v + \dot{\psi}a - \dot{\delta}e}{u}\right) - \delta\cos(\eta) \ . \tag{B.98}$$

Its linearized expression is then

$$\alpha_1 = \beta + \frac{a}{V}r - \frac{e}{V}\dot{\delta} - \delta\cos(\eta) \ . \tag{B.99}$$

The virtual displacement of the center of the contact area of the front wheel is

$$\delta u_1 = \left\{ \begin{array}{c} \delta x \\ \delta y + \delta\psi a - e\delta\delta \end{array} \right\} \ . \tag{B.100}$$

The virtual work of forces F_{x_i} and F_{y_i} and of the moment M_{z_i} acting between wheel and ground is

$$\delta\mathcal{L}_1 = F_{x_1}\delta x + F_{y_1}\left[\delta y + \delta\psi x_i - e\delta\delta\right] + M_{z_i}\left[\delta\psi + \delta\delta\cos(\eta)\right] \ . \tag{B.101}$$

The generalized forces to be introduced into the first equations of motion are those already seen in the previous model. The force included in the fifth equation is

$$Q_\delta = -eF_{y_1} + M_{z_i}\cos(\eta) \ . \tag{B.102}$$

Proceeding as in the previous models, it follows that

$$Q_y = Y_v v + Y_r\dot{\psi} + Y_{\dot{\delta}}\dot{\delta} + Y_\phi\phi + Y_\delta\delta + F_{y_e} \ , \tag{B.103}$$

$$Q_\psi = N_v v + N_r\dot{\psi} + N_{\dot{\delta}}\dot{\delta} + N_\phi\phi + N_\delta\delta + M_{z_e} \ , \tag{B.104}$$

where the already defined derivatives of stability are not changed,

$$Y_{\dot{\delta}} = C_1\frac{e}{V} \ , \tag{B.105}$$

$$N_{\dot{\delta}} = \left[C_1 a - (M_{z_1})_{,\alpha}\right]\frac{e}{V} \ . \tag{B.106}$$

The expression of Q_ϕ is the same as seen for the locked controls model

$$Q_\phi = M_v v + M_r\dot{\psi} + M_{\dot{\delta}}\dot{\delta} + M_\phi\phi + M_\delta\delta \ , \tag{B.107}$$

where

$$\left\{ \begin{array}{l} M_v = \frac{1}{V}\left[C_1 e + (M_{z_1})_{,\alpha}\cos(\eta)\right] \ , \\ M_r = \frac{a}{V}C_1\left[C_1 e + (M_{z_1})_{,\alpha}\cos(\eta)\right] \ , \\ M_{\dot{\delta}} = -\frac{e}{V}\left[C_1 e + (M_{z_1})_{,\alpha}\cos(\eta)\right] \ , \\ M_\phi = -e(F_{y_1})_{,\gamma} \ , \\ M_\delta = -\left[C_1 e + (M_{z_1})_{,\alpha}\cos(\eta)\right]\cos(\eta) \ . \end{array} \right. \tag{B.108}$$

B.5.2 Final expression of the linearized, free controls equations

The four equations describing the lateral free controls motions are

$$\begin{bmatrix} m & 0 & -mh & 0 \\ & J_z & J_{xz} & J_{z1}\cos(\eta) + J_{xz1}\sin(\eta) \\ & & J_x & -J_{z1}\sin(\eta) + J_{xz1}\cos(\eta) \\ & \text{symm.} & & J_{z1} \end{bmatrix} \begin{Bmatrix} \dot{v} \\ \ddot{\psi} \\ \ddot{\phi} \\ \ddot{\delta} \end{Bmatrix} +$$

$$+ \begin{bmatrix} -Y_v & mV - Y_r & 0 & -Y_{\dot{\delta}} \\ -N_v & -N_r & N_g & -N_{\dot{\delta}} - S^* \\ -L_v & -mhV - VN_g & 0 & -VC^* \\ -M_v & -M_r + VS^* & +VC^* & -M_{\dot{\delta}} + c_\delta \end{bmatrix} \begin{Bmatrix} v \\ \dot{\psi} \\ \dot{\phi} \\ \dot{\delta} \end{Bmatrix} + \tag{B.109}$$

$$+ \begin{bmatrix} 0 & 0 & -Y_\phi & -Y_\delta \\ 0 & 0 & mh\dot{V} + \dot{V}\left(\frac{J_{p1}}{R_{e_1}} + \frac{J_{p2}}{R_{e_2}}\right) - N_\phi & -N_\delta - \dot{V}S^* \\ 0 & 0 & -mgh - L_\phi & -\dot{V}C^* \\ 0 & 0 & -M_\phi & -M_\delta \end{bmatrix} \begin{Bmatrix} y \\ \psi \\ \phi \\ \delta \end{Bmatrix} =$$

$$= \begin{Bmatrix} Y_\delta \delta + F_{y_e} \\ N_\delta \delta + M_{z_e} \\ 0 \\ M_g \end{Bmatrix},$$

where

$$S^* = \frac{J_{p_1}}{R_{e_1}}\sin(\eta) \ , \quad C^* = \frac{J_{p_1}}{R_{e_1}}\cos(\eta) \ .$$

From matrices **M**, **C** and **K**, defined in the configurations space, it is immediately possible to obtain the dynamic matrix in the state space. In this case the first two equations are first- order differential equations, while the others are second-order equations. The order of the set of equations is then 6 and the dynamic matrix has 6 rows and columns.

B.5.3 Free controls stability

The stability with free controls may be studied simply by searching the eigenvalues of the dynamic matrix **A**. The eigenproblem usually yields two real eigenvalues and two complex conjugated pairs.

Out of the real solutions, one is negative and has practically no importance in the behavior of the system, while the other is positive and hence unstable. As in the locked control model, the latter corresponds to the capsize mode and must be stabilized by the driver or by some control device. This eigenvalue decreases with increasing speed, as gyroscopic moments of the wheels reduce the velocity at which the motorcycle falls on its side.

The two complex conjugate pairs are related to the so-called weave and wobble modes: The first, already seen in the locked control study, is primarily a

yaw oscillation of the whole vehicle but involves the roll and steering degrees of freedom as well, while the other is primarily an oscillation of the steering system about its axis. The weave frequency is lower than the wobble frequency, and is usually more dependent on speed.

While the first mode is usually damped, the latter can become unstable, particularly at high speed. To stabilize wobble motion it is possible to introduce a steering damper, which has been included in the present mathematical model. The damper has the effect of reducing wobble instability, but may affect weave negatively. Too large a damping can trigger weave instability: The value of coefficient c_δ must be chosen with care and the present mathematical model can supply useful guidelines.

Wobble motion

A simplified model may also be built for wobble motion. If the steering system is considered separately from the vehicle using a model similar to that seen in Fig. B.3 for the vehicle body, the following equation of motion is obtained,

$$J\ddot{\delta} + \frac{C_1 e^2 \cos^2(\eta)}{V}\dot{\delta} + eC_1\delta\cos^2(\eta) = 0, \tag{B.110}$$

where J is the moment of inertia of the steering system about the steering axis. If a steering damper is present, its damping coefficient must be added to the term

$$\frac{C_1 e^2 \cos^2(\eta)}{V}$$

multiplying $\dot{\delta}$. Note that the damping of the steering damper must also be added in the equation related to weave.

The pole for wobble motion is

$$s = \cos(\eta)\,\frac{-C_1 e^2 \cos(\eta) \pm \sqrt{C_1^2 e^4 \cos^2(\eta) - 4V^2 JeC_1}}{2VJ}. \tag{B.111}$$

At low speed there are two negative real poles, so that wobble motion is stable. Starting from the speed

$$V = \frac{e\cos(\eta)}{2}\sqrt{\frac{C_1 e}{J}}, \tag{B.112}$$

the roots become complex and the motion is oscillatory. It is initially damped, but with increasing speed the real part may become positive, producing an unstable motion.

Example B.3 *Study the free controls stability of the motorcycle studied in the previous example and plot the eigenvalues as functions of the speed and the roots locus.*

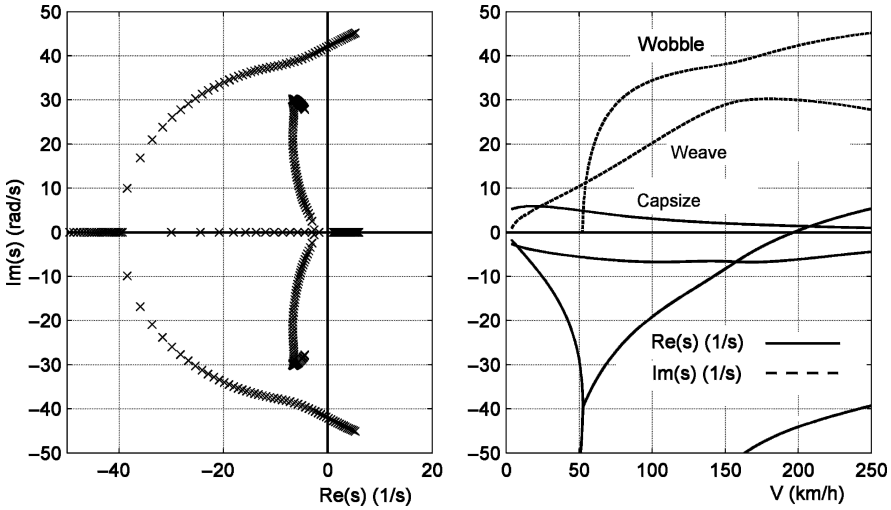

FIGURE B.6. Free controls stability study for the motorcycle of Appendix E.10. Roots locus and plot of the eigenvalues versus the speed

Operating as seen in the previous examples, the plots shown in Fig. B.6 are obtained.

Wobble motion becomes unstable starting from about 200 km/h.

The values of the natural frequencies and the time constant for capsize at three values of the speed are

V	s_{cap}	τ_{cap}	s_{weave}	s_{wob}
km/h	*1/s*	*s*	*1/s*	*1/s*
0	*4.37*	*0.228*	–	–
100	*3.07*	*0.326*	*–6.74±20.29 i*	*–19.04±34.46 i*
200	*1.40*	*0.711*	*–6.11±29.95 i*	*+0.43±42.35 i*

V	τ^*_{cap}	τ^{**}_{cap}	s^*_{weave}	s^*_{wob}
km/h	*s*	*s*	*1/s*	*1/s*
0	*0.33*	*0.33*	–	–
100	*0.33*	*0.37*	*–10.8±17.6i*	*–2.60±38.89 i*
200	*0.33*	*0.41*	*–4.26±17.8 i*	*–1.11±36.03 i*

*Wobble motion becomes unstable at about 200 km/h. The values obtained using the simplified models (values with *) are reported together with those obtained using the present model.*

The computation was repeated assuming that a steering damper with $c_\delta = 25$ Nms/rad is present. The relevant results are plotted in Fig. B.7. The damper stabilizes wobble motion up to more than 250 km/h, but reduces weave stability.

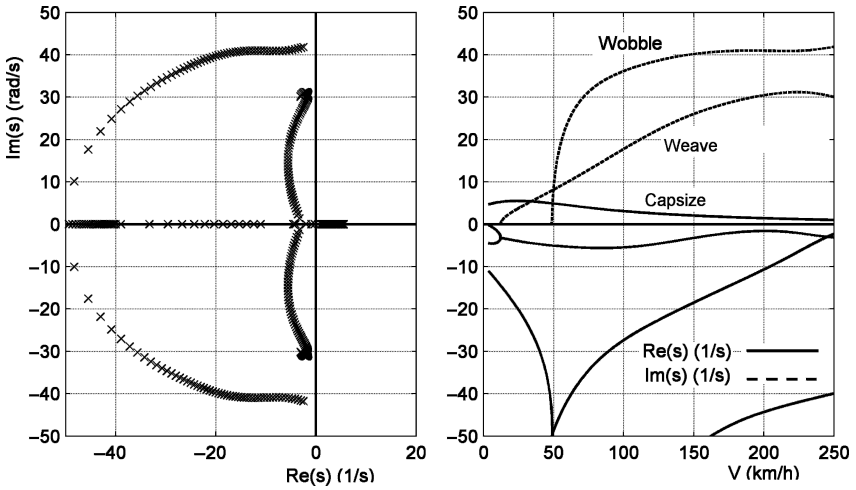

FIGURE B.7. Free controls stability study for the motor cycle of Appendix E.10. Roots locus and plot of the eigenvalus versus the speed. Steering damper with $c_\delta = 25$ Nms/rad

B.5.4 Steady-state response

The steady-state response may be obtained directly from Eq. (B.109) by introducing the steering moment M_s as an unknown. The equation is

$$\begin{bmatrix} C_{11} & K_{13} & K_{14} & 0 \\ C_{21} & K_{23} & K_{24} & 0 \\ C_{31} & K_{33} & K_{34} & 0 \\ C_{41} & K_{43} & K_{44} & -1 \end{bmatrix} \begin{Bmatrix} V\beta \\ \phi \\ \delta \\ M_s \end{Bmatrix} = r \begin{Bmatrix} -C_{12} \\ -C_{22} \\ -C_{32} \\ -C_{42} \end{Bmatrix} + \begin{Bmatrix} F_{y_e} \\ M_{z_e} \\ -hF_{y_e} \\ eF_{y_{e_1}} \end{Bmatrix} . \quad \text{(B.113)}$$

It is then possible to obtain, together with the path curvature gain, the sideslip angle gain and the roll angle gain, as well as the steering moment gain M_s/δ.

B.6 STABILITY AT LARGE ROLL ANGLES

B.6.1 Locked controls motion

In fast driving the roll angle of a motorcycle may become even larger than 45°. In these conditions the linearized model seen in the previous sections cannot be used. However, even when managing a curve at high speed, the sideslip angles and the steering angle are not large, and the only source of nonlinearity is the roll angle. In these conditions stability may be studied by linearizing the equations about a static equilibrium condition, characterized by a value ϕ_0 of the roll angle, that may be computed for example using Eq. (25.45).

Assuming that the displacement from the equilibrium condition is small, the roll angle is

$$\phi = \phi_0 + \phi_1 \ , \tag{B.114}$$

where angle ϕ_1 is small and then

$$\sin(\phi) = \sin(\phi_0) + \phi_1 \cos(\phi_0) \ , \tag{B.115}$$

$$\cos(\phi) = \cos(\phi_0) - \phi_1 \sin(\phi_0) \ . \tag{B.116}$$

Remembering that ϕ_0 is constant and its derivatives vanish, the locked controls equations reduce to

$$\left\{\begin{array}{l} m\left[\dot{V} + h\ddot{\psi}\sin(\phi_0)\right] = Q_x \\ m\left[\dot{v}+V\dot{\psi} - h\ddot{\phi}_1\cos(\phi_0)\right] = Q_y \\ \ddot{\psi}\left[J_z\cos^2(\phi_0) + J_y^*\sin^2(\phi_0)\right] + \ddot{\phi}_1 J_{xz}\cos(\phi_0)+mh\dot{V}\sin(\phi_0)+ \\ \qquad +mh\dot{V}\phi_1\cos(\phi_0) + \dot{V}\sin(\phi_0)\left(\frac{J_{p_1}}{R_{e_1}} + \frac{J_{p_2}}{R_{e_2}}\right) + \\ \qquad + \dot{V}\phi_1\cos(\phi_0)\left(\frac{J_{p_1}}{R_{e_1}} + \frac{J_{p_2}}{R_{e_2}}\right) + V\dot{\phi}_1\cos(\phi_0)\left(\frac{J_{p_1}}{R_{e_1}} + \frac{J_{p_2}}{R_{e_2}}\right) = Q_\psi \\ \ddot{\phi}J_x^* + \ddot{\psi}J_{xz}\cos(\phi_0) - mh\cos(\phi_0)\dot{v} - V\dot{\psi}\cos(\phi_0)\left(mh + \frac{J_{p_1}}{R_{e_1}} + \frac{J_{p_2}}{R_{e_2}}\right) + \\ \qquad -mgh\sin(\phi_0) - mgh\phi_1\cos(\phi_0) = Q_\phi \ . \end{array}\right. \tag{B.117}$$

The generalized forces are

$$\left\{\begin{array}{l} Q_x = F_{x_1} + F_{x_2} + F_{xa} \ , \\ Q_y = F_{y_1} + F_{y_2} + F_{ya} \ , \\ Q_\psi = F_{y_1}a - F_{y_2}b + M_{z_1} + M_{z_2} - F_{xa}h\sin(\phi_0) - F_{xa}h\phi_1\cos(\phi_0) + M_{za} \ , \\ Q_\phi = -hF_{ya}\cos(\phi_0) - F_{za}h\sin(\phi_0) - F_{za}h\phi_1\cos(\phi_0) + M_{xa} \ . \end{array}\right. \tag{B.118}$$

Assuming that the expression for the sideslip angles of the wheels is that seen for small roll angles(an assumption that may be justly criticized at least for the front wheel), the expression for Q_y and for the derivatives of stability Y_v, Y_r, Y_ϕ and Y_δ are those already seen.

Q_ψ and the derivatives of stability N_v, N_r and N_δ are not changed, but derivative N_ϕ becomes

$$N_\phi = a(F_{y_1})_{,\gamma} - b(F_{y_2})_{,\gamma} - \frac{1}{2}\rho V_r^2 ShC_x\cos(\phi_0) \tag{B.119}$$

and a moment

$$N_0 = -\frac{1}{2}\rho V_r^2 SC_x h\sin(\phi_0)\,, \tag{B.120}$$

due to aerodynamic drag, must be added to the external moment M_{z_e}.

As far as Q_ϕ is concerned, derivatives L_v and L_ϕ become

$$\left\{\begin{array}{l} L_v = \frac{1}{2}\rho V_r S\left[l(C_{M_x})_{,\beta} - h(C_y)_{,\beta}\cos(\phi_0)\right] \ , \\ \\ L_\phi = -\frac{1}{2}\rho V_r^2 ShC_z\cos(\phi_0) \ , \end{array}\right. \tag{B.121}$$

and a term

$$L_0 = -\frac{1}{2}\rho V_r^2 S C_z h \sin(\phi_0) \tag{B.122}$$

must be added.

B.6.2 Equilibrium condition

The computation of the steady-state equilibrium condition at constant speed reduces to the computation of either v, $\dot{\psi}$ and ϕ_0 (in this condition ϕ_1 is equal to zero) at a given value of δ or v, δ and ϕ_0 for a given value of $\dot{\psi}$. As usual the linearized equations may be uncoupled and longitudinal dynamics does not affect handling.

The other three equations may be written as

$$\left\{\begin{array}{l} Y_v v + (Y_r - mV)\,\dot{\psi} + Y_\phi \phi_0 + Y_\delta \delta + F_{y_e} = 0\ , \\ N_v v + N_r r + N_\phi \phi_0 + N_\delta \delta + N_0 + M_{z_e} = 0\ , \\ V\dot{\psi}\cos(\phi_0)\left(mh + \frac{J_{p1}}{R_{e_1}} + \frac{J_{p2}}{R_{e_2}}\right) + L_\phi \phi_0 + \\ \qquad + L_v v + L_0 + mgh\sin(\phi_0) = 0\ . \end{array}\right. \tag{B.123}$$

Because unknown ϕ_0 is present in an explicit way in the trigonometric functions and also in an implicit way in N_ϕ, N_0, L_v, L_ϕ and L_0, it may be expedient to choose a value of ϕ_0 and then solve the equations in v, $\dot{\psi}$ and δ, i.e., choose a value of the roll angle and then compute the parameters of the resulting path, obviously after also choosing a value for the speed. If the steady-state values are v_0 and $\dot{\psi}_0$, the equation becomes

$$\left[\begin{array}{ccc} -Y_v & mV - Y_r & -Y_\delta \\ -N_v & -N_r & -N_\delta \\ -L_v & -V\cos(\phi_0)\left(mh + \frac{J_{p1}}{R_{e_1}} + \frac{J_{p2}}{R_{e_2}}\right) & 0 \end{array}\right] \left\{\begin{array}{c} v_0 \\ \dot{\psi}_0 \\ \delta_0 \end{array}\right\} = \tag{B.124}$$

$$= \left\{\begin{array}{c} Y_\phi \phi_1 + F_{y_e} \\ N_\phi \phi_1 + N_\delta \delta + N_0 + M_{z_e} \\ L_\phi \phi_0 + L_0 + mgh\sin(\phi_0) \end{array}\right\}.$$

It is immediately clear that, if the aerodynamic terms are neglected, the last equation uncouples and becomes

$$\tan(\phi_0) = -\frac{V\dot{\psi}}{mgh}\left(mh + \frac{J_{p1}}{R_{e_1}} + \frac{J_{p2}}{R_{e_2}}\right), \tag{B.125}$$

which coincides with Eq. (25.45)[2].

[2]The (−) sign comes from the fact that if the curve is toward the left (positive $\dot{\psi}$) the vehicle tilts to the left (negative ϕ).

B.6.3 Stability at constant speed

The term $\ddot{\psi}$ present in the first equation of motion weekly couples this equation to the others. If this term is neglected, and stating that

$$v = v_0 + v_1 \ , \quad \dot{\psi} = \dot{\psi}_0 + \dot{\psi}_1$$

(because motion occurs with locked controls $\delta = \delta_0$), it follows that

$$\begin{bmatrix} m & 0 & -mh\cos(\phi_0) \\ 0 & J_z\cos^2(\phi_0) + J_y^*\sin^2(\phi_0) & J_{xz}\cos(\phi_0) \\ -mh\cos(\phi_0) & \ddot{\psi}J_{xz}\cos(\phi_0) & J_x^* \end{bmatrix} \begin{Bmatrix} \dot{v}_1 \\ \ddot{\psi}_1 \\ \ddot{\phi}_1 \end{Bmatrix} + \tag{B.126}$$

$$+ \begin{bmatrix} -Y_v & mV - Y_r & 0 \\ -N_v & -N_r & N_g\cos(\phi_0) \\ -L_v & -(mhV + N_g)\cos(\phi_0) & 0 \end{bmatrix} \begin{Bmatrix} v_1 \\ \dot{\psi}_1 \\ \dot{\phi}_1 \end{Bmatrix} + \tag{B.127}$$

$$+ \begin{bmatrix} 0 & 0 & -Y_\phi \\ 0 & 0 & -N_\phi \\ 0 & 0 & -mgh\cos(\phi_0) - L_\phi \end{bmatrix} \begin{Bmatrix} y \\ \psi \\ \phi_1 \end{Bmatrix} = \mathbf{0}.$$

Locked controls stability in the small for a motorcycle managing a curve in steady-state condition with an arbitrarily large roll angle can thus be studied.

B.6.4 Free controls model

Operating as seen in previous models, the following equations may be written

$$\begin{cases} m\left[\dot{V} + h\ddot{\psi}\sin(\phi_0)\right] = Q_x \ , \\ m\left[\dot{v} + V\dot{\psi} - h\ddot{\phi}_1\cos(\phi_0)\right] = Q_y \ , \\ \ddot{\psi}\left[J_z\cos^2(\phi_0) + J_y^*\sin^2(\phi_0)\right] + \ddot{\delta}\left[J_{z1}\cos(\eta) + J_{xz1}\sin(\eta)\cos(\phi_0)\right] + \\ \quad + \ddot{\phi}_1 J_{xz}\cos(\phi_0) - V\frac{J_{p1}}{R_{e_1}}\dot{\delta}\sin(\eta)\cos(\phi_0) - \dot{V}\frac{J_{p1}}{R_{e_1}}\delta\sin(\eta)\cos(\phi_0) + \\ \quad + mh\dot{V}\phi_1\cos(\phi_0) + \dot{V}\sin(\phi_0)\left(\frac{J_{p1}}{R_{e_1}} + \frac{J_{p2}}{R_{e_2}}\right) + mh\dot{V}\sin(\phi_0) + \\ \quad + \dot{V}\phi_1\cos(\phi_0)\left(\frac{J_{p1}}{R_{e_1}} + \frac{J_{p2}}{R_{e_2}}\right) + V\dot{\phi}_1\cos(\phi_0)\left(\frac{J_{p1}}{R_{e_1}} + \frac{J_{p2}}{R_{e_2}}\right) = Q_\psi \ , \end{cases} \tag{B.128}$$

$$
\begin{cases}
\ddot{\phi}J_x^* + \ddot{\psi}J_{xz}\cos(\phi_0) + \ddot{\delta}\left[-J_{z1}\sin(\eta) + J_{xz1}\cos(\eta)\right] - mh\dot{v}\cos(\phi_0) + \\
\quad -V\dot{\psi}\cos(\phi_0)\left(mh + \frac{J_{p_1}}{R_{e_1}} + \frac{J_{p_2}}{R_{e_2}}\right) - V\frac{J_{p_1}}{R_{e_1}}\dot{\delta}\cos(\eta) + \\
\quad -\dot{V}\frac{J_{p_1}}{R_{e_1}}\delta\cos(\eta) - mgh\sin(\phi_0) - mgh\phi_1\cos(\phi_0) = Q_\phi \ , \\
J_{z1}\ddot{\delta} + \ddot{\psi}\left[J_{z1}\cos(\eta) + J_{xz1}\sin(\eta)\cos(\phi_0)\right] + \ddot{\phi}\left[-J_{z1}\sin(\eta) + \right. \\
\quad \left. + J_{xz1}\cos(\eta)\right] + V\frac{J_{p_1}}{R_{e_1}}\left[\dot{\psi}\sin(\eta)\cos(\phi_0) + \dot{\phi}\cos(\eta)\right] = Q_\delta \ .
\end{cases}
$$

The four equations describing the lateral free controls motion about a position defined by the values v_0, $\dot{\psi}_0$, ϕ_0 and δ_0 (in this case δ is a variable and may be written as $\delta_0 + \delta_1$) and thus allowing free controls stability to be studied, are

$$
\begin{bmatrix}
m & 0 & -mh\cos(\phi_0) & 0 \\
 & J_z^{**} & J_{xz}\cos(\phi_0) & J_{z1}\cos(\eta) + J_{xz1}\sin(\eta)\cos(\phi_0) \\
 & & J_x^* & -J_{z1}\sin(\eta) + J_{xz1}\cos(\eta) \\
 & \text{symm.} & & J_{z1}
\end{bmatrix}
\begin{Bmatrix} \dot{v}_1 \\ \ddot{\psi}_1 \\ \ddot{\phi}_1 \\ \ddot{\delta}_1 \end{Bmatrix} +
$$

$$
+ \begin{bmatrix}
-Y_v & mV - Y_r & 0 & -Y_{\dot{\delta}} \\
-N_v & -N_r & N_g\cos(\phi_0) & -N^* \\
-L_v & -(mhV + N_g)\cos(\phi_0) & 0 & -VC^* \\
-M_v & -M_r + VS^* & VC^* & -M_{\dot{\delta}} + c_\delta
\end{bmatrix}
\begin{Bmatrix} v_1 \\ \dot{\psi}_1 \\ \dot{\phi}_1 \\ \dot{\delta}_1 \end{Bmatrix} + \tag{B.129}
$$

$$
+ \begin{bmatrix}
0 & 0 & -Y_\phi & -Y_\delta \\
0 & 0 & -N_\phi & -N_\delta \\
0 & 0 & -mgh\cos(\phi_0) - L_\phi & 0 \\
0 & 0 & -M_\phi & -M_\delta
\end{bmatrix}
\begin{Bmatrix} y \\ \psi \\ \phi_1 \\ \delta_1 \end{Bmatrix} = \mathbf{0} \ ,
$$

where

$$
J_z^{**} = J_z\cos^2(\phi_0) + J_y^*\sin^2(\phi_0) \ , \quad S^* = \frac{J_{p_1}}{R_{e_1}}\sin(\eta) \ , \tag{B.130}
$$

$$
C^* = \frac{J_{p_1}}{R_{e_1}}\cos(\eta) \ , \quad N^* = N_{\dot{\delta}} + VS^*\cos(\phi_0) \ . \tag{B.131}
$$

Appendix C

WHEELED VEHICLES FOR EXTRATERRESTRIAL ENVIRONMENTS

Humankind has been exploring space surrounding its home planet, the Earth, and the nearest celestial bodies since the late 1950s. Such exploration is not an occasional enterprise, but the beginning of a trend that will see our species build a true spacefaring civilization, one based on many worlds, initially in our solar system and then beyond it.

There is no doubt that the great difficulties now being encountered and those that will emerge in the future will make this expansion a slow one, requiring decades or more likely centuries to yield important results. Owing to the size of the Universe, it is an expansion that will never end. Certainly it will require technological advancements that today cannot even be imagined. But it is also true that such difficulties are only partially technological. Economical, social and political factors will play an even more significant role.

Beginning with the first experiences of robotic and human exploration of other celestial bodies, a need was felt for vehicles able to carry instruments, objects of various kinds and finally the explorers themselves.

The vehicles for planetary exploration used up to now have all been robotic vehicles operating on wheels, designed and built using technologies that have little in common with standard automotive technologies. This is due in part to their small size and above all to their low speed, which ranges from a maximum of 1,5 km/h, for the Lunokhod, to some tens of m/h, for the automatic vehicles used for Mars exploration.

At these speeds suspensions based on spring and damper systems are not necessary, although articulated systems to suitably distribute the load on the ground were needed, because all these vehicles have more than 3 wheels.

Kinematic steering is more than adequate to control the trajectory.

The only exception is the vehicle used in the last *Apollo* missions to grant the needed mobility to the astronauts. Even if more than 30 years have passed since this vehicle was used, it remains an interesting case.

C.1 THE LUNAR ROVING VEHICLE (LRV) OF THE APOLLO MISSIONS

The LRV is an electric four wheel drive and steering (4WDS) vehicle able to carry two people in space suits at a speed of 18 km/h for a maximum distance of 120 km (Fig. C.1).

The main characteristics of the LRV were[1]

- Mass: 210 kg,
- Payload: 450 kg,
- Length (overall): 3,099 mm,
- Wheelbase: 2,286 mm,
- Track: 1,829 mm,
- Maximum speed: 18 km/h,
- Maximum manageable slope: 25°,

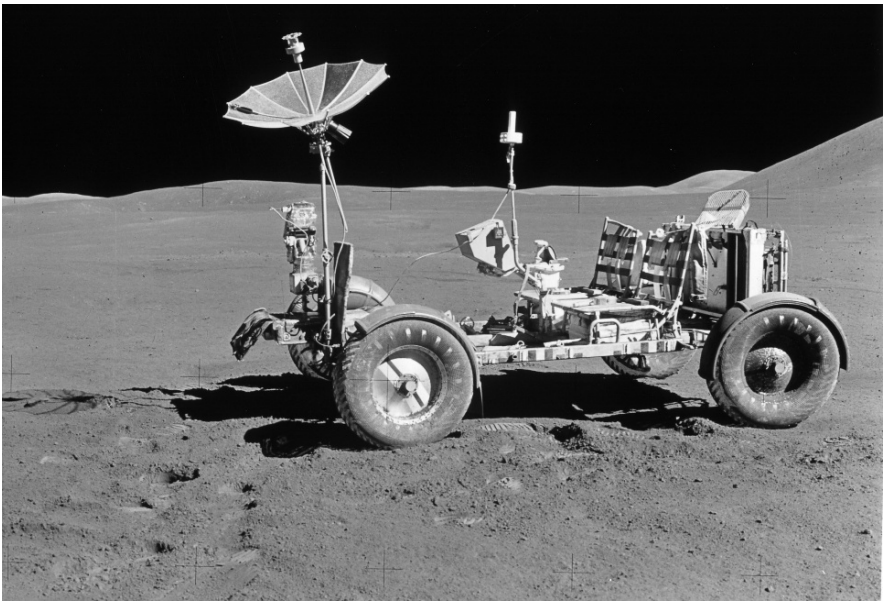

FIGURE C.1. The *Lunar Roving Vehicle* (LRV) of the last three *Apollo* missions on the Lunar surface (NASA image)

[1]A. Ellery, *An Introduction to Space Robotics*, Springer Praxis, Chichester, 2000, – – –, *Lunar Roving Vehicle Operations Handbook*, ttp://www.hq.nasa.gov/office /pao/History/alsj/lrvhand.html.

- Maximum manageable obstacle: 300 mm height,
- Maximum manageable crevasse: 700 mm length,
- Range: 120 km in four traverses,
- Operating life: 78 h.

At the time it was designed the LRV was a concentrate of high automotive technology adapted to the peculiar operating conditions that could be found on the Lunar surface. It marked the first time a vehicle with four steering and driving wheels was built, with each wheel having its own motor in the hub. Steering was by wire.

The project was deeply conditioned by the mass and size constraints driven by the need to be carried to the Moon along with the astronauts by the *Lunar Excursion Module* (LEM). Apart from the need to minimize its structural mass, these constraints forced designers to use a foldable architecture; it is likely that these considerations were determinant in the use of a by-wire configuration, in that era a completely immature technology.

A short analysis of the various subsystems and some considerations on what is still viable today and what, on the contrary, has been out-paced by technological advances, is reported in the following sections.

C.1.1 Wheels and tires

Pneumatic or solid rubber tires were discarded primarily to reduce the vehicle mass. In their place tires made with an open steel wire mesh, with a number of titanium alloy plates acting as treads in the ground contact zone, were built. Inside the tire a smaller, more rigid frame acted as a stop to avoid excessive deformation under high impact loads. The outer diameter of the tire was 818 mm.

Although the possibility of using standard pneumatic tires on a planet without an atmosphere may be raised, the lack of air is not the point. The short duration of use predicted (a single mission and few working hours) allowed such an innovative technology to be chosen without the need to perform long duration tests. In future missions aimed at building permanent outposts, things will be different and more traditional solutions may be needed. It must be noted that the version of the vehicle used to train the astronauts on Earth had standard pneumatic tires.

C.1.2 Drive and brake system

The LRV had 4 independent, series wound DC brush electric motors mounted in the wheel hubs together with harmonic drive reduction gears[2]. Each motor

[2] *Harmonic drives* are reduction gears based on a compliant gear wheel that meshes inside an internal gear having one tooth more than the former wheel. An eccentric (wave generator)

was rated 180 W, with a maximum speed of 17,000 rpm. The gear ratio of the harmonic drives was 80:1. The nominal input voltage was 36 V, controlled by PWM from the Electronic Control Unit. The drive unit was sealed, maintaining an internal pressure of about 0.5 bar for proper lubrication and brush operation.

The energy needed for motion was supplied by two silver-zinc primary batteries with a nominal voltage of 36 V and a capacity of 115 Ah (4,14 kWh) each. The use of primary batteries derives from the fact that each vehicle had to be used for a single mission, and for a limited time.

The LRV had four cable actuated drum brakes directly mounted on the wheels. As will be seen later, braking torques are low in vehicles operating in low gravity conditions and drum brakes are a reasonable solution. They are also preferable because of dust, which may create problems for disc brakes because they are more exposed to external contamination. Even if the braking power is much smaller than that typical of vehicles used on Earth, the lack of air may cause overheating problems.

The driver interface for longitudinal control was the same T handle that actuated the steering. Advancing the joystick actuated the motors forward. Pulling it back actuated reverse, but only if the reverse switch were engaged. Actuating the brakes required the handle to be pivoted backward about the brake pivot point.

The wheels could be disengaged from the drive-brake system into a free-wheeling condition.

C.1.3 Suspensions

Suspensions were fairly standard SLA suspensions, with the upper and lower arms almost parallel. No anti-dive or anti-squat provisions seem to have been included. Springs were torsion bars applied to the two arms, while a conventional shock absorber was located as a diagonal of the quadrilateral. The ground clearance varied from full load and unloaded conditions by 76 mm (between 356 and 432 mm). These values yield a vertical stiffness of the suspension-tire assembly of 2.40 kN/m, a very low value. Assuming that the tire was much harder than the suspension, the natural frequency in bounce was just 0.6 Hz for the fully loaded vehicle or 1.1 Hz in empty conditions.

C.1.4 Steering

Steering controlled all wheels and was electrically actuated (steer by wire). The geometry was designed with kinematic steering in mind: Ackermann steering on each axle and opposite steering of the rear axle with equal angles at front

---

deforms the first wheel so that for each revolution of the eccentric the flexible wheel moves by one pitch. Very high gear ratios can thus be obtained while maintaing good efficiency and little backlash, but the high cost of such devices allows their use only in selected applications, primarily in robotics.

and rear wheels. The kinematic wall-to-wall steering radius was 3.1 m. Each steering mechanism was actuated by an electric motor through a reduction gear and a spur gear sector; in case of malfunction of one of the two steering devices, the relevant steering could be centered and blocked and the vehicle driven with steering on one axle only.

The same T handle controlling the motors and brakes operated the steering by lateral displacement. A feedback loop insured that the wheels were steered by an angle proportional to the lateral displacement of the handle, but there was no force feedback except for a restoring force increasing linearly with the steering angle up to a 9° handle angle, then increasing with a step and finally increasing again linearly with greater stiffness.

Steering control may be the most outdated part of the LRV, although in a way it was a forerunner of the 4WS and steer by wire systems currently available. The 4WS logic was based strictly on kinematic steering. The low top speed justifies this choice, but only to a point: The low gravitational acceleration of the Moon implies that sideslip angles are much higher, for a given trajectory and a given speed, than on Earth. The very concept of kinematic steering is thus applicable only at speeds much lower than on Earth. Because centrifugal acceleration is proportional to the square of the speed, the top speed $V_{max} = 18$ km/h is equivalent, from this viewpoint, to the speed at which dynamic effect starts to appear. No modern 4WS vehicle has such prominent rear axle steering. Today a much more sophisticated rear steering strategy is present in even the simplest vehicle with all-wheel steering.

A second difference is that today steer by wire systems are reversible and the driver interface is haptic, i.e. there is an actuator supplying a feedback that allows the driver to feel the wheel reaction, as in conventional mechanical steering systems. The fact that it is possible to drive without a feedback is proven by the fact that vehicles in videogames and radio controlled model cars can be operated (the control of the LRV has surprising similarities with that of R/C model cars) but it is considered unsafe and difficult to operate a full size car in this way. Because *Apollo* astronauts needed much training to operate the LRV, a purposely designed trainer simulating its performance had to be built, it being impossible to operate the lunar vehicle on Earth.

C.2 TYPES OF MISSIONS

The types of missions requiring the use of vehicles on celestial bodies can be tentatively subdivided into the following classes[3].

1. Robotic exploration missions
2. Robotic exploitation missions

[3]G. Genta, M. A. Perino, *Teleoperation Support for Early Human Planetary Missions*, New Trends in Astrodynamics and Applications II, Princeton, June 2005.

3. Human exploration missions with robotic rovers to help humans in exploration duties

4. Human exploration missions with vehicles to enhance human mobility

5. Human exploration-exploitation missions requiring construction-excavation devices.

Vehicle for unmanned missions (1 and 2) are usually very small and slow, more similar to moving robots than to vehicles, while those for missions 2 and 5 are more similar to earth moving and construction machinery. Even if a good knowledge of vehicle dynamics is needed to design them properly, these are machines having little in common with automotive technology. Missions of type 3 require small machines, more similar to robots than to vehicles.

Missions of type 4 require true vehicles that may differ from those used on our planet due to the different environmental conditions in which they must operate. But because the goal is essentially the same, namely to transport personnel and goods from one place to the other, with the required velocity and safety and in an economical and energetically efficient way, there will be many points in common.

The first essential difference is that of operating in an environment in which human life is impossible without suitable protection. The designer has to chose between two alternatives: A simple mobility device, without any life-support capability, whose task is to carry humans protected by their own space suit, and a vehicle providing a true shirt-sleeve environment.

The first solution, like the LRV, allows the us of small and very light vehicles, the minimum size being that of a city car. Vehicles of the second type, which are true mobile habitats, are larger and more complex machines. A modular approach may be followed, with a chassis containing all devices offering the required mobility, on which a habitat may be mounted. Current vehicles similar to this solution are military vehicles in which the inner space is completely insulated from the outside to provide some protection from chemical or bacteriological attacks. The smallest size for vehicles of this type is that of a small van.

C.3 ENVIRONMENTAL CONDITIONS

The first difference between Earth and other celestial bodies is gravitational acceleration. All celestial bodies to be explored (with the exception of Venus, where $g = 8,87$ m/s^2, but whose environment is so difficult in terms of temperature, atmospheric density and pressure that no operation on its surface is planned in the foreseeable future) are characterized by a gravitational acceleration much lower than that of Earth. (Table C.1).

All asteroids except the largest have a very low gravitational acceleration, and their irregular form causes the gravitational acceleration to be variable from

TABLE C.1. Values of the gravitational acceleration, in m/s^2, on the surface of the Moon, some rocky planets, satellites of giant planets and asteroids.

Planets	Mars	3,77	Mercury	3,59
Satellites	Moon	1,62		
	Io	1,80	Europa	1,32
	Ganimedes	1,43	Callisto	1,24
	Titan	1,35	Triton	0,78
Asteroids	Pallas	0,31	Vesta	0,28
	Ceres	0,26	Juno	0,09

place to place and not perpendicular to the ground. For instance, the gravitational acceleration on Eros varies between 0.0023 and 0.0055 m/s^2.

A low gravitational acceleration g has some advantages, from the possibility of human explorers carrying very bulky life support equipment to reduced structural stresses and to reduced power requirements for motion. Another important advantage is that the weight the vehicle-ground contact must carry is low, making floating possible. But performance of vehicles whose mobility is produced by friction forces is drastically reduced.

Although this does not limit mobility in a strict sense, i.e. the possibility for the vehicle to move, it does lower the longitudinal and lateral acceleration of the vehicle and the top speed it can travel. The maximum longitudinal and lateral accelerations of the vehicle can be assumed to be proportional to the gravitational acceleration, if the ideal braking and steering approach is used.

The second point is the thin atmosphere. On the Moon there is no atmosphere at all, as is true of all asteroids, comets and most satellites of the outer planets. The atmosphere on Mars is so thin that it can be neglected when dealing with ground locomotion, although thick enough to support aerodynamic vehicles or balloons. The only body among those mentioned in Table C.1 having an atmosphere comparable in density to Earth is Titan.

The lack of an atmosphere with a non-negligible density means no aerodynamic drag and thus no constraint to the outer shape of the vehicle. This may, however, be a negligible advantage if the speed of the vehicle is low due to poor traction. Moreover, the lack of an atmosphere makes it impossible to use aerodynamic forces to increase the forces on the ground and thus traction.

A third point is the absence of humidity. The Moon, Mars and asteroid surfaces are completely of from water. Because the presence of mud produces the most difficult mobility for wheeled vehicles, this is without any doubt a positive feature. The surfaces of comets and outer planets' satellites are rich in ice but conditions are such that the ice is far from its melting point and the pressure of the vehicle on the ground is low. The surface of the ice does not melt under the wheels, offering good traction in these conditions. The soil of Titan may contain liquid hydrocarbons, but it is unknown whether these produce conditions similar to muddy ground on Earth.

A final point is the absence of products of biological origin, important in giving the peculiar characteristics to the wide variety of soils that can be found on Earth. Celestial bodies likely to be explored first are covered with regolith, pulverized rock and gravel, with characteristics that are less variable than those of soils encountered on Earth.

The Moon, for instance, is covered with a layer of regolith about 2 or 3 m thick on the so-called maria and 3 to 16 m thick on the highlands. The mean size of grains varies between 40 and 270 μm, with a preponderance of the smallest size. The porosity of the soil is high at the surface ($40 \div 43\%$), leading to a density as low as about 1000 kg/m^3. Porosity reduces with depth and only 200 mm below the surface the density doubles to about 2000 kg/m^3.

The most important parameter for locomotion is the cohesive bearing strength, which is about 300 Pa on the surface, increasing about ten fold at 200 mm depth[4].

Maria are fairly flat, offering few obstacles and a good mobility, as demonstrated by the last *Apollo* missions. On the highlands, on the other hand, there are many craters and mountains with high slopes and obstacles. To travel through them expeditiously it will be necessary to prepare tracks as soon as the first outposts are built.

The surface of Mars is also covered with regolith, with even thinner grains owing to a more complex geological history, with erosion due to water (present in very ancient times) and wind. The types of obstacles are much more varied than on the Moon, and mobility may be quite difficult above all in the zones that are more scientifically interesting, owing to ravines, canyons, cliffs and boulders of all sizes.

C.4 MOBILITY

The low value of the pressure on the ground and the lack of water, and thus of mud, make the use of tracks less convenient than on Earth. The choice of wheeled vehicles is also suggested by their lower mass (until it is possible to build vehicles there, vehicles will be carried from Earth), complexity and energy consumption, along with their greater reliability. Other solutions, such as legged vehicles, were often considered for robots, but never for transportation vehicles.

The experience gained with the LRV confirms these considerations: That vehicle never experienced mobility problems and showed no tendency to sink into the regolith. All the pictures taken on the Moon show that the wheels of the vehicle, even when fully loaded, ride lightly on the surface (Fig. C.2a).

The sinking of a wheel with a contact area 100 mm in width is plotted versus the pressure on the ground for 3 different values of the friction angle in Fig. C.2b. The ratio between tractive and normal force F_t/F_n, in conditions of

[4] A. Ellery, *An Introduction to Space Robotics*, Springer Praxis, Chichester, 2000.

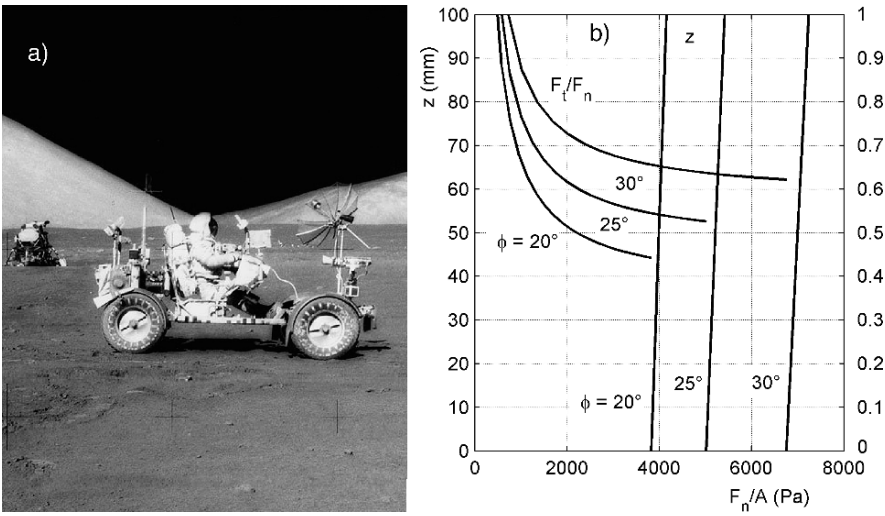

FIGURE C.2. a) Image of the Lunar Rover (LRV) with astronaut Eugene Cernan on board taken during the third extra-vehicular activity (EVA) in the *Apollo* 17 mission (NASA image). b): Sinking z and ratio between tractive and normal force F_t/F_n as functions of the normal pressure on the ground for 3 different values of the friction angle for a wheel 100 mm wide

no sinking[5] is also reported versus pressure in the same figure. The values of the friction angle here considered are reasonable, owing to the lack of humidity.

The carrying capacity of the ground seems to be low, but it is more than enough to support quite a massive vehicle owing to low gravity. Moreover, the density and the cohesive strength of regolith increase with depth. Thus the carrying capacity increases quickly with small values of sinking, much more than that shown in the figure. The figure was plotted assuming that the properties of the ground are constant, equal to those characterizing the surface layer.

Finally, rolling resistance is expected to be quite low, owing to the limited sinking. Its order of magnitude should be similar to that found on roads with a natural surface on Earth and thus, for a pneumatic wheel, f_0 should be about 0,05.

Similar considerations should also hold for Mars, where the soil is also composed of dry regolith.

In terms of obstacle management, wheels can manage at low speed obstacles whose height is on the order of magnitude of their radius or more if particular types of suspensions are used, and can traverse ditches whose width is no more than 70% of their diameter, unless the vehicle layout allows operation with some wheels off the ground.

[5]G. Genta, *Design of Planetary Exploration Vehicles,* ESDA 2006, Torino, Luglio 2006.

C.5 BEHAVIOR OF VEHICLES IN LOW GRAVITY

As previously stated, the primary difference between operating a ground vehicle on Earth and on the Moon or Mars or the other bodies to be explored is low gravity. In vehicles using friction forces to propel and brake the vehicle or control its trajectory, performance depends upon the forces exerted on the ground and, if no aerodynamic force is present, on weight. In the following sections only ideal conditions will be considered; i.e. it is assumed that all wheels work with the same longitudinal or side force coefficient.

C.5.1 Longitudinal performance

The deceleration that a vehicle may develop in ideal braking conditions is

$$\frac{dV}{dt} = \mu_x g \ . \tag{C.1}$$

It follows that if the longitudinal force coefficient μ_x is equal to 0.5, a reasonable value on non-prepared ground, the maximum deceleration that may be obtained on the Moon ($g = 1,62$ m/s^2) is 0,8 m/s^2. Obviously the deceleration the vehicle may actually reach is lower, and may be computed in the usual way.

Load transfer does not depend upon the gravitational acceleration, but only upon the longitudinal force coefficient: If a vehicle brakes with a certain value of μ_x, it has the same load shift (obviously in a relative sense) on Earth and on the Moon. The curve $\eta_f(\mu_x)$ is then the same, for a given braking system. Note that the variability of μ_x may be lower on the Moon than on Earth, because it is influenced by the presence of water or ice on the ground (possible only on Earth). A good knowledge of the lunar ground thus makes it possible to design braking system operating at higher efficiency than usual.

The distance needed to stop the vehicle, computed assuming uniformly decelerated motion for values of the deceleration included between 0,2 and 1 m/s^2, is shown in Fig. C.3.

The same holds for acceleration: On Earth the limitations in acceleration are set primarily by the available power, except for very powerful vehicles or extremely poor road conditions; on the Moon it is likely that the limitations come from the power that can be transferred to the ground. A layout with all wheel drive is advisable to ensure reasonable performance in acceleration.

The low traction available and the simultaneous presence of longitudinal load transfer makes the use of ABS and traction control devices necessary, even more so than on Earth, although the lessened variability of ground characteristics make these systems less useful.

Reduced gravitational acceleration has no effect on the ability to manage slopes, but does reduce the required power. The steepest slope that can be managed by a 4WD vehicle, assuming ideal driving conditions (i.e. that all wheels work with the same longitudinal force coefficient) is given by the usual formula

$$\tan(\alpha_{max}) = i_{max} = \mu_{x_p} \ . \tag{C.2}$$

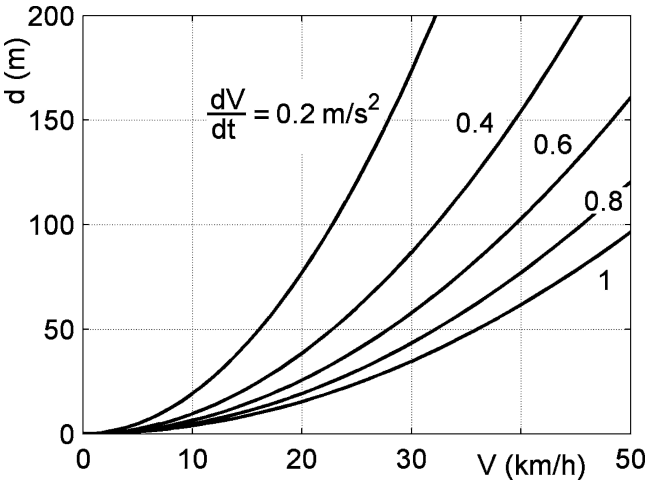

FIGURE C.3. Distance needed to stop the vehicle at constant deceleration versus the speed for values of the deceleration included between 0,2 and 1 m/s^2.

Assuming a value of the force coefficients $\mu_x = 0.5$, a maximum slope $\alpha_{max} = 27°$, i.e. a 46% grade, is obtained. This can, however, be obtained only in ideal conditions, and only when using accurate slip control of the wheels.

Taking the difference of the force coefficient at the front and rear wheels into account, if the height of the center of mass on the ground is $h_G = a/2$, the values $\alpha_{max} = 22°$, corresponding to $i_{\max} = 38\%$, are obtained for a 4WD vehicle. These values are fairly good, particularly if the low value of the force coefficient used is considered.

The specific power in W/kg (kW/ton) needed to travel on a slope on the Moon is reported in Fig. C.4 as a function of the slope. A power of just 2 kW allows a 1 ton vehicle to travel on level road at more than 50 km/h and to overcome a 40 % grade at 10 km/h.

C.5.2 Handling

Referring to the concept of ideal steering, if there are no aerodynamic forces and the road is level, the maximum centrifugal acceleration is

$$\frac{V^2}{R} = g\mu_y \ , \tag{C.3}$$

where the value of μ_y is that of the whole vehicle. The relationship between the minimum radius of the trajectory and the speed in the lunar environment for various values of μ_y is shown in Fig. C.5. It has been assumed in plotting the figure that the value of μ_y for the vehicle is 70% of that referred to the tires.

Again, in spite of the poor performance, the transversal load transfer is not less than on Earth, with higher centrifugal accelerations but the same value of

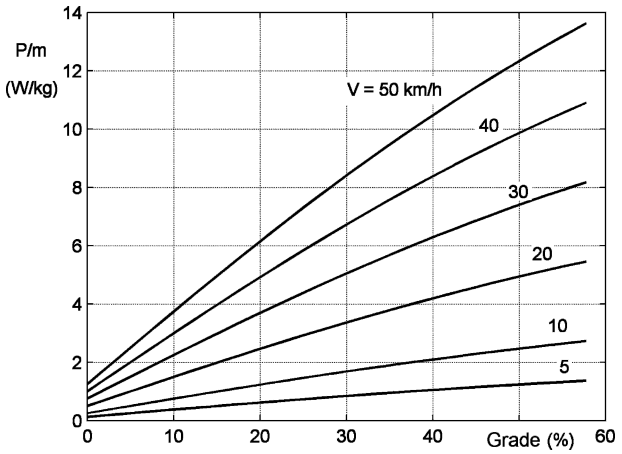

FIGURE C.4. Specific power in W/kg (kW/ton) needed to travel on a slope on the Moon at various speeds, with $f_0 = 0,05$ and $\eta_t = 0,9$.

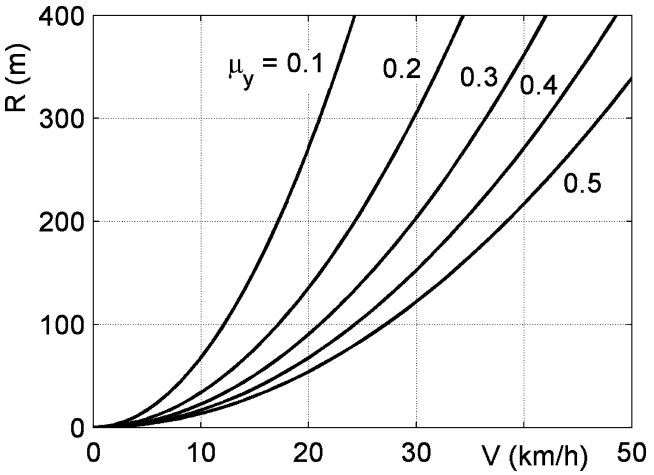

FIGURE C.5. Relationship between the radius of the trajectory and the maximum speed for a vehicle on the Moon with different values of the cornering force coefficient μ_y. The sliding factor is assumed to be 70% of the cornering force coefficient of the wheel

the force coefficient μ_y. The only point is that the tires are likely to be oversized owing to the low load (see below), and may work in the part of the $C(F_z)$ (cornering stiffness-load) curve where load transfer is less important, at least using linearized models.

In spite of the low speed, the very low cornering forces available may make the use of modern stability enhancement (ESP, VDC, etc.) systems worthwhile.

C.5.3 Comfort

Comfort is little influenced by the gravitational acceleration of the planet on which the vehicle moves: The criteria for bounce and pitch motions, suspension damping and other suspension characteristics developed for vehicles on Earth hold on other worlds. There is even an advantage: One limitation to spring softness in vehicular suspensions comes from the need to limit suspension travel with changing load. In low gravity, if the springs are designed with dynamic considerations in mind, the static deflection under load is small presenting no constraints upon suspension softness. The only limit in this area is the need to avoid bounce and pitch frequencies that are too low. These may cause motion sickness.

The human side is another matter. We know little about how a human body accustomed to no gravity after a few days of space travel will react to vibration under low gravity conditions. The usual guidelines may not apply as they do on Earth. The LRV, for example, had a bounce frequency in full loaded conditions that was too low for comfort, but it is not known that any astronaut suffered from motion sickness while driving on the Moon. Further studies are needed, but they must be conducted on site, because low gravity cannot be properly simulated on Earth.

However, low gravity does cause an unwanted effect on bounce and pitch motion: The wheels tend to lift from the ground, as is apparent in the movies taken in the *Apollo* missions[6]. It is obvious that at reduced gravitational acceleration, inertia forces become more important with respect to weight, causing the difficulty in maintaining a good wheel-ground contact when travelling on uneven ground to increase. This effect can be evidenced by plotting the ratio between the minimum vertical force (static value minus amplitude of the dynamic force) and the static force as a function of the frequency when driving on a road with a harmonic profile of a given amplitude.

A plot of this type for a quarter car with two degrees of freedom with a sprung mass of 240 kg, unsprung mass of 38 kg, tire stiffness 135 kN/m, suspension stiffness 15,7 kN/m and optimum damping (1,52 kNs/m) is shown in Fig. C.6. The results for the lunar environment are compared with those obtained for Earth.

From the figure it is clear that while on Earth the suspension maintains contact with the ground even at an amplitude of 10 mm, on the Moon an amplitude as small as 2 mm causes the wheel to bounce at a frequency of about 9 Hz. For larger amplitudes, the contact of the wheel on the ground is quite uncertain, with ensuing reduction of the already poor traction and cornering forces. This problem may be lessened by increasing the damping of the shock absorber or decreasing the stiffness of the spring, but this would in turn lessen comfort.

---

[6]If a further clue were needed, those moves demonstrate that the astronauts were actually on the Moon. At the speed reached by the LRV, the dynamic behavior of the vehicle is inconsistent with conditions on Earth.

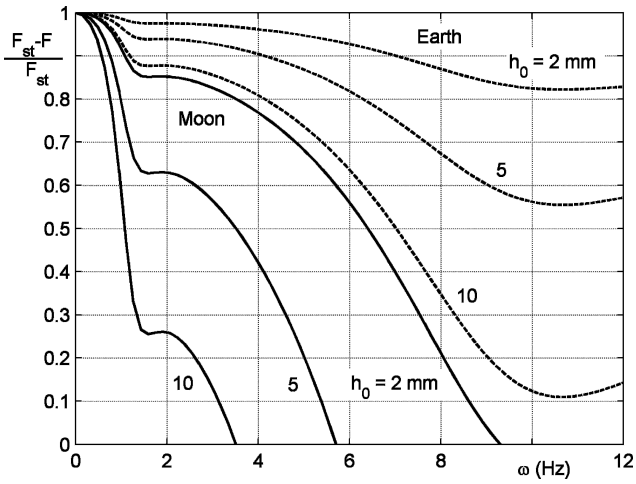

FIGURE C.6. Ratio between the minimum vertical force on the ground and the static force for a quarter car model as a function of the frequency when driving on Earth (dashed lines) and on the Moon (full lines) on a road with harmonic profile at a given amplitude h_0.

The ground contact problem could suggest the use of at least semi-active suspensions, or even fully active ones. An interesting possibility is the use of electromagnetic damping because of the difficulties of cooling standard shock absorbers in the vacuum of space (Moon) or in a very thin atmosphere (Mars).

C.6 POWER SYSTEM

Travelling in low gravity conditions requires much less power than on our planet: Rolling resistance is much lower, aerodynamic drag is absent (and at low speeds like those that can be reached in these conditions it would be negligible even in an Earth-like atmosphere). Low traction prevents accelerations requiring high power from being obtained.

The low top speed, linked to the difficulties in acceleration, braking and cornering, reduces the power requirements in unstationary conditions. In these conditions electric drive powered by batteries seems to be a good solution, especially because the cost problems that prevent the use of high performance batteries on normal vehicles are much less important. If the vehicle must be used for prolonged periods of time, rechargeable batteries will be used instead of the primary batteries used on the LRV. They will be charged by the solar (or better nuclear) power system of the outpost.

An alternative may be fuel cells, using locally produced oxidizer and fuel.

Other more conventional solutions, such as internal combustion engines of a more or less traditional type fed by locally produced fuel are also viable. On

Mars, for instance, production of oxygen and methane from ice, surely present in many places on the planet, and from the abundant atmospheric carbon dioxide seems a good choice.

Radioisotope thermoelectric generators (RTG) may be a good choice for small vehicles, while larger ones may use, at least in principle, a small nuclear reactor directly, even if the use of batteries recharged from a stationary reactor seems more convenient.

Some power is also needed for thermal control. On the Moon, for instance, thermal excursions are extreme and the vehicle, even if not operating, must be protected from the cold during a night that lasts 14 days. The thermal control systems are not different from those used on space vehicles, and will not be dealt with here. The same is true of life support systems, although these may not be a part of the vehicle, but may be a part of the habitat carried on board.

C.7 CONCLUSIONS

The examples above dealt mostly with the Moon, the body where the most likely need for ground transportation will first arise. On Mars the effects will be less severe, but the situation will be more or less similar.

When vehicles for the exploration and the exploitation of asteroids are designed, significantly different problems will be encountered, because of the low gravitational acceleration and the small size of these bodies. The first feature makes it necessary to proceed with extreme caution to ensure that inertial forces do not make the vehicle lift off and become lost in space. The second makes it useless to move at speeds above a low value. It is likely that vehicles used on asteroids and comets will have little in common with automotive technology and will be small space vehicles.

On the other hand, the vehicles that will carry explorers and then colonists on the surface of the Moon and then on Mars will be essentially similar to motor vehicles and their designers will need a good knowledge of automotive technology. Unlike of what was feared in 1960, lunar and martian soil is not at all difficult and, at least in the flatter zones, offers good carrying capacity and fair traction because of the lack of humidity. There is no problem in moving at moderate speed, even without building permanent infrastructures.

It will be harder to reach places in more difficult areas, which on Mars are the most interesting from a scientific viewpoint, and it is likely that it will be necessary to build, at the least, dirt roads or tracks.

Worse problems will be encountered when mobility at higher speed is necessary. Here the worst problems will come from the low gravitational acceleration. Roads with a good surface and large radii may be a partial solution, but it is likely that other approaches will be followed, such as hopping vehicles (performing parabolic flights is not energetically infeasible, owing to low gravity), and above all guided vehicles on rails or, more likely, maglev vehicles. The latter may

be particularly suitable to low gravity conditions, but these are solutions for a more distant future, when traffic density will justify building costly infrastructures.

In the short and medium term robotic and manned vehicles will be based on more or less standard automotive technology, benefiting from the recent advances of the latter. Drive and brake by wire may allow performance satisfying the needs of planetary exploration with the required safety, while semi-active and active suspensions will increase comfort to acceptable levels.

Appendix D
PROBLEMS RELATED TO ROAD ACCIDENTS

As discussed in Part III, the cost of accidents due to the use of motor vehicles, both in terms of human lives and economic losses, is quite high. the goal of increasing the safety of motor vehicles is generally considered a technical and social priority.

The actions taken to reduce both the number and severity of accidents are both technical and legal and involve many disciplines. Automotive engineers are involved both in the design of the vehicle and, as a consultant of courts or law makers, in the reconstruction of accidents. Their aim is to ascertain responsibilities and introduce into the standards and rules those provisions necessary to prevent accidents or reduce their consequences.

It must be noted that the reconstruction of an accident is often a difficult task. The expert, who usually acts as a consultant of the court or of one of the persons involved, may have only a partial knowledge of the situation. The only known data are in many cases the positions of the vehicles after the accident plus any marks that may remain on the road, and sometimes even these are uncertain and affected by large errors. A road accident, occurring in a very short time and usually in an unexpected way, can have a large psychological impact on witnesses and protagonists. This, together with the limited technical knowledge of the persons involved and the economic interests at stake, may make the reports of witnesses difficult to interpret and weigh correctly, particularly when they lead to conflicting reconstructions.

The traditional methods used in the reconstruction of accidents are based on rough approximations, which are, however, justified by the uncertainties and sometimes the quick variations of the parameters of the problem. Only the use of more elaborated numerical models, implemented on computers, can produce higher accuracy.

D.1 VEHICLE COLLISION: IMPULSIVE MODEL

A frequent scenario in the reconstruction of accidents is a collision between vehicles or between a vehicle and an obstacle. The simplest model deals with the collision as an impulsive phenomenon, i.e., it assumes that the time during which the vehicles remain in contact (typically on the order of 0.1 s) is vanishingly short and that the forces they exchange are infinitely large. Mathematically the forces may be represented by a Dirac impulse function. Their study is based on the momentum theorem, stating that the variation of the momenta of the vehicles is equal to the impulse of the forces they exchange.

Because the forces the vehicles exchange during the collision are larger by orders of magnitude than the other forces acting on them, this approach is quite correct, even if it has the disadvantage of not allowing us to study what happens during the impact but only how the motion changes between instant t_1 preceding the collision and instant t_2 following it.

Remark D.1 *It is meaningless to ask what happens during a phenomenon whose duration is zero by definition.*

D.1.1 Central head-on collision

The simplest case is that of a head-on collision in which the velocities of the centres of mass of the vehicles lie along the same straight line (Fig. D.1a). Actually, if the velocities $\dot{x}_A$ and $\dot{x}_B$ have the same sign a rear collision occurs while a head-on collision is characterized by opposite signs of the velocities.

The relative velocity

$$V_R = \dot{x}_B - \dot{x}_A \tag{D.1}$$

must be negative; otherwise the vehicles do not approach each other.

During the collision the absolute value of the relative velocity decreases between times t_1 and time t_i, when the centres of mass are at their minimum distance. In the rebound phase, between times t_i and t_2, the relative velocity

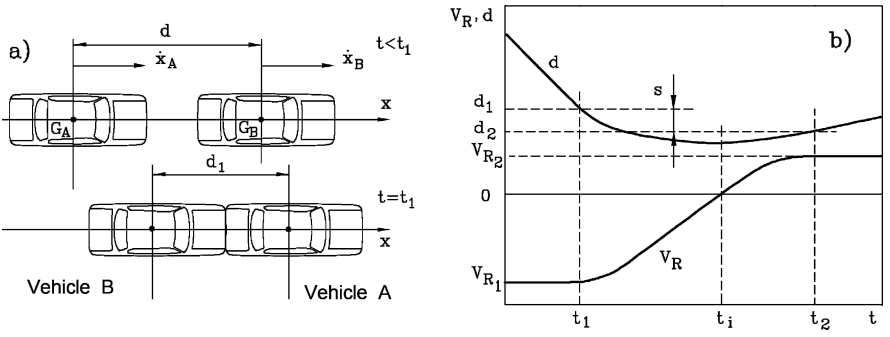

FIGURE D.1. Central head-on collision. (a) Situations before the collision and at time t_1; (b) relative velocity and distance between the centres of gravity as functions of time.

becomes positive (Fig. D.1b). The distance between the centres of mass is plotted in the same figure. The final crush s of the vehicles is the difference between d_1 and d_2.

As already said, however, the impulsive model does not show what happens between t_1 and t_2. The conservation of momentum allows the relationship to be written as

$$m_A \dot{x}_{A_1} + m_B \dot{x}_{B_1} = m_A \dot{x}_{A_2} + m_B \dot{x}_{B_2} \ . \tag{D.2}$$

Because the collision is generally inelastic, the kinetic energy is not conserved

$$\frac{1}{2} m_A \dot{x}_{A_1}^2 + \frac{1}{2} m_B \dot{x}_{B_1}^2 \geq \frac{1}{2} m_A \dot{x}_{A_2}^2 + \frac{1}{2} m_B \dot{x}_{B_2}^2 \ ; \tag{D.3}$$

the two sides being equal in the case of a perfect elastic collision.

The position and the velocity of the centre of mass of the system made by the two vehicles are simply

$$x_G = \frac{m_A x_A + m_B x_B}{m_A + m_B} \ , \tag{D.4}$$

$$\dot{x}_G = \frac{m_A \dot{x}_A + m_B \dot{x}_B}{m_A + m_B} \ . \tag{D.5}$$

A consequence of the conservation of the momentum is the conservation of the velocity of the centre of mass of the system:

$$\dot{x}_{G_1} = \dot{x}_{G_2} \ .$$

The velocities of the vehicles can thus be expressed as functions of the velocity of the centre of mass, which remains constant, and of the relative velocity, a function of time

$$\dot{x}_A = \dot{x}_G - V_R \frac{m_B}{m_A + m_B} \ , \qquad \dot{x}_B = \dot{x}_G + V_R \frac{m_A}{m_A + m_B} \ . \tag{D.6}$$

The kinetic energy of the system can thus be written in the form

$$\mathcal{T} = \frac{1}{2} \left[\dot{x}_G^2 (m_A + m_B) + V_R^2 \frac{m_A m_B}{m_A + m_B} \right] \ . \tag{D.7}$$

As the velocity of the centre of mass is constant, the maximum energy dissipation occurs when the relative velocity vanishes. It is therefore possible to state a lower and an upper bound to the kinetic energy after the collision

$$\frac{1}{2} \dot{x}_G^2 (m_A + m_B) \leq \mathcal{T}_2 \leq \frac{1}{2} \left[\dot{x}_G^2 (m_A + m_B) + V_{R_1}^2 \frac{m_A m_B}{m_A + m_B} \right] \ . \tag{D.8}$$

The minimum kinetic energy (expression on the left) occurs when the collision is perfectly inelastic and the two vehicles remain attached to each other.

In the case of a perfectly elastic collision, the absolute value of the relative velocity after the impact is equal to that at time t_1:

$$V_{R_2} = -V_{R_1} \ .$$

A restitution coefficient e^* is usually defined as[1]

$$e^* = -\frac{V_{R_2}}{V_{R_1}} \ . \tag{D.9}$$

In case of a perfectly elastic collision $e^* = 1$, while $e^* = 0$ for inelastic impacts. In all actual impacts $0 < e^* < 1$.

The energy dissipated during the collision is then

$$\mathcal{T}_2 - \mathcal{T}_1 = \frac{1}{2}\frac{m_A m_B}{m_A + m_B}\left(V_{R_1}^2 - V_{R_2}^2\right) = \frac{1}{2}\frac{m_A m_B}{m_A + m_B} V_{R_1}^2 \left(1 - e^{*^2}\right) \ . \tag{D.10}$$

In the first part of the collision, from time t_1 to time t_i, the relative velocity decreases to zero and the kinetic energy reduces to a minimum, given by the expression on the left side of Eq. (D.8). The energy related to velocity V_{R_1} transforms partly into elastic deformation energy, with part of it dissipated as heat. In the second part of the collision, from time t_i to time t_2, a fraction of this energy is transformed back to kinetic energy. The ratio between the energy restituted in the second phase and that subtracted from the kinetic energy in the first is e^{*2}.

In motor vehicle collisions the value of e^* is low, typically in the range of $0.05 \div 0.2$ for impacts with large permanent deformations. It depends, however, on the relative velocity and may be higher in low speed collisions, tending to unity when no permanent deformations are left.

The velocities of the vehicles after the impact are

$$\begin{cases} \dot{x}_{A_2} = \dot{x}_{A_1} + m_B V_{R_1} \dfrac{1 + e^*}{m_A + m_B} \\ \\ \dot{x}_{B_2} = \dot{x}_{B_1} - m_A V_{R_1} \dfrac{1 + e^*}{m_A + m_B} \ . \end{cases} \tag{D.11}$$

D.1.2 Oblique collision

Seldom is the situation as described in Fig. D.1; usually the velocity vectors of each of the two vehicles do not pass through the centre of mass of the other as in Fig. D.2. If the collision is considered as an impulsive phenomenon, the conservation of momentum still holds

$$\begin{cases} m_A \dot{x}_{A_1} + m_B \dot{x}_{B_1} = m_A \dot{x}_{A_2} + m_B \dot{x}_{B_2} \\ \\ m_A \dot{y}_{A_1} + m_B \dot{y}_{B_1} = m_A \dot{y}_{A_2} + m_B \dot{y}_{B_2} \ , \end{cases} \tag{D.12}$$

[1]Symbol e^* will be used for the restitution coefficient instead of e to avoid confusion with the base of natural logarithms.

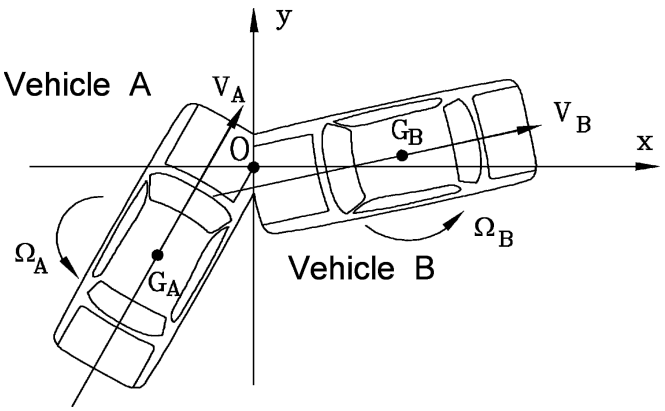

FIGURE D.2. Oblique collision.

but does not allow us to solve the problem of projecting the situation after the collision from that preceding it. Nor does the assessment of a coefficient of restitution allow us to obtain a solution, because the conditions to be stated are two and not one (Eq. (D.12) contains two conditions and 4 unknowns).

Assume that the contact surface at the moment of maximum deformation is flat and state a reference frame Oxy centred at point O in which the resultant of the contact forces is applied, with the x-axis perpendicular to the contact area. Note that the components of velocities V_i of the vehicles are plotted in the figure in the direction of the positive axes: Practically speaking, some of them are negative. The vehicles may also have an angular velocity Ω; if not at time t_1, then surely at time t_2.

The impulsive model implies that the duration of the impact is zero: It may thus be thought of as the collision between two rigid bodies, predeformed as shown in the figure.

The velocity of point O, considered as belonging alternatively to vehicle A and vehicle B, is

$$\vec{V}_{A_O} = \left\{ \begin{array}{l} \dot{x}_{G_A} - \Omega_A y_A \\ \\ \dot{y}_{G_A} + \Omega_A x_A \end{array} \right\}, \qquad \vec{V}_{B_O} = \left\{ \begin{array}{l} \dot{x}_{G_B} - \Omega_B y_B \\ \\ \dot{y}_{G_B} + \Omega_B x_B \end{array} \right\}, \tag{D.13}$$

where x_A, y_A, etc. are the coordinates of the centres of mass in the Oxy frame. Note that both x_A and y_A are negative in the figure.

The relative velocity of vehicle B with respect to vehicle A at point O is

$$\vec{V}_R = \vec{V}_{B_O} - \vec{V}_{A_O} = \left\{ \begin{array}{l} \dot{x}_{G_B} - \dot{x}_{G_A} - \Omega_B y_B + \Omega_A y_A \\ \\ \dot{y}_{G_B} - \dot{y}_{G_A} + \Omega_B x_B - \Omega_A x_A \end{array} \right\}. \tag{D.14}$$

The x component of the relative velocity, hereafter written as $V_{R_\perp}$ is the velocity at which the two surfaces approach each other, or better, move away

from each other, as a positive value means that the distance between the surfaces increases. The y component $V_{R_\parallel}$ is the velocity at which the surfaces slide over each other and can be either positive or negative.

As in the case of the central impact, it is possible to define a restitution coefficient

$$e^* = -\frac{V_{R_{\perp_2}}}{V_{R_{\perp_1}}} \ .$$

Each vehicle receives an impulse from the other that is equal to its change of momentum. Indicating with $\vec{I}$ the impulse received by vehicle A from vehicle B (the impulse received by vehicle B from vehicle A is then $-\vec{I}$), the momentum theorem applied to the two vehicles may be written in the form

$$\begin{cases} I_x = m_A \left(\dot{x}_{A_2} - \dot{x}_{A_1}\right) \\ I_y = m_A \left(\dot{y}_{A_2} - \dot{y}_{A_1}\right) \end{cases} \qquad \begin{cases} -I_x = m_B \left(\dot{x}_{B_2} - \dot{x}_{B_1}\right) \\ -I_y = m_B \left(\dot{y}_{B_2} - \dot{y}_{B_1}\right) \ . \end{cases} \tag{D.15}$$

Similarly the conservation of the angular momentum can be written in the form

$$\begin{cases} I_x y_A - I_y x_A = J_A \left(\Omega_{A_2} - \Omega_{A_1}\right) \\ \\ I_x y_B - I_y x_B = -J_B \left(\Omega_{B_2} - \Omega_{B_1}\right) \ . \end{cases} \tag{D.16}$$

A single relationship is still needed. It is possible to relate the components of the impulse in a direction perpendicular to the impact surface I_x to the tangential component I_y using a simple relationship

$$I_y = \lambda I_x \ , \tag{D.17}$$

where λ is a kind of friction coefficient in the zone where the two vehicles are in contact. Because the vehicles usually interlock with each other, its value may be far higher than that of an actual coefficient of friction. Moreover, its value changes in time and only an average value is required. Its sign is the same as that of ratio $V_{R_\perp}/V_{R_\parallel}$.

By introducing equations (D.15) and (D.16) into Eq. (D.14), it follows that

$$V_{R_{\perp_2}} = V_{R_{\perp_1}} - I_x \left(a - \lambda b\right) \ , \tag{D.18}$$

where

$$\begin{cases} a = \dfrac{1}{m_A} + \dfrac{1}{m_B} + \dfrac{y_A^2}{J_A} + \dfrac{y_B^2}{J_B} \\ \\ b = \dfrac{x_A y_A}{J_A} + \dfrac{x_B y_B}{J_B} \ . \end{cases}$$

The value of the x component of the impulse is then

$$I_x = V_{R_{\perp_1}} \frac{1 + e^*}{a - \lambda b} \ . \tag{D.19}$$

The direct problem, i.e. that of finding the conditions after the collision (time t_2) from those at time t_1 is now easily solved. Once the components $V_{R_{\perp_1}}$ and $V_{R_{\parallel_1}}$ are computed, the sign of λ is known and the impulse can be computed from equations (D.19) and (D.17). The velocities after the collision are thus computed through equations (D.15) and (D.16).

For the inverse problem, i.e. that of finding the conditions before the collision (time t_1) from those at time t_2, Eq. (D.19) can be modified as

$$I_x = -V_{R_{\perp_2}} \frac{1 + e^*}{e^* (a - \lambda b)} \tag{D.20}$$

and a procedure similar to the previous one can be followed.

The problem is the assessment of the values of coefficients λ and e^* and of the positions of the centres of mass of the vehicles with respect to point O, because the position of the latter cannot usually be evaluated with precision. It is possible to repeat the computation with different values of the uncertain parameters in order to define zones in the parameter space where the solutions must lie and to rule out possible reconstructions of the accident. Some solutions can be ruled out by remembering that $a - \lambda b$ must be positive, as both I_x and V_{i_1} are negative, if vehicle A is in the half plane with negative x.

D.1.3 Collision against a fixed obstacle

A particular case is that of the collision against a fixed obstacle (Fig. D.3). The equations seen above still apply, provided that

$$\frac{1}{m_B} = \frac{1}{J_B} = \dot{x}_B = \dot{y}_B = 0 \ ,$$

i.e. the fixed obstacle is considered as a vehicle with infinite mass travelling at zero speed.

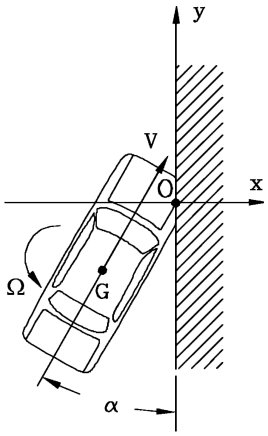

FIGURE D.3. Collision against a fixed obstacle.

It then follows that

$$\vec{V}_R = \left\{ \begin{array}{l} -V\cos(\alpha) - \Omega y_G \\ \\ -V\sin(\alpha) + \Omega x_G \end{array} \right\} , \tag{D.21}$$

$$I = \frac{mr^2(1+e^*)[-V_1\cos(\alpha) - \Omega_1 y_G]}{r^2 + y_G(y_G - \lambda x_G)} , \tag{D.22}$$

where

$$r = \sqrt{\frac{J}{m}}$$

is the radius of gyration of the vehicle.

If the angular velocity Ω_1 is negligible, the expressions for the velocity after the impact are

$$\left\{ \begin{array}{l} \dot{x}_2 = \dot{x}_1 \dfrac{y_G(y_G - \lambda x_G) - r^2 e^*}{y_G(y_G - \lambda x_G) + r^2} \\ \\ \dot{y}_2 = \dot{y}_1 - \dot{x}_1 \dfrac{\lambda r^2(1+e^*)}{y_G(y_G - \lambda x_G) + r^2} \\ \\ \Omega_2 = \dot{x}_1 \dfrac{(y_G - \lambda x_G)(1+e^*)}{y_G(y_G - \lambda x_G) + r^2} . \end{array} \right. \tag{D.23}$$

If $\dot{x}_2 > 0$ or $\Omega_2 > 0$ the vehicle has a second collision with the obstacle with the rear part of the body or, in practice, it undergoes a deformation that displaces the point of contact rearward, with a change in the values of x_G and y_G: It is impossible that $\dot{x}_2 > 0$ after a collision. In case of a perfectly inelastic impact the vehicle finally slides along the obstacle. The deformations are such that

$$y_G - \lambda x_G \approx 0 , \quad \dot{x}_2 = \Omega_2 = 0 , \quad \dot{y}_2 = \dot{y}_1 - \lambda \dot{x}_1 .$$

If the obstacle is a flat surface, λ is the coefficient of friction.

D.1.4 Non-central head-on collision

Consider a head-on collision in which the velocities of the centres of mass of the vehicles do not lie along the same straight line (Fig. D.4).

If the vehicles have no angular velocity before the collision, it follows that

$$\dot{y}_{A_1} = \dot{y}_{B_1} = \Omega_A = \Omega_B = 0 , \ \dot{x}_{A_1} = V_A , \ \dot{x}_{B_1} = V_B .$$

The components of the relative velocity are then

$$V_{R_{\perp_1}} = V_B - V_A , \ V_{R_{\parallel_1}} = 0$$

and, because the slip velocity is nil, λ can be assumed to vanish.

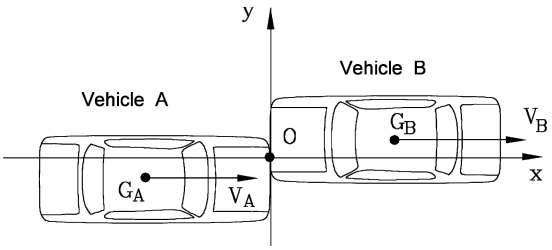

FIGURE D.4. Non-central head-on collision.

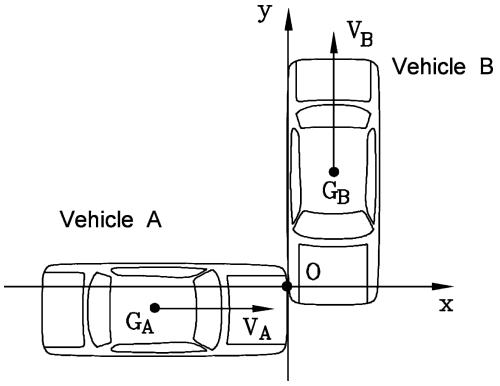

FIGURE D.5. Lateral collision.

The expressions for the velocities after the impact are

$$\begin{cases} \dot{x}_{A_2} = V_A + (V_B - V_A)\,\dfrac{1+e^*}{am_A} \\ \dot{x}_{B_2} = V_B - (V_B - V_A)\,\dfrac{1+e^*}{am_B} \\ \Omega_{A_2} = (V_B - V_A)\,\dfrac{y_A(1+e^*)}{aJ_A} \\ \Omega_{B_2} = -\,(V_B - V_A)\,\dfrac{y_B(1+e^*)}{aJ_B}\ . \end{cases} \tag{D.24}$$

D.1.5 Lateral collision

Consider a lateral collision in which the velocities of the centres of mass of the vehicles are perpendicular to each other (Fig. D.5).

If the angular velocities of the vehicles are vanishingly small before the collision

$$\dot{y}_{A_1} = \dot{x}_{B_1} = \Omega_A = \Omega_B = 0\ ,\ \ \dot{x}_{A_1} = V_A\ ,\ \ \dot{y}_{B_1} = V_B\ ,$$

it follows that

$$V_{R_{\perp_1}} = -V_A \ , \quad V_{R_{\parallel_1}} = V_B$$

and then

$$I_x = -V_A \frac{1+e^*}{a-\lambda b} \ , \tag{D.25}$$

where λ is negative if both V_A and V_B are positive.

The expressions for the velocities after the impact are

$$\begin{cases} \dot{x}_{A_2} = V_A \left[1 - \dfrac{1+e^*}{m_A(a-\lambda b)}\right] \\ \dot{y}_{A_2} = -V_A \lambda \dfrac{1+e^*}{m_A(a-\lambda b)} \\ \Omega_{A_2} = -\left(y_A - \lambda x_A\right) \dfrac{(1+e^*)}{J_A(a-\lambda b)} \\ \dot{x}_{B_2} = V_A \dfrac{1+e^*}{m_B(a-\lambda b)} \\ \dot{y}_{B_2} = V_B + V_A \lambda \dfrac{1+e^*}{m_A(a-\lambda b)} \\ \Omega_{B_2} = \left(y_B - \lambda x_B\right) \dfrac{(1+e^*)}{J_A(a-\lambda b)} \ . \end{cases} \tag{D.26}$$

D.1.6 Simplified approach

The problem is often simpler. If the directions of the velocity vectors of the vehicles before and after the impact can be estimated independently, there is no need to assume the values of e^* and λ. With reference to Fig. D.6, Eq. (D.12) can be written as

$$\begin{cases} m_A V_{A_1} \cos(\theta_{A_1}) + m_B V_{B_1} \cos(\theta_{B_1}) = m_A V_{A_2} \cos(\theta_{A_2}) + m_B V_{B_2} \cos(\theta_{B_2}) \\ m_A V_{A_1} \sin(\theta_{A_1}) + m_B V_{B_1} \sin(\theta_{B_1}) = m_A V_{A_2} \sin(\theta_{A_2}) + m_B V_{B_2} \sin(\theta_{B_2}) \ . \end{cases} \tag{D.27}$$

If all angles θ_i at times t_1 and t_2 are known or can be assumed, both the direct or the inverse problem are easily solved. Once the velocities have been computed it is possible to obtain the angular velocities, the components of the impulse, e^* and λ.

In the inverse problem, the velocity after the impact is usually obtained from the distance travelled by the two vehicles between time t_2 and the instant t_3 in which all motion ceases. The wheels are often assumed to be blocked, which is correct only if the deformations due to the collision are sufficiently large, or if the sideslip angles are sizeable enough to cause the wheels to slide on the ground.

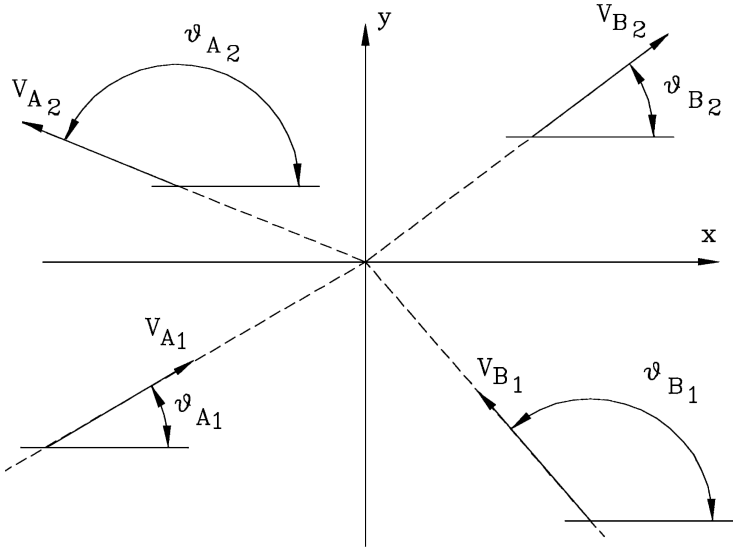

FIGURE D.6. Simplified approach: velocities at times t_1 and t_2.

If the vehicle slides for a distance d before coming to a stop without hitting any other obstacle, the velocity V_2 can be computed by equating the kinetic energy of the vehicle after the collision with the energy dissipated by friction, that is the product of the friction force mgf by the distance travelled d:

$$V_2 = \sqrt{2gdf}\ , \tag{D.28}$$

where f is the coefficient of friction between the tires and the road.

If at time t_3 the vehicle hits an obstacle with a speed V_3 after sliding for a distance d, it follows that

$$V_2 = \sqrt{2gdf + V_3^2}\ . \tag{D.29}$$

Velocity V_3 may be assessed only from the damage suffered by the vehicle during the secondary collision, a difficult and process that is affected by large uncertainties and errors.

Remark D.2 *The larger the value of the friction coefficient f or the distance d, the less significant are the errors in the estimate of V_3.*

Another source of uncertainties is the evaluation of f, which is affected not only by road conditions and the possibility that some of the wheels are rolling instead of slipping but also by the actual motion of the vehicle.

The motion of the vehicle on the road after the collision is actually not a simple translational motion but a combination of translation and rotation. As already seen, the angular velocity of the vehicle after the collision may be computed even if only approximately for the position of the point of application of the shock load can only be guessed. At first glance it would seem that the

rotation $\psi_3 - \psi_2$ of the vehicle during the time from t_2 to t_3 could be computed the same way as the translational motion

$$\psi_3 - \psi_2 = \frac{J_z \Omega_2^2}{2mg\overline{d}f} \,, \tag{D.30}$$

where $\overline{d}$ is the average distance between the centre of mass and the centres of the contact areas of the wheels.

This is, however, incorrect as the coefficient of friction cannot be applied to translational and rotational motions separately. But as it will be shown in Section D.3.1, it is possible to approximate the correct results by studying the two motions separately with two "equivalent" friction coefficients, both of which are smaller in magnitude than the actual coefficient f.

Example D.1 *Two cars collided at the intersection of two urban three-lanes streets. Evaluate the speed of the vehicles at the instant of the collision, knowing only the final positions at which they stopped and their directions at time t_1. Vehicle A stopped without any secondary collision while vehicle B ended up against a wall. From the deformations caused by the secondary impact, a value $V_3 \approx 11$ m/s ≈ 40 km/h is assumed.*

With reference to the xy frame shown in Fig. D.7, the coordinates of the centres of mass of the vehicles at time t_3 are $x_{A_3} = 9.2$ m, $y_{A_3} = 12.8$ m, $x_{B_3} = 13.2$ m and $y_{B_3} = 12.0$ m. The masses of the vehicles are $m_A = 850$ kg and $m_B = 870$ kg.

Because the exact position of the vehicles at time t_1 is unknown, each of them will be assumed to have traveled in the centre of the right, centre and left lane. As a result, nine possible positions of the impact point will be considered. With simple geometrical computations, the values of y_{A_1} and y_{B_1} as functions of the position of vehicle A and those of x_{A_1} and x_{B_1} as functions of the position of vehicle B are

	Vehicle A		*Vehicle B*	
Lane	y_{A_1}	y_{B_1}	x_{A_1}	x_{B_1}
Right	-9.8	10.2	6.0	8.6
centre	-6.3	-6.7	2.6	5.2
Left	-2.8	-3.2	-0.8	1.8

It is straightforward to compute the distances d_A and d_B for the nine cases under study. Vehicle A stops without hitting any obstacle. As its velocity was almost perpendicular to its longitudinal axis and some rotation occurred, owing to the fact that the front wheels were blocked as a consequence of the impact, a fairly high value of the friction coefficient can be assumed, namely $f_A = 0,45$.

Vehicle B had only one wheel locked and moved in a direction less inclined with respect to its longitudinal axis; an average value of the friction coefficient, $f_B = 0,30$ is then assumed. In all nine cases the values of V_{A_2} and V_{B_2} can be easily obtained

$$V_{A_2} = \sqrt{2gd_A f_A} \,, \qquad V_{B_2} = \sqrt{2gd_B f_B + V_{B_3}^2} \,.$$

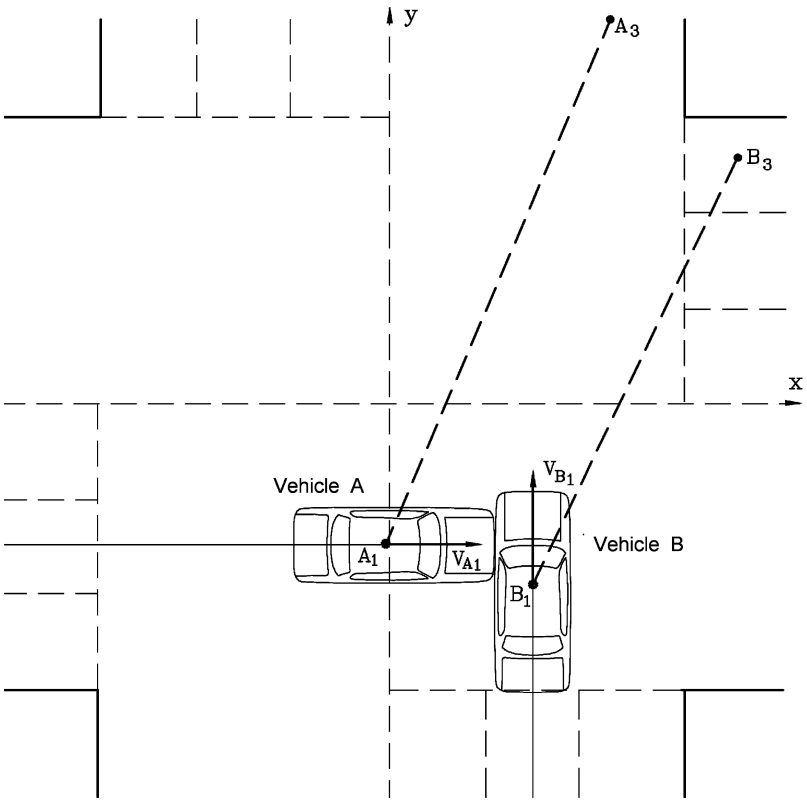

FIGURE D.7. Example D.1; positions of the vehicles.

Angles θ_{A_1} *and* θ_{B_1} *are respectively* $\theta_{A_1} = 0$ *and* $\theta_{B_1} = 90°$. *Angles* θ_{A_2} *and* θ_{B_2} *can be computed as*

$$\theta_{A_2} = \arcsin\left(\frac{y_{A_3} - y_{A_1}}{d_A}\right) , \qquad \theta_{B_2} = \arcsin\left(\frac{y_{B_3} - y_{B_1}}{d_B}\right) .$$

By solving Eq. (D.27) in V_{A_1} *and* V_{B_1}, *the following values of the velocities are obtained:*
Velocity V_{A_1} *(in km/h)*

		Vehicle A		
	Lane	*Right*	*centre*	*Left*
Vehicle B	*Left*	*49.3*	*53.3*	*59.0*
	centre	*34.9*	*38.5*	*42.8*
	Left	*19.1*	*21.2*	*24.1*

Velocity V_{B_1} (in km/h)

		Vehicle A		
	Lane	*Right*	*centre*	*Left*
Vehicle B	*Left*	*99.7*	*91.4*	*81.7*
	centre	*103.3*	*95.7*	*86.8*
	Left	*105.5*	*98.6*	*90.7*

It is very unlikely that vehicle B was in the left lane, as this would yield too low a value for the velocity of vehicle A. However, its position has little effect on the value of the velocity of vehicle B, which, in this case, is the most important parameter to be determined. Some uncertainty in this result remains, because values between 81.7 and 105.5 km/h are possible.

This approach, which may be defined as traditional, still carries a wide uncertainty margin, primarily linked to the evaluation of the friction coefficients and the velocities after the impact, in case a vehicle stops by hitting an obstacle. Its simplicity allows one to perform the computations several times and to obtain upper and lower bounds of the results. The values of the initial velocities can then be used to perform more accurate numerical simulations.

Example D.2 *Two cars collided at the intersection of two urban streets (Fig. D.8). Both the collision point and the final positions at which they stopped (both vehicles stopped without hitting any obstacle) are known. Compute the speeds at which the two vehicles reached the intersection and the positions taken by the vehicles after the impact.*

The inertial properties of the vehicles, the coordinates of their centre of mass and their yaw angles at times t_2 and t_3 with reference to the frame xy shown in the figure are $m_A = 1130$ kg, $m_B = 890$ kg, $J_A = 1780$ kg m^2, $J_B = 1400$ kg m^2, $x_{A_1} = 0.3$ m, $y_{A_1} = 0.6$ m, $x_{B_1} = 0.7$ m, $y_{B_1} = 1.4$ m, $x_{A_3} = -4.4$ m, $y_{A_3} = 8.5$ m, $x_{B_3} = 1.7$ m, $y_{B_3} = 4.9$ m, $\psi_{A_1} = 90^\circ$, $\psi_{B_1} = 180^\circ$, $\psi_{A_3} = 120^\circ$ and $\psi_{B_3} = 20^\circ$.

The positions of the centres of mass of the vehicle with reference to frame $x'y'$ centred on the impact zone are $x'_{G_A} = -0.825$ m, $y'_{G_A} = -0.80$ m, $x'_{G_B} = 1.575$ m and $y'_{G_B} = 0$.

For the computation of the velocities after the impact a value $f_A = 0.15$ was assumed for the first vehicle (after the impact it travelled with little sideslip) and $f_B = 0.50$ was assumed for the second. As the distances travelled after the collision are $d_A = 9.123$ m and $d_B = 3.640$ m, the velocities at time t_2, computed through Eq. (D.28), are $V_{A_2} = 18.7$ m/s = 67.3 km/h and $V_{B_2} = 5.98$ m/s = 21.5 km/h.

The velocity vectors are then

$$\vec{V}_{A_2} = \left\{ \begin{array}{r} -9.65 \\ 16.22 \end{array} \right\} \text{ m/s}\,, \qquad \vec{V}_{B_2} = \left\{ \begin{array}{r} -1.64 \\ 5.75 \end{array} \right\} \text{ m/s}\,.$$

The velocities before the collision are easily obtained from Eq. (D.27)

$$\vec{V}_{A_1} = \left\{ \begin{array}{r} 0 \\ 20.75 \end{array} \right\} \text{ m/s}\,, \qquad \vec{V}_{B_1} = \left\{ \begin{array}{r} -13.89 \\ 0 \end{array} \right\} \text{ m/s}\,.$$

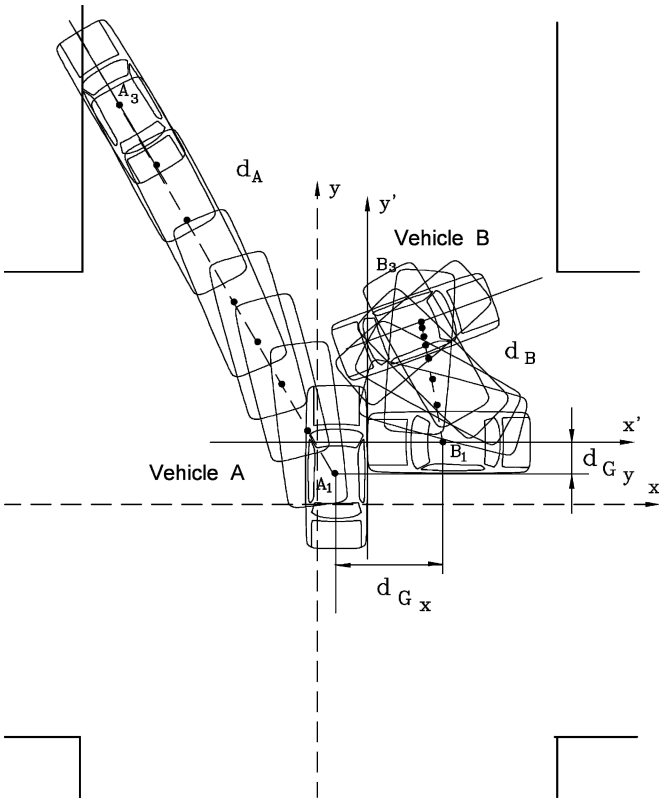

FIGURE D.8. Example D.2; positions of the vehicles at times t_1 and t_3 and reconstruction of the accident; computed positions at times 0.05, 0.1, 0.15, 0.2, 0.3 and 0.5 s from time t_2.

The two cars were then travelling at 74.7 km/h and 50.0 km/h.

This result was obtained using a much simplified model. A more detailed approach can be used to confirm the results, using equations (D.25) and following, the only difference being that in this case vehicle B hits vehicle A. Because $V_{R_{\perp_1}} = V_{B_1} = 13.89$ *m/s and* $V_{R_{\parallel_1}} = -V_{A_1} = -20.75$ *m/s, it follows that*

$$I_x = V_B \frac{1+e^*}{a-\lambda b} = -\frac{13,890(1+e^*)}{2.368-0.371\lambda} \,.$$

The components of the impulse can be easily computed from the velocities before and after the impact: $I_x = -10,905$ *Ns and* $I_y = -5,119$ *Ns. The value* $\lambda = 0.469$ *is easily obtained, a high but realistic value owing to the possibility of the vehicles becoming interlocked.*

By equating the two values of I_x *the value* $e^* = 0.723$ *for the restitution coefficient is obtained. It is also quite high, but is again justified by the small permanent deformations found on the vehicles.*

The angular velocities after the impact are then obtained

$$\Omega_{A_2} = \frac{I_x y'_A - I_y x'_A}{J_A} = 2.52 \; rad/s \, ,$$

$$\Omega_{B_2} = \frac{-I_x y'_B + I_y x'_B}{J_B} = -5.75 \; rad/s \, .$$

To compute the rotations of the vehicles during the accident Eq. (D.30) can be used. The value $f = 0.7$ *can be used for both vehicles (see Sec. D.3.1). The geometrical parameters are* $\overline{d}_A = 1.45$ *m and* $\overline{d}_B = 1.35$ *m. The results are*

$$|\psi_{A_3} - \psi_{A_2}| = 0,502 \; rad = 29^\circ \, ,$$

$$|\psi_{B_3} - \psi_{B_2}| = 2,813 \; rad = 161^\circ \, .$$

which are close to those measured on the road. The positions of the vehicle at times between t_2 *and* t_3 *are reported in Fig. D.8.*

D.2 VEHICLE COLLISION: SECOND APPROXIMATION MODEL

D.2.1 Head on collision against a fixed obstacle

The model studied in the previous sections was based on the assumption that the collision is an impulsive phenomenon. Consequently, it was impossible to assess what might happen during the impact. The shock, however, has a short but finite duration, making it possible to study how the displacement, velocity and acceleration change between t_1 and t_2.

Consider first a head-on collision against a fixed obstacle, like that occurring during a crash test (Fig. D.9). The force that the vehicle receives from the obstacle has a time history of the type shown in Fig. D.10a. The curve is not smooth because the compliance of the front of the vehicle changes strongly as it is crushed, owing to geometric nonlinearities, buckling and other phenomena. The experimental law may, however, be approximated by a smooth curve $F(t)$ while retaining the most important features of the actual behavior of the vehicle (dashed curve in the figure).

The linkage of force and acceleration is complex, as the vehicle's configuration changes in time, with each point of the vehicle having its own acceleration. However, with the exception of the front part, which is crushed, the vehicle may be considered as a rigid body.

The position of the centre of mass may be considered as fixed to the undeformed part of the vehicle. The acceleration can thus be obtained directly from the force $F(t)$; in an actual crash test the acceleration is usually measured by accelerometers located on the vehicle and the force is obtained from these readings.

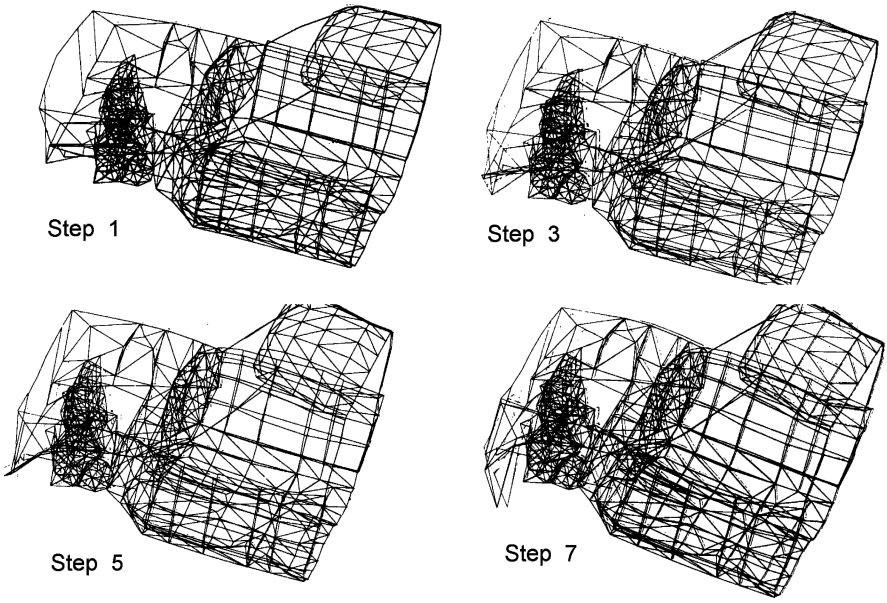

FIGURE D.9. Numerical simulation of a crash test against a rigid barrier: Deformation of the vehicle at various instants (fuinite element method).

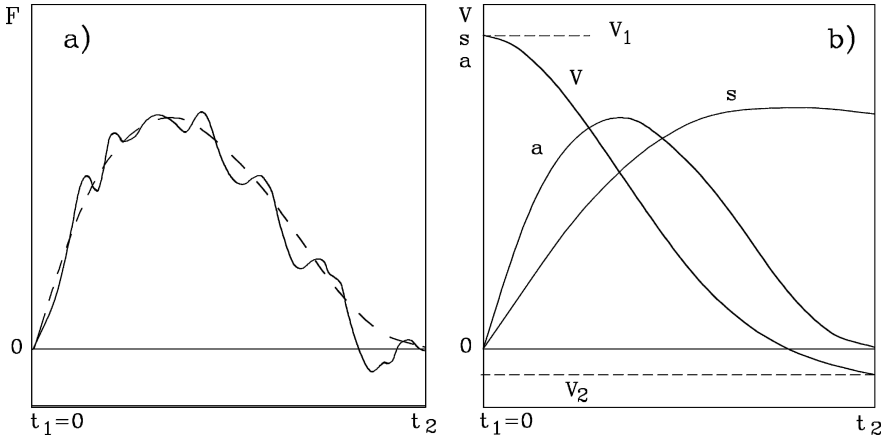

FIGURE D.10. (a) Force the vehicle receives from the obstacle during a crash test as a function of time. Experimental curve and mathematical empirical law. (b) Time histories $V(t)$, $a(t)$ and $s(t)$ obtained from the empirical law $F(t)$.

From the acceleration it is straightforward to compute the velocity and the deformation of the vehicle.

A law approximating the acceleration is[2]

$$a = \tau(1-\tau)^{\beta}\frac{cV_1}{t_2} \ , \tag{D.31}$$

where t_2 is the duration of the impact,

$$\tau = \frac{t}{t_2} \qquad (0 \le \tau \le 1)$$

is the nondimensional time and c and β are nondimensional constants.

Such a law has a vanishing derivative (jerk equal to zero) at the end of the collision ($t = t_2$) while the jerk at the beginning of the collision ($t = 0$) is other than zero; both these features comply with the intuitive physical interpretation of the phenomenon.

The velocity may be obtained by integrating Eq. (D.31):

$$V = -cV_1\left[\frac{(1-\tau)^{\beta+1}}{\beta+1} - \frac{(1-\tau)^{\beta+2}}{\beta+2}\right] + K \ . \tag{D.32}$$

The constant of integration K can be computed because at time $t = 0$ the speed is $V = V_1$

$$K = V_1\left[1 + \frac{c}{(\beta+1)(\beta+2)}\right] \ . \tag{D.33}$$

By remembering the definition of the restitution coefficient

$$e^* = -\frac{V_2}{V_1} \ ,$$

it is possible to compute the value of constant c. By computing the velocities at times t_2 and t_1, i.e. for $\tau = 0$ and $\tau = 1$, and equating their ratio to $-e^*$, it follows that

$$c = -(1+e^*)(\beta+1)(\beta+2) \ . \tag{D.34}$$

The final expression of the velocity is thus

$$V = V_1\left\{(1+e^*)\left[1+\tau(\beta+1)\right](1-\tau)^{\beta+1} - e^*\right\} \ . \tag{D.35}$$

A further integration gives the distance travelled s

$$s = V_1 t_2\left\{-(1+e^*)\left[(1-\tau)^{\beta+2} - \frac{\beta+1}{\beta+3}(1-\tau)^{\beta+3}\right] - e^*\tau + K_1\right\} \ . \tag{D.36}$$

If at time $t = 0$ the distance is assumed to be nil, s describes the crushing of the front part of the vehicle. This statement allows the value of the integration constant K_1 to be computed

$$K_1 = \frac{2(1+e^*)}{\beta+3} \ . \tag{D.37}$$

---

[2]R.H. Macmillan, *Dynamic of Vehicle Collisions*, Inderscience Enterprises, Jersey 1983.

The final expression of the displacement is thus

$$s = V_1 t_2 \left(\frac{1+e^*}{\beta+3} \left\{ 2 - (1-\tau)^{\beta+2} \left[2 + (\beta+1)\tau \right] \right\} - e^* \tau \right) . \tag{D.38}$$

At time $\tau = 1$, the displacement directly yields the residual crushing of the vehicle s_2

$$s_2 = V_1 t_2 \left[\frac{2(1+e^*)}{\beta+3} - e^* \right] . \tag{D.39}$$

In case of an elastic collision, the residual crushing must vanish: If $e^* = 1$ then $s_2 = 0$. From this statement a first relationship between β and e^* can be stated: $\beta = 1$ if $e^* = 1$.

Parameters β and e^* characterizing the impact depend on many factors, beginning with the structural characteristics of the vehicle and including the type of impact and, in the case of head-on collision against a fixed obstacle, the impact velocity V_1 and time t_2.

A primary characteristic of the vehicle is its stiffness at the instant it enters into contact with the obstacle, namely its *crushing modulus* (Fig. D.11). With simple kinematic considerations it follows that

$$K = m \left(\frac{da}{ds} \right)_{\tau=0} = m \left(\frac{da}{dt} \right)_{\tau=0} \left(\frac{ds}{dt} \right)^{-1}_{\tau=0} = \frac{m}{V_1} \left(\frac{da}{dt} \right)_{\tau=0} . \tag{D.40}$$

By introducing the expression (D.31) of the acceleration into Eq. (D.40), it follows that

$$K = m \frac{(1+e^*)(\beta+1)(\beta+2)}{t_2^2} . \tag{D.41}$$

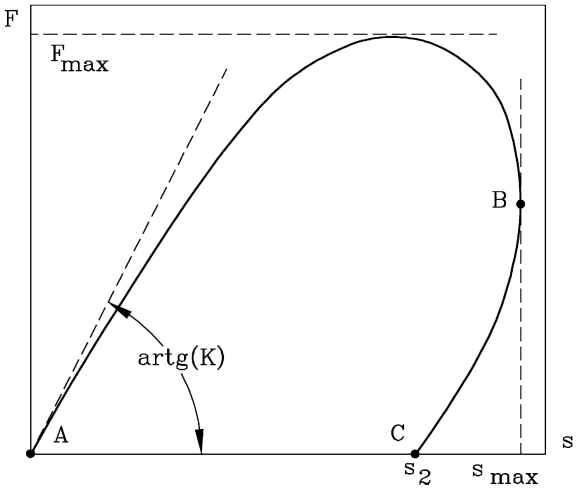

FIGURE D.11. Force received by the vehicle during a head-on collision against the obstacle as a function of the crushing s.

The value of K can be obtained from crash tests. Values between 1 and 2 MN/m are found in the literature.

The crushing process is far from linear. A qualitative plot of force F against the displacement s is reported in Fig. D.11: The inelastic behavior of the vehicle and the hysteresis cycle are clearly shown. The area below the line from point A to point B is the energy absorbed by the vehicle from time t_1 to the instant t_i at which the maximum displacement is reached. In the case of collision against a fixed rigid obstacle it is equal to the kinetic energy of the vehicle.

The area below the line from point B to point C is the energy that is transformed back into kinetic energy during the rebound phase from time t_i to t_2. If $e^* = 0$ such an area vanishes and $s_2 = s_{max}$. If, on the contrary $e^* = 1$ line BC is superimposed to line AB and the area of the hysteresis cycle vanishes.

The plot is usually obtained from a crash test, either performed on an actual vehicle or simulated by computer. The numerical simulation is a complex task, owing to the complex geometry of the front part of the vehicle and the nonlinearities of all types involved. A large and fast computer is thus required. Some results obtained through the finite element method, which at present is the only method allowing problems of this complexity to be tackled, are reported in Fig. D.9. The computation has been performed through step by step integration in time of the equations of motion; the deformed mesh at four different time values has been reported in the figure.

The law $F(s)$, obtained through the empirical law $F(t)$ defined above, is often assumed to be independent of the deformation rate ds/dt. Such an assumption has no theoretical background but is justified by the fact that it is substantiated by experimental evidence, at least when the deformation rate is low.

The mean value of the force received by the vehicle

$$\overline{F} = \frac{1}{t_2} \int_0^{t_2} F dt \tag{D.42}$$

can be easily computed by remembering that the total impulse received by the vehicle is equal to the change of the momentum

$$\overline{F} = m \frac{V_2 - V_1}{t_2} = -m \frac{V_1}{t_2} (1 + e^*) \, . \tag{D.43}$$

If the mean value of force F is small, the permanent deformations are usually negligible and the impact is close to being elastic, i.e. $e^* \approx 1$. With increasing $\overline{F}$ the collision becomes more and more inelastic, i.e. e^* decreases with increasing $\overline{F}$. It is possible to approximate the dependence of the restitution coefficient e^* on the average force $\overline{F}$ with an exponential law (Fig. D.12)

$$e^* = e^{-\overline{F}/K_r} \, , \tag{D.44}$$

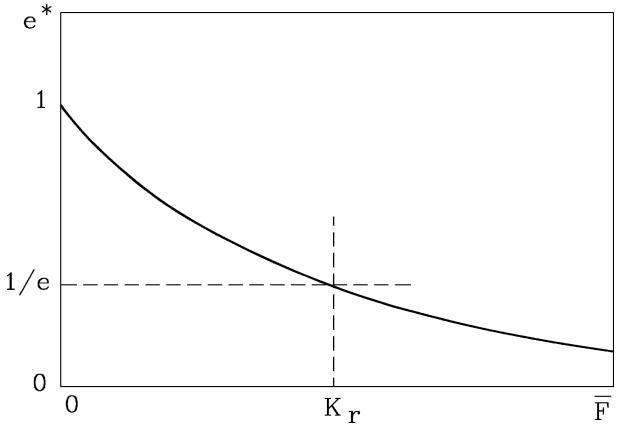

FIGURE D.12. Law $e^*(\overline{F})$ approximated by Eq. (D.44).

where K_r, usually referred to as the *impact resistance modulus*, is the value of $-\overline{F}$ at which the coefficient of restitution takes the value

$$e^* = \frac{1}{e} = 0.368 \ .$$

K_r can also be obtained from a crash test. From Equations. (D.41) and (D.44), it follows that

$$K_r = m\frac{V_1(1+e^*)}{t_2 \ln(1/e^*)} \ , \tag{D.45}$$

which allows K_r to be calculated from quantities that can be measured or computed. Values between 40 and 100 kN have been reported for K_r in the literature.

As seen above, constant β depends on e^*: It takes a unit value when $e^* = 1$ and increases when e^* decreases. Assume that, at least in the case of strongly inelastic impacts, i.e. near the condition $e^* = 0$, the law $\beta(e^*)$ may be approximated as

$$\beta = \beta_0 - (\beta_0 - 1)e^* \ , \tag{D.46}$$

which, although assumed for $e^* \approx 0$, gives the correct result also for $e^* = 1$.

Because $\beta > 1$, β_0 is always larger than unity. Also β_0, which is nondimensional, may be considered as a characteristic of the vehicle, and will be referred to as the *structural index*. A large value of β_0 characterizes vehicles with a very stiff front section, while a compliant front section is typical of vehicles with low β_0. Its values are usually close to 2.

Parameters K, K_r and β_0 completely characterize a vehicle in terms of head-on collision against a rigid obstacle. Once they have been measured, it is possible to compute the laws $F(t)$, $a(t)$ and $s(t)$ from the collision conditions, namely the velocity V_1 and the mass of the vehicle m.

TABLE D.1. Parameters obtained from crash tests on some European passenger vehicles.

	BMC Mini	BMC 1100	Ford Anglia	BMC 1800
m [kg]	720	950	1000	1250
V_1[m/s]	14	11,5	14	14
e^*	0,10	0,08	0,5	0,11
t_2[ms]	92	102	103	97
β_0	2,35	2,79	2,89	2,16
K [MN/m]	1,27	1,67	1,81	1,80
K_r [kN]	52,3	45,8	47,6	90,7

TABLE D.2. Parameters obtained from crash tests on some American passenger vehicles.

	Sub compact	Compact	Interm.	Standard 71/72	Standard 73/74
m [kg]	1135	1545	1820	2045	2045
V_1[m/s]	12	12	10,5	10	10,3
e^*	0,01	0,01	0,20	0,20	0,20
t_2[ms]	102	102	151	147	143
β_0	2,50	2,50	2,00	2,00	2,00
K [MN/m]	1,60	2,17	1,03	1,09	1,16
K_r [kN]	28,6	38,8	96,7	93,6	108,8

The values reported in Tables D.1 and D.2 have been obtained from crash tests published by manufacturers[3]. The values in the first table are not exactly comparable with the others because they have been computed from well documented tests, while not all the parameters were known for the others and the values of β_0 and s_2 had to be assumed.

To solve the direct problem, i.e. to obtain the conditions after the collision, mainly s_2 and V_2, from V_1, it is possible to compute t_2 from Eq. (D.45) and to introduce it into Eq. (D.41), obtaining

$$KmV_1^2 = K_r^2 \left[\ln\left(\frac{1}{e^*}\right)\right] \frac{(\beta+1)(\beta+2)}{1+e^*} \,. \tag{D.47}$$

Substituting Eq. (D.46) into Eq. (D.47) the latter yields

$$\frac{KmV_1^2}{K_r^2} = \left[\ln\left(\frac{1}{e^*}\right)\right] \frac{(\beta_0+1)(\beta_0+2) - e^*(\beta_0-1)(2\beta_0+3) + e^{*^2}(\beta_0-1)^2}{1+e^*} \,, \tag{D.48}$$

which can be solved numerically in e^* and then allows the direct problem to be solved.

[3]R.H. Macmillan, *Dynamic of Vehicle Collisions*, Inderscience Enterprises, Jersey 1983.

The inverse problem, i.e. obtaining the conditions before the collision, primarily V_1, from the crushing s_2, is also easily solved. From Equations. (D.37), (D.41) and (D.45) it follows that

$$s_2 \frac{K}{K_r} = \ln\left(\frac{1}{e^*}\right) \frac{(\beta+1)(\beta+2)\left[2(1+e^*)-(\beta+3)e^*\right]}{\beta+3} \,. \tag{D.49}$$

Substituting Eq. (D.46) into Eq. (D.49) the latter yields

$$s_2 \frac{K}{K_r} = \ln\left(\frac{1}{e^*}\right) \left[e^{*^2}(\beta_0-1)^2 - e^*(2\beta_0^2+\beta_0-3)+3\beta_0+\beta_0+2\right] \times \frac{e^*(e^*-1)(\beta_0-1)+2}{-e^*(\beta_0-1)+\beta_0+3}, \tag{D.50}$$

which may be solved numerically in e^* and allowing the inverse problem to be solved.

Example D.3 *Consider a car with $\beta_0 = 2$, K = 1.2 MN/m, K_r = 65 kN and m = 1000 kg impacting an obstacle at 20 m/s. Compute the parameters of the impact and laws $F(t)$, $a(t)$ $V(t)$ and $s(t)$.*

The numerical solution of Eq. (D.48) yields e^* = 0.0416 and then β = 1.958, t_2 = 0.1 s. The laws $F(t)$, $a(t)$ $V(t)$ and $s(t)$ for this case are plotted in Fig. D.13; the residual crush is s_2 = 757 mm.

D.2.2 Head-on collision between vehicles

The head-on collision between vehicles may be studied using the same model seen in the previous section, provided the contact surface is assumed to remain planar

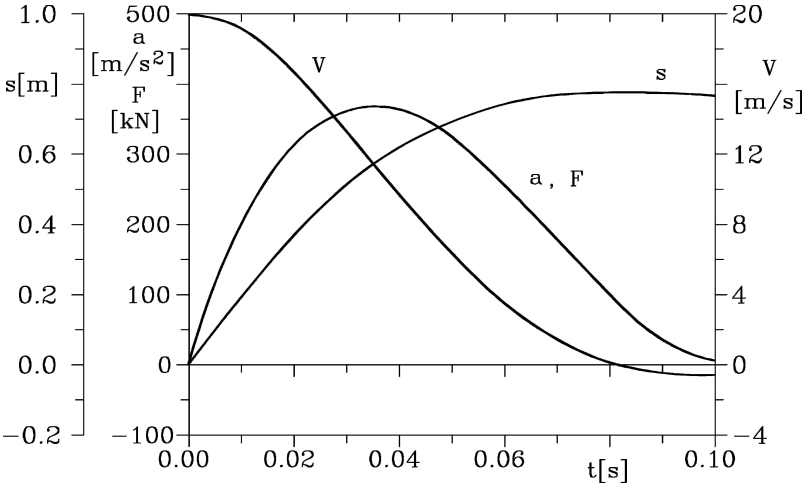

FIGURE D.13. Laws $F(t)$, $a(t)$, $V(t)$ and $s(t)$ for Example D.3.

and the characteristics of the impact, and particularly law $F(s)$, are independent of the deformation rate. Each vehicle can thus be assumed to impact against a moving massless obstacle (Fig. D.13a). Each vehicle is modelled as a point mass, provided with a nonlinear spring, whose characteristics (K, K_r and β_0) are those seen for the collision against a fixed obstacle.

The deformation rates

$$\begin{cases} \dot{s}_A = \dot{x}_b - \dot{x}_A \\ \\ \dot{s}_B = -\dot{x}_b + \dot{x}_B \end{cases} \tag{D.51}$$

are positive when the springs are compressed.

The relative velocity V_R is then

$$V_R = \dot{x}_B - \dot{x}_A = -(\dot{s}_A + \dot{s}_B) \; . \tag{D.52}$$

If the curves $F(s)$ for the two vehicles are known, a plot of the type shown in Fig. D.14b can be drawn. As the total force acting on the virtual obstacle must vanish,

$$|F_A| = |F_B|$$

for each value of time. The intersections of the curves $|F_A(s_A)|$ and $|F_B(s_B)|$ with any line $F =$ constant thus yield the deformations s_A and s_B in the same instant. A third curve in which the force is plotted as a function of the total deformation $s = s_A + s_B$, i.e. of the change of distance between the centres of mass, can be plotted.

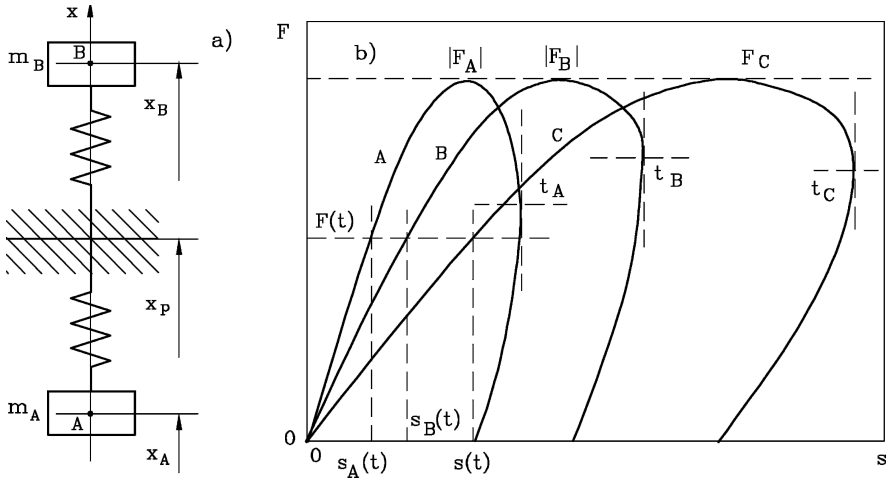

FIGURE D.14. Head-on collision between vehicles. (a) model; (b) forces as functions of the crush of the vehicles.

The maximum values of the deformations need not be reached at the same time: In the figure the maximum deformation is reached at time t_A and t_B for the two vehicles, while the distance between the centres of mass is at its minimum at time t_C.

Because the forces acting on the vehicles are simply

$$F_A = m_A \ddot{x}_A \ , \quad F_B = m_B \ddot{x}_B,$$

it follows that

$$F_A = -F_B = \dot{V}_R \frac{m_A m_B}{m_A + m_B} \ . \tag{D.53}$$

If the derivative of the relative velocity has a time history which is of the same type as that assumed for the acceleration in Eq. (D.31),

$$\dot{V}_R = -\frac{cV_{R_1}}{t_2} \tau (1-\tau)^\beta \ , \tag{D.54}$$

where, as usual,

$$\tau = \frac{t}{t_2} \ ,$$

the same model used for the collision against an obstacle is sufficient for the present case as well.

Instead of m, K, V and s, the relevant equations now contain

$$m_C = \frac{m_A m_B}{m_A + m_B} \ , \qquad K_C = \frac{K_A K_B}{K_A + K_B} \ , \qquad V_R \ , \qquad s_C = s_A + s_B \ .$$

Assume that the characteristics of the vehicles and the residual deformation of one of them, say s_{A_2}, are known. Because curve $F(s)$ has been assumed to be the same as that characterizing the impact against the barrier, from s_{A_2} it is possible to compute e_A^* directly from Eq. (D.50) and then velocity V'_{A_1} [4] which causes the same residual deformation s_{A_2} in an impact with a rigid obstacle.

The maximum value F_{max_A} of the force received by the first vehicle is

$$F_{max_A} = K_{r_A} \beta_A^{\beta_A} \ln \left(\frac{1}{e_A^*} \right) \frac{(\beta_A + 1)(\beta_A + 2)}{(\beta_A + 1)^{\beta_A + 1}} \ . \tag{D.55}$$

The absolute value of such force is equal to the maximum force acting on vehicle B. It is thus possible to write an equation identical to Eq. (D.55) with the characteristics of the second vehicle. Because

$$\beta_B = \beta_{0_B} - (\beta_{0_B} - 1) e_B^* \ ,$$

it is possible to obtain e_B^* and then t_{B_2}, V_{B_1} and s_{B_2}.

[4] V' is the velocity in the equivalent collision against a rigid obstacle.

The two equivalent collisions against a rigid obstacle are thus completely characterized. As the curves $F(s)$ are the same in the actual collision and its equivalents, the energy dissipated in the former is equal to that dissipated in the latter

$$\Delta E = \Delta E_A + \Delta E_B = \frac{1}{2} m_A V_{A_1}^2 \left(1 - e_A^{*^2}\right) + \frac{1}{2} m_B V_{B_1}^2 \left(1 - e_B^{*^2}\right) . \quad \text{(D.56)}$$

It is thus possible to consider the actual collision, described by curve C in Fig. D.14b, by using the same equations seen in the previous chapter with the mentioned substitutions. The maximum force, already expressed by Eq. (D.55), and the energy dissipated take the values

$$F_{max} = \frac{s_{C_2} K_C \beta_C^{\beta_C} (\beta_C + 3)}{(\beta_C + 1)^{\beta_C + 1} \left[2 - e_C^* (\beta_C + 1)\right]} , \quad \text{(D.57)}$$

$$\Delta E = \frac{1}{2} m_C V_{C_1}^2 \left(1 - e_C^{*^2}\right) . \quad \text{(D.58)}$$

Equations (D.57) and (D.58) contain 3 unknowns β_C, e_C^* and V_R (or V_{C_1}, which is the same). A third equation may be obtained considering that force F_{max} can also be expressed as

$$F_{max} = K_C V_R t_2 \frac{\beta_C^{\beta_C}}{(\beta_C + 1)^{\beta_C + 1}} . \quad \text{(D.59)}$$

Because

$$t_2^2 = \frac{m_C}{K_C} (1 + e_C^*)(\beta_C + 1)(\beta_C + 2) , \quad \text{(D.60)}$$

computing V_R from Eq. (D.58) and substituting the value so obtained into Equations. (D.59) and (D.60), it follows that

$$F_{max}^2 = K_C \frac{2 \Delta E \beta^{2\beta} (\beta + 2)}{(1 - e^*)(\beta + 1)^{2\beta + 1}} . \quad \text{(D.61)}$$

The last equation can be solved in e^*, obtaining

$$e^* = 1 - K_C \frac{2 \Delta E \beta^{2\beta} (\beta + 2)}{F_{max}^2 (\beta + 1)^{2\beta + 1}} . \quad \text{(D.62)}$$

Finally, introducing Eq. (D.62) into Eq. (D.57), the equation

$$F_{max} = s_C K_C \frac{\beta^\beta (\beta + 3)}{(\beta + 1)^{\beta + 1}} \left[1 - \beta + \frac{2 \Delta E K_C}{F_{max}^2} (\beta + 2) \left(\frac{\beta}{\beta + 1}\right)^{2\beta}\right]^{-1} , \quad \text{(D.63)}$$

is obtained, which may be easily solved numerically in β. It is thus possible to obtain the values of e^* and V_R, solving the problem.

The inverse problem, consisting in obtaining the parameters characterizing the collision once the relative velocity V_R is known, is more difficult as it must be solved in an iterative way. A value of the final crushing s_2^* of one of the two vehicles is assumed and from it the relative velocity V_R^* can be computed as seen above. A new value of the residual crushing, for example obtained as

$$s_2^{**} = s_2^* \frac{V_R}{V_R^*} \ ,$$

can then be computed and a new relative velocity, which is closer to the correct one, is obtained. The procedure should converge quickly to the required result. The velocities of the vehicle after the collisions can then be obtained without further problems.

Example D.4 *Consider the head-on collision between two cars whose characteristics are known from crash tests, e.g. the vehicles of the first and fourth columns of Table D.1.*

The characteristics are then $m_A = 720$ *kg,* $m_B = 1250$ *kg,* $\beta_{0_A} = 2.35$, $\beta_{0_B} = 2.16$, $K_A = 1.27$ *MN/m,* $K_B = 1.80$ *MN/m,* $K_{r_A} = 52.3$ *kN and* $K_{r_B} = 90.7$ *kN. The residual crush of the first vehicle is* $s_{A_2} = 400$ *mm. Compute the parameters of the impact and the relative velocity at time* t_1*.*

The parameters characterizing the collision are $m_C = 456.85$ *kg and* $K_C = 0.745$ *MN/m. The coefficient of restitution for the first vehicle is easily computed from the residual crush by numerically solving Eq. (D.50):* $e_A^* = 0.105$*. The values of* β_A, t_{A_2} *and* V_{A_1} *are then* $\beta_A = 2.208$, $t_{A_2} = 0.092$ *s and* $V_{A_1} = 13.63$ *m/s.*

Equations (D.55), (D.46), (D.41) and (D.45) yield $F_{max} = 218$ *kN,* $e_B^* = 0.252$, $\beta_B = 1.87$, $t_{B_2} = 0.098$ *s,* $V_{B_1} = 7.85$ *m/s and* $s_{B_2} = 202$ *mm.*

The energy dissipated and the total crush are then $\Delta E = 102$ *kJ and* $s_C = 602$ *mm.*

Solving Eq. (D.63) in β *and using Equations (D.58) and (D.62), the final results are obtained:*

$$\beta = 2,037 \ , \quad e^* = 0,159 \ , \quad V_R = 21,43 \ m/s \ .$$

Example D.5 *Consider the vehicles of the previous examples colliding head-on with velocities* $V_{A_1} = 26.7$ *m/s = 96 km/h and* $V_{B_1} = -13.1$ *m/s =* -47 *km/h. Compute the velocities after the impact.*

The relative velocity is $V_R = 39.8$ *m/s. By assuming a residual crush of the first vehicle* $s_{A_2} = 400$ *mm in the previous example a relative velocity* $V_R = 21.43$ *m/s has been obtained.*

Correcting the assumed residual crush linearly, a new trial value $s_{A_2} = 743$ *mm is obtained, which yields a relative velocity* $V_R = 36.16$ *m/s that is already close to the correct values.*

With two further iterations a crush $s_{A_2} = 823$ *mm is obtained, together with* $e^* = 0.048$, $F_{max} = 378$ *kN and* $\Delta E = 360$ *kJ.*

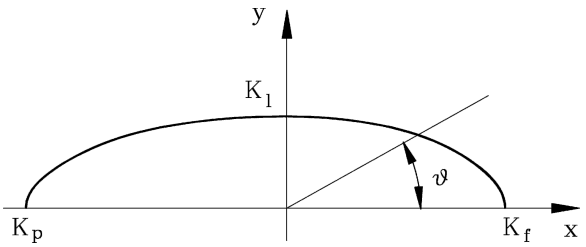

FIGURE D.15. Polar diagram $K(\theta)$ approximated by two arcs of ellipse.

As final results, the velocities after the collision are obtained:

$$\begin{aligned} V_{A_2} &= 0,234 \ m/s = 0,84 \ km/h \ , \\ V_{B_2} &= 2,144 \ m/s = 7,72 \ km/h \ . \end{aligned}$$

D.2.3 Oblique collision between vehicles

The first issue in the study of oblique collisions is the evaluation of the characteristics of the vehicle: If it is already difficult to obtain the values of K, K_r and β_0 for head-on collisions, it is almost impossible to obtain them for a generic impact direction. If it is possible to find the relevant values for side or rear impacts, the dependence of the characteristics upon angle θ (Fig. D.15) may be approximated by two arcs of ellipse, one for the front and one for the rear.

Following the notation of the figure, function $K(\theta)$ may be expressed as

$$\begin{aligned} &\frac{K_f K_l}{\sqrt{K_f^2 \sin^2(\theta) + K_l^2 \cos^2(\theta)}} && \text{for} \quad 0 \le \theta \le 90^\circ, \\ &\frac{K_p K_l}{\sqrt{K_p^2 \sin^2(\theta) + K_l^2 \cos^2(\theta)}} && \text{for} \quad 90^\circ \le \theta \le 180^\circ \ . \end{aligned} \tag{D.64}$$

Similar relationships may be written to approximate the other characteristics of the vehicle.

If the collision, albeit oblique, were central, i.e. the two velocities were aligned, and the two angular velocities were equal to zero (Fig. D.16a), the procedure seen above for the head-on collision would still hold, provided that the correct characteristics of the vehicles were used.

In case of non-central oblique collisions the vehicles are subject also to angular accelerations about the yaw axis z. An approximated but simple way to take this into account is to substitute the mass of the vehicle against which each vehicle collides with an effective mass, lower than the actual one. It is questionable whether it is worthwhile to attempt to refine this model further, because the assumptions on which the present models are based and the uncertainties in the data do not allow high precision to be obtained.

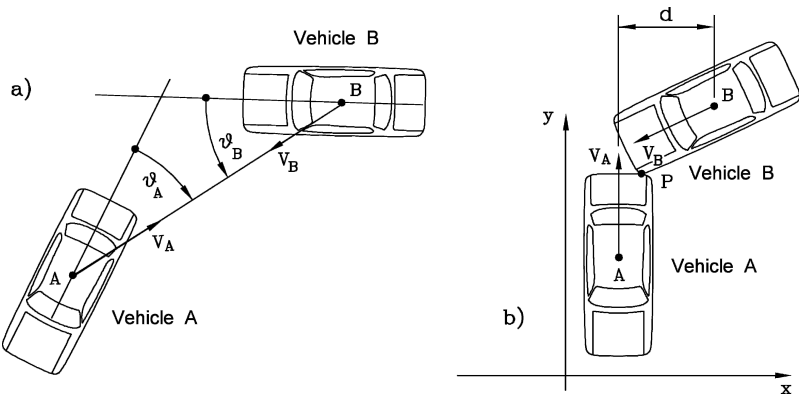

FIGURE D.16. (a) Central oblique collision. (b) Oblique collision in which vehicle A hits the front part of vehicle B.

Consider the situation of Fig. D.16b: Vehicle A hits the front part of vehicle B. Neglecting the friction in the contact area ($\lambda = 0$), the x component of the momentum of the second vehicle does not change and the impulse reduces to its y component. Vehicle B undergoes an acceleration in the y direction and an angular acceleration

$$\ddot{y}_{G_B} = \frac{F}{m_B} , \qquad \ddot{\theta}_B = \frac{Fd}{J_{z_B}} . \tag{D.65}$$

The acceleration of point P, seen as belonging to vehicle B, is then

$$\ddot{y}_{P_B} = \ddot{y}_{G_B} + d\ddot{\theta}_B = \frac{F}{m_B}\left(1 - \frac{d^2}{r_B^2}\right) , \tag{D.66}$$

where r_B is the radius of gyration. The acceleration of the contact point is thus equal to the acceleration of the centre of mass of a vehicle having a *reduced mass*

$$m_{r_B} = m_B \frac{r_B^2}{r_B^2 + d^2} .$$

If neither vehicle collides head-on with the other, reference must be made to the surface in collision, as seen in Section D.1.2. If no allowance is taken for the friction between the vehicles, the reduced masses of the two vehicles can be computed with reference to the perpendicular to these surfaces (Fig. D.17a). If friction is taken into account, reference must be made to a direction inclined at an angle $\arctan(\lambda)$ with respect to the perpendicular to the collision surface (Fig. D.17b).

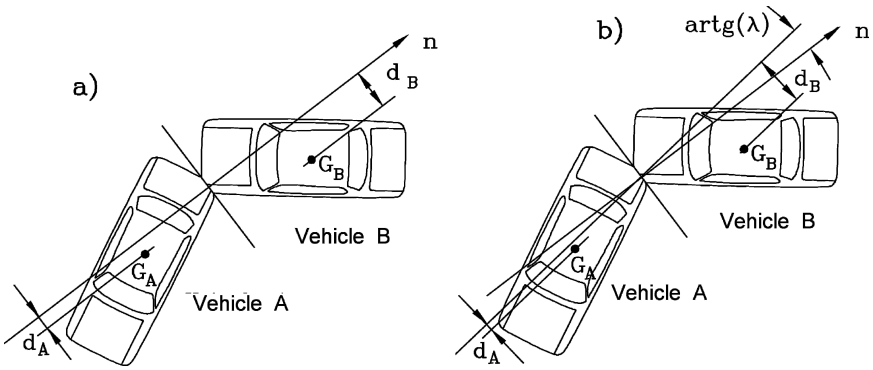

FIGURE D.17. Oblique collision; definition of distances d_A and d_B for the computation of the reduced mass. (a) No friction ($\lambda = 0$) and (b) $\lambda \neq 0$.

D.3 MOTION AFTER THE COLLISION

D.3.1 Vehicle with locked wheels

If, after the collision, the motion of the vehicle is simply translational, the distance travelled may be easily computed as seen in Section D.1.6. This, however, is seldom the case: After the impact a certain yaw velocity $\Omega = \dot{\psi}$ is usually present. It is thus incorrect to take translational and rotational motion into account independently.

Consider a vehicle that, after the collision, moves with the wheels completely locked, as if the brakes were fully applied or the deformations of the body were sufficient to prevent the wheels from rotating. With reference to Fig. D.18a, the components of the velocity of the centre of contact P_i of the ith wheel u_i and v_i in the directions of axes x and y fixed to the vehicle are

$$\begin{cases} u_i = V\cos(\beta) - \Omega r_i \sin(\chi_i) \\ v_i = V\sin(\beta) + \Omega r_i \cos(\chi_i)\ , \end{cases} \tag{D.67}$$

where r_i and χ_i are linked to the coordinates x_i and y_i of point P_i by the obvious relationships

$$r_i = \sqrt{x_i^2 + y_i^2}\ , \qquad \chi_i = \arctan\left(\frac{y_i}{x_i}\right)\ .$$

The absolute value of force F_i exchanged by the ith locked wheel is simply

$$|F_i| = fZ_i$$

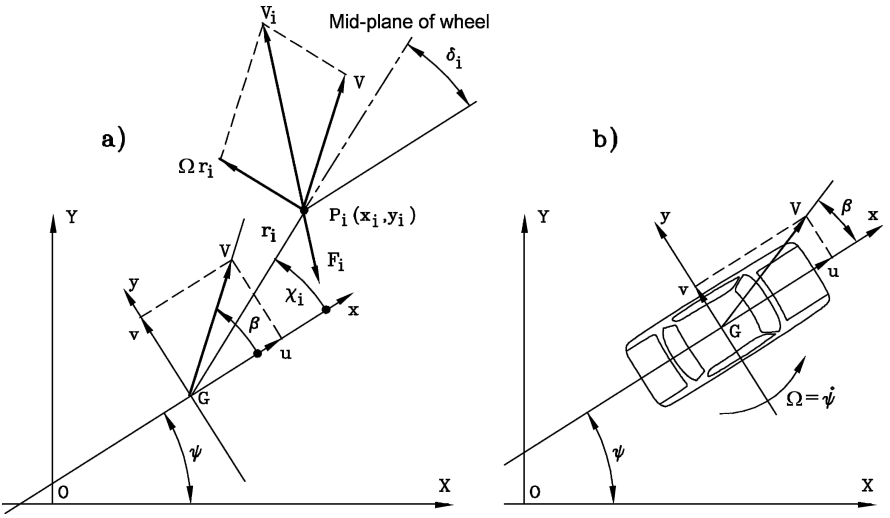

FIGURE D.18. (a) Velocity of the centre of contact of the i-th wheel; (b) inertial reference frame and variables of motion.

and its direction is equal to that of the velocity V_i, with opposite sign. The components of force F_i are then

$$\begin{cases} F_{x_i} = -fZ_i \dfrac{u_i}{|V_i|} = fZ_i \dfrac{-V\cos(\beta) + \Omega r_i \sin(\chi_i)}{|V_i|} \\ F_{y_i} = -fZ_i \dfrac{v_i}{|V_i|} = -fZ_i \dfrac{V\sin(\beta) + \Omega r_i \cos(\chi_i)}{|V_i|} \end{cases} , \tag{D.68}$$

where

$$|V_i| = \sqrt{V^2 + \Omega^2 r_i^2 + 2V\Omega r_i \sin(\beta - \chi_i)} \, . \tag{D.69}$$

The moment of force F_i about the yaw axis z is

$$M_i = F_{y_i} r_i \cos(\chi_i) - F_{X_i} r_i \sin(\chi_i) = fZ_i r_i \frac{\Omega r_i + V\sin(\beta - \chi_i)}{|V_i|} \, . \tag{D.70}$$

The trajectory can thus be easily computed by numerical integration of the equations of motion. No linearization is possible in this case, because the slip angle of the vehicle β may be quite large. The equations of motion are Eq. (25.65), where the forces acting on the wheels are those expressed by Eq. (D.68) rotated in the inertial reference frame by multiplying them by a suitable rotation matrix. The model here used is essentially a three-degrees of freedom, rigid body model in which all forces except those due to tire-road interaction have been neglected. It would in any case be difficult to take aerodynamic forces into account when angle β_a is large and rapidly varying.

At time $t = 0$, coinciding with time t_2 immediately after the collision, the position and the velocity of the vehicle and also angle

$$\beta = \arctan\left(\frac{\dot{x}'}{\dot{y}'} - \psi\right)$$

are known and the numerical integration can be started.

Owing to the impossibility of linearizing the equations of motion, it is impossible to work in terms of axles. The wheels must therefore be considered one by one; in particular velocity V_i is different for the wheels of the same axle. It is difficult to take load transfer between the wheels of the same axle into account with a model based on the assumption of a rigid body. The load transfer can be strongly influenced in these conditions by roll rotations so that a more complete model is required if this effect is to be included. Forces F_{x_i} and F_{y_i} and moment M_i change continuously during motion. The total forces and moments acting on the vehicle also change, but to a lesser extent.

A simple approach that can be used to study the motion of the vehicle without having to perform a numerical simulation is to substitute the actual contact area between the vehicle and the ground with a circle having a radius r equal to the average distance of the centres of the contact areas of the wheels and the centre of mass (Fig. D.19a).

The force and the moment exerted on an arc of amplitude $d\theta$ of such a circumference may be expressed by equations of the same type as equations (D.68) and (D.70). Assuming that the vertical load mg exerted on the contact area is evenly distributed on the circumference, the components of the force and the yawing momentare

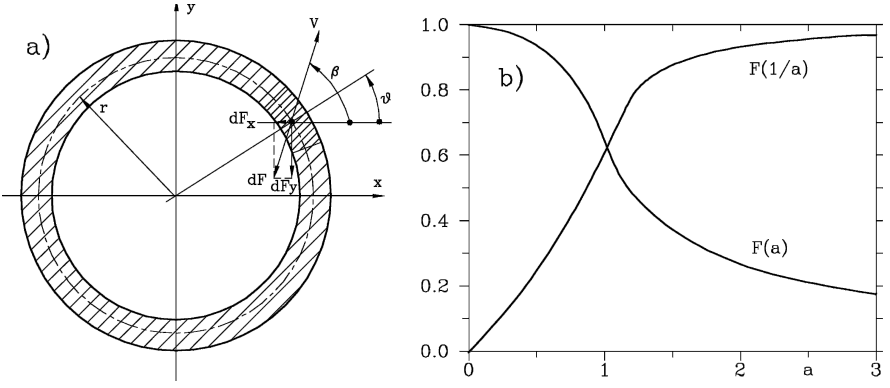

FIGURE D.19. (a) Simplified model for the study of the trajectory of a vehicle moving with locked wheels. Circular contact area that is substituted for the actual contact area. (b) Functions $F(a)$ and $F(1/a)$ for a spanning between 0 and 3.

$$\begin{cases} dF_x = f\dfrac{mg}{2\pi}\dfrac{-V\cos(\beta)+\Omega r\sin(\theta)}{\sqrt{V^2+\Omega^2r^2+2V\Omega r\sin(\beta-\theta)}}d\theta \\ dF_y = -f\dfrac{mg}{2\pi}\dfrac{V\sin(\beta)+\Omega r\cos(\theta)}{\sqrt{V^2+\Omega^2r^2+2V\Omega r\sin(\beta-\theta)}}d\theta \\ dM = -f\dfrac{mgr}{2\pi}\dfrac{V\sin(\beta-\theta)+\Omega r}{\sqrt{V^2+\Omega^2r^2+2V\Omega r\sin(\beta-\theta)}}d\theta\ . \end{cases} \tag{D.71}$$

Force dF may be decomposed along directions parallel and perpendicular to the velocity V. The first component, which is tangential to the trajectory, is

$$dF_{\parallel} = dF_x\cos(\beta)+dF_y\sin(\beta) = -f\frac{mg}{2\pi}\frac{V+\Omega r\sin(\beta-\theta)}{\sqrt{V^2+\Omega^2r^2+2V\Omega r\sin(\beta-\theta)}}d\theta\ . \tag{D.72}$$

Its effect is to reduce the speed of the vehicle. The second component, acting in a direction perpendicular to the trajectory and thus bending the path of the vehicle, is

$$dF_{\perp} = -dF_x\sin(\beta)+dF_y\cos(\beta) = -f\frac{mg}{2\pi}\frac{\Omega r\cos(\beta-\theta)}{\sqrt{V^2+\Omega^2r^2+2V\Omega r\sin(\beta-\theta)}}d\theta\ . \tag{D.73}$$

By integrating the expression of the forces and moments, it follows that

$$\begin{cases} F_{\parallel} = -f\dfrac{mg}{2\pi}\displaystyle\int_0^{2\pi}\frac{1+a\sin(\zeta)}{\sqrt{1+a^2+2a\sin(\zeta)}}d\zeta \\ F_{\perp} = -f\dfrac{mg}{2\pi}\displaystyle\int_0^{2\pi}\frac{a\cos(\zeta)}{\sqrt{1+a^2+2a\sin(\zeta)}}d\zeta = 0 \\ M = -f\dfrac{mgr}{2\pi}\displaystyle\int_0^{2\pi}\frac{1+\frac{1}{a}\sin(\zeta)}{\sqrt{1+\left(\frac{1}{a}\right)^2+\frac{2}{a}\sin(\zeta)}}d\zeta\ , \end{cases} \tag{D.74}$$

where

$$\zeta = \beta - \theta$$

(because β does not depend on θ, $d\zeta = d\theta$) and the nondimensional parameter a is the ratio between the component of the velocity due to rotation and velocity V

$$a = \frac{\Omega r}{V}\ .$$

The component of force F perpendicular to the trajectory is equal to zero: This means that the trajectory is straight, at least within the assumptions used in the present model. If a more accurate model were used the trajectory would bend, although only slightly.

TABLE D.3. Values of functions $F(a)$ and $F(1/a)$ for some values of a.

a	$F(a)$	$F(1/a)$	a	$F(a)$	$F(1/a)$
0	1	0	1,4	0,3860	0,8566
0,2	0,9899	0,1005	1,6	0,3306	0,8936
0,4	0,9587	0,2043	1,8	0,2900	0,9177
0,6	0,9028	0,3158	2,0	0,2587	0,9342
0,8	0,8125	0,4441	2,5	0,2043	0,9587
1,0	0,6366	0,6366	3,0	0,1691	0,9716
1,2	0,4685	0,7926	∞	0	1

The integrals which appear in the expressions of the forces and the moments are functions of parameter a only. By introducing the function $F(a)$ defined as

$$F(a) = \frac{1}{2\pi} \int_0^{2\pi} \frac{1 + a\sin(\zeta)}{\sqrt{1 + a^2 + 2a\sin(\zeta)}} d\zeta \ , \tag{D.75}$$

the expressions of $F_{\parallel}$ and M are simply

$$\begin{cases} F_{\parallel} = -fmgF(a) \\ \\ M = -fmgrF\left(\frac{1}{a}\right) \ . \end{cases} \tag{D.76}$$

Function $F(a)$ must be obtained numerically. Its plot is reported in Fig. D.19b and some values are reported in Table D.3.

The equations governing the motion of the vehicle are two differential equations

$$\begin{cases} \dfrac{dV}{dt} = -fgF\left(\dfrac{r\Omega}{V}\right) \\ \\ \dfrac{d\Omega}{dt} = -fgr\dfrac{m}{J_z}F\left(\dfrac{V}{r\Omega}\right) \ . \end{cases} \tag{D.77}$$

These must be integrated numerically, because parameter a changes continuously during motion and function $F(V/r\Omega)$ cannot be expressed in closed form. Once laws $V(t)$ and $\Omega(t)$ are known, the yaw angle and the position on the trajectory can be obtained by further integration

$$\psi = \int_0^t \Omega(u)du \ , \qquad s = \int_0^t V(u)du \ . \tag{D.78}$$

Example D.6 *Consider a vehicle with m = 1000 kg, J_z = 2000 kg m^2, a = 1.4 m, b = 1.4 m and t = 1.08 m. After the collision, the vehicle moves with a speed V = 7.36 m/s, angular velocity $\Omega = -5.19$ rad/s and angle β equal to 53°. Compute the trajectory and the positions taken by the vehicle until it stops.*

The results obtained by numerically integrating the equations of motion are reported in Fig. D.20a, curves A. A value of 0.7 for the friction coefficient has been

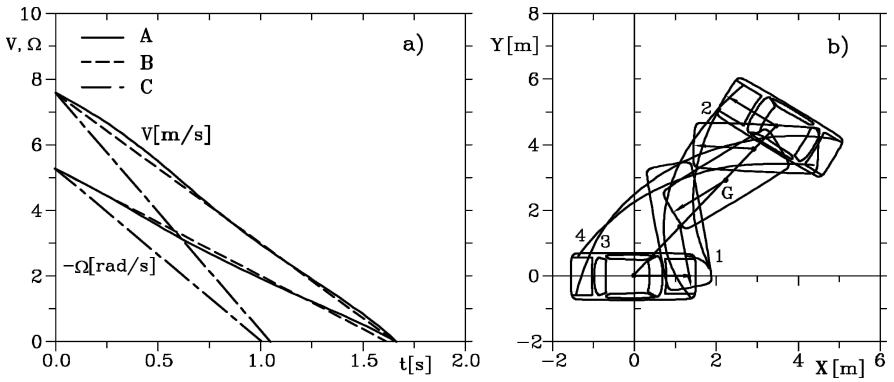

FIGURE D.20. Motion of a vehicle with locked wheels after a collision. (a) Time histories $V(t)$ and $\Omega(t)$ computed through numerical integration of the equations of motion (curves A), numerical integration of Eq. (D.77) (B) and by considering translations and rotations (C) separately. (b) Trajectory corresponding to curve (A).

assumed. The integration was performed using a time step $\Delta t = 0.01$ s. The trajectory is reported in Fig. D.20b. The vehicle stops in a time of 1.70 s, after a displacement of 6.33 m and a rotation of 4.19 rad (240°).

Similar results are obtained by integrating Eq. (D.77) (curves B). The values of function $F(a)$ used for the integration were taken from Table D.3 and interpolated linearly. The time needed to extinguish the motion, the displacement and the rotation are respectively 1.62 s, 6.11 m and 4.06 rad (233°).

Incorrect results would have been obtained by considering translational and rotational motion (curves C) separately. The time needed to extinguish the motion, the displacement and the rotation would have been respectively 1.01 s, 3.94 m and 2.62 rad (150°).

Laws $V(t)$ and $\Omega(t)$ are almost linear. If they were exactly linear the value of a would remain constant during the motion and no numerical integration would be required: A constant rate deceleration with the values of dV/dt and $d\Omega/dt$ given by Eq. (D.77) would occur. Note that this is equivalent to studying the motion as a translation and a rotation occurring separately, with "reduced" coefficients of friction equal to $fF(a)$ and $fF(1/a)$ respectively. In the example, immediately after the collision the value of a is 1.05, $F(a) = 0.62$ and $F(1/a) = 0.66$. By multiplying the friction coefficient by these values and considering the two motions separately, a time of 1.7 s for coming to a standstill is obtained. This value is close to that obtained through more complex models.

D.3.2 Vehicle with free wheels

In most cases the wheels of the vehicle, or at least some of them, remain free to rotate after the collision. There is little difficulty in numerically integrating the equations of motion, obviously written without any linearization. Equation (25.65) can be used, together with Eq. (25.94) yielding the sideslip angles of the

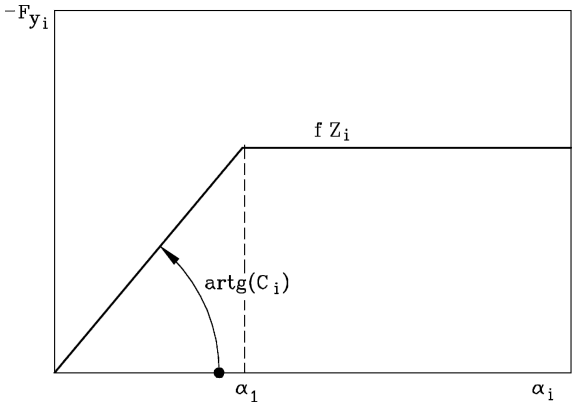

FIGURE D.21. Cornering force of the tire as a function of the sideslip angle. Simplified model in which the curve $F_y(\alpha)$ is approximated by two straight lines.

wheels. A model of the tire which can be used for all values of α from 0 to 360° is needed. The "magic formula" is at present probably the best and most precise choice.

The only difference from the nonlinear model is that some of the wheels may be locked. However, if the angular velocity of the vehicle is high, the sideslip angles remain at high values for a long time and the importance of accurately modelling the behavior of the tires at low sideslip angle is not great. In this situation a simple model for the cornering force of the tire as the one shown in Fig. D.21 may be used. With reference to the figure, the force the tire receives from the road is

$$\begin{cases} F_{x_i} = F_{z_i} \dfrac{\mu_i}{|\mu_i|} \left[-f_r \cos(\delta_i) - f \sin(\delta_i) \right] \\ \qquad\qquad\qquad\qquad\qquad\qquad \text{if} \quad \alpha > \alpha_1 \quad , \\ F_{y_i} = F_{z_i} \dfrac{\mu_i}{|\mu_i|} \left[-f_r \sin(\delta_i) + f \cos(\delta_i) \right] \end{cases}$$

$$\begin{cases} F_{x_i} = F_{z_i} \dfrac{\mu_i}{|\mu_i|} \left[-f_r \cos(\delta_i) - \dfrac{\alpha_i}{C_i} f \sin(\delta_i) \right] \\ \qquad\qquad\qquad\qquad\qquad\qquad \text{if} \quad \alpha \leq \alpha_1 \quad , \\ F_{y_i} = F_{z_i} \dfrac{\mu_i}{|\mu_i|} \left[-f_r \sin(\delta_i) + \dfrac{\alpha_i}{C_i} f \cos(\delta_i) \right] \end{cases} \tag{D.79}$$

where f_r is the rolling coefficient.

The moment about the z-axis is expressed by the first part of Eq. (D.70). The rolling drag is usually small compared to the other forces and might be neglected but, because the equation must in any case be integrated numerically, there is no need to do so.

Example D.7 *Repeat the study of Example D.6 assuming that the wheels are free and all steer angles δ_i are equal to zero.*

By assuming a law $F_y(\alpha)$ of the type shown in Fig. D.21 with $\alpha_1 = 8°$ and $f_r = 0.02$ the results shown in Fig. D.22 are obtained through numerical integration. The

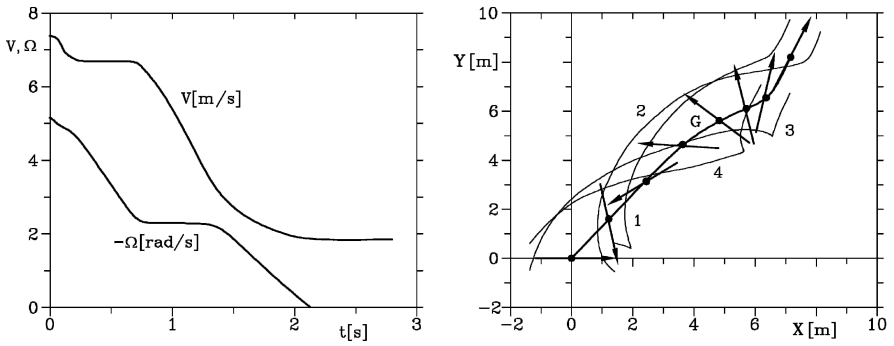

FIGURE D.22. Motion of a vehicle with free wheels after a collision. (a) Time histories $V(t)$ and $\Omega(t)$ computed through numerical integration of the equations of motion and (b) trajectories of the centre of mass and of the points of contact of the wheels.

computations were repeated with different values of angle α_1, obtaining practically the same results in all cases. With $\alpha_1 = 0$ the laws $V(t)$ and $\Omega(t)$ do not change, except for some oscillations due to numerical problems.

The vehicle at the end of the simulation is aligned with its velocity and rolls forward freely. In other cases the simulation may end with the vehicle rolling away in reverse.

D.4 ROLLOVER

D.4.1 Quasi-static rollover

As discussed in Part IV, rollover of a rigid vehicle in static or quasi-static conditions is usually impossible, except in the case of vehicles with particularly narrow track or high centre of mass: The conditions for slipping are reached well before those needed for rollover.

Rollover on a flat surface is controlled by parameter

$$\frac{t}{2h_G} ,$$

which is sometimes referred to as the rollover threshold: This constitutes the limit to the ratio between the lateral acceleration and the gravitational acceleration a_y/g. If the road has a transversal slope

$$i_t = \tan(\alpha_t)$$

the threshold becomes

$$\frac{t}{2h_G} - i_t .$$

The threshold increases linearly with the slope if the external part of the curve is raised and decreases otherwise.

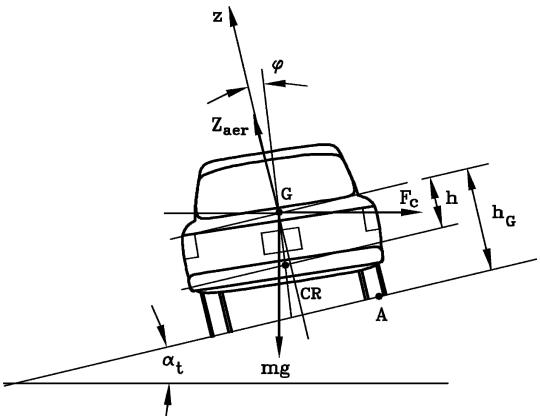

FIGURE D.23. Quasi-static rollover of a vehicle on elastic suspensions.

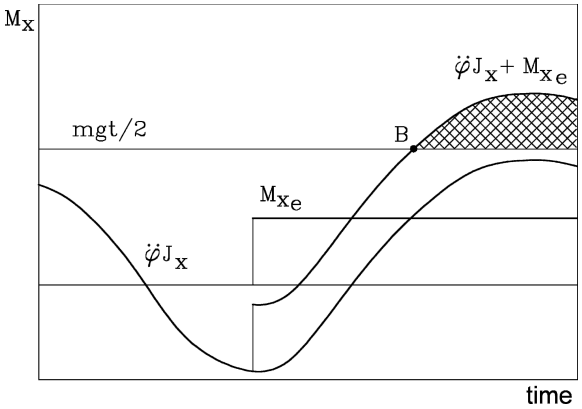

FIGURE D.24. Roll inertia torques causing rollover: In B the conditions for rollover are reached.

If

$$i_t = \frac{t}{2h_G}$$

the vehicle overturns naturally without the application of external forces, but this can occur only in case of off-road motion, because the adverse slope must be quite large.

To release the assumption of a rigid vehicle, the roll of the vehicle body must be accounted for. With reference to Fig. D.24, the forces acting in the direction parallel and perpendicular to the road surface are

$$\begin{cases} F_{\parallel} = \dfrac{mV^2}{R}\cos(\alpha_t) - mg\sin(\alpha_t) \\ \\ F_{\perp} = \dfrac{mV^2}{R}\sin(\alpha_t) + mg\cos(\alpha_t) - Z_{aer}\ . \end{cases} \tag{D.80}$$

If the inertia of the unsprung masses and the compliance of the tires are neglected and the roll angle is small enough, its value is

$$\phi \approx \frac{F_{\parallel} h}{K_t} , \tag{D.81}$$

where h is the height of the centre of mass over the roll axis and K_T is the torsional stiffness of the vehicle.

The vehicle rolls over if

$$\frac{F_{\parallel}}{F_{\perp}} > \frac{t - 2h\phi}{2h_G} . \tag{D.82}$$

Neglecting aerodynamic lift and assuming that the road surface is flat, the above equations may be solved in the lateral acceleration, yielding

$$\frac{V^2}{Rg} > \frac{t}{2h_G} \frac{1}{1 + \dfrac{mgh^2}{K_t h_G}} . \tag{D.83}$$

The fraction on the right hand side is a factor smaller than one expressing the reduction of resistance to rollover due to the presence of suspensions. The rollover threshold decreases with increasing roll compliance $1/K_t$ of the suspensions and distance h between the centre of mass and the roll centre. A stiff suspension with high roll centre can substantially reduce rollover danger and bring the rollover conditions close to those characterizing the rigid vehicle.

The rollover threshold can be reduced, owing to roll compliance, by a few percent (typically 5%) in passenger vehicles, with lower reductions in sports cars and greater in large luxury saloon cars.

The compliance of the tires increases this effect slightly, and some effects may be due to the exact geometry of the suspensions, particularly in terms of their lateral deflection, the lateral deflection of the tires and the inclination of the roll axis due to the differences between front and rear suspensions. To account for all these factors, a detailed mathematical model of the vehicle must be built and analyzed on a computer.

Alternatively, the whole vehicle can be put on a "tilt-table", i.e. on a platform that can be inclined laterally, and the lateral slope can be increased until the load on the less loaded wheels reduces almost to zero, denoting that the threshold of rollover has been reached. Note that the tilt-table arrangement exactly simulates rollover due to the lateral slope of the road, as may occur in off-road driving, but does not exactly reproduce conditions on flat road. The difference may be small if the vehicle rolls over on a lateral slope that is not too steep, i.e. about $20° \div 25°$, while the errors build up when the lateral slope reaches values as high as $45°$, where errors of about 30% may be present. To avoid this problem, a "cable-pull" test can be devised, in which the lateral forces are applied by cables directly to the vehicle at the location of the centre of mass.

In spite of these effects, static rollover remains a rare occurrence for all vehicles but those with very high centre of mass and narrow track, because the available lateral forces on the tires are not high enough to prevent lateral slipping before rollover.

D.4.2 Dynamic rollover

Dynamic conditions linked to roll oscillations, on the other hand, can lead to rollover if the external rolling moment adds to an inertia torque due to roll accelerations.

If a step roll input is applied to the vehicle, the response is a damped roll oscillation about the static equilibrium position that would have been reached if the same input had been applied slowly. Note that an input is applied slowly if its characteristic times are larger than the period of the lowest natural frequency involved; because the roll period is usually on the order of one second, most roll inputs, being faster than that, have the characteristics of a dynamic load.

Remark D.3 *If the vehicle were critically damped in roll no oscillations would take place. The roll angle would increase monotonically, reaching the static value asymptotically.*

Because all vehicles are underdamped in roll, the roll angle overshoots and then oscillates; the lower the damping ratio of the system the higher the overshoot and thus the danger of rollover. The presence of anti-roll bars makes things worse from this viewpoint. When anti-roll bars are added to an existing suspension the roll stiffness is increased but roll damping is usually unchanged, because the damping of shock absorbers is optimized for bounce and pitch behavior. The effect is an increase of the natural frequency and the underdamped behavior of the system. While the static roll angle is decreased by the added stiffness, both the overshoot and the natural frequency of roll oscillations are increased, the latter effect increasing roll inertia torques.

Consider a vehicle undergoing roll oscillations (Fig. D.24). The inertia torque $J_x\ddot{\phi}$ due to roll oscillations is sketched as a function of time in the figure. It is always lower than $mgt/2$, the restoring moment due to weight on level road, and hence no danger of rollover is present. However, if an external force causing the rolling moment M_{x_e} is applied, the conditions for incipient rollover occur in B.

From this point on the wheels at one side lose contact with the ground. The weight stabilizes, until a large enough roll rotation to bring the weight force outside point A in Fig. D.24 is completed, but the vehicle continues the roll over motion. Note that this simple model is inadequate to predict what happens when some of the wheels are no longer in contact with the ground and the roll angle is magnified.

A fast-reacting driver may prevent rollover even in these conditions by giving appropriate steering inputs, as testified by stunt drivers who can proceed with the car on two wheels, without either rolling over or rolling back onto four wheels,

but it is most unlikely that a normal driver in normal conditions would perform stunts of this type. In most cases, once rollover starts it proceeds to its inevitable consequences.

Roll dynamics is closely coupled with yaw dynamics and rollover is no exception. During a sinusoidal steering input the lateral tire forces on the rear wheels are delayed with respect to those on the front wheels; this delay is larger in longer vehicles and the effect is even more pronounced in articulated vehicles. The combined roll-yaw dynamics with its resonances may facilitate rollover, particularly when selected frequencies are present in the excitation.

Tractor-trailer combinations are particularly subject to rollover due to sudden steering inputs: The roll of the trailer is delayed with respect to that of the tractor and can be large enough to cause the former to rollover. A hitch providing roll coupling between trailer and tractor helps in this case, because the latter collaborates in resisting the tendency of the former to overturn.

D.4.3 Lateral collision with the curb

Consider a vehicle modelled as a rigid body and assume that its velocity V is not contained in the plane of symmetry (Fig. D.25). Both wheels on one side enter into contact at time t_1 with the curb. At time t_1 the components of the velocity are[5]

$$u = u_1 \ , \quad v = v_1 \ , \quad w = p = q = r = 0 \ ,$$

i.e. the velocity of the vehicle is contained in a plane parallel to the road and the angular velocity is nil.

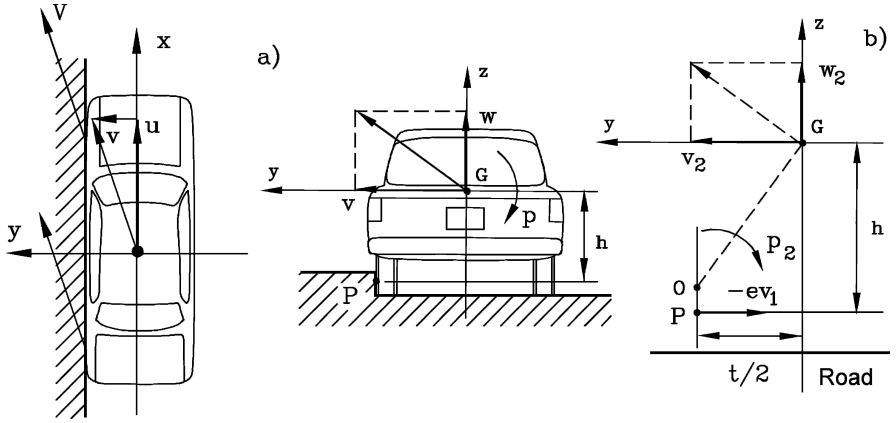

FIGURE D.25. Side impact against the curb. (a) Sketch; (b) determination of the centre of rotation at time t_2.

[5]The components Ω_x, Ω_y and Ω_z of the angular velocity are here indicated as p, q and r, and the component V_z of the velocity is indicated with w.

If friction between the vehicle and the curb is neglected, the component u of the velocity along the x-axis remains constant and the components q and r of the angular velocity along the y and z axes remain vanishingly small. The other components of the velocity after the impact, i.e. at time t_2, are

$$v = v_2 \ , \quad w = w_2 \ , \quad p = p_2 \ .$$

The component of the velocity in a direction perpendicular to the impact surface in P at time t_1 is

$$V_{\perp_1} = v_1 \ .$$

Assuming a partially inelastic impact with coefficient of restitution e^*, at time t_2 the same velocity is

$$V_{\perp_2} = -e^* v_1 \ .$$

If the condition that the motion of point P between time t_1 and t_2 occurs in a plane parallel to the ground is added, the position of the centre of rotation at time t_2 can be easily found and a relationship linking w_2 and p_2 to v_1 can be obtained.

With reference to Fig. D.25b it follows that

$$\begin{cases} p_2 = -\dfrac{v_2 + e^* v_1}{h} \\ \\ w_2 = -p_2 \dfrac{t}{2} = (v_2 + e^* v_1)\, \dfrac{t}{2h} \ , \end{cases} \tag{D.84}$$

The components of the impulse the vehicle receives during the impact can be related to the variations of the momentum and the angular momentum

$$\begin{cases} I_y = m(v_1 - v_2) \\ \\ I_z = -m w_2 \\ \\ I_y h - I_z \dfrac{t}{2} = -J_x p_2 \ . \end{cases} \tag{D.85}$$

By introducing Eq. (D.84) into Eq. (D.85) it follows that

$$\begin{cases} v_2 = -v_1 \dfrac{A^2 - e^*(1 + B^2)}{1 + A^2 + B^2} \\ \\ p_2 = -v_1 \dfrac{A^2(1 + e^*)}{h(1 + A^2 + B^2)} \ , \end{cases} \tag{D.86}$$

where

$$A = \frac{2h}{t} \ , \qquad B = \frac{2}{t}\sqrt{\frac{J_x}{m}} \ .$$

Rollover motion starts at time t_2. If the component of the velocity of point P in the y direction vanishes rapidly owing to the friction of the road, rollover actually occurs if the centre of mass crosses a line perpendicular to the road in P. This means that the vehicle rolls over only if its centre of mass moves above a distance Δh equal to

$$\Delta h = \sqrt{\frac{t^2}{4} + h^2} - h = h\left(\sqrt{1 + \frac{1}{A^2}} - 1\right) . \tag{D.87}$$

This can occur only if the kinetic energy associated with velocities v_2, w_2 and p_2 is at least equal to the potential energy $mg\Delta h$. With simple computations it can be shown that the condition for completing rollover is

$$v_2^2 + w_2^2 + \frac{J_x}{m} p_2^2 \geq 2hg\left(\sqrt{1 + \frac{1}{A^2}} - 1\right) . \tag{D.88}$$

Because

$$v_2^2 + w_2^2 = p_2^2\left(\frac{t^2}{4} + h^2\right) ,$$

the condition for rollover becomes

$$v_1^2 \frac{A^2(1+e^*)^2}{1 + A^2 + B^2} \geq 2hg\left(\sqrt{1 + \frac{1}{A^2}} - 1\right) . \tag{D.89}$$

Consider for instance a vehicle with $A = 0.6$ and $B = 0.7$ hitting a curb in a perfectly elastic way ($e^* = 1$), which is the most dangerous condition. From Eq. (D.89) the rollover condition is

$$v_1^2 \geq 2.42gh .$$

Equation (D.89) may be written explicitly in terms of forward velocity V and impact angle θ

$$V^2 \sin^2(\theta) \geq 2hg \frac{1 + A^2 + B^2}{A^2(1+e^*)^2}\left(\sqrt{1 + \frac{1}{A^2}} - 1\right) . \tag{D.90}$$

If $h = 0.36$ m and the impact angle is $\theta = 15°$, the vehicle in question will roll over for forward velocities greater than 11 m/s (40 km/h). Note that this result depends strongly on the value of e^*: The ratio between the velocities V needed for rollover when $e^* = 0$ and $e^* = 1$ is equal to $\sqrt{2}$. It makes sense that in this case the restitution coefficient e^* is greater than in the case of impacts between vehicles, but in general it depends upon the impact conditions.

It must also be noted that if the height of the curb is low, and consequently the value of h is large, the vehicle tends not to engage against the curb but to drive over it, making the whole study inapplicable. The assumption of a rigid body is also questionable: The impact usually occurs between the curb and the unsprung mass and the latter can undergo plastic and elastic deformations, accompanied by deformations of the tires.

D.4.4 Effect of the transversal slope and the curvature of the road

The above model is based upon the assumptions that the road is flat and that the curb is straight. To account for the transversal slope of the road it is sufficient to assume that the y-axis is inclined. The only difference is that of changing the expression of the potential energy due to the vertical displacement of the centre of mass of the vehicle, because a vertical line passing through point P is no longer perpendicular to the road.

If the curb is not straight the motion is more complex and it is not possible to study the motion in the yz plane independently of that in the x direction. However, if the curb follows a circular path with a radius far greater than the length of the vehicle and of the displacements in the y direction involved in the rollover motions, it is possible to simplify the problem.

Consider the situation shown in Fig. D.26a. The motion in the yz plane can be studied with reference to the non-inertial xyz frame, rotating about line CC′ with angular velocity

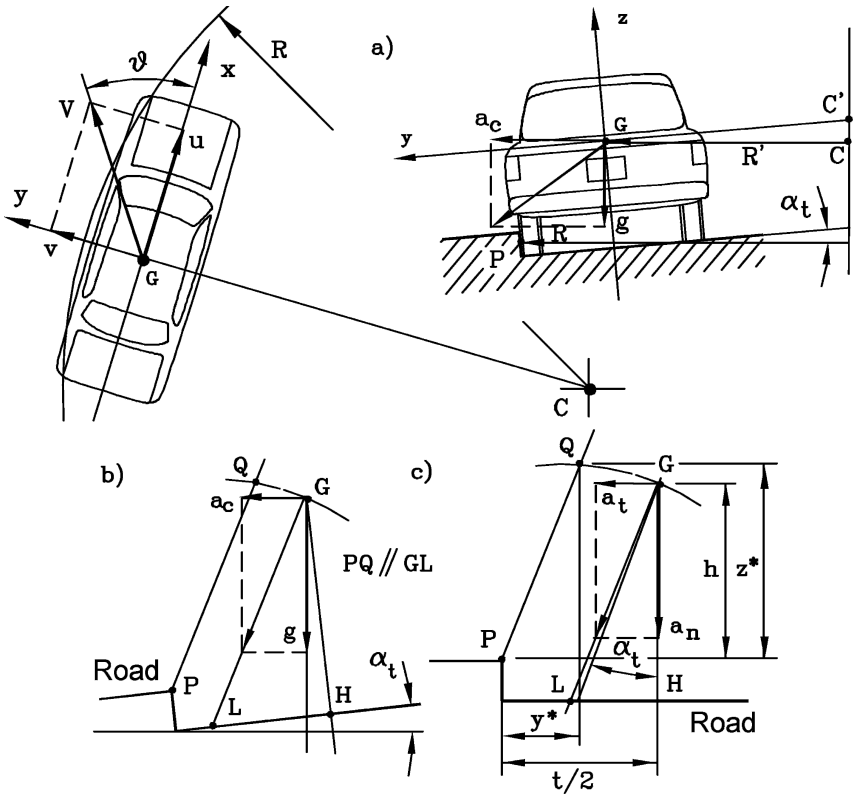

FIGURE D.26. Side impact against a curb following a circular path. (a) Sketch at time t_2; (b) accelerations broken into vertical and horizontal directions and (c) in directions parallel and perpendicular to the road.

$$\frac{V\cos(\theta)}{R} \ .$$

Both centrifugal and Coriolis acceleration must be introduced in the study of the motion starting from time t_2.

Centrifugal acceleration is directed radially while Coriolis acceleration acts in the x direction. Their values are, respectively,

$$\begin{cases} a_c = \dfrac{u^2}{R'} = \dfrac{V^2}{R'}\cos^2(\theta) \\ \\ a_{cor} = -2\dfrac{V}{R'}\cos(\theta)\left[v_2\cos(\alpha_t) + w_2\sin(\alpha_t)\right] \ . \end{cases} \tag{D.91}$$

Only centrifugal acceleration needs to be considered in the study of the motion in the yz plane. It can be considered constant, neglecting the fact that R' and u change during the rollover motion. The method used in the previous case may be repeated by simply introducing the resultant of centrifugal and gravitational accelerations (here broken into directions parallel and perpendicular to the road surface)

$$\begin{cases} a_\perp = g\cos(\alpha_t) - a_c\sin(\alpha_t) \\ \\ a_\parallel = g\sin(\alpha_t) + a_c\cos(\alpha_t) \ . \end{cases} \tag{D.92}$$

for the gravitational acceleration (Fig. D.26a,b). The vehicle will roll over if its centre of mass goes beyond line PQ, whose direction is that of the resultant of the two accelerations. The coordinates of point Q are then linked to each other by the relationship

$$\frac{y^*}{z^*} = \frac{a_\parallel}{a_\perp} \ .$$

Point Q lies on a circle centred in P passing through point G. It then follows that

$$y^{*^2} + z^{*^2} = h^2 + \frac{t^2}{4} \ . \tag{D.93}$$

By intersecting the circle with line PQ it follows that

$$y^* = h\frac{\sqrt{1+\frac{1}{A^2}}}{\sqrt{1+\left(\frac{a_\perp}{a_\parallel}\right)^2}} \ , \qquad z^* = h\frac{\sqrt{1+\frac{1}{A^2}}}{\sqrt{1+\left(\frac{a_\parallel}{a_\perp}\right)^2}} \ , \tag{D.94}$$

where

$$A = \frac{2h}{t} \ .$$

The total increase of potential energy in the motion from G to Q to be substituted for $mg\Delta h$ in the rollover condition is

$$\Delta\mathcal{U} = mha_\perp\left\{\sqrt{\left(1+\frac{1}{A^2}\right)\left[1+\left(\frac{a_\perp}{a_\parallel}\right)^2\right]} - 1 - \frac{a_\parallel}{Aa_\perp}\right\}, \tag{D.95}$$

The final form of the rollover condition is thus

$$v_1^2 \frac{A^2(1+e^*)^2}{1+A^2+B^2} \geq 2ha_\perp \left\{ \sqrt{\left(1+\frac{1}{A^2}\right)\left[1+\left(\frac{a_\perp}{a_\parallel}\right)^2\right]} - 1 - \frac{a_\parallel}{Aa_\perp} \right\} . \quad \text{(D.96)}$$

Clearly if

$$\frac{a_\perp}{a_\parallel} = A,$$

the vehicle rolls over even for $v_1 = 0$: Points G and Q coincide and the system is statically on the verge of instability. If the curb is along a straight line ratio $a_\parallel/a_\perp$ is equal to $\tan(\alpha_t) = i_t$, transversal slope of the road.

If on the contrary the road is flat but curved,

$$\frac{a_\parallel}{a_\perp} = \frac{a_c}{g} = V^2 \frac{\cos^2(\theta)}{Rg} .$$

The nondimensional velocity $v_1/\sqrt{a_\perp h}$ needed for rollover is plotted against ratio $a_\parallel/a_\perp$ for various values of e^* in Fig. D.27. The plot has been obtained for $A = 0.6$ and $B = 0.7$.

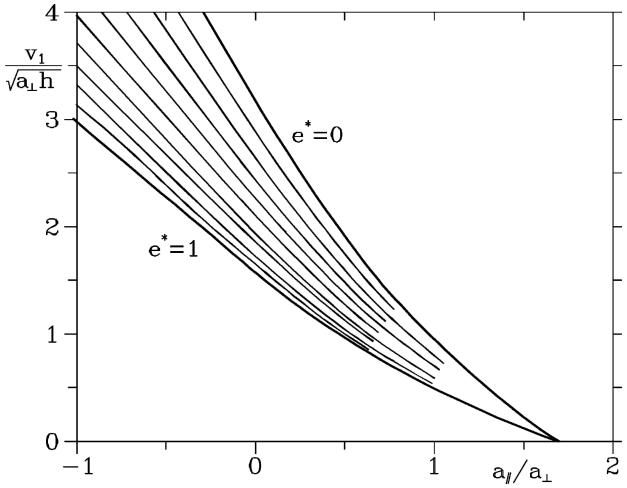

FIGURE D.27. Nondimensional velocity $v_1/\sqrt{a_\perp h}$ needed for rollover as a function of $a_\parallel/a_\perp$ for various values of e^*. Vehicle with $A = 0.6$ and $B = 0.7$.

D.5 MOTION OF TRANSPORTED OBJECTS DURING THE IMPACT

D.5.1 Free objects

The study of the motion of objects onboard vehicles during a collision is important both for understanding their effects on passengers and for devising suitable restraint systems for people and packaging for objects.

If the object is simply supported on a surface parallel to the road, when the vehicle stops abruptly because of a collision (which in the following will be considered as a central impact against a fixed object) it will continue its motion until it collides with the front wall of the load compartment. This first part of the collision process is easily studied under the assumption that the mass of the object is negligible with respect to that of the vehicle. The motion of the former does not influence that of the latter.

Consider the situation sketched in Fig. D.28, in which the elastic and damping properties of the transported object are modelled by a spring-damper system. The motion of the vehicle is assumed to follow the model described in Section D.2.1 and the motion of the object will be studied with reference to the xz frame centred in the position of point P, belonging to the front part of the object, at time t_1, when the vehicle hits the obstacle.

Neglecting friction, the motion of point P immediately after the collision is described by the law

$$x_P = V_1 t = V_1 t_2 \tau \ , \tag{D.97}$$

where V_1 is the velocity of the vehicle before the collision and the nondimensional time

$$\tau = \frac{t}{t_2}$$

is defined with respect to the duration of the collision t_2.

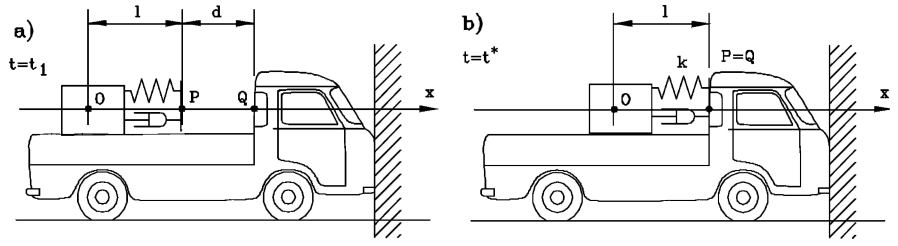

FIGURE D.28. Motion of the object O free to move on a vehicle hitting a rigid barrier. The elastic and damping properties of the object are modelled by a spring-damper system. (a) Situation at time t_1. (b) Situation at time t^*, when the object hits the front wall of the load compartment.

Assuming the model of Section D.2.1 to describe the motion of the vehicle, the x coordinate of point Q is

$$x_Q = d + V_1 t_2 \left(\frac{1+e^*}{\beta+3} \left\{ 2 - [2 + (\beta+1)\tau] (1-\tau)^{\beta+2} \right\} - e^* \tau \right) . \tag{D.98}$$

The object hits the front wall of the load compartment at time t^*, when the distance between points P and Q vanishes, i.e. when

$$\tau^* - \frac{2 - [2 + (\beta+1)\tau^*] (1-\tau^*)^{\beta+2}}{\beta+3} = \frac{d}{V_1 t_2 (1+e^*)} . \tag{D.99}$$

Equation (D.99) can be easily solved in τ^*; however this solution holds only if $\tau^* \leq 1$, i.e. if the object collides before time t_2. If this condition does not hold the secondary collision inside the vehicle occurs when the latter has started its motion backward after rebounding from the obstacle and Eq. (D.98) does not apply. The condition for which Eq. (D.99) holds, i.e. for which $\tau^* \leq 1$, is simply

$$d \leq V_1 t_2 (1+e^*) \frac{\beta+1}{\beta+3} . \tag{D.100}$$

If condition (D.100) is satisfied, the relative velocity is easily computed by considering that at time τ^* the velocities of the object and the vehicle are both known

$$V_R = V_1 (1+e^*) \left\{ 1 - [1 + (\beta+1)\tau^*] (1-\tau^*)^{\beta+1} \right\} . \tag{D.101}$$

If, on the contrary, condition (D.100) is not satisfied, the computation is even simpler. If the rebound velocity is considered constant,

$$V_2 = -e^* V_1 ,$$

after time t_2, the relative velocity is simply

$$V_R = V_1 (1+e^*) .$$

The time at which the secondary collision takes place can be assumed to be

$$t^* = t_2 + t_3 ,$$

where t_3 is the time needed to travel at the velocity V_R defined above for a distance d_2 that still separates the object and the vehicle at time t_2. d_2 can be computed stating $\tau = 1$ into Eq. (D.98), i.e. by Eq. (D.100) with '='. Operating in this way, it follows that

$$t_3 = \frac{d}{V_1 (1+e^*)} - t_2 \frac{\beta+1}{\beta+3} . \tag{D.102}$$

The motion of the object after it hits the wall of the load compartment may be analyzed in different ways.

It is possible to resort to a semi-empirical time history, as was done for the vehicle colliding against an obstacle, or to model the mechanical properties of the object and to use that model to obtain the equation of motion.

By assuming that the object and the wall are rigid bodies with an interposed linear spring-damper system, as sketched in Fig. D.28, the equation of motion of point O for $t > t^*$ is

$$m\ddot{x}_O + c(\dot{x}_O - \dot{x}_Q) + k(x_O + l - x_Q) = 0 \,, \tag{D.103}$$

with the initial conditions

$$x_O = x_Q - l \quad \text{and} \quad \dot{x}_O = V_1 \qquad \text{for} \;\; t = t^* \,. \tag{D.104}$$

By introducing the nondimensional coordinate

$$\chi = \frac{x_O + l - x_Q}{V_1 t_2}$$

and the nondimensional time τ, the equation of motion reduces to

$$\frac{d^2\chi}{d\tau^2} + \frac{ct_2}{m}\frac{d\chi}{d\tau} + \frac{kt_2^2}{m}\chi = \frac{d^2\chi_Q}{d\tau^2} \,, \tag{D.105}$$

with the initial conditions

$$\chi = 0 \qquad \text{and} \qquad \frac{d\chi}{d\tau} = 1 - \left(\frac{d\chi_Q}{d\tau}\right)_{\tau=\tau^*} \qquad \text{for} \qquad t = t^*.$$

The expressions of $d^2\chi_Q/d\tau^2$ and of $d\chi_Q/d\tau$ can be easily computed from t^* to t_2 $(0 \le \tau \le 1)$ from Equations. (D.31) and (D.35) while for $t > t_2$ $(\tau > 1)$ they are simply

$$\frac{d^2\chi_Q}{d\tau^2} = 0 \;\;, \quad \frac{d\chi_Q}{d\tau} = -e^* \,.$$

If the secondary collision occurs before time t_2 the equation of motion of the object is

$$\begin{aligned} &\frac{d^2\chi}{d\tau^2} + \frac{ct_2}{m}\frac{d\chi}{d\tau} + \frac{kt_2^2}{m}\chi = (\beta+1)\,(\beta+2)\,(1+e^*)\,\tau\,(1-\tau)^\beta \qquad \text{for} \;\; \tau^* < \tau < 1, \\ &\frac{d^2\chi}{d\tau^2} + \frac{ct_2}{m}\frac{d\chi}{d\tau} + \frac{kt_2^2}{m}\chi = 0 \qquad\qquad\qquad\qquad\qquad\qquad\quad \text{for} \;\; \tau > 1, \end{aligned} \tag{D.106}$$

with the initial conditions $\chi = 0$ and

$$\frac{d\chi}{d\tau} = (1+e^*)\left\{1 - [1 + (\beta+1)\tau^*]\,(1-\tau)^{\beta+1}\right\}$$

for $t = t^*$.

If the secondary shock occurs during the rebound phase, after the vehicle has lost contact with the obstacle, the equation of motion is the second of Equations. (D.106) and the initial condition on $d\chi/d\tau$ reduces to

$$\frac{d\chi}{d\tau} = (1 + e^*) \ .$$

These equations of motion hold only up to the time in which the object rebounds, losing contact with the wall of the load compartment. This instant can be easily computed by looking for the time at which the acceleration of the object vanishes, because the force acting between points P and Q reduces to zero.

The acceleration may can be computed as

$$\begin{aligned} \frac{d^2\chi_0}{d\tau^2} &= \frac{V_1}{t_2}\left[\frac{d^2\chi}{d\tau^2} - (\beta+1)(\beta+2)(1+e^*)\,\tau\,(1-\tau)^\beta\right] && \text{if } \ \tau^* < \tau < 1, \\ \frac{d^2\chi_0}{d\tau^2} &= \frac{V_1}{t_2}\frac{d^2\chi}{d\tau^2} && \text{if } \ \tau > 1. \end{aligned} \tag{D.107}$$

This expression of the acceleration is one of the most interesting results of this study, because the aim of the elastic system with stiffness k and damping c is to allow the object to survive the shock of the collision, which means reducing its acceleration within allowable limits.

Another important result is the value of the maximum displacement χ, i.e. the maximum compression of the spring. This value cannot be higher than a given allowable limit, beyond which the elastic system is crushed or, at least, shows nonlinear characteristics with increasing stiffness. In practice, to limit the acceleration the spring must be soft but the decrease of the value of k is limited by the available space because it causes the maximum travel to increase.

The whole process is governed by five nondimensional parameters: β and e^*, linked to the way the vehicle collides with the obstacle, ratio

$$\frac{d}{V_1 t_2} \ ,$$

linked to the clearance between the object and the wall, and

$$\frac{kt_2^2}{m} \quad \text{and} \quad \frac{ct_2}{m} \ ,$$

related to the elastic and damping characteristics of the object.

Parameter kt_2^2/m can be written in the form

$$\frac{kt_2^2}{m} = (\omega_n t_2)^2 = 4\pi^2 \left(\frac{t_2}{T_n}\right)^2 \ , \tag{D.108}$$

where ω_n and T_n are the circular frequency and the period of the undamped free oscillations of a spring-mass system with mass m and stiffness k. If this parameter has a value equal to π^2 the half-period of the undamped oscillations is equal to t_2.

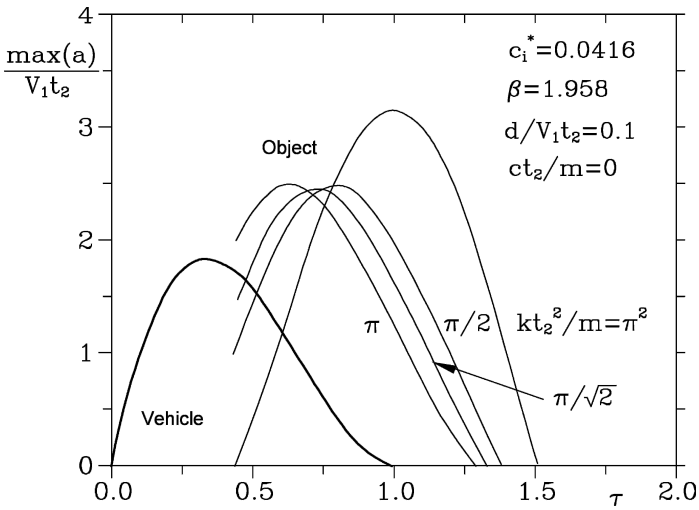

FIGURE D.29. Time history of the acceleration for the vehicle studied in Fig. D.13 hitting a fixed obstacle at 20 m/s and for an object carried by it.

Parameter ct_2/m is linked to kt_2^2/m and to the damping ratio ζ by the relationship

$$\frac{ct_2}{m} = \zeta\sqrt{2}\sqrt{\frac{kt_2^2}{m}} \,. \tag{D.109}$$

The absolute value of the acceleration of an object onboard the vehicle studied in Fig. D.13 hitting a fixed obstacle at 20 m/s is plotted against time in Fig. D.29. The value of kt_2^2/m has been assumed to be equal to π^2; the various curves correspond to different values of ct_2/m. In the case studied, the lowest maximum acceleration is obtained for

$$\frac{ct_2}{m} = \pi/\sqrt{2} \,,$$

i.e. for $\zeta = 0.5$.

This value of the damping ratio coincides with the "optimum value" defined in Section 6.8.1 for the quarter car model with a single degree of freedom. As the two models are different, such instances cannot be generalized and the values of ζ minimizing the acceleration must be obtained for each case, as can be verified by plotting the same figure with different values of the parameters.

The maximum values of the acceleration and the displacement are plotted versus parameter kt_2^2/m in Fig. D.30. The plot has been obtained with the same values of β and e^* used for Fig. D.29, with the added assumption of a damping ratio equal to 0.5. From the figure it is clear that the distance d must be kept to a minimum to provide low values for the acceleration. From the maximum allowable value of the displacement χ it is possible to obtain the minimum value of k and then the value of the peak acceleration occurring during the impact.

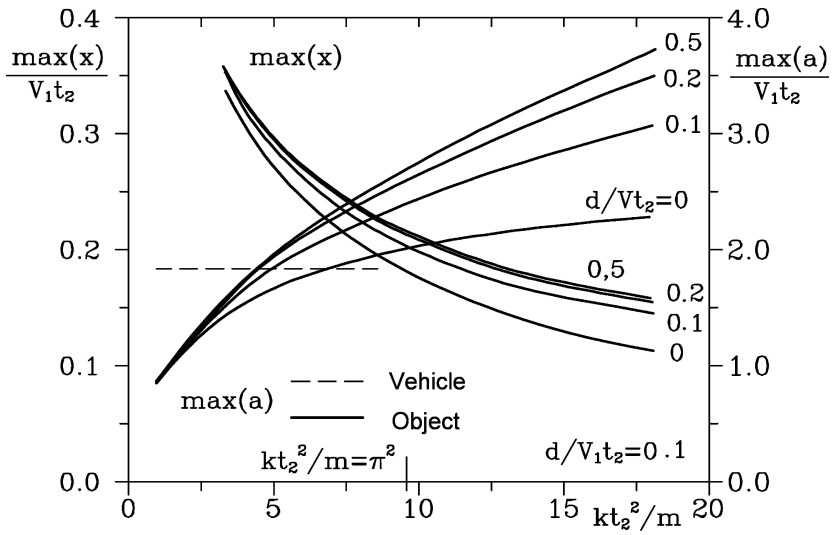

FIGURE D.30. Peak values of the acceleration and of the displacement as a function of the stiffness of the spring for various values of the clearance d. Same vehicle as in Fig.D.29; damping equal to half of the critical damping (ζ =0.5).

The results shown in Figs. D.29 and D.30 were obtained by numerical integration of the equation of motion in time.

The simple models here shown allow basic and straightforward qualitative assessments, with a limited number of parameters involved. There is, however, no difficulty in building more complete models that result in good quantitative predictions of the actual behavior of the system.

D.5.2 Constrained objects

The behavior of an object constrained onboard a vehicle is not qualitatively different from that seen for free objects. In the case of constrained objects the distance d, i.e. the clearance of the restraining device, is smaller and may even be equal to zero.

The motion of a constrained object can be studied in four distinct phases (Fig. D.31).

1. The first phase begins in the instant the vehicle encounters the obstacle starting its deceleration and ends at time t^* when the object contacts the restraining system. Usually, if the clearance is not too large, time t^* occurs before time t_2.

2. The second phase extends between time t^* and time t_2. The collision of the vehicle against the obstacle is completed and the object is retained by the constraining device. At the end the vehicle rebounds freely.

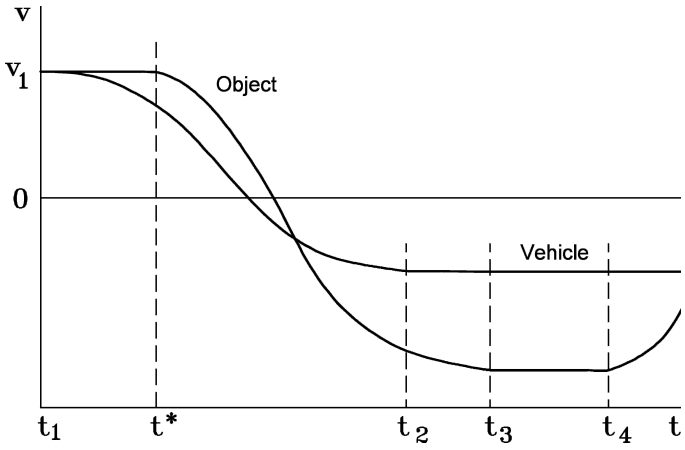

FIGURE D.31. Time history of velocity of the motion of the vehicle and of an object constrained on board.

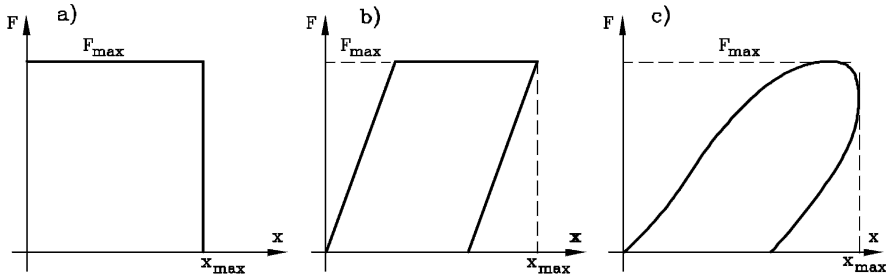

FIGURE D.32. Force exerted by the restraining system as a function of the deformation x; the energy dissipated is the area under the curve. (a) Perfectly plastic, (b) elasto-plastic and (c) actual behaviour.

3. The third phase is between time t_2 and time t_3. The object rebounds backward and, at the end, loses contact with the restraining system. The vehicle moves backward, with a speed that is low if the collision is strongly inelastic.

4. The fourth phase goes from time t_3 to time t_4 when the object, moving backward at a speed higher than that of the vehicle, hits the back wall of the load compartment.

The study may then continue, because at this point there may be a further rebound, which can be particularly dangerous.

A case of particular importance that can be studied, at least as a first approximation, with the present technique, is that of the motion of a person wearing a seat belt. The collision with the seat at time t_4 can be the most dangerous event under these circumstances.

To increase the adequacy of the model to supply quantitative information as well it is possible to factor in the nonlinearities that are always present in actual cases. A nonlinear law stating the dependence of the force provided by the restraint as a function of the displacement x and of the velocity $\dot{x}$ may be introduced without adding greatly to the complexity of the numerical simulation.

The restraining system should have a perfectly plastic behavior to reduce the acceleration peak to a minimum, as in this case the energy dissipation is maximum for a given value of applied force and displacement (Fig. D.32a).

A more realistic behavior is an elasto-plastic law (Fig. D.32b) while actual systems show a more complex force-displacement characteristic (Fig. D.32c).

Appendix E
DATA ON VARIOUS VEHICLES

This appendix contains fairly complete data on different vehicles: The small cars of the A, B, C and D sections, two sports cars, a van, an articulated truck and a racing motorcycle

Some of the data here reported were used throughout the text in the examples and may be used by the reader to repeat the computations shown for different kinds of motor vehicles.

Although not an exact description of any actual vehicle, the characteristics shown here are typical.

E.1 Small car (a)

The vehicle is a typical late model small car with five seats and a 1.2 liter spark ignition engine.

The primarygeometrical data and inertial properties of the vehicle are:

length = 3,540 mm	width = 1,580 mm	height = 1,540 mm
$a = 923$ mm	$b = 1,376$ mm	$l = 2,299$ mm
$m = 860 \div 1{,}020$[1] kg	$t_1 = 1{,}370$ mm	$t_2 = 1{,}360$ mm
$J_x = 500$ kg m^2	$J_y = 1{,}000$ kg m^2	$J_z = 1{,}225$ kg m^2
$h_G = 600$ mm		
J_r(each) = 0.59 kg m^2	$J_m = 0.088$ kg m^2	$J_t = 0.05$ kg m^2

[1]The first value is the mass of the empty vehicle; the second includes two passengers and is consistent with the values of the moments of inertia the height of the center of mass.

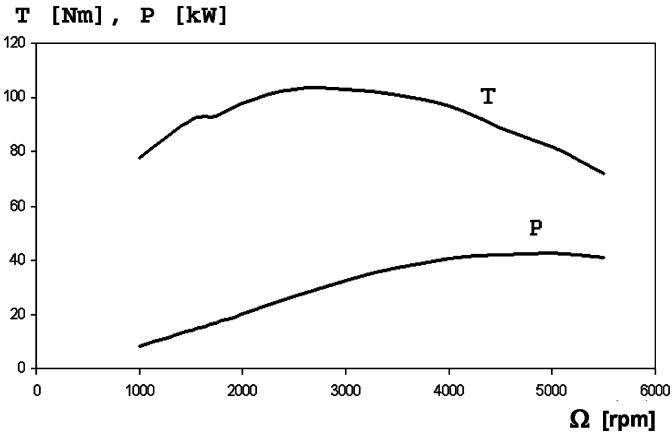

FIGURE E.1. Maximum power and torque curves of the engine.

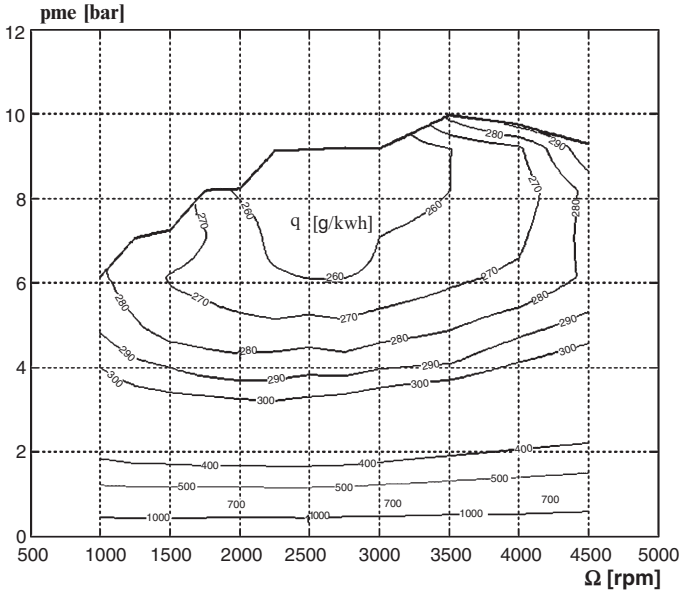

FIGURE E.2. Map of the specific fuel consumption of the engine; the consumption at idle (700 rpm) is 340 g/h.

The maximum engine power and torque are

$P_{max} = 43$ kW at 5000 rpm; $T_{max} = 103$ Nm at 3000 rpm.

The performance curves of the engine are reported in Fig. E.1; the map of specific fuel consumption is shown in Fig. E.2.

The data for the computation of rolling resistance and for the computation of longitudinal and lateral forces (equations (2.34, 2.35, 2.36, 2.37)) for the 155/70 R 13 tires used on this car are reported in the following table:

$$R_e = 279 \text{ mm}$$

$f_0 = 0.011$	$K = 2.6 \cdot 10^{-8}$ s^2/m^2
$p_{Cx1} = 1.62$	$p_{Cy1} = 1.711$
$p_{Dx1} = 0.941$	$p_{Dy1} = 0.900$
$p_{Dx2} = 5.84 \cdot 10^{-2}$	$p_{Dy2} = -0.273$
$p_{Dx3} = -2.45 \cdot 10^{-5}$	$p_{Dy3} = 5.45 \cdot 10^{-4}$
$p_{Ex1} = 0.804$	$p_{Ey1} = 5.84 \cdot 10^{-2}$
$p_{Ex2} = -0.312$	$p_{Ey2} = -0.616$
$p_{Ex3} = -0.416$	$p_{Ey3} = -1.49 \cdot 10^{-5}$
$p_{Ex4} = -3.79 \cdot 10^{-6}$	$p_{Ey4} = 2.59 \cdot 10^{-5}$
$p_{Kx1} = 41.3$	$p_{Ky1} = -12.4$
$p_{Kx2} = 15.5$	$p_{Ky2} = 1.08$
$p_{Kx3} = -5.44 \cdot 10^{-3}$	$p_{Ky3} = 0.767$
$p_{Hx1} = -5.27 \cdot 10^{-8}$	$p_{Hy1} = -2.26 \cdot 10^{-8}$
$p_{Hx2} = 5.60 \cdot 10^{-8}$	$p_{Hy2} = 2.07 \cdot 10^{-7}$
	$p_{Hx3} = -5.36 \cdot 10^{-7}$
$p_{Vx1} = -8.54 \cdot 10^{-8}$	$p_{Vy1} = 6.37 \cdot 10^{-8}$
$p_{Vx2} = 3.48 \cdot 10^{-7}$	$p_{Vy2} = 8.13 \cdot 10^{-7}$
	$p_{Vy3} = -1.40 \cdot 10^{-6}$
	$p_{Vy4} = 7.80 \cdot 10^{-7}$

Aerodynamic data:

$$S = 2.04 \text{ m}^2 \qquad C_x = 0.33$$

Gear ratios (front wheel drive):

$\tau_I = 3.909$	$\tau_{II} = 2.157$	$\tau_{III} = 1.48$	$\eta_t = 0.93$
$\tau_{IV} = 1.121$	$\tau_V = 0.897$	$\tau_f = 3.438$	

E.2 Small car (b)

The vehicle is a typical 1990s small car with five seats and a 1 liter spark ignition engine of the 1990s. The performance curves of the engine and map of specific fuel consumption are shown in Fig. E.3.

The primary geometrical data and the inertial properties of the vehicle, wheels and driveline are:

length = 3,640 mm	width = 1,560 mm	height = 1,410 mm
$a = 870$ mm	$b = 1,290$ mm	$l = 2,160$ mm
$m = 830$ kg	$t_1 = 1{,}284$ mm	$t_2 = 1{,}277$ mm
$J_x = 290$ kg m^2	$J_y = 1{,}094$ kg m^2	$J_z = 1{,}210$ kg m^2
$J_{xz} = -84$ kg m^2		
J_r(each) = 0.4 kg m^2	$J_m = 0.085$ kg m^2	$J_t = 0.05$ kg m^2

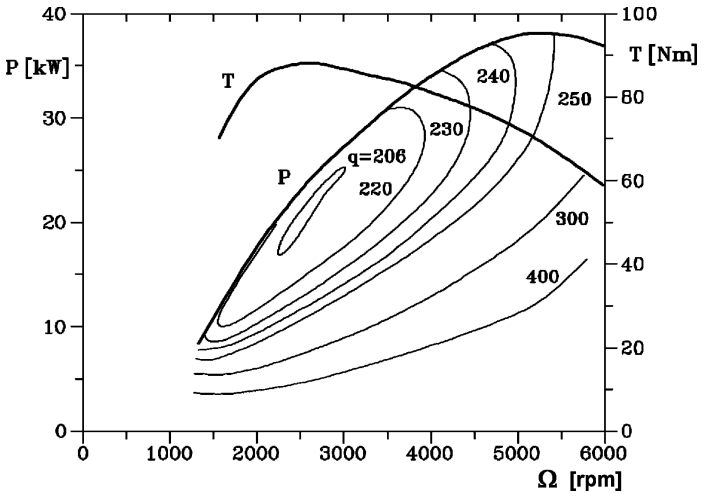

FIGURE E.3. Maximum torque and power curves and map of the specific fuel consumption of the engine; the consumption at idle (700 rpm) is 27 g/h.

The maximum engine power and torque are
$P_{max} = 38.3$ kW at 5200 rpm; $T_{max} = 87$ Nm at 3,000 rpm.

The data for the computation of rolling resistance and longitudinal and lateral forces (equations (2.23, 2.28, 2.29)) for the 145 R 13 tires used on this car are reported in the following table:

$f_0 = 0.013$	$K = 6.5 \cdot 10^{-6}$ s^2/m^2	$R_e = 257$ mm
$a_0 = 1.30$	$a_1 = -53.3$	$a_2 = 1,190$
$a_3 = 588$	$a_4 = 2.52$	$a_5 = 0$
$a_6 = -0.519$	$a_7 = 1.00$	$a_8 = 0$
$a_9 = 0$	$a_{10} = 0$	$a_{111} = 0$
$a_{112} = 0$	$a_{12} = 0$	$a_{13} = 0$
$c_0 = 2.40$	$c_1 = -4.40$	$c_2 = -1.36$
$c_3 = -4.10$	$c_4 = -3.28$	$c_5 = 0.245$
$c_6 = 0$	$c_7 = -0.0792$	$c_8 = 0$
$c_9 = 1.00$	$c_{10} = 0$	$c_{11} = 0$
$c_{12} = 0$	$c_{13} = 0$	$c_{14} = 0$
$c_{15} = 0$	$c_{16} = 0$	$c_{17} = 0$
$A = 1.12$	$C = 0.625$	$D = 1$
$n = 0.6$	$k = 46$	$d = 5$

Aerodynamic data:

$S = 1.7$ m^2	$C_x = 0.32$	$C_z = -0.21$
$C_{M_y} = -0.09$	$(C_y)_{,\beta} = -2.2$ 1/rad	$(C_{M_z})_{,\beta} = -0.6$ 1/rad

Driveline (front wheels drive):

$$\tau_I = 4.64 \qquad \tau_{II} = 2.74 \qquad \tau_{III} = 1.62$$
$$\tau_{IV} = 1.05 \qquad \tau_f = 3.47 \qquad \eta_t = 0.91$$

E.3 Small car (c)

The vehicle is a typical late-model small car with five seats and a 1.3 liter direct injection diesel engine.

The main geometrical data and inertial properties of the vehicle, wheels and engine are:

length = 4,030 mm	width = 1,690 mm	height = 1,490 mm
$a = 958$ mm	$b = 1,552$ mm	$l = 2,510$ mm
$m = 1{,}090 \div 1{,}250$[2] kg	$t_1 = 1{,}440$ mm	$t_2 = 1{,}420$ mm
$J_x = 960$ kg m^2	$J_y = 2{,}058$ kg m^2	$J_z = 2{,}663$ kg m^2
$h_G = 550$ mm		
J_r(each) = 0.77 kg m^2	$J_m = 0.16$ kg m^2	$J_t = 0.06$ kg m^2

The maximum engine power and torque are
$P_{max} = 51$ kW at 4,000 rpm; $T_{max} = 180$ Nm at 1,800 rpm.

The performance curves of the engine are reported in Fig. E.4; the map of specific fuel consumption is shown in Fig. E.5.

The data for the computation of rolling resistance and longitudinal and lateral forces (equations (2.34, 2.35, 2.36, 2.37)) for the 175/65 R 15 tires used on this car are reported in the following table:

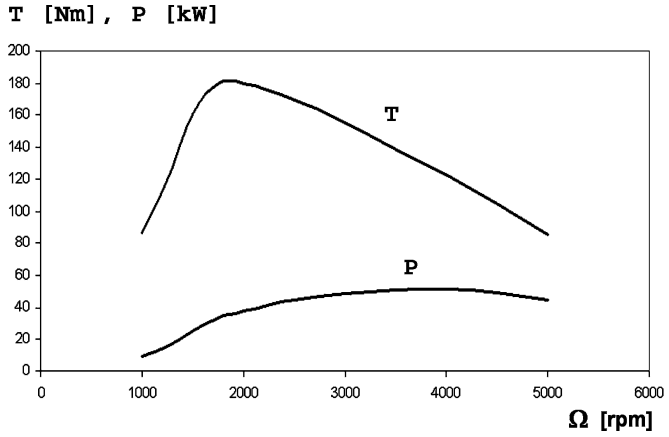

FIGURE E.4. Maximum power and torque curves of the engine.

[2]The first value is the mass of the empty vehicle; the second includes two passengers and is consistent with the values of the moments of inertia and height of the center of mass.

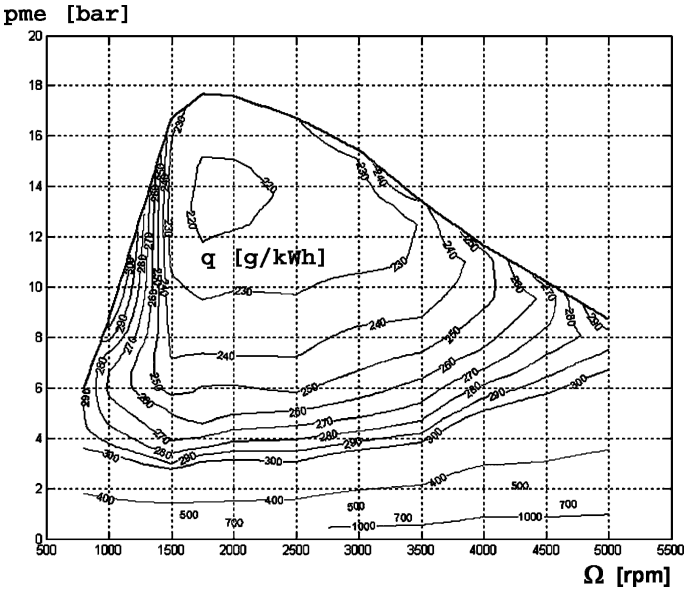

FIGURE E.5. Map of the specific fuel consumption of the engine; the consumption at idle (800 rpm) is 300 g/h.

$$R_e = 296 \text{ mm}$$

$f_0 = 0.0096$	$K = 2.7 \cdot 10^{-8}$ s^2/m^2
$p_{Cx1} = 1.45$	$p_{Cy1} = 1.11$
$p_{Dx1} = 1.00$	$p_{Dy1} = 0.982$
$p_{Dx2} = 0.0$	$p_{Dy2} = -0.16$
$p_{Dx3} = 0.0$	$p_{Dy3} = -2.47$
$p_{Ex1} = 8.58 \cdot 10^{-7}$	$p_{Ey1} = 0.571$
$p_{Ex2} = -7.60 \cdot 10^{-6}$	$p_{Ey2} = -0.261$
$p_{Ex3} = -2.24 \cdot 10^{-5}$	$p_{Ey3} = -0.323$
$p_{Ex4} = -202$	$p_{Ey4} = -22.66$
$p_{Kx1} = 25.1$	$p_{Ky1} = -20.22$
$p_{Kx2} = -5.11 \cdot 10^{-6}$	$p_{Ky2} = 2.72$
$p_{Kx3} = 0.399$	$p_{Ky3} = 0.0811$
$p_{Hx1} = -8.71 \cdot 10^{-6}$	$p_{Hy1} = 3.39 \cdot 10^{-3}$
$p_{Hx2} = -1.0 \cdot 10^{-5}$	$p_{Hy2} = 1.58 \cdot 10^{-3}$
	$p_{Hy3} = 9.83 \cdot 10^{-2}$
$p_{Vx1} = 1.42 \cdot 10^{-5}$	$p_{Vy1} = 4.51 \cdot 10^{-4}$
$p_{Vx2} = 8.62 \cdot 10^{-5}$	$p_{Vy2} = 0.0161$
	$p_{Vy3} = 0.438$
	$p_{Vy4} = -0.378$

Aerodynamic data:

$$S = 2.14 \text{ m}^2 \qquad C_x = 0.35$$

Driveline (front wheels drive):

$\tau_I = 3.909$ $\tau_{II} = 2.238$ $\tau_{III} = 1.444$ $\eta_t = 0.93$
$\tau_{IV} = 1.029$ $\tau_V = 0.767$ $\tau_f = 3.563$

E.4 Medium size saloon car (a)

The vehicle is a typical late-model saloon car with five seats and a 1.9 liter direct injection diesel engine.

The main geometrical data and inertial properties of the vehicle, wheels and engine are:

length = 4,250 mm	width = 1,760 mm	height = 1,530 mm
$a = 1,108$ mm	$b = 1,492$ mm	$l = 2,600$ mm
$m = 1{,}320 \div 1{,}400$[3] kg	$t_1 = 1{,}506$ mm	$t_2 = 1{,}498$ mm
$J_x = 545$ kg m^2	$J_y = 1{,}936$ kg m^2	$J_z = 2{,}038$ kg m^2
$h_G = 565$ mm		
J_r(each) = 0.86 kg m^2	$J_m = 0.27$ kg m^2	$J_t = 0.08$ kg m^2

The maximum engine power and torque are
$P_{max} = 85$ kW at 4,000 rpm; $T_{max} = 280$ Nm at 2,000 rpm.

The performance curves of the engine are reported in Fig. E.6; the map of specific fuel consumption is shown in Fig. E.7.

The data for the computation of rolling resistance and longitudinal and lateral forces (equations (2.34, 2.35, 2.36, 2.37)) for the 195/65 R 15 tires used on this car are reported in the following table:

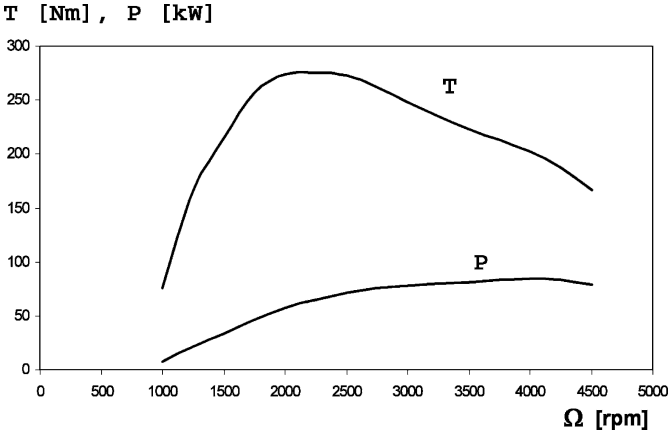

FIGURE E.6. Maximum power and torque curves of the engine.

[3]The first value is the mass of the empty vehicle; the second includes two passengers and is consistent with the values of the moments of inertia and height of the center of mass.

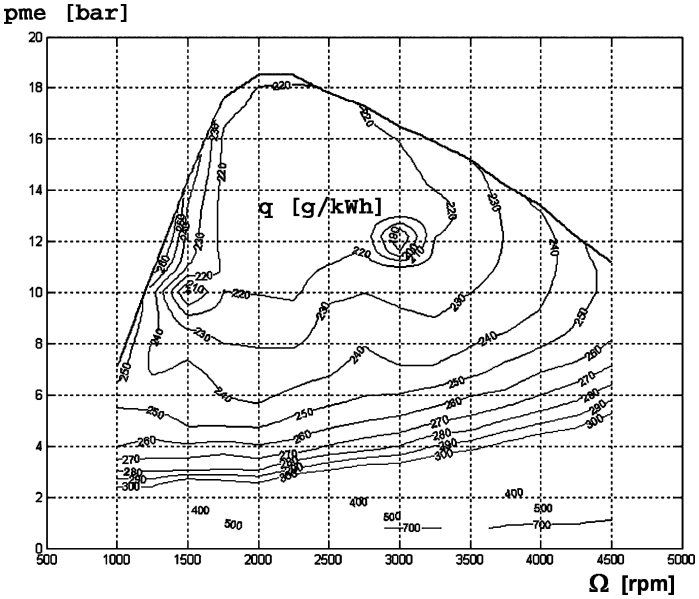

FIGURE E.7. Map of the specific fuel consumption of the engine; the consumption at idle (850 rpm) is 520 g/h

$$R_e = 307 \text{ mm}$$

$f_0 = 0.0124$	$K = 0.23 \cdot 10^{-8}$ s^2/m^2
$p_{Cx1} = 1.53$	$p_{Cy1} = 0.0486$
$p_{Dx1} = 1.20$	$p_{Dy1} = 18.1$
$p_{Dx2} = -0.129$	$p_{Dy2} = -2.21$
$p_{Dx3} = 0.0$	$p_{Dy3} = 1.71$
$p_{Ex1} = 0.456$	$p_{Ey1} = 0.106$
$p_{Ex2} = 0.420$	$p_{Ey2} = 0.0767$
$p_{Ex3} = 0.024$	$p_{Ey3} = -1.57$
$p_{Ex4} = 0.174$	$p_{Ey4} = 28.9$
$p_{Kx1} = 60.9$	$p_{Ky1} = -24.03$
$p_{Kx2} = 0.0807$	$p_{Ky2} = 1.70$
$p_{Kx3} = 0.567$	$p_{Ky3} = 0.388$
$p_{Hx1} = -5.99 \cdot 10^{-5}$	$p_{Hy1} = 3.07 \cdot 10^{-3}$
$p_{Hx2} = 5.76 \cdot 10^{-4}$	$p_{Hy2} = -3.55 \cdot 10^{-3}$
	$p_{Hx3} = 0.0796$
$p_{Vx1} = 0.0347$	$p_{Vy1} = -0.0153$
$p_{Vx2} = 0.0221$	$p_{Vy2} = -0.0468$
	$p_{Vy3} = -0.0522$
	$p_{Vy4} = 0.217$

Aerodynamic data:

$$S = 2.15 \text{ m}^2 \qquad C_x = 0.34$$

Driveline (front wheels drive):

$\tau_I = 3.58$	$\tau_{II} = 1.89$	$\tau_{III} = 1.19$	$\eta_t = 0.93$
$\tau_{IV} = 0.85$	$\tau_V = 0.69$	$\tau_f = 3.63$	

E.5 Medium size saloon car (b)

The vehicle is a typical saloon car with a 2 liter spark ignition supercharged engine from the late 1980s.

The performance curves of the engine are reported in Fig. E.8.

The main geometrical data and inertial properties of the vehicle, wheels and driveline are:

length = 4,690 mm	width = 1,830 mm	height = 1,450 mm
$a = 1,064$ mm	$b = 1,596$ mm	$l = 2,660$ mm
$m = 1{,}150$ kg	$t_1 = 1{,}490$ mm	$t_2 = 1{,}482$ mm
$J_x = 530$ kg m^2	$J_y = 1{,}630$ kg m^2	$J_z = 1{,}850$ kg m^2
$h_G = 570$ mm		
$J_{xz} = -120$ kg m^2		
J_r(each) = 0.6 kg m^2	$J_m = 0.19$ kg m^2	$J_t = 0.07$ kg m^2

The maximum engine power and torque are

$P_{max} = 122$ kW at 5,500 rpm; $T_{max} = 255$ Nm at 2,500 rpm, with the possibility of short surges up to 284 Nm at 2,750 rpm (*overboost*).

The data for the computation of rolling resistance and longitudinal and lateral forces (equations (2.23, 2.28, 2.29)) for the 195 R 14 tires used on this car are reported in the following table:

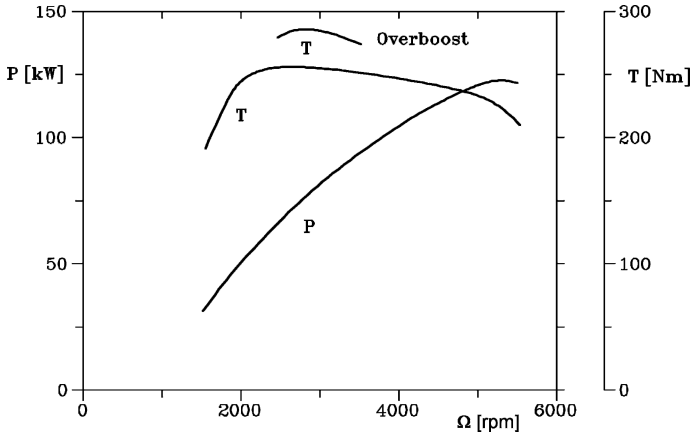

FIGURE E.8. Maximum power and torque curves of the engine

$f_0 = 0.013$ $K = 6.5 \times 10^{-6}$ s^2/m^2 $R_e = 287$ mm
$a_0 = 1.69$ $a_1 = -55.2$ $a_2 = 1,270$
$a_3 = 1.600$ $a_4 = 6.49$ $a_5 = 4.80 \cdot 10^{-3}$
$a_6 = -0.388$ $a_7 = 1.00$ $a_8 = -4.54 \cdot 10^{-2}$
$a_9 = 4.28 \cdot 10^{-3}$ $a_{10} = 8.65 \cdot 10^{-2}$ $a_{111} = -7.97$
$a_{112} = -0.223$ $a_{12} = 7.61$ $a_{13} = 45.9$
$b_0 = 1.65$ $b_1 = -7.61$ $b_2 = 1,122$
$b_3 = -7.36 \cdot 10^{-3}$ $b_4 = 145$ $b_5 = -7.66 \cdot 10^{-2}$
$b_6 = -3.86 \cdot 10^{-3}$ $b_7 = 8.50 \cdot 10^{-2}$ $b_8 = 7.57 \cdot 10^{-2}$
$b_9 = 2.36 \cdot 10^{-2}$ $b_{10} = 2.36 \cdot 10^{-2}$
$c_0 = 2.22$ $c_1 = -3.04$ $c_2 = -9.23$
$c_3 = 0.500$ $c_4 = -5.57$ $c_5 = -0.260$
$c_6 = -1.30 \cdot 10^{-3}$ $c_7 = -0.358$ $c_8 = 3.74$
$c_9 = -15.2$ $c_{10} = 2.11 \cdot 10^{-3}$ $c_{11} = 3.46 \cdot 10^{-4}$
$c_{12} = 9.14 \cdot 10^{-3}$ $c_{13} = -0.244$ $c_{14} = 0.101$
$c_{15} = -1.40$ $c_{16} = 0.444$ $c_{17} = -0.999$

Aerodynamic data:

$S = 2.06$ m^2 $C_x = 0.36$ $C_z = -0.12$
$C_{M_y} = -0.05$ $(C_y)_{,\beta} = -1.8$ 1/rad $(C_{M_z})_{,\beta} = -0.5$ 1/rad

Driveline (front wheel drive)

$\tau_I = 3.750$ $\tau_{II} = 2.235$ $\tau_{III} = 1.518$ $\eta_t = 0.91$
$\tau_{IV} = 1.132$ $\tau_V = 0.82$ $\tau_f = 2.95$

E.6 Sports car (a)

The vehicle is a recent two-seater sports car with a 4.2 liter spark ignition engine.

The main geometrical data and inertial properties of the vehicle, wheels, engine and transmission are

length = 4,510 mm width = 1,920 mm height = 1,210 mm
$a = 1,461$ mm $b = 1,199$ mm $l = 2,660$ mm
$m = 1{,}590 \div 1{,}690$[4] kg $t_1 = 1{,}670$ mm $t_2 = 1{,}600$ mm
$J_x = 626$ kg m^2 $J_y = 2{,}165$ kg m^2 $J_z = 2{,}220$ kg m^2
$h_G = 470$ mm
J_r (total) $= 2.2$ kg m^2 $J_m = 0.28$ kg m^2 $J_t = 0.07$ kg m^2

The maximum engine power and torque are
$P_{max} = 290$ kW at 7,000 rpm; $T_{max} = 460$ Nm at 4,400 rpm.

The performance curves of the engine are reported in Fig. E.9; the map of specific fuel consumption is shown in Fig. E.10.

[4]The first value is the mass of the empty vehicle; the second includes two passengers and is consistent with the values of the moments of inertia and height of the center of mass.

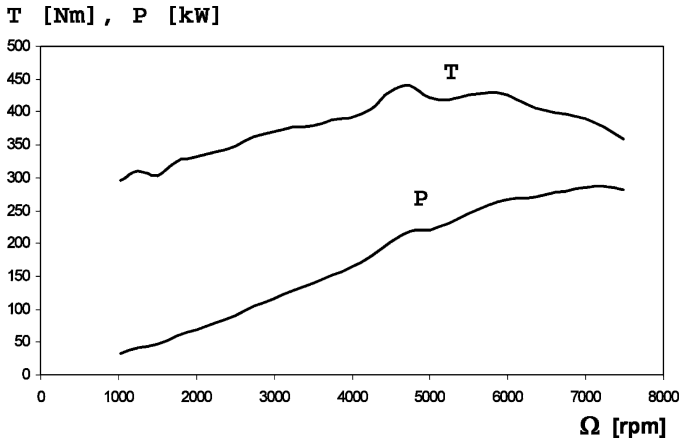

FIGURE E.9. Maximum power and torque curves of the engine.

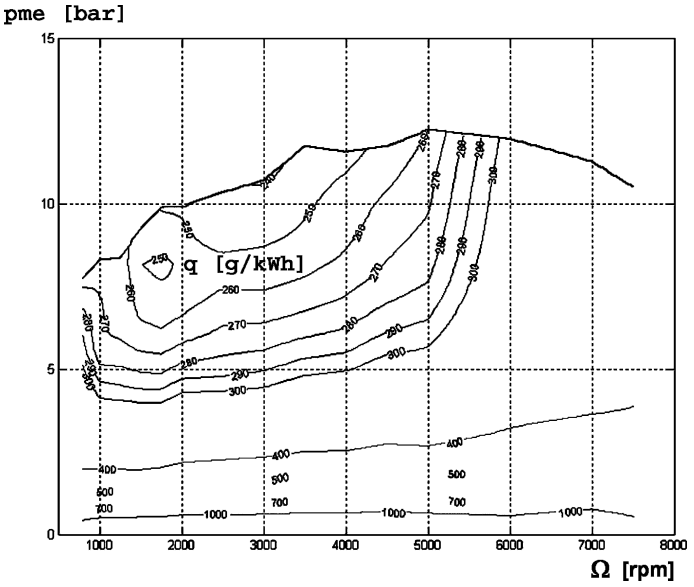

FIGURE E.10. Map of the specific fuel consumption of the engine; the consumption at idle (850 rpm) is 520 g/h

The data for the computation of rolling resistance and longitudinal and lateral forces (equations (2.34, 2.35, 2.36, 2.37)) for the front 245/40 R 18 and rear 285/40 R 18 tires used on this car are reported in the following table:

$f_0 = 0.014$	$K = 0.5 \cdot 10^{-7}$ s^2/m^2
$p_{Cx1} = 1.44$	$p_{Cy1} = 1.84$
$p_{Dx1} = 1.27$	$p_{Dy1} = 1.19$
$p_{Dx2} = -0.0824$	$p_{Dy2} = -0.181$
$p_{Dx3} = 0.0$	$p_{Dy3} = 3.85$
$p_{Ex1} = -2.37 \cdot 10^{-5}$	$p_{Ey1} = -1.89 \cdot 10^{-4}$
$p_{Ex2} = -3.93 \cdot 10^{-5}$	$p_{Ey2} = 5.17 \cdot 10^{-5}$
$p_{Ex3} = 8.57 \cdot 10^{-6}$	$p_{Ey3} = 1060$
$p_{Ex4} = -201$	$p_{Ey4} = 1490$
$p_{Kx1} = 35.8$	$p_{Ky1} = -3050$
$p_{Kx2} = 4.73 \cdot 10^{-4}$	$p_{Ky2} = 299$
$p_{Kx3} = 0.143$	$p_{Ky3} = 0.224$
$p_{Hx1} = -7.69 \cdot 10^{-5}$	$p_{Hy1} = -4.70 \cdot 10^{-4}$
$p_{Hx2} = 1.35 \cdot 10^{-4}$	$p_{Hy2} = -1.24 \cdot 10^{-4}$
	$p_{Hy3} = -8.04 \cdot 10^{-3}$
$p_{Vx1} = 3.32 \cdot 10^{-4}$	$p_{Vy1} = -0.0153$
$p_{Vx2} = 5.72 \cdot 10^{-4}$	$p_{Vy2} = -0.00210$
	$p_{Vy3} = -0.857$
	$p_{Vy4} = -0.380$

$$R_e = 333 \text{ mm}$$

$f_0 = 0.0124$	$K = 0.23 \cdot 10^{-8}$ s^2/m^2
$p_{Cx1} = 1.52$	$p_{Cy1} = 1.41$
$p_{Dx1} = 1.49$	$p_{Dy1} = 1.18$
$p_{Dx2} = -0.102$	$p_{Dy2} = -0.158$
$p_{Dx3} = 0.0$	$p_{Dy3} = 1.87$
$p_{Ex1} = -0.277$	$p_{Ey1} = 0.358$
$p_{Ex2} = -0.422$	$p_{Ey2} = -0.691$
$p_{Ex3} = 0.251$	$p_{Ey3} = 0.196$
$p_{Ex4} = -1.04$	$p_{Ey4} = -6.03$
$p_{Kx1} = 27.6$	$p_{Ky1} = -60.1$
$p_{Kx2} = -10.1$	$p_{Ky2} = 3.51$
$p_{Kx3} = 0.432$	$p_{Ky3} = 0.271$
$p_{Hx1} = -6.34 \cdot 10^{-4}$	$p_{Hy1} = 2.74 \cdot 10^{-3}$
$p_{Hx2} = -3.87 \cdot 10^{-4}$	$p_{Hy2} = -2.29 \cdot 10^{-4}$
	$p_{Hy3} = 0.0197$
$p_{Vx1} = 0.0127$	$p_{Vy1} = 0.0369$
$p_{Vx2} = 0.0214$	$p_{Vy2} = -0.0262$
	$p_{Vy3} = -0.47$
	$p_{Vy4} = -0.565$

Aerodynamic data:

$$S = 2.21 \text{ m}^2 \qquad C_x = 0.35$$

Driveline (rear wheel drive):

$\tau_I = 3.29$	$\tau_{II} = 2.16$	$\tau_{III} = 1.61$	$\tau_{IV} = 1.27$	$\eta_t = 0.91$
$\tau_V = 1.04$	$\tau_{VI} = 0.88$	$\tau_f = 4.19$		

E.7 Sports car (b)

The vehicle is a mid-engine two-seater sports car with a 3.5 liter spark ignition supercharged engine.

The performance curves of the engine and the map of specific fuel consumption are shown in Fig. E.11.

The main geometrical data and inertial properties of the vehicle, wheels, engine and transmission are

length = 4,250 mm	width = 1,900 mm	height = 1,160 mm
$m = 1{,}480$ kg	$t_1 = 1{,}502$ mm	$t_2 = 1{,}578$ mm
$J_x = 590$ kg m^2	$J_y = 1{,}730$ kg m^2	$J_z = 1{,}950$ kg m^2
$J_{xz} = -50$ kg m^2	J_{r_1} (each) $= 7$ kg m^2	J_{r_2} (each) $= 7$ kg m^2
$J_m = 0.7$ kg m^2	$J_t = 0.08$ kg m^2	

$P_{max} = 235$ kW at 7,200 rpm; $T_{max} = 324$ Nm at 5,000 rpm.

Data for rolling coefficient and for the "magic formula" for lateral forces, longitudinal forces and aligning torque of tires:

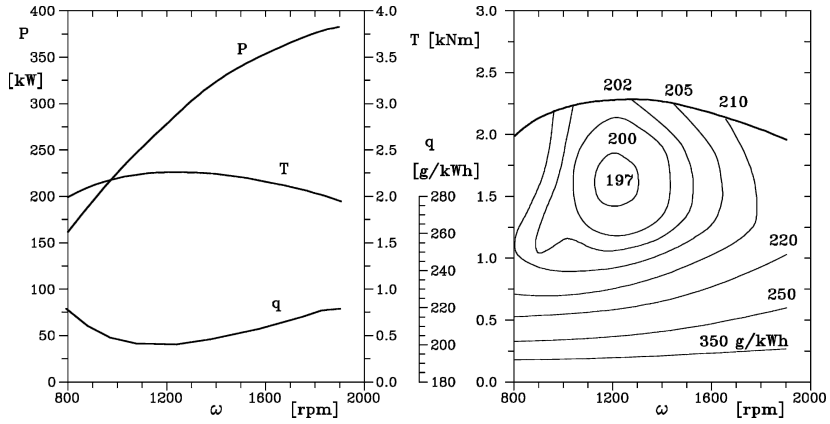

FIGURE E.11. Maximum torque and power curves and map of the specific fuel consumption of the engine.

$f_0 = 0.013$	$K = 6.5 \times 10^{-6}$ s^2/m^2	$R_{e_1} = 310$ mm
$R_{e_2} = 315$ mm		
$a_0 = 1.7990$	$a_1 = 0$	$a_2 = 1688.0000$
$a_3 = 4140.0000$	$a_4 = 6.0260$	$a_5 = 0$
$a_6 = -0.3589$	$a_7 = 1.0000$	$a_8 = 0$
$a_9 = -6.1110 \times 10^{-3}$	$a_{10} = -3.2240 \times 10^{-2}$	$a_{111} = 0$
$a_{112} = 0$	$a_{12} = 0$	$a_13 = 0$
$b_0 = 1.65$	$b_1 = 0$	$b_2 = 1688$
$b_3 = 0$	$b_4 = 229$	$b_5 = 0$
$b_6 = 0$	$b_7 = 0$	$b_8 = -10$
$b_9 = 0$	$b_{10} = 0$	
$c_0 = 2.0680$	$c_1 = -6.4900$	$c_2 = -21.850$
$c_3 = 0.4160$	$c_4 = -21.3100$	$c_5 = 2.9420 \times 10^{-2}$
$c_6 = 0$	$c_7 = -1.1970$	$c_8 = 5.2280$
$c_9 = -14.8400$	$c_{10} = 0$	$c_{11} = 0$
$c_{12} = -3.7360 \times 10^{-3}$	$c_{13} = 3.8910 \times 10^{-2}$	$c_{14} = 0$
$c_{15} = 0$	$c_{16} = 0.6390$	$c_{17} = 1.6930$

Aerodynamic data:

$S = 1.824$ m^2	$C_x = 0.335$	$C_z = -0.34$
$C_{M_y} = 0$	$(C_y)_{,\beta} = -2.3$ 1/rad	$(C_N)_{,\beta} = -0.3$ 1/rad

Transmission (rear wheel drive) (the value of τ_f is inclusive of the reduction gears located between engine and gearbox):

$\tau_I = 1/3.214$	$\tau_{II} = 1/2.105$	$\tau_{III} = 1/1.458$
$\tau_{IV} = 1/1.094$	$\tau_V = 1/0.861$	$\tau_f = 1/4.051$
$\eta_t = 0.87$		

E.8 Van

The vehicle is a van with a carrying capacity of 1.4 t (fully loaded mass 3,500 kg) with a 2.3 l direct injection diesel engine.

The main geometrical data and inertial properties of the vehicle, wheels, engine and transmission are

length = 5,400 mm	width = 2,050 mm	height = 2,500 mm
$a = 1,204$ mm	$b = 2,246$ mm	$l = 3,450$ mm
$m = 2{,}020 \div 2{,}100$[5] kg	$t_1 = 1{,}810$ mm	$t_2 = 1{,}790$ mm
$J_x = 1{,}400$ kg m^2	$J_y = 6{,}000$ kg m^2	$J_z = 6{,}230$ kg m^2
$h_G = 679$ mm		
J_r(each) = 1.07 kg m^2	$J_m = 0.335$ kg m^2	$J_t = 0.32$ kg m^2

[5]The first value is the mass of the empty vehicle; the second includes one passenger and luggage and is consistent with the values of the moments of inertia and height of the center of mass. The effect of the payload must then be added.

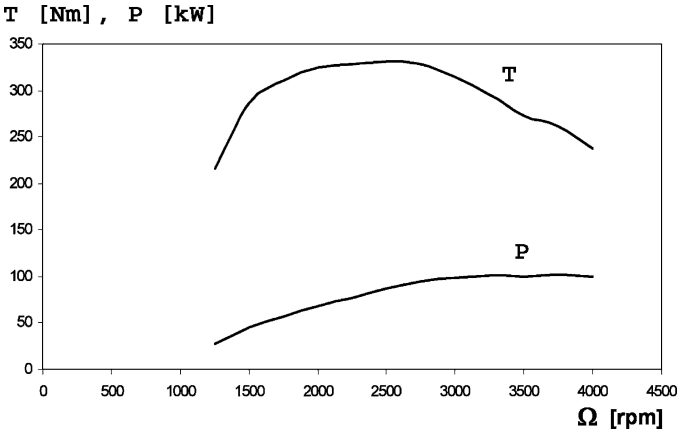

FIGURE E.12. Maximum power and torque curves of the engine.

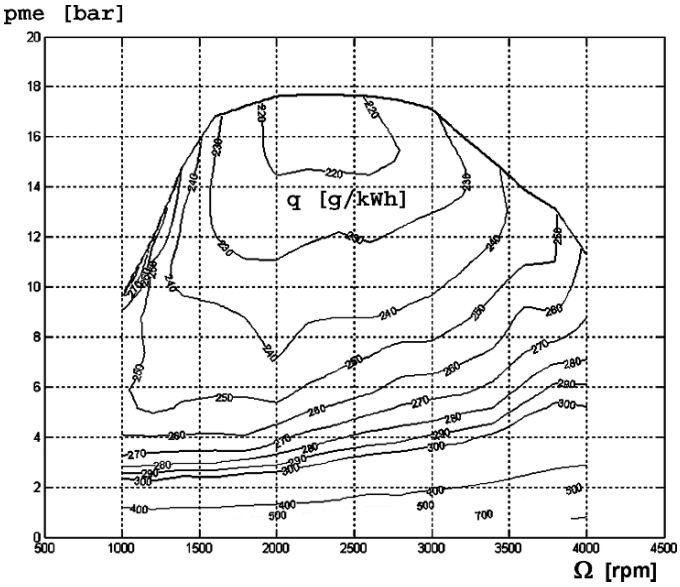

FIGURE E.13. Map of the specific fuel consumption of the engine; the consumption at idle (800 rpm) is 500 g/h.

The maximum engine power and torque are

$P_{max} = 103$ kW at 3,750 rpm; $T_{max} = 330$ Nm at 2,500 rpm.

The performance curves of the engine are reported in Fig. E.12; the map of specific fuel consumption is shown in Fig. E.13.

Aerodynamic data:

$$S = 4.4 \text{ m}^2 \qquad C_x = 0.37$$

Driveline (rear wheels drive):

$\tau_I = 4.99$ $\tau_{II} = 2.6$ $\tau_{III} = 1.52$ $\eta_t = 0.93$
$\tau_{IV} = 1.00$ $\tau_V = 0.777$ $\tau_f = 3.72$

The data for the computation of rolling resistance and longitudinal and lateral forces (equations (2.34, 2.35, 2.36, 2.37)) for the 225/65 R 16 tires used on this vehicle are reported in the following table:

$R_e = 339$ mm

$f_0 = 0.0094$	$K = 0.43 \cdot 10^{-8}$ s^2/m^2
$p_{Cx1} = 1.76$	$p_{Cy1} = 1.3$
$p_{Dx1} = 1.09$	$p_{Dy1} = -0.857$
$p_{Dx2} = -0.0312$	$p_{Dy2} = -0.0702$
$p_{Dx3} = 0.0$	$p_{Dy3} = 0.0$
$p_{Ex1} = 0.552$	$p_{Ey1} = 0.00117$
$p_{Ex2} = 0.370$	$p_{Ey2} = -0.0106$
$p_{Ex3} = -0.170$	$p_{Ey3} = -8.68 \cdot 10^{-5}$
$p_{Ex4} = 0.0$	$p_{Ey4} = 0.0$
$p_{Kx1} = 19.1$	$p_{Ky1} = -15.3$
$p_{Kx2} = -0.466$	$p_{Ky2} = 2.93$
$p_{Kx3} = 0.483$	$p_{Ky3} = 0.0$
$p_{Hx1} = -5.45 \cdot 10^{-4}$	$p_{Hy1} = 0.00571$
$p_{Hx2} = 2.09 \cdot 10^{-4}$	$p_{Hy2} = 0.00283$
	$p_{Hy3} = 0.0$
$p_{Vx1} = 0.0$	$p_{Vy1} = 0.0207$
$p_{Vx2} = 0.0$	$p_{Vy2} = 0.00421$
	$p_{Vy3} = 0.0$
	$p_{Vy4} = 0.0$

E.9 Heavy articulated truck

The vehicle is an articulated truck with a two-axle tractor and a three-axle trailer. The geometrical data regarding the positions of the axles and centers of mass in the xz plane are reported in Fig. E.14.

E.9.1 Tractor

The main geometrical data and inertial properties of the vehicle, wheels, engine and transmission are:

$m = 7{,}150$ kg $t_1 = 2{,}100$ mm $t_2 = 1{,}835$ mm
$J_x = 4{,}500$ kg m^2 $J_y = 25{,}800$ kg m^2 $J_z = 27{,}000$ kg m^2
$J_{xz} = -3{,}800$ kg m^2 $J_r = 2.5$ kg m^2 (each)
$J_m = 2.55$ kg m^2 $J_t = 1.1$ kg m^2

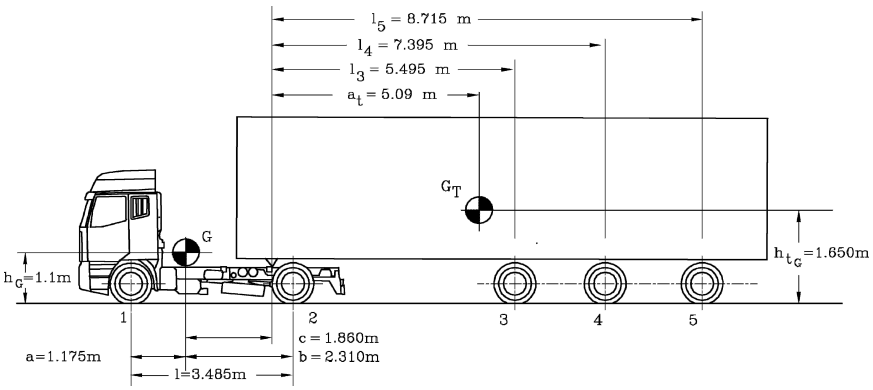

FIGURE E.14. Sketch of an articulated truck with 5 axles.

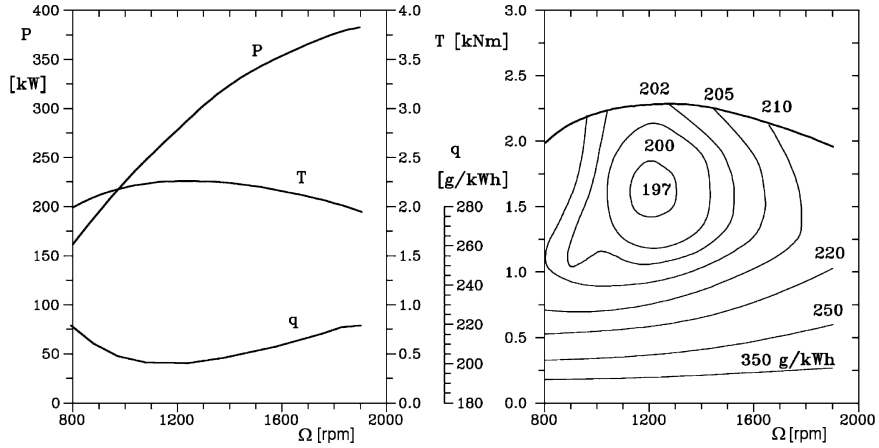

FIGURE E.15. Maximum torque and power curves and map of the specific fuel consumption of the engine.

The vertical and torsional stiffnesses of the suspensions are:

$K_1 = 2{,}100$ N/m $\quad K_2 = 2{,}800$ N/m $\quad K_{t_1} = 3{,}790$ Nm/rad
$K_{t_2} = 3{,}790$ Nm/rad

Aerodynamic data:

$S = 5.14$ m^2 $\quad C_x = 0.45$ (tractor) $\quad C_x = 0.65$ (whole vehicle)
$C_z = 0$ $\quad (C_y)_{,\beta} = -2.2$ 1/rad $\quad (C_{M_z})_{,\beta} = -1.5$ 1/rad

The curves of the maximum power and torque of the engine are reported in Fig. E.15 together with the map of the specific fuel consumption

Driveline (rear wheels drive):

$\tau_I = 12.5$	$\tau_{II} = 8.35$	$\tau_{III} = 6.12$
$\tau_{IV} = 4.56$	$\tau_V = 3.38$	$\tau_{VI} = 2.47$
$\tau_{VII} = 2.14$	$\tau_{VIII} = 1.81$	$\tau_{IX} = 1.57$
$\tau_X = 1.35$	$\tau_{XI} = 1.17$	$\tau_{XII} = 1.00$
$\tau_{XIII} = 0.87$	$\tau_f = 4.263$	$\eta_{tI} = 0.81$
$\eta_{tII} = 0.84$	$\eta_{tIII} = 0.84$	$\eta_{tIV} = 0.84$
$\eta_{tV} = 0.89$	$\eta_{tVI} = 0.87$	$\eta_{tVII} = 0.84$
$\eta_{tVIII} = 0.87$	$\eta_{tIX} = 0.84$	$\eta_{tX} = 0.87$
$\eta_{tXI} = 0.84$	$\eta_{tXII} = 0.93$	$\eta_{tXIII} = 0.89$

E.9.2 Trailer

Inertial properties of the trailer:

$m = 32{,}000$[6] kg	$t_3 = 1{,}835$ mm	$t_4 = 1{,}835$ mm
$t_5 = 2{,}100$ mm	$J_x = 30{,}000$ kg m^2	$J_y = 285{,}000$ kg m^2
$J_z = 285{,}000$ kg m^2		

Vertical and torsional stiffnesses of the suspensions:

$K_3 = 2{,}150$ N/m	$K_4 = 2{,}150$ N/m	$K_5 = 1{,}380$ N/m
$K_{t3} = 3{,}200$ Nm/rad	$K_{t4} = 3{,}200$ Nm/rad	$K_{t5} = 2{,}800$ Nm/rad

Aerodynamic data:

$S = 7.5$ m^2	$C_x = 0.25$	$C_z = 0$
$(C_y)_{,\beta} = -2.35$ 1/rad	$(C_{M_z})_{,\beta} = -0.6$ 1/rad	(referred a l_5)

E.9.3 Tires

Axles 1 and 5 have single tires, axles 2, 3 and 4 have twin tires. Data for rolling coefficient and basic data for cornering forces and aligning torque using a simplified magic formula (equations (2.23, 2.28, 2.29)):

$f_0 = 0.008$	$K = 0$	$R_e = 460$ mm
$a_3 = 5019.3$	$a_4 = 65.515$	
$c_3 = -0.6100$	$c_4 = -2.3400$	$c_5 = 0.02727$

E.10 Racing motorcycle

The vehicle is a racing motorcycle. The geometrical sketch of the vehicle and the torque and power curves of the engine are reported in Fig. E.16.

[6] Fully loaded mass.

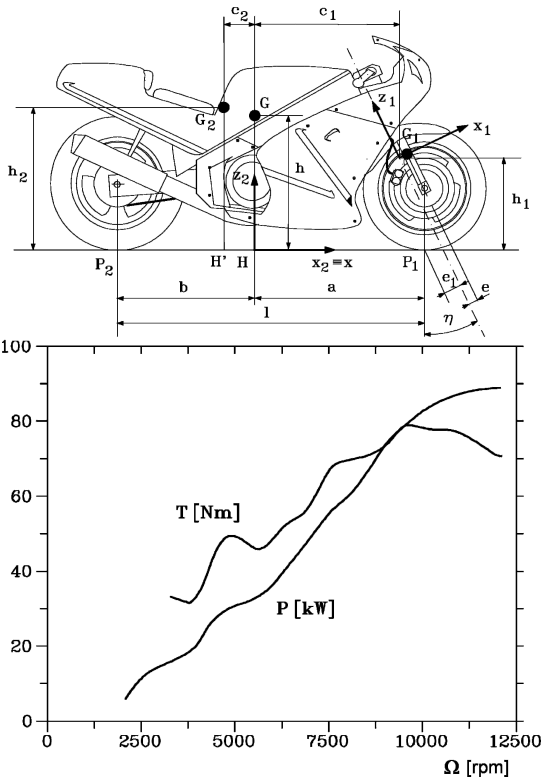

FIGURE E.16. Geometrical sketch of the vehicle and torque and power curves of the engine.

The main geometrical data and inertial properties of the vehicle (moment of inertia J_x is referred to an axis lying on the ground), wheels, engine, transmission are:

$m_1 = 20$ kg	$m_2 = 200$ kg	$m_d = 70$ kg (driver)
$J_x = 80$ kg m^2	$J_y = 110$ kg m^2	$J_z = 40$ kg m^2
$J_{xz} = 0$	$J_{1_z} = 2$ kg m^2	$J_{1_{xz}} = 1$ kg m^2
$J_{p_1} = 0.4$	$J_{p_2} = 0.4$ kg m^2	$J_e = 0.08$ kg m^2
$l = 1320$ mm	$a = 642$ mm	$b = 678$ mm
$c_1 = 561.5$ mm	$c_2 = 54.2$ mm	$e = 50$ mm
$e_1 = 95$ mm	$h = 495.6$ mm	$h_1 = 432$ mm
$h_2 = 500$ mm	$\eta = 23°$	$c_\delta = 8$ Nms/rad

$P_{max} = 88$ kW a 11.900 rpm; $T_{max} = 76$ Nm a 9.750 rpm.

Wheels and tires, geometrical and linearized data:

$R_{e1} = 300$ mm	$R_{e2} = 300$ mm	$r_{t_1} = 70$ mm
$r_{t_2} = 110$ mm	r_t (average) $= 90$ mm	
$f_0 = 0.01$	$K = 4 \cdot 10^{-6}$ s^2/m^2	$\mu_{x_{max}} = 1.1$
$(C_1)_{,Z} = 27.27$ 1/rad	$(C_2)_{,Z} = 30.0$ 1/rad	
$(M_{z_2})_{,\alpha,Z} = 0.228$ m/rad	$(F_{y_1})_{,\gamma,Z} = -1.177$ 1/rad	
$(M_{z_1})_{,\alpha,Z} = 0.210$ m/rad	$(F_{y_2})_{,\gamma,Z} = -1.367$ 1/rad	

Data for the "magic formula" for lateral forces, longitudinal forces and aligning torque, front tire (Equations (2.23, 2.28, 2.29)):

$a_0 = 1.50$	$a_1 = -27.9$	$a_2 = 1,280$
$a_3 = -1000$	$a_4 = 4.00$	$a_5 = 0.015$
$a_6 = -0.35$	$a_7 = -1.99$	$a_8 = 0.058$
$a_9 = 0$	$a_{10} = 0$	$a_{11} = 5$
$a_{12} = 0$	$a_{13} = 0$	
$b_3 = 49.6$	$b_4 = 226$	$b_5 = 0.069$
$c_0 = 2.40$	$c_1 = -2.72$	$c_2 = -2.28$
$c_3 = 1.86$	$c_4 = 2.73$	$c_5 = 0.11$
$c_6 = 0.030$	$c_7 = -0.07$	$c_8 = 0.643$
$c_9 = -4.04$	$c_{10} = -0.07$	$c_{11} = -0.015$
$c_{12} = 0$	$c_{13} = 0$	$c_{14} = -0.066$
$c_{15} = 0.945$	$c_{16} = 0$	$c_{17} = 0$

Data for the "magic formula" for lateral forces, longitudinal forces and aligning torque, rear tire (Equations (2.23, 2.28, 2.29)):

$a_0 = 1.50$	$a_1 = -27.9$	$a_2 = 1,275$
$a_3 = -1.100$	$a_4 = 4.00$	$a_5 = 0.010$
$a_6 = -0.35$	$a_7 = -1.99$	$a_8 = 0.058$
$a_9 = 0$	$a_{10} = 0$	$a_{11} = 5$
$a_{12} = 0$	$a_{13} = 0$	
$b_3 = 49.6$	$b_4 = 226$	$b_5 = 0.069$
$c_0 = 2.40$	$c_1 = -2.72$	$c_2 = -2.28$
$c_3 = 1.86$	$c_4 = 2.73$	$c_5 = 0.11$
$c_6 = 0.03$	$c_7 = -0.070$	$c_8 = 0.643$
$c_9 = -4.04$	$c_{10} = -0.07$	$c_{11} = -0.015$
$c_{12} = 0$	$c_{13} = 0$	$c_{14} = -0.066$
$c_{15} = 0.945$	$c_{16} = 0$	$c_{17} = 0$

Aerodynamic data:

$S = 1$ m^2	$C_x = 0.23$	$C_z = 0.10$
$C_{M_y} = 0$	$(C_y)_{,\beta} = 0.026$ 1/rad	$(C_{M_z})_{,d} = 0.065$ 1/rad

Transmission (the values of τ_i are inclusive of the reduction gear located between engine and gearbox):

$$\begin{array}{lll} \tau_I = 4.91 & \tau_{II} = 3.84 & \tau_{III} = 3.22 \\ \tau_{IV} = 2.81 & \tau_V = 2.5 & \tau_{VI} = 2.29 \\ \tau_f = 3.00 & \eta_t = 0.88 & \end{array}$$

BIBLIOGRAPHY OF VOLUME 2

Part III

1. Data S., Ugo A., *Objective Evaluation of Steering System Quality*, FISITA International Congress, Prague, 1996.

2. The Auto - Oil II Program, *A report from the services of the European Commission*, Bruxelles, 2000.

3. Lenz H. P. *et alii*, *Transport emissions in EU - 15*, ACEA, Bruxelles, 2002.

4. Caviasso G., Data S., Pascali L., Tamburro A., *Customer Orientation in Advanced Vehicle Design*, SAE Paper 2002-01-1576, 2002.

5. Data S., Frigerio F., *Objective Evaluation of Handling Quality*, Journal of Automotive Engineering, 3, 2002.

6. - , *Road Accidents 1980 - 2000*, ACEA, Bruxelles, 2002.

7. - , *Panorama of Transport*, Eurostat, Luxenbourg, 2003.

8. - , *Autoincifre 2004*, ANFIA, Torino, 2004.

9. Bargero R., Brizio P., Celiberti L., Falasca V., *Objective Evaluation of Vibroacustical Quality*, Congresso SAE, Detroit, 2004.

10. - , *Car Park 1995 - 2002*, ACEA, Bruxelles, 2004.

11. - , *Energy, Transport and Environment Indicators*, Eurostat, Luxenbourg, 2005.

12. Putignano C., *Statistiche dei trasporti 2002 - 2003*, ISTAT, Rome, 2005.

13. - , *European Automotive Industry Report 2005*, ACEA, Bruxelles, 2005.

14. - , *Segments and Bodies 1990 - 2004*, ACEA, Bruxelles, 2005.

Part IV

1. E. Koenig, R. Fachsenfield, *Aerodynamik des Kraftfahrzeuge*, Verlag der Motor, Rundshou-Umsha Verlag, Frankfurt A.M. 1951.

2. Bussien, *Automobiltechnisches Handbuch*, Technischer Verlag H Cam. Ber-lin, 1953.

3. M. Bencini, *Dinamica del veicolo*, Tamburini, Milan, 1956.

4. C. Deutsch, *Dynamique des vehicules routiers*, Organisme National de Sécurité Routière.

5. W. Steeds, *Mechanics of Road Vehicles*, Iliffe & Sons, London, 1960.

6. G.H. Tidbury, *Advances in Automobile Engineering*, Pergamon Press, London, 1965.

7. F. Pernau, *Die entscheidenden Reifeneigenschaften*, Vortragstext, Eszter, 1967.

8. J.R. Ellis, *Vehicle Dynamics*, Business Books Ltd., London, 1969.

9. G. Pollone, *Il veicolo*, Levrotto & Bella, Turin, 1970.

10. H.C.A Van Eldik Thieme, H.B. Pacejka, *The Tire as a Vehicle Component*, Vehicle Res. Lab., Delft University of Technology, 1971.

11. M. Mitschke, *Dinamik der Kraftfahzeuge*, Springer, Berlin, 1972.

12. A. Morelli, *Costruzioni automobilistiche*, in *Enciclopedia dell'Ingegneria*, ISEDI, Milan, 1972.

13. A.J. Scibor Ryilski, *Road Vehicle Aerodynamics*, Pentech Press, Londra, 1975.

14. M.D. Artamonov, V.A. Ilarionov, M.M. Morin, *Motor Vehicles, Fundamentals and Design*, MIR, Moscow, 1976.

15. W.H. Hucho, *The Aerodynamic Drag of Cars. Current Understanding, Unresolved Problems, and Future Prospects*, in *Aerodynamic drag mechanism of bluff bodies and road vehicles*, Plenum Press, New York, 1978.

16. R. H. Macmillan, *Dynamics of Vehicle Collisions*, Inderscience Enterprises, Jersey, 1983.

17. E. Fiala, *Ingegneria automobilistica*, in Manuale di ingegneria meccanica, part 2, EST, Milano, 1985.

18. G.G. Lucas, *Road Vehicle Performance*, Gordon & Breach, London, 1986.

19. J.C. Dixon, *Tyres, Suspension and Handling*, Cambridge University Press, Cambridge, 1991.

20. T. D. Gillespie, *Fundamentals of Vehicle Dynamics*, Society of Automotive Engineers, Warrendale, 1992.

21. D. Bastow, G.P. Howard, *Car Suspension and Handling*, Pentech Press, London, and Society of Automotive Engineers, Warrendale, 1993.

22. W.F. Milliken, D.L. Milliken, *Race Car Vehicle Dynamics*, Society of Automotive Engineers, Warrendale, 1995.

23. J. Reimpell, H. Stoll, J.W. Betzler, *The Automotive Chassis: Engineering Principles*, Butterworth, Oxford, 2001.

24. W.F. Milliken, D.L. Milliken, *Chassis Design, Principles and Analysis*, SAE, Warrendale, 2002.

25. D. Karnopp, *Vehicle Stability*, Marcel Dekker, New York, 2004.

26. Rajesh Rqajamqni, *Vehicle Dynamics and Control*, Springer, New York, 2006.

INDEX